

18th Australian Wine Industry Technical Conference

Lead Guest Editor: Markus J. Herderich

Guest Editors: Paul Petrie, Leigh Schmidtke, and Paul Kilmartin





**18th Australian Wine Industry Technical
Conference**

Australian Journal of Grape and Wine Research

**18th Australian Wine Industry
Technical Conference**

Lead Guest Editor: Markus J. Herderich

Guest Editors: Paul Petrie, Leigh Schmidtke, and
Paul Kilmartin



Copyright © 2023 Hindawi Limited. All rights reserved.

This is a special issue published in "Australian Journal of Grape and Wine Research." All articles are open access articles distributed under the Creative Commons Attribution License, which permits unrestricted use, distribution, and reproduction in any medium, provided the original work is properly cited.

Chief Editor






Stefano Poni , Italy

Academic Editors







Malcolm Allen , Australia
Kym Anderson, Australia
Eveline Bartowsky , Australia
Keren Bindon , Australia
Rob Bramley , Australia
Michela Centinari, USA
Armando Corsi, Australia
Gregory Dunn, United Kingdom
Katherine Evans , Australia
Marianna Fasoli, Italy
Leigh Francis , Australia
Paul R. Grbin , Australia
Andrew Hall , Australia
Megan Hall, USA
James Harbertson , USA
Paul Kilmartin , New Zealand
Yishai Netzer, Israel
Vinay Pagay, Australia
Anne Pellegrino , France
Paul Petrie , Australia
Hayley Ridgway , New Zealand
Renata Ristic , Australia
Paolo Sabbatini, Italy
Anthony Saliba , Australia
Leigh Schmidtke, Australia
Mark Sosnowski , Australia
Chris Steel , Australia
Marie Thiollet-Scholtus, France
Bin Tian , New Zealand
Steve Tyerman, Australia
Justine Vanden Heuvel , USA
Rob Walker, Australia
Liz Waters , Australia
Kerry Wilkinson , Australia
Ji-Cheng Zhan, China

Contents









Using a Camera System for the In-Situ Assessment of Cordon Dieback due to Grapevine Trunk Diseases

Julie Tang , Olivia Yem, Finn Russell, Cameron A. Stewart , Kangying Lin, Hiranya Jayakody, Matthew R. Ayres, Mark R. Sosnowski , Mark Whitty , and Paul R. Petrie 
Research Article (15 pages), Article ID 8634742, Volume 2023 (2023)




Underpinning Terroir with Data: Integrating Vineyard Performance Metrics with Soil and Climate Data to Better Understand Within-Region Variation in Marlborough, New Zealand

R. G. V. Bramley , J. Ouzman , A. P. Sturman , G. J. Grealish , C. E. M. Ratcliff , and M. C. T. Trought 
Research Article (23 pages), Article ID 8811402, Volume 2023 (2023)




The Role of Potent Thiols in “Empyreumatic” Flint/Struck-Match/Mineral Odours in Chardonnay Wine

Damian Espinase Nandorfy , Tracey Siebert, Eleanor Bilogrevic , Desireé Likos , Flynn Watson, Sheridan Barter , Lisa Pisaniello, Allie Kulcsar, Robert A. Shellie , Russell Keast , Leigh Francis , and Marlize Bekker 
Research Article (17 pages), Article ID 8847476, Volume 2023 (2023)




The Genome Assembly of *Vitis vinifera* cv. Shiraz

Cristobal A. Onetto , Christopher M. Ward , and Anthony R. Borneman 
Research Article (14 pages), Article ID 6686706, Volume 2023 (2023)




Performance of a Leaf-Galling Phylloxera (*Daktulosphaira vitifoliae*) on Roots of Diverse *Vitis* spp. Rootstocks in North East Victoria, Australia

C. W. Clarke , K. S. Powell , S. Norng, B. M. Carmody, M. Walpole, and J. P. Cunningham 
Research Article (12 pages), Article ID 1328258, Volume 2023 (2023)








Evaluating the Potential of High-Resolution Visible Remote Sensing to Detect Shiraz Disease in Grapevines

Yeniu Mickey Wang , Bertram Ostendorf , and Vinay Pagay 
Research Article (9 pages), Article ID 7376153, Volume 2023 (2023)








Climate Services for Agriculture: Tools for Informing Decisions Relating to Climate Change and Climate Variability in the Wine Industry

Leanne Webb , Carly Tozer, Lynette Bettio , Rebecca Darbyshire, Bella Robinson, Aysha Fleming, Sigrid Tijs, Roger Bodman , and Mahesh Prakash
Research Article (13 pages), Article ID 5025359, Volume 2023 (2023)

Modelling Smoke Flavour in Wine from Chemical Composition of Smoke-Exposed Grapes and Wine

Mango Parker , WenWen Maddy Jiang , Eleanor Bilogrevic , Desireé Likos , John Gledhill, Adrian D. Coulter , Geoff D. Cowey, Con A. Simos, I. Leigh Francis , and Markus J. Herderich 
Research Article (14 pages), Article ID 4964850, Volume 2023 (2023)



Erratum to “Assessing the Short-Term Effects of No-Till on Crop Yield, Greenhouse Gas Emissions, and Soil C and N Pools in a Cover-Cropped, Biodynamic Mediterranean Vineyard”

Cristina Lazcano , Noelymar Gonzalez-Maldonado , Erika H. Yao , Connie T. F. Wong, Mia Falcone, Jean Dodson Peterson , L. Federico Casassa , Bwalya Malama , and Charlotte Decock 
Erratum (1 page), Article ID 9843618, Volume 2023 (2023)








Distribution of 3-Isobutyl-2-methoxypyrazine across Rachis Components of *Vitis vinifera* Shiraz and Cabernet Sauvignon

Ross D. Sanders , Paul K. Boss , Dimitra L. Capone , Catherine M. Kidman , Emily L. Nicholson , and David W. Jeffery 
Research Article (10 pages), Article ID 2428791, Volume 2023 (2023)

Using Zeolites to Cold Stabilize White Wines






Tim Reilly, Pawel Mierczynski, Andri Suwanto, Satriyo Krido Wahono, Waldemar Maniukiewicz, Krasimir Vasilev, Keren Bindon , and Agnieszka Mierczynska-Vasilev 
Research Article (12 pages), Article ID 7259974, Volume 2023 (2023)

Assessing the Short-Term Effects of No-Till on Crop Yield, Greenhouse Gas Emissions, and Soil C and N Pools in a Cover-Cropped, Biodynamic Mediterranean Vineyard

Cristina Lazcano , Noelymar Gonzalez-Maldonado , Erika H. Yao , Connie T. F. Wong, Mia Falcone, Jean Dodson Peterson , L. Federico Casassa , Bwalya Malama , and Charlotte Decock 
Research Article (12 pages), Article ID 8100818, Volume 2022 (2022)

Research Article

Using a Camera System for the In-Situ Assessment of Cordon Dieback due to Grapevine Trunk Diseases

Julie Tang ¹, Olivia Yem,¹ Finn Russell,¹ Cameron A. Stewart ¹, Kangying Lin,¹
Hiranya Jayakody,¹ Matthew R. Ayres,² Mark R. Sosnowski ^{2,3}, Mark Whitty ¹
and Paul R. Petrie ^{1,2,3,4}

¹School of Mechanical and Manufacturing Engineering, University of New South Wales, Kensington, NSW 2052, Australia

²Crop Sciences, South Australian Research and Development Institute, Waite Research Precinct, Urrbrae, SA 5064, Australia

³School of Agriculture, Food and Wine, Waite Research Institute, The University of Adelaide, Glen Osmond, SA 5064, Australia

⁴College of Science and Engineering, Flinders University, Adelaide, SA 5001, Australia

Correspondence should be addressed to Julie Tang; julie.tang92@gmail.com

Received 20 January 2023; Revised 1 August 2023; Accepted 17 August 2023; Published 18 October 2023

Academic Editor: Chris Steel

Copyright © 2023 Julie Tang et al. This is an open access article distributed under the Creative Commons Attribution License, which permits unrestricted use, distribution, and reproduction in any medium, provided the original work is properly cited.

Background and Aims. The assessment of grapevine trunk disease symptoms is a labour-intensive process that requires experience and is prone to bias. Methods that support the easy and accurate monitoring of trunk diseases will aid management decisions. **Methods and Results.** An algorithm was developed for the assessment of dieback symptoms due to trunk disease which is applied on a smartphone mounted on a vehicle driven through the vineyard. Vine images and corresponding expert ground truth assessments (of over 13,000 vines) were collected and correlated over two seasons in Shiraz vineyards in the Clare Valley, Barossa, and McLaren Vale, South Australia. This dataset was used to train and verify YOLOv5 models to estimate the percentage dieback of cordons due to trunk diseases. The performance of the models was evaluated on the metrics of highest confidence, highest dieback score, and average dieback score across multiple detections. Eighty-four percent of vines in a test set derived from an unseen vineyard were assigned a score by the model within 10% of the score given by experts in the vineyard. **Conclusions.** The computer vision algorithms were implemented within the phone, allowing real-time assessment and row-level mapping with nothing more than a high-end mobile phone. **Significance of the Study.** The algorithms form the basis of a system that will allow growers to scan their vineyards easily and regularly to monitor dieback due to grapevine trunk disease and will facilitate corrective interventions.

1. Introduction

Grapevine trunk diseases (GTDs), such as Eutypa and Botryosphaeria dieback, are a pervasive and growing issue across the Australian wine industry that gradually reduces vineyard performance. Other trunk diseases, such as esca, Petri disease, Phomopsis dieback, and black foot disease, cause significant issues in other countries but have little impact in Australia [1]. Eutypa dieback causes leaves to become distorted and yellow, shoots to stunt, and cordons to dieback. Botryosphaeria dieback has no distinct foliar symptoms but causes similar cordon dieback. GTDs are detected by the visual assessment of experts, and the control

treatments for GTDs can be labour-intensive and most effective when administered preventively, early in the life of the vineyard [1–4]. Regular vineyard surveys are not feasible for many growers due to the labour resources required.

Methods for estimating GTD dieback from aerial imagery are well-established but are limited by ground vegetation [5]. Recent work by Ouyang et al. [6] used 3D point clouds collected using an unmanned aerial vehicle to detect GTD with an accuracy of 87.4%.

Deep learning techniques are part of a rapidly growing area of machine learning research that is especially effective for image analysis such as the detection of GTD. Deep learning methods typically result in higher classification

accuracy and faster testing times than using traditional machine learning methods, but most critically for this research, they eliminate the need for hand-crafted features [7]. These advantages over traditional machine learning have caused deep learning image analysis to be used in a wide variety of agricultural applications, including disease identification [8–11]. Researchers applied combinations of different networks, both existing and custom architectures, on datasets that they had collected and augmented themselves [7–9, 11, 12].

Mohanty et al. [12] previously achieved an overall accuracy of 99.35% when detecting crop-disease pairs from images of leaves using DL techniques, but there are key differences in the scope of research programs. They identified 26 different diseases in 14 crop species, but the images used were of a single leaf, taken in a controlled environment against a consistent background. Our research aims to detect the presence of a single disease in real time from images taken in the field, which introduces a number of complications. The in-field images introduce uncontrolled backgrounds and conditions, which can reduce the accuracy of the detection.

For in-field images, there has been a wide variety of work in object detection for agriculture, most notably fruit detection. Kuznetsova et al. [13] applied the YOLOv5 algorithms for apple detection with a false positive rate of 3.5% and a false negative rate of 2.8%. For strawberry detection, Chen et al. [14] achieved a false positive rate of 5.7 to 15.4% and a false negative rate between 4.6% and 18.1% on mature fruit. Wang et al. [15] studied various attributes of fruit detection using YOLOv5 and recommended that for single-class object detection, a minimum of 2500 objects should be labelled and used in training.

Beyond object detection, the classification of severity or other fruit attributes has also been studied. In addition to their mature strawberry detection, Chen et al. [14] investigated flower and immature fruit detection, with limited success. Wang et al. [16] adapted a VGG-16 classification model for estimating apple flower distributions, focussing on the maturity stage rather than the frequency of each class. They showed it to be more accurate and slightly faster than YOLOv5 when running on a personal computer.

The aim of this research was to develop an automated edge computing system that would allow growers to quantify the severity of cordon dieback caused by GTDs at a temporal (every season) and spatial (whole vineyard) scale. The system had to use a standard camera mounted on a vineyard vehicle and intelligent algorithms to monitor and map trunk disease and be implemented in such a way that it could be accessed by nontechnical users.

The aim can be split into two components:

- (1) Algorithms for cordon dieback assessment
- (2) System for data collection, processing, and display

This paper presents the first component of the research and evaluates its performance. The algorithm for cordon dieback assessment will be a machine-learning-based image processing algorithm trained using vineyard images collected on a standard camera and will be assessed on the

similarity of the algorithm's results to expert assessment on unseen vines. The scope of this research is limited to vines with bilateral cordons with spurs, trained on a single wire, due to these being more common than quadrilateral cordons in an Australian context.

2. Materials and Methods

2.1. Data. The data used to evaluate the dieback assessment networks were collected in October of 2020 and 2021 in eleven vineyards (cv. Shiraz, *Vitis vinifera* L.) in the McLaren Vale and the Clare and Barossa Valleys, South Australia. Images of the vines were collected using a mobile phone app developed for the purpose and operating on a pair of Samsung Galaxy S21+ phones (model SM-G996B) running Android 11. These phones were mounted on a trailer approximately 300 mm from the ground and the middle of the interrow, with the image sensor facing the vines and the phone orientated so the cordon wire was near the centre of the image. See Figure 1 for the experimental setup. The trailer was driven throughout the vine rows at a speed of approximately 7–9 km/h while imagery was captured and processed by the phone. Images were captured by each phone at a rate of at least 5 frames per second and a resolution of 1280 × 720 pixels. When combined with the wide field of view lens in the phone, this enabled the majority of each vine to be captured, with the trunk at the centre of the image. Further analysis of the achievable framerate is given in Section 4.3.

The proportion of cordon dieback on each vine was also visually assessed by two experts in the vineyard, and the score was recorded for each of the assessed vines [4, 17]. Cordon dieback in these vineyards is predominantly caused by GTDs, as evidenced by the presence of *Eutypa* dieback foliar symptoms, but it should be acknowledged that other factors such as nematodes, viruses, and other vineyard management practices may have contributed to the cordon dieback [18]. Each cordon was assigned a score in the range of (0, 50) in increments of 5, representing the percentage of dieback on the cordon as a total of the vine. Class 0 represents a complete and healthy canopy, and class 50 represents a cordon with no shoots or leaves. The assessment of dieback can vary between experts, and there is a particular difficulty in differentiating between the lower classes of 0, 5, and 10. These scores were matched with the images of the vines, and the images were labelled with bounding boxes around the trunk and around each cordon with the dieback score. During the growing season for the 2021 vintage, 12,642 bilateral cordon vines were scored and imaged, with 5,570 in the McLaren Vale and 7,072 in the Clare Valley. In the 2022 vintage growing season, an additional 1,149 bilateral cordon vines were scored and imaged, 568 from the McLaren Vale and 581 from the Clare Valley. The vines imaged in the 2022 vintage growing season were also imaged in the previous growing season. Overall, 13,791 vines were imaged and scored.

2.2. Algorithm Development. The model chosen for the dieback assessment network was YOLOv5s, as it is small enough to deploy on edge computers while maintaining



FIGURE 1: Two pairs of smartphones mounted facing the opposite rows for continuous data collection. This prototype setup also includes two action cameras and two vertically orientated phones; note that only images collected from the horizontally orientated phones were included here. Other than a companion phone to control these phones from the driver’s seat, no additional infrastructure was needed. See Figure 2 for an example image.

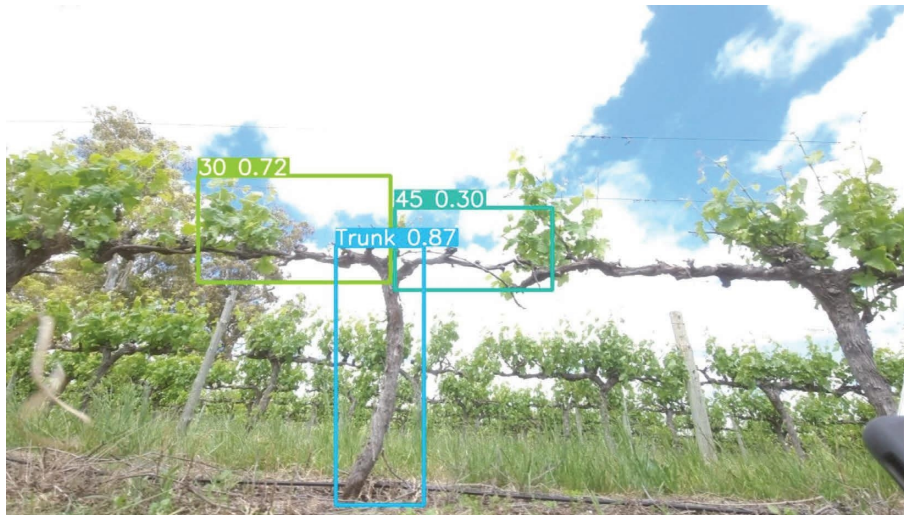


FIGURE 2: Detection from the unseen test set. The dieback on the right cordon is underestimated as the shoots from the adjacent cordon extend into the bounding box.

good detection results. The total dataset of all scored vine image across each vineyard resulted in an unequal number of instances between cordon classes (Figure 3(a)). This class imbalance can result in the assessment network overfitting to certain classes, artificially increasing the probability of assessing certain classes. This is particularly detrimental to the classes with very few training examples, such as classes 45 and 50 (Figure 3(a)). A subset of the total dataset with a balanced class distribution was created and used as the balanced training dataset for the network (Figure 3(b)). The number of training examples was greatly reduced when a balanced training dataset was created, as the number of training examples in each class was reduced to approximately the number of instances in the smallest class (class 50), and the majority of training examples consisted of classes 5, 10, and 15. Experimentation was used to explore the effects of various combinations of training sets across years.

Data augmentation techniques were used to increase the number of training examples, so that the network would be more robust to changes in orientation and variable environmental conditions. Each training image was flipped horizontally with a probability of 85%, which would simulate driving the vehicle carrying the camera in each direction along the row of vines, capturing images of both sides of the vine. A Gaussian blur was applied to the training images to increase the number of training instances and to increase the robustness of the algorithm to lower-quality images which may occur when capturing images from a moving platform. The weather conditions greatly affected the brightness of the grapevine images, so each of the images had its brightness both increased and decreased using a gamma correction function to simulate a range of weather conditions. Gamma correction applies a mathematical function to each pixel that either lightens or darkens the image overall, depending on the parameters used. The augmentations applied increased

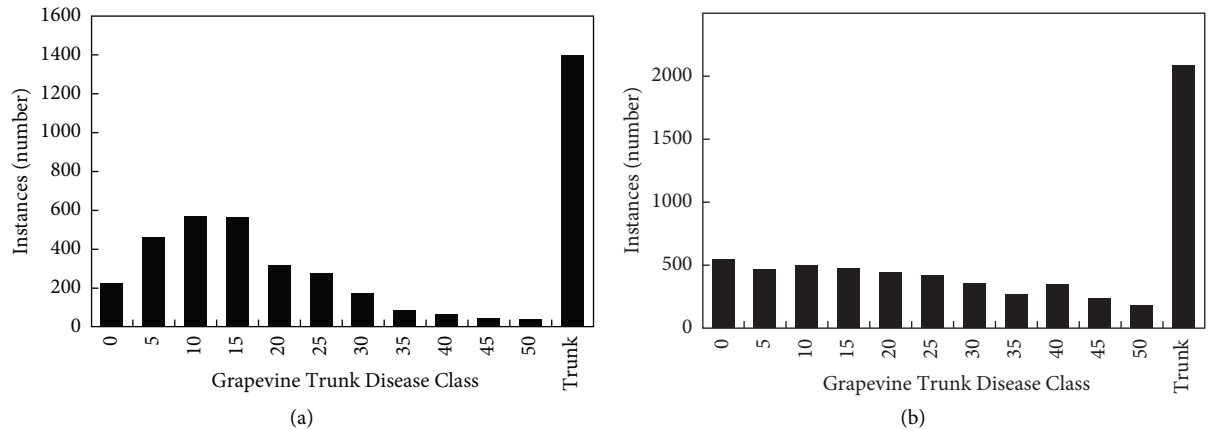


FIGURE 3: (a) The distribution of vine cordon GTD labels for imagery collected in the 2022 vintage. (b) The more balanced distribution of vine cordon GTD labels used for training the models, using data collected from both 2021 and 2022 vintages. Zero indicates no GTD symptoms observed, and 50 indicates complete dieback for that cordon. The total number of cordons is approximately twice the number of vines as indicated by the number of trunks identified.

the number of training images from 2084 images to 13076 images. The validation and test set images were not augmented in any way (Table 1).

Experiments were carried out to evaluate the suitability of the proposed algorithm by varying the hyperparameters and the data used for training each model (Supplementary Table 1 to Supplementary Table 6). The Ultralytics YOLOv5 version 6.1 Python library was used to implement the algorithm [19]. Training was carried out on a personal computer with 16 Intel® Core™ i9-9900KF CPUs using Python 3.7.3 and Ubuntu 18.04.6 LTS. The data used to train a deep learning image processing network is crucial and one of the defining factors in the results.

All models were evaluated on an unseen test set consisting of all the assessed vines in one block. This was to ensure that there was no overlap between the training and test data and that the results of each experiment could be directly comparable. The primary variables that were investigated were the data used to train the network and the training hyperparameters. All experiments were trained to completion, with completion being defined as the trend of the accuracy on the validation set across training epochs appearing to stabilise, with training lasting at least 300 epochs.

The most accurate model was evaluated not only on the unseen test set (Block 4) but also on a much larger set of images from the remaining blocks, again ensuring that these images were not included in either the training or validation sets.

2.2.1. Algorithm Evaluation Metrics. The success of the dieback assessment algorithm was measured using the following criteria:

- (i) Percentage of trunks detected
- (ii) Percentage of cordons detected
- (iii) Percentage of cordons with dieback scores identified correctly (class accuracy)
- (iv) Percentage of cordons with dieback scores identified within 5% of correct score (variation accuracy $\pm 5\%$)

- (v) Percentage of cordons with dieback scores identified with 10% of correct score (variation accuracy $\pm 10\%$)

The percentage of trunks detected should be as high as possible, as the system used to analyse the images relies on the detection of a trunk or half cordon to denote the results of the dieback assessment algorithm. By detecting the trunk and using images only where the trunk appeared close to the centre of the image, double-counting of successive half cordons was avoided. The algorithm must be able to detect the grape vine cordons in order to identify the extent of dieback, so the successful detection of cordons must occur for the algorithm to be effective. The assessment of the extent of dieback is subjective and can vary between experts. Therefore, the identification of the dieback score for each cordon will be assessed on an exact match to the in-field scoring as well as with a margin of 5% or 10% error.

2.3. System Overview. To manage, control, and observe the scanning process with ease, a smartphone-based two-application system was designed with a “controller” and a “scanner” application (Figures 4 and 5). The system only needs to connect to external devices on two occasions: for the initial fast localisation of the GNSS system or when downloading the map data for display on a computer. The system is able to process the images and automatically generate a map of the GTD in real time using only the “scanner” phone, the results of which are displayed on the “controller” phone or a computer. Further details of the system are outside the scope of this paper and available on request.

3. Results

3.1. Dieback Assessment Algorithm. Following the experiments used for training the dieback assessment algorithms, model 6 gave the best overall performance (Table 2). The trunk class was excluded from the confusion matrix (Figure 6) for the best performing model (model six) as all

TABLE 1: Number of images in each data subset.

Data subset	Number of images
All data	13,791
Balanced training data	2,084
Augmented balanced training data	13,076
Balanced validation data	821
Test data from a single unseen vineyard with no augmentations or balancing	172

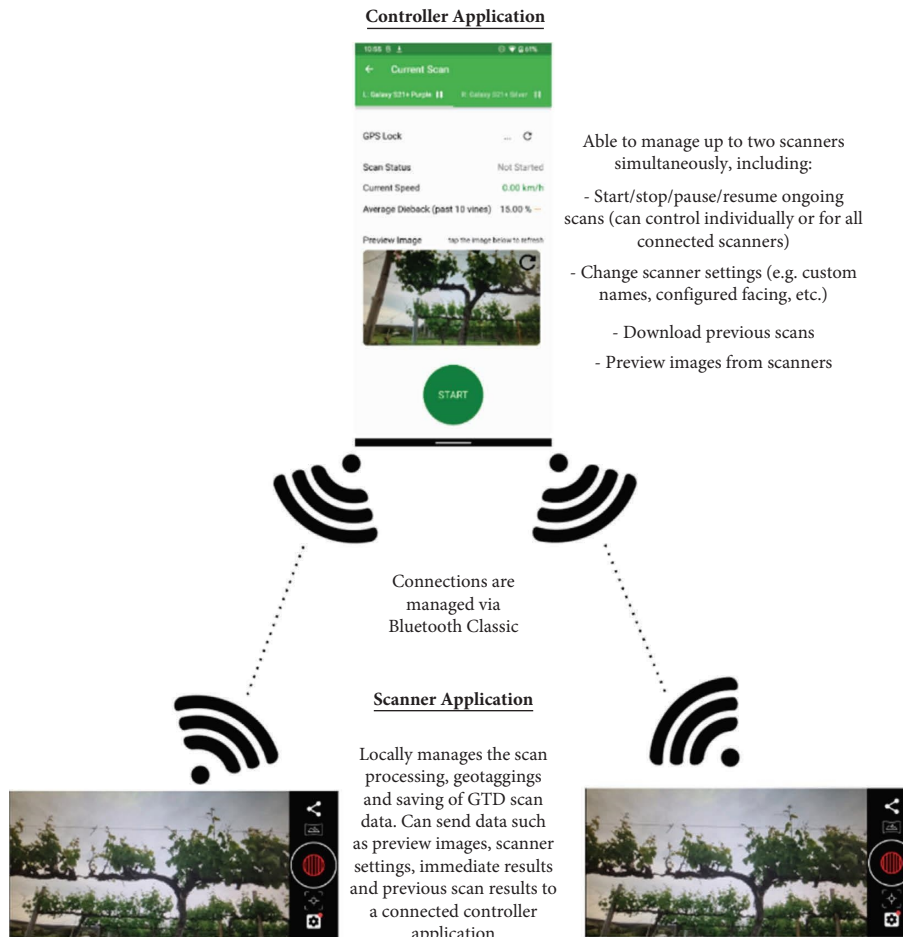


FIGURE 4: Application ecosystem overview.

trunks were correctly detected in the test set. Missing cordons, which are cordons that were labelled, but not detected by the algorithm, were designated a separate class (“M”) in the confusion matrix.

Model 6 was applied to images collected in the same blocks used for training. Even though these vines and images were not seen by the model during training or validation, excellent correlation with ground truth is seen, with over 99% of vines having an estimated GTD dieback severity within 10% of the manual ground truth (Table 2 and Figure 6(b)).

When the most successful model (model 6) was applied to the unseen test set; that is, with vines from a block completely unseen in the training or validation, the shape of the distribution is well matched against ground truth data (Figure 7(a)). Similar patterns were seen for the blocks used

as part of the validation (within the training process) (Supplementary Figure 1). Examples of detections in images are shown in Figures 8 and 9.

3.2. Evaluation of the Selected Model across Eleven Test Sites.

Data from the eleven sites used for training and validating the algorithm were processed with model 6 using the smartphone—with an additional block in the Barossa Valley also mapped (Block 1). Histograms were used to display the distribution of GTD severity across the block (Supplementary Figure 1). The vines and severity of GTD were georeferenced and plotted on aerial images (Figures 10–12).

In Block 1 (Figure 10), the mapped data displayed a high degree of average severity uniformly distributed across all of the surveyed vines. Whilst there are pockets of higher-

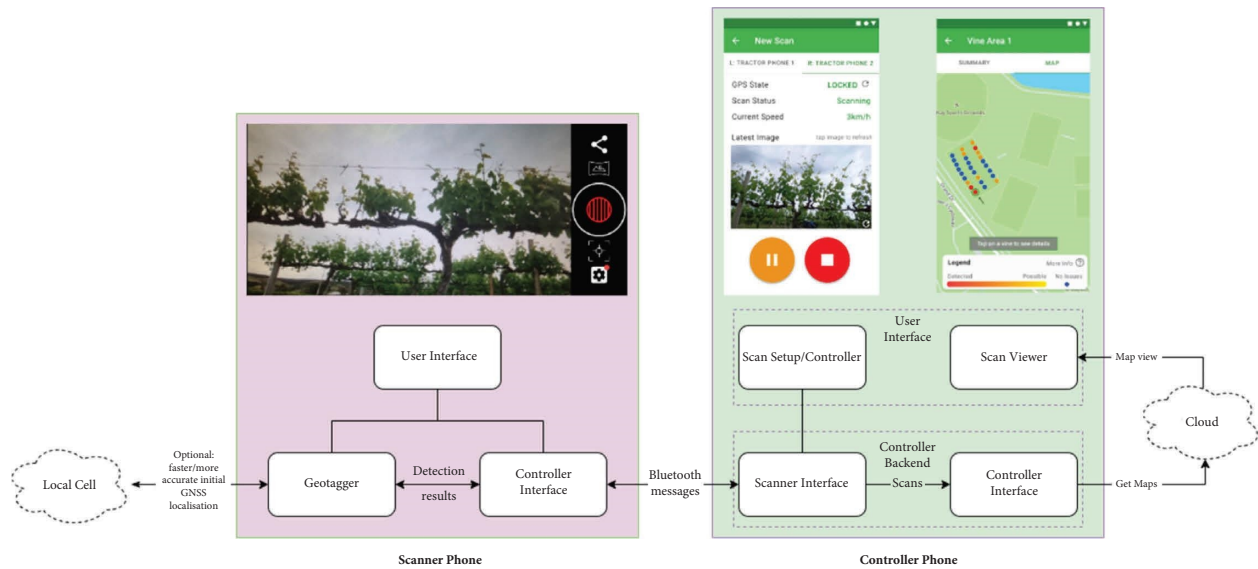


FIGURE 5: System overview diagram. The internal phone GNSS receiver is used to geotag each image. As such, the positional accuracy is dependent on having mobile phone reception on initial setup.

severity vines (such as in the centre of the top row), most vines exhibit symptom severities in the 40–60 percent range. This could indicate an older block, where the disease has had time to spread throughout most vines and less attention has been placed on remedial treatment.

In Block 5 (Figure 11), a high concentration of vines exhibiting severe symptoms were located at the northern end of the rows. Grapevine trunk disease does not normally follow a spatial pattern—so the grouping of the affected vines in one section of the vineyard was surprising. On further investigation, it was identified that the northern end of the block had reduced vigour as it is prone to frost, and a frost event had occurred several weeks before the assessment. Regardless of the cause, this gives growers an indicator that this is an area where the vines are performing poorly. A further manual inspection would often be made of the worst-affected areas to confirm the cause of an unusually concentrated area of increased dieback.

The mapping of Block 8 (Figure 12) exhibits less severe symptom severity. The high-symptom severity vines are clustered into small groups and distributed across the eastern portions of the block.

Vine symptom severity was usually normally distributed across the respective block, with a skew towards lower levels of severity (Figure 13). The results across blocks were typically clustered to a 10–20% range with some outliers. Blocks 3 and 5 exhibit results with a wider spread, with lower peaks, and a flatter distribution. In Block 5, this was a cause of the severe concentration of vine symptom severity in a small section of the block (see Figure 11).

3.3. Application Performance and Optimisation. The target framerate (5 FPS) was achieved consistently as a result of optimisation of the phone application. Images were captured at 1280×720 pixels and processed at 640×360 pixels using model 6. The two test phones used (128 GB and 256 GB

models of the SM-G996B Samsung Galaxy S21+ 5G) were both able to maintain a throughput of at least 5 FPS, shown as the ability to process individual images consistently in less than 200 ms over 110 minutes (Figure 14). The increase in processing time observed in the 128 GB model at the 60 minute mark is likely due to processor throttling as the phone heated up over time; however, the 200 ms threshold was not exceeded.

4. Discussion

4.1. GTD Detection Algorithm

4.1.1. Trunk and Cordon Detection. Trunk detection was high across all the experiments, with at least 97% of trunks being detected in each experiment and trunk detection as high as 100% in two of the trained models. Trunk detection was consistently high because of the number of instances in the training data and the appearance of the trunks. The trunks are visually distinct from the cordons, most notably due to their orientation. For every grapevine, there is a single trunk and two bilateral cordons with spurs; quadrilateral-cordon vines were considered out of scope for this research due to their distinctly different appearance. Given that the cordons are broken down into 10 classes based on the extent of dieback, the number of instances of trunks is much higher than any other class. Deep learning object detection algorithms require many examples to accurately detect objects in images; therefore, the high number of training instances for trunks ensures that the trunk detection was successful.

The algorithm must detect the grapevine cordons in order to classify them based on the extent of dieback, which makes the percentage of cordons detected critical to the overall performance of the algorithm. The percentage of detected cordons rose with the number of training examples and the increase in the left-right flip during training. The increase of the left-right flip hyperparameter also effectively

TABLE 2: Results of training GTD detection algorithm when applied to a completely unseen test set (Block 4).

Identifier	Training data	Training hyperparameters	Trunks detected (%)	Cordons detected (%)	Class accuracy (%)	Variation accuracy ($\pm 5\%$)	Variation accuracy ($\pm 10\%$)
Model 1	V2022 training and validation data. No augmentations applied	See Supplementary Table 1	99.42	15.79	6.43	11.68	14.02
Model 2	V2022 training and validation data. No augmentations. 85% left-right flip applied	See Supplementary Table 2	99.42	82.56	24.12	56.09	71.49
Model 3	V2022 training and validation data. Exposure and blur augmentations applied	See Supplementary Table 3	100.00	88.66	24.99	63.35	77.00
Model 4	V2021 and V2022 training and validation data. No augmentations. 85% left-right flip applied	See Supplementary Table 4	97.09	85.17	26.74	60.74	74.96
Model 5	V2021 and V2022 balanced training and validation data. No augmentations	See Supplementary Table 5	98.84	97.1	25.72	64.39	81.52
Model 6	V2021 and V2022 balanced training and validation data. Exposure and blur augmentations applied. 85% left-right flip applied	See Supplementary Table 6	100.00	99.42	26.16	63.56	84.18



FIGURE 6: Confusion matrices for cordon class detections for model 6 (as described in Table 2). (a) Images for the unseen test set were collected from vineyards where other images from those vineyards were used in training. (b) Images for the unseen vines comprised of vines from Block 4 which had not been used for any model training or validation the yellow off-diagonal terms have been highlighted as ± 10 threshold has been applied in the evaluation of results in this paper. The general diagonal form of the results is evident, with some outliers (discussed below).

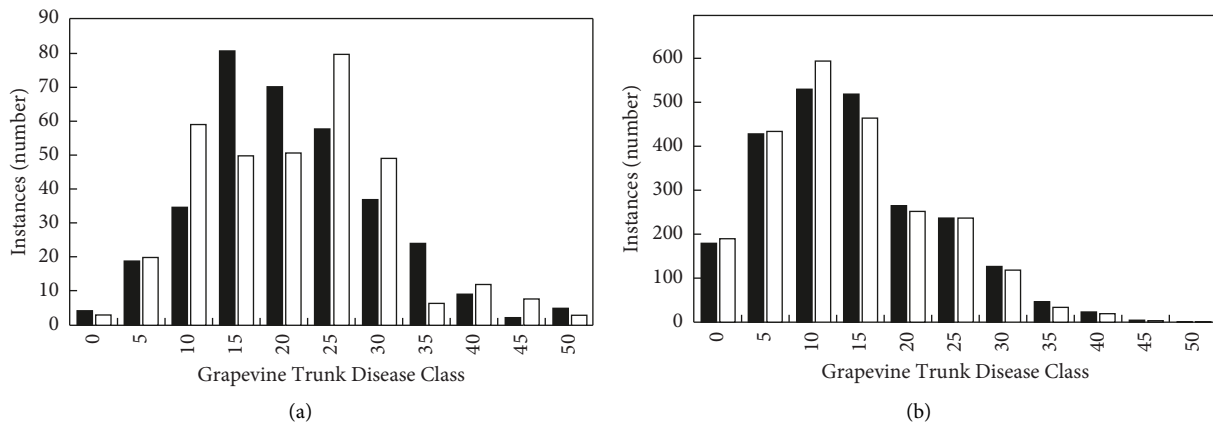


FIGURE 7: A comparison of manually assessed and detected severity of grapevine trunk disease in test sets when using model 6 described in Table 2 for (a) images collected from Block 4 and (b) unseen vines in vineyards used for training the algorithm. Black bars indicate manually assessed severity and white bars show detected severity. A score of 0 represents no cordon dieback and a score of 50 represents no foliage present.

increased the number of training images as the images are reversed horizontally, as most clearly seen in the 67% increase in the detected cordons between experiments 1 and 2 when a 0.85 left-right flip was applied. The effects of increasing the training examples diminished as more training examples were used, but the network achieved the correct detection of 99% of cordons in the unseen test set which underpins the rest of the analysis.

Two cordons were not detected in the test set. In the first example of a missing cordon, the cordon was not detected as

there was a tree in the background with the foliage extending above and below the cordon, so the cordon was not distinguished from the background (Figure 15). For the second missed cordon detection, the photo is blurred and the leaves are pale in the image, but the cordon is not unrecognisable to a human observer (Figure 16). There are other considerations for the algorithm in this example. First, the right cordon was detected with a confidence score of 0.41, low compared to the majority of cordon confidence scores, which suggests that the light conditions and the blur (more

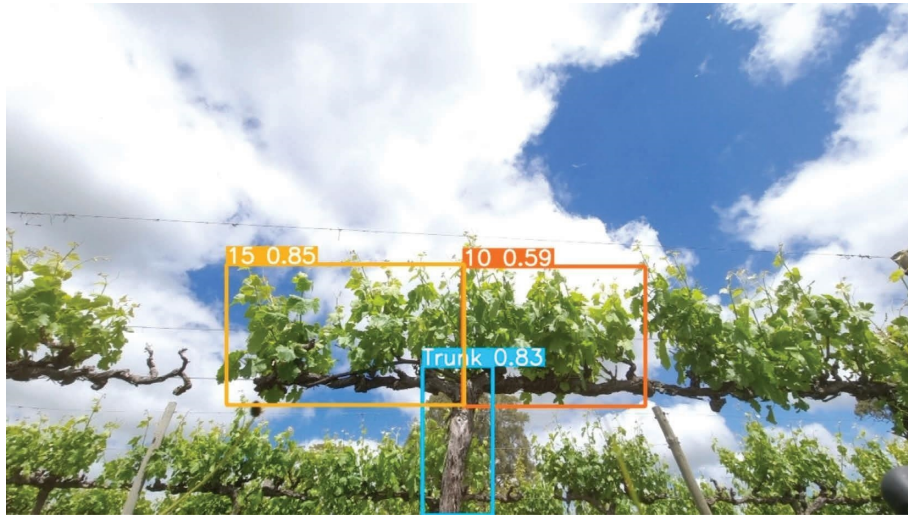


FIGURE 8: Detections from model 6. The labelled classes were 15 on the left and 15 on the right. The detected classes were 15 for the left cordon and 10 for the right, as the detected classes are given first in the bounding box labels. The decimal in the bounding box is the confidence score, an expression of how sure the algorithm is of what is detected.

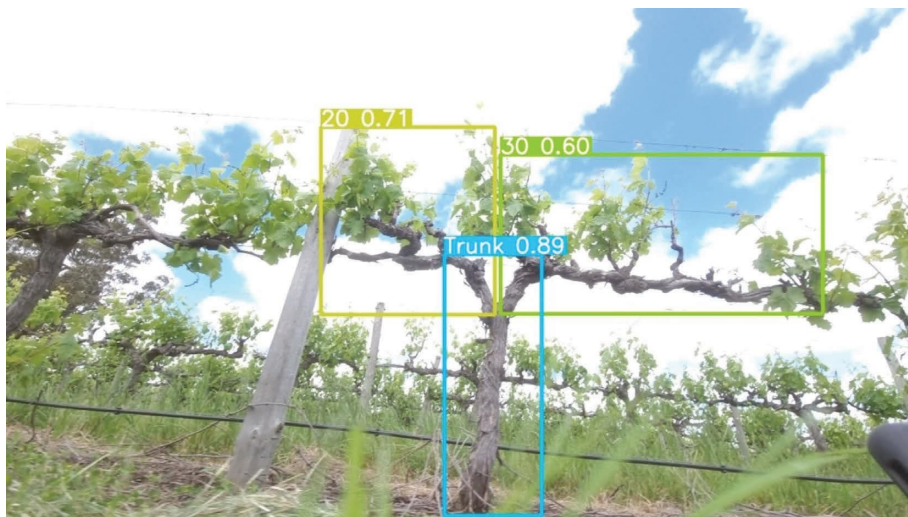


FIGURE 9: Detections from model 6. The labelled classes were 25 on the left and 30 on the right. The detected classes were 20 for the left cordon and 30 for the right, as the detected classes are given first in the bounding box labels. The decimal in the bounding box is the confidence score, an expression of how sure the algorithm is of what is detected.

significant on the left cordon) were a major factor in any detections of the left cordon falling under the confidence threshold of 0.25. The bounding box for the trunk is also much wider than the typical trunk bounding boxes as the trunk itself is slanted (Figure 16). The cordons do not originate from the centre of the trunk bounding box, as is the norm, and combined with the thinness of the left cordon, this creates additional difficulties for the detection of this cordon.

In terms of pure object detection accuracy using YOLOv5, Kuznetsova et al. [13] obtained an accuracy of 97.1% in counting apples in general images. It is not surprising that the trunk detection results in this work are slightly higher in accuracy given the size and uniqueness of the shape compared with apples.

4.1.2. GTD Dieback Detection. Detecting trunks and cordons in vineyard images allows the algorithm to fulfill the aim of detecting the extent of dieback. Model 4 had the highest class accuracy, with 27% of cordons classified by the algorithm matching the labels given in the vineyard (Table 2). As previously stated (see Section 3.1), the dieback scoring is subjective and can vary between different experts, and there is particular difficulty in differentiating between classes 0, 5, and 10. When the variation accuracy within 5% and 10% was considered, model 6 had the highest $\pm 10\%$ variation accuracy (84%), as well as a higher $\pm 5\%$ variation accuracy and more cordons detected than model 4. Models 4 and 6 had slightly different training hyperparameters, but the main difference between these models was the training data



FIGURE 10: Block 1 vine symptom mapping—each point represents the overall vine assessment combining both cordons.



FIGURE 11: Block 5 vine symptom mapping—each point represents the overall vine assessment combining both cordons.



FIGURE 12: Block 8 vine symptom mapping—each point represents the overall vine assessment combining both cordons.

used. Model 6 used the V2021 and V2022 augmented data, resulting in many more training examples which improved the performance similarly to the cordon detection. The augmented data adjusted the exposure and blur of the training images, which theoretically would make the algorithm more robust to changing light conditions and changes in photo quality, as shown by Wang et al. [15]. However, the test set images were taken on a single day using one model of phone. Therefore, the effects of changing illumination due to weather conditions and changing the photo quality due to the camera used were not directly assessed.

The $\pm 10\%$ variation accuracy is quite reasonable given that some classes included as little as 50 training images (prior to augmentation), and Wang et al. [15] recommended 2500 training images for a single class. The detection algorithm is more likely to overestimate the extent of the dieback rather than underestimate it, with 19 cordons underestimated by at least 15% and 28 cordons overestimated by at least 15%, the manual scoring factors in all the shoots extending from each cordon, including when a shoot extends over the adjacent cordon, although this is not common. The detection algorithm estimates the extent of dieback based on the volume of leaves around the cordon, as the training images were labelled with a bounding box around the cordon, and the volume of leaves in the bounding box is largely consistent with the

amount of dieback. If a shoot extends to another cordon, the algorithm will estimate the extent of dieback incorrectly (see Figure 2). The right cordon in this example was given a manual score of 50, but the detection algorithm assigned a score of 30 due to the shoots from the adjacent cordon extending into the bounding box. The accuracy of 84% on an individual vine level compares well with that of Ouyang et al. [6], who achieved 87% accuracy on an aggregated row level. The number of classes of severity used by Ouyang et al. [6] was slightly smaller, which would also lead to improved results.

When the frequencies of each class in the manual scoring and detections were compared between a set of vines from a vineyard that was not used in training (Figure 7(a)) and a larger test set consisting of the unseen vines in vineyards that were used in training the algorithm (Figure 7(b)), the algorithm performed better on the unseen vines in vineyards used in training. The images of the unseen vineyard are often overexposed, although some of the unseen vines in the training blocks are overexposed as well, these are a higher proportion in the unseen vineyard. The images in the unseen vineyard are blurred in addition to the light conditions that would cause more difficulties in accurately estimating the dieback.

There are two possible courses of action to potentially improve the results. The training images could be given new scores based on the volume of leaves around each cordon.

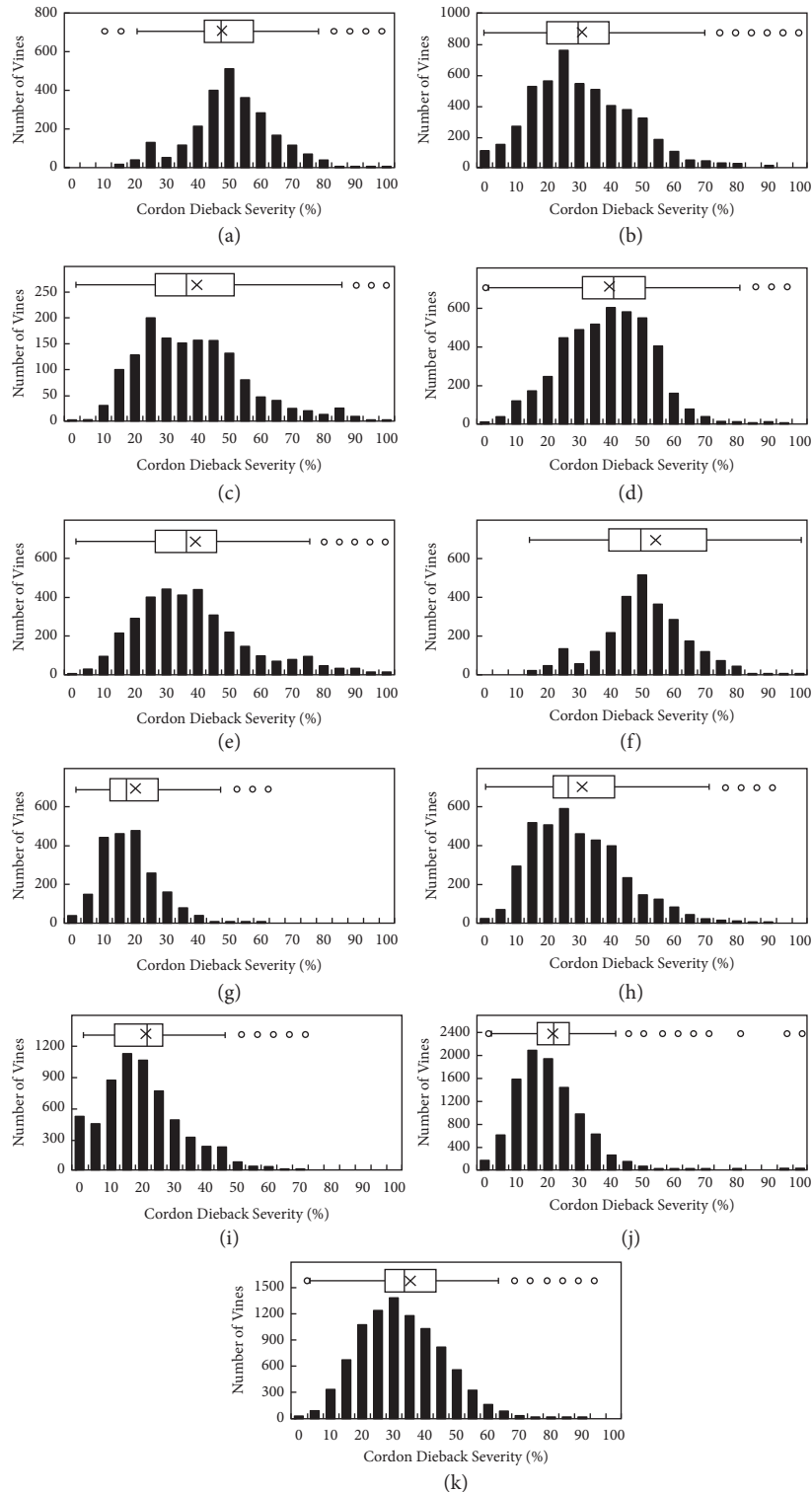


FIGURE 13: Cordon dieback severity distribution across blocks, relative to 25% of total number of vines scanned in that block. Subfigures (a–k) correspond to Blocks 1 to 11, respectively.

This would not reflect the manual scoring system as closely but may align more with the needs of the growers. The presence of growth in the area is more important than exactly which vine it extends from. Alternatively, semantic segmentation could be used to identify exactly which shoots

extend from each cordon to align with the manual scoring more closely. Semantic segmentation would not appear to currently be a feasible technique for real-time processing on a mobile phone due to the need to classify each pixel rather than identify three bounding boxes. The training data would

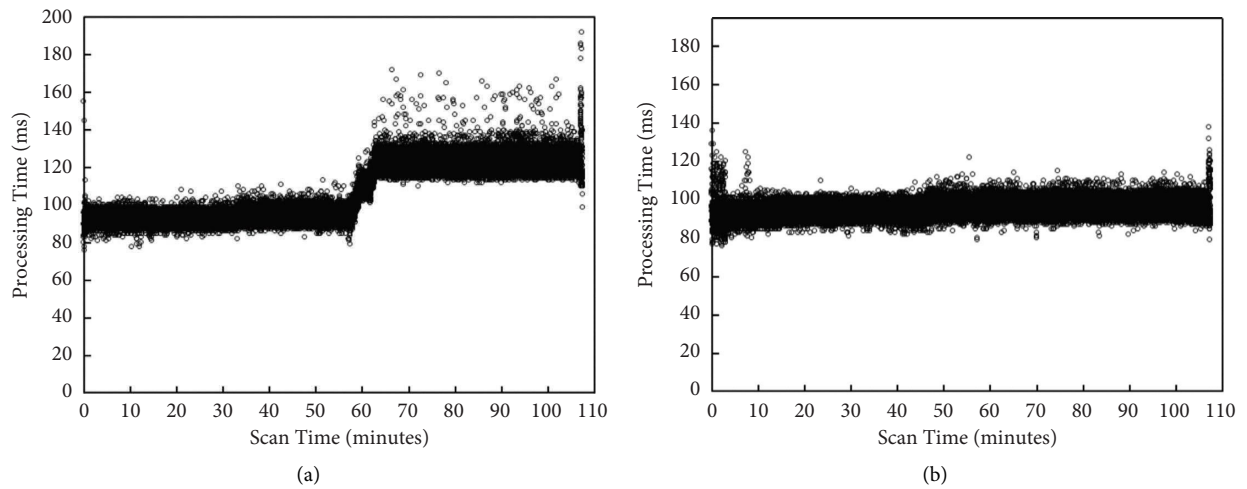


FIGURE 14: Sustained processing time of GTD dieback scanning across different S21+ models—128 GB (a) and 256 GB (b).



FIGURE 15: A missing cordon detection from the test set.



FIGURE 16: Another missing cordon detection from the test set.

also need to be labelled by experts in manually scoring dieback as correctly allocating each shoot to the correct cordon is very important.

4.2. Evaluation of the Selected Model across Eleven Test Sites. By comparing the results across all the test sites, significant variation in the spatial pattern, incidence, and severity of GTD dieback symptoms was observed. This may be due to different ages of vines, different GTDs involved, or local climatic conditions. The incidence and severity of GTDs increases with age of vines [3, 4, 20]. The distribution of pathogens that cause *Eutypa* and *Botryosphaeria* dieback varies between Australian regions [21, 22] which may also explain some of the variability observed between regions in the current study. Rainfall is required for infection, and certain temperature and humidity conditions favour the different causal pathogen species [23, 24]. Nonetheless, this work lays the foundation for the analysis of data over multiple seasons or before and after remediation activities to monitor changes in GTD symptoms.

Very few blocks have a low average severity (Supplementary Figure 1), partially due to grapevines being a natural system and not growing uniformly despite the best endeavours of growers. It also highlights the potential for growers to tend to underestimate the severity throughout their blocks, as once the canopy is more fully grown, shoots will tend to spread out and disguise diseased sections of the cordon.

4.3. Evaluation of Smartphone Application. After running for many hours in-field conditions, the smartphone “scanner” application was able to successfully collect, process, and geo-reference all the images across the eleven test sites. Despite the hard requirement of 5 FPS processing, the phone was able to sustain this performance consistently in tests lasting more than an hour. Compared with the aerial method of Ouyang et al. [6], the ability to undertake the survey using only a mobile phone mounted on a vehicle is somewhat simpler yet of comparable accuracy, giving greater opportunity for industry adoption.

5. Conclusions

This paper presents and evaluates an algorithm to detect and map grapevine trunk disease dieback using only a smartphone. The YOLOv5-based algorithm was successfully applied in a smartphone app to collect and process data from more than 13,000 vines in the McLaren Vale, Clare Valley, and Barossa Valley regions of South Australia across two growing seasons and ten vineyards.

The algorithm was effective, as it was able to classify 99% of cordons within 10% of expert visual dieback assessment on unseen vines from the same blocks as used in the training and validating the model. When tested on vines from a different block, again unseen by the model, a classification accuracy of 84% was achieved and 99.5% of cordons were detected.

Furthermore, the algorithm reliably operated at a frame rate of 5 FPS on a commercially available smartphone,

including capturing, processing, and mapping the data with GNSS.

Further research into the robustness of the algorithm under different weather conditions and image quality is recommended to ensure that the system remains effective for many models of phone used and that the system is not reliant on good weather conditions. A variation of the algorithm that can be used in vineyards with different training systems (e.g., multiple cordons) would also be a recommended area of further research. A reliance on existing deep learning algorithms mean the GTD level had to be discretised; further work could examine methods for providing a continuous numerical output.

Being able to transform a deep learning model trained on a server to run in real-time on a smartphone has provided a powerful tool for growers to attach to a vehicle and obtain maps of GTD dieback symptoms. This opens the potential for rapid assessment of GTD more widely across the industry on bilateral cordon-trained vines. It also highlights the potential for deep learning models to be trained to detect visual symptoms of other diseases and to be applied in the field with just a smartphone.

Data Availability

The underlying data for this study are stored in the UNSW Data Archive. The data used to support the findings of this study are available from the corresponding author upon reasonable request.

Conflicts of Interest

The authors declare that they have no conflicts of interest.

Acknowledgments

This work was funded by the South Australian Wine Industry Development Scheme (2020) and was led by the South Australian Research and Development Institute (SARDI). Fieldwork, ground truth assessment, system testing, and grower liaison were undertaken by SARDI, and the algorithm and system were developed by UNSW Sydney (UNSW). This research would not have been completed without the assistance of DJs Growers, especially Mr. Joe Siebert, and the Clare Valley Wine and Grape Association, especially Ms. Anna Baum, who provided advice and access to a number of growers who in turn made their blocks available for the study. We appreciate the support provided by the growers in the McLaren Vale and the Clare Valley in allowing us to access their vineyards.

Supplementary Materials

Supplementary Tables 1 to 6 include the training hyperparameters used to train the YOLOv5s object detection network to identify grapevine trunks and assess the dieback, resulting in the results given as experiments 1 to 6. Supplementary Figure 1 shows validation results on blocks used during training, albeit with images not contributing to the training process. (*Supplementary Materials*)

References

- [1] D. Gramaje, J. R. Úrbez-Torres, and M. R. Sosnowski, "Managing grapevine trunk diseases with respect to etiology and epidemiology: current strategies and future prospects," *Plant Disease*, vol. 102, no. 1, pp. 12–39, 2018.
- [2] M. R. Sosnowski, T. J. Wicks, and E. S. Scott, "Control of Eutypa dieback in grapevines using remedial surgery," *Phytopathologia Mediterranea*, vol. 50, pp. S277–S284, 2011.
- [3] M. Sosnowski and D. Mundy, "Prevalence of grapevine trunk disease in New Zealand – observations from vineyard surveys," *New Zealand Winegrower*, vol. 117, pp. 116–121, 2019.
- [4] M. Sosnowski, "Grapevine trunk disease—best practice management guide," 2021, <https://www.wineaustralia.com/growing-making/pest-and-disease-management/eutypa-dieback>.
- [5] C. Poblete-Echeverria, S. Fuentes, S. Ortega-Farias, J. Gonzalez-Tallice, and J. A. Yuri, "Digital cover photography for estimating leaf area index (LAI) in apple trees using a variable light extinction coefficient," *Sensors*, vol. 15, no. 2, pp. 2860–2872, 2015.
- [6] J. Ouyang, R. De Bei, and C. Collins, "Assessment of canopy size using UAV-based point cloud analysis to detect the severity and spatial distribution of canopy decline," *OENO One*, vol. 55, no. 1, pp. 253–266, 2021.
- [7] N. Zhu, X. Liu, Z. Liu et al., "Deep learning for smart agriculture: concepts, tools, applications, and opportunities," *International Journal of Agricultural and Biological Engineering*, vol. 11, no. 4, pp. 21–28, 2018.
- [8] Q. Zhang, Y. Liu, C. Gong, Y. Chen, and H. Yu, "Applications of deep learning for dense scenes analysis in agriculture: a review," *Sensors*, vol. 20, no. 5, p. 1520, 2020.
- [9] L. Santos, F. N. Santos, P. M. Oliveira, and P. Shinde, "Deep learning applications in agriculture: a short review," in *Iberian Robotics Conference*, pp. 139–151, Springer, Cham, Switzerland, 2019.
- [10] K. G. Liakos, P. Busato, D. Moshou, S. Pearson, and D. Bochtis, "Machine learning in agriculture: a review," *Sensors*, vol. 18, no. 8, p. 2674, 2018.
- [11] A. Kamilaris and F. X. Prenafeta-Boldú, "A review of the use of convolutional neural networks in agriculture," *The Journal of Agricultural Science*, vol. 156, no. 3, pp. 312–322, 2018.
- [12] S. P. Mohanty, D. P. Hughes, and M. Salathé, "Using deep learning for image-based plant disease detection," *Frontiers in Plant Science*, vol. 7, p. 1419, 2016.
- [13] A. Kuznetsova, T. Maleva, and V. Soloviev, "Detecting apples in orchards using YOLOv3 and YOLOv5 in general and close-up images," in *Advances in Neural Networks—ISNN 2020*, M. Han, S. Qin, and N. Zhang, Eds., vol. 12557, Cham, Switzerland, Springer, 2020.
- [14] Y. Chen, W. S. Lee, H. Gan et al., "Strawberry yield prediction based on a deep neural network using high-resolution aerial orthoimages," *Remote Sensing*, vol. 11, no. 13, p. 1584, 2019.
- [15] X. Wang, J. Tang, and M. Whitty, "Data-centric analysis of on-tree fruit detection: experiments with deep learning," *Computers and Electronics in Agriculture*, vol. 194, Article ID 106748, 2022.
- [16] X. Wang, J. Tang, and M. Whitty, "DeepPhenology: estimation of apple flower phenology distributions based on deep learning," *Computers and Electronics in Agriculture*, vol. 185, Article ID 106123, 2021.
- [17] B. Henderson, M. R. Sosnowski, M. G. McCarthy, and E. S. Scott, "Incidence and severity of Eutypa dieback in grapevines are related to total surface area of pruning wounds," *Australian Journal of Grape and Wine Research*, vol. 27, no. 1, pp. 87–93, 2021.
- [18] P. O'Brien, R. De Bei, M. Sosnowski, and C. Collins, "A review of factors to consider for permanent cordon establishment and maintenance," *Agronomy*, vol. 11, no. 9, p. 1811, 2021.
- [19] Ultralytics, "YOLOv5," 2022, <https://github.com/ultralytics/yolov5>.
- [20] J. A. Duthie, G. P. Munkvold, and J. J. Marois, "Relationship between age of vineyard and incidence of Eutypa dieback," *Phytopathology*, vol. 81, p. 1183, 1991.
- [21] W. Pitt and R. Huang, "Identification, distribution and current taxonomy of Botryosphaeriaceae species associated with grapevine decline in New South Wales and South Australia," *Australian Journal of Grape and Wine Research*, vol. 16, no. 1, pp. 258–271, 2010.
- [22] F. P. Trouillas, W. M. Pitt, M. R. Sosnowski et al., "Taxonomy and DNA phylogeny of Diatrypaceae associated with *Vitis vinifera* and other woody plants in Australia," *Fungal Diversity*, vol. 49, no. 1, pp. 203–223, 2011.
- [23] J. R. Úrbez-Torres, "The status of Botryosphaeriaceae species infecting grapevines," *Phytopathologia Mediterranea*, vol. 50, pp. 5–45, 2011.
- [24] J. S. Mayorquin, D. H. Wang, M. Twizeyimana, and A. Eskalen, "Identification, distribution, and pathogenicity of Diatrypaceae and Botryosphaeriaceae associated with citrus branch canker in the southern California desert," *Plant Disease*, vol. 100, no. 12, pp. 2402–2413, 2016.

Research Article

Underpinning Terroir with Data: Integrating Vineyard Performance Metrics with Soil and Climate Data to Better Understand Within-Region Variation in Marlborough, New Zealand

R. G. V. Bramley ¹, J. Ouzman ¹, A. P. Sturman ², G. J. Grealish ^{3,4}, C. E. M. Ratcliff ¹,
and M. C. T. Trought ⁵

¹CSIRO, Waite Campus, Urrbrae, SA 5064, Australia

²School of Earth and Environment, University of Canterbury, Christchurch 8140, New Zealand

³Manaaki Whenua-Landcare Research, Palmerston North 4442, New Zealand

⁴CSIRO, Black Mountain Science and Innovation Park, Canberra, ACT 2601, Australia

⁵Innovative Winegrowing, 9A Ward Street, Blenheim 7201, New Zealand

Correspondence should be addressed to R. G. V. Bramley; rob.bramley@csiro.au

Received 26 January 2023; Revised 11 April 2023; Accepted 3 June 2023; Published 4 September 2023

Academic Editor: Andrew Hall

Copyright © 2023 R. G. V. Bramley et al. This is an open access article distributed under the Creative Commons Attribution License, which permits unrestricted use, distribution, and reproduction in any medium, provided the original work is properly cited.

Background and Aims. Previous work in Australia has demonstrated the value of data-driven approaches to terroir analysis but, like other terroir research, focussed predominantly on the natural resources (soils, topography, and climate) on which winegrowing depends. In only very few cases have metrics of production performance also been considered. In this study, focussed on the Marlborough region of New Zealand, we integrated data pertaining to vineyard performance with biophysical data (soils and climate) describing the conditions under which grapes are grown to give a more holistic indication of regional-scale variation in the terroir of the Marlborough production system. **Methods and Results.** Digital map layers describing variation in climate, soil properties, and the yield and harvest date of Sauvignon Blanc (*Vitis vinifera* L.) were assembled and analysed for similarity in their patterns of spatial variation over six vintages (2014–2019) using *k*-means clustering. The results suggest that the Marlborough region has a characteristically variable Sauvignon Blanc production with crop phenology and harvest date strongly influenced by variation in temperature, and yield variation impacted by soil properties. Spatial variation in seasonal rainfall did not appear to impact on vineyard performance. Importantly, the Wairau and Awatere valleys which, hitherto, have been considered together as parts of a single Marlborough region, are shown to be distinct. **Conclusions.** This analysis is strongly suggestive of the Marlborough terroir being variable at the within-region scale. It also lends weight to the idea that estimates of vineyard performance in some parts of the region may be used to predict performance in others. **Significance of the Study.** The results have potentially important implications for the management of both vineyard operations and winery logistics, for wine marketing and for whole-of-industry planning around expansion or contraction. The methods used are free of any bias introduced to many previous studies of terroir zoning through adherence to historical or geopolitical boundaries, expert opinion of wines, and other heuristics.

1. Introduction

The development of the Marlborough grape-growing region, located in the northeast corner of the South Island of New Zealand, has occurred over the past 50 years. Starting from initial plantings in the early 1970s, largely in the central

Wairau Plains, the region expanded to first cover the southern valleys of the Wairau, before progressively increasing in the mid-2000s into the Awatere Valley to the south, towards the coast of the Wairau Plains from the early 2010s, and then more recently to the upper valleys of the Wairau and Awatere valleys. The current area planted is approximately 28,883 ha

(71% of the total New Zealand vineyard area), with 23,290 ha (or 81%) planted to Sauvignon Blanc (*Vitis vinifera* L.) predominantly as a single mass-selected clone of UCD1 (<https://www.nzwine.com/media/21915/1-vineyard-report-2022.pdf>). Marlborough Sauvignon Blanc was first recognised as a distinctive style, reflecting the *terroir* of the region, in the early 1990s when success, particularly in the United Kingdom market, resulted in increasing consumer demand; it is now a recognisable international wine style.

Terroir is a multivariate concept which describes the interaction between the conditions under which grapes are grown and wine is made and the sensory and chemical attributes of wine [1–6]. Thus, whilst there is no literal English translation of *terroir*, it can be considered to encompass many factors—soil, topography, climate, landscape, biodiversity, and management [7]—which give a wine its “sense of place” [8]. In a New Zealand context, *terroir* aligns closely to the Māori concept of *tūrangawaewae* [9–11]—literally, ‘a place to stand.’

Whilst management of both grapegrowing and winemaking are included in the *terroir* concept, much of the past research into *terroir* and *terroir* zoning (e.g., 12–19) has focussed solely on biophysical factors, especially climate and soil physical properties. It has also relied on analysis of entire winegrowing regions rather than focussing just on the land used for winegrape production. In many instances, especially in ‘Old World’ countries, the notion of *terroir* aligns closely to national appellation systems, such as the French ‘Appellation d’Origine Contrôlée’ (AOC) system (see Robinson and Harding [20] for a summary) and to the specification of product characteristics—as in the ‘Protected Designation of Origin’ (PDO) system used more broadly throughout the European Union [21]. As a consequence, *terroir* zoning research in these regions has generally been constrained by conformity to the boundaries of existing denominations. This, coupled with a reliance on heuristics/presumptions of inter-regional difference and expert opinion of wines, in addition to land classification approaches based on thematic mapping [22], has led to the distinctiveness of some *terroir* zones being called into question [23, 24]. It has also led to a call for “unbiased scientific approaches” to be brought to bear on the study of *terroir* [25], focussed on process-based understanding of the complex functional relationships between *terroir* factors and the attributes of wine [26].

Recent research has demonstrated how a data-driven approach might be applied to the biophysical aspects of *terroir* zoning at the regional scale. This work has used methods of spatial analysis which have become common in the study of vineyard variability at the within-vineyard scale (e.g., 27, 28) and which have underpinned the development of precision viticulture [29]. Thus, in studies of biophysical variation in the Margaret River [30] and Barossa Zone [24] geographical indications (GIs) of Australia, *k*-means clustering of map layers, describing regional-scale variation in viticulturally important climate indices and soil properties, enabled the delineation of ‘zones’ within these winegrowing regions. These zones were suggested as an appropriate underpinning basis for subsequent sensory and chemical analysis of the wines produced in them, potentially leading to the delineation of subregions within these GIs for which ‘distinctiveness’ might be demonstrated. There is much interest in such subregionalisation in Australia, in the

belief that it might convey marketing advantages to wine producers in these regions. However, it has also been suggested [24, 30, 31] that greater benefit might accrue from better understanding the various biophysical factors which affect final wines in terms of opportunities for improved management of the grape and wine production process. A key aspect of this recent Australian work was the observation that a different zonation resulted when soil and climate data pertaining to just that land which is used for winegrape production was included in the analysis, compared to when it was undertaken for the winegrowing region as a whole (i.e., the entire GI). This was important given that, in the Margaret River and Barossa GIs, only approximately 3 and 11% of the land is under vine. Note however, that neither of these studies included vineyard performance metrics or sensory or chemical analysis of wines.

In a third study conducted in the Marlborough region of New Zealand, Bramley et al. [22] collected data on the yield and harvest date of Sauvignon Blanc from approximately 525–750 vineyards over five vintages (2014–18) and used these to interpolate regional-scale maps of yield and harvest date variation. A key motivation for this work was to see whether vineyard performance in one location might be used to inform decisions in another. The seasonal maps showed remarkably similar patterns of variation in both yield and harvest date, despite interannual variation in the mean yield resulting from seasonal variation in climatic conditions. This similarity in patterns of variation was strongly suggestive of it reflecting a regional *terroir*, with both soil and temperature variation nominated as possible drivers of the variation in vineyard performance. However, this Marlborough study did not draw on any data describing soils or climate variation as was done in the Australian studies. Thus, the objectives of the present study were to incorporate such soil and climate data, along with the vineyard performance metrics, into a more holistic analysis of the Marlborough *terroir*. In particular, we wished to see whether the variation in vineyard performance could be explained by variation in biophysical factors. We also wished to take the opportunity to enhance the robustness of the previous analysis [22] through the incorporation of data from an additional vintage season and, across all seasons studied, from additional vineyards.

2. Methods and Materials

Marlborough, one of 16 local government regions in New Zealand, is located in the northeast of the South Island, with the District Council based in Blenheim, the largest town in the region (Figure 1). Whilst Marlborough is well known for its wine production, the rapid increase in the vineyard area over the last 30 years means there is currently no separately defined ‘wine region’ as in the case, for example, of the Australian GI or French AOC systems. Accordingly, for the purposes of this study, a map coverage of land under vineyard was obtained from the Marlborough District Council and from this, a regional grapegrowing ‘boundary’ was defined (Figure 1). In turn, this boundary was used as the basis for developing a 1 ha raster grid (i.e., pixels of 100 m × 100 m) which was used as the base for all subsequent mapping.

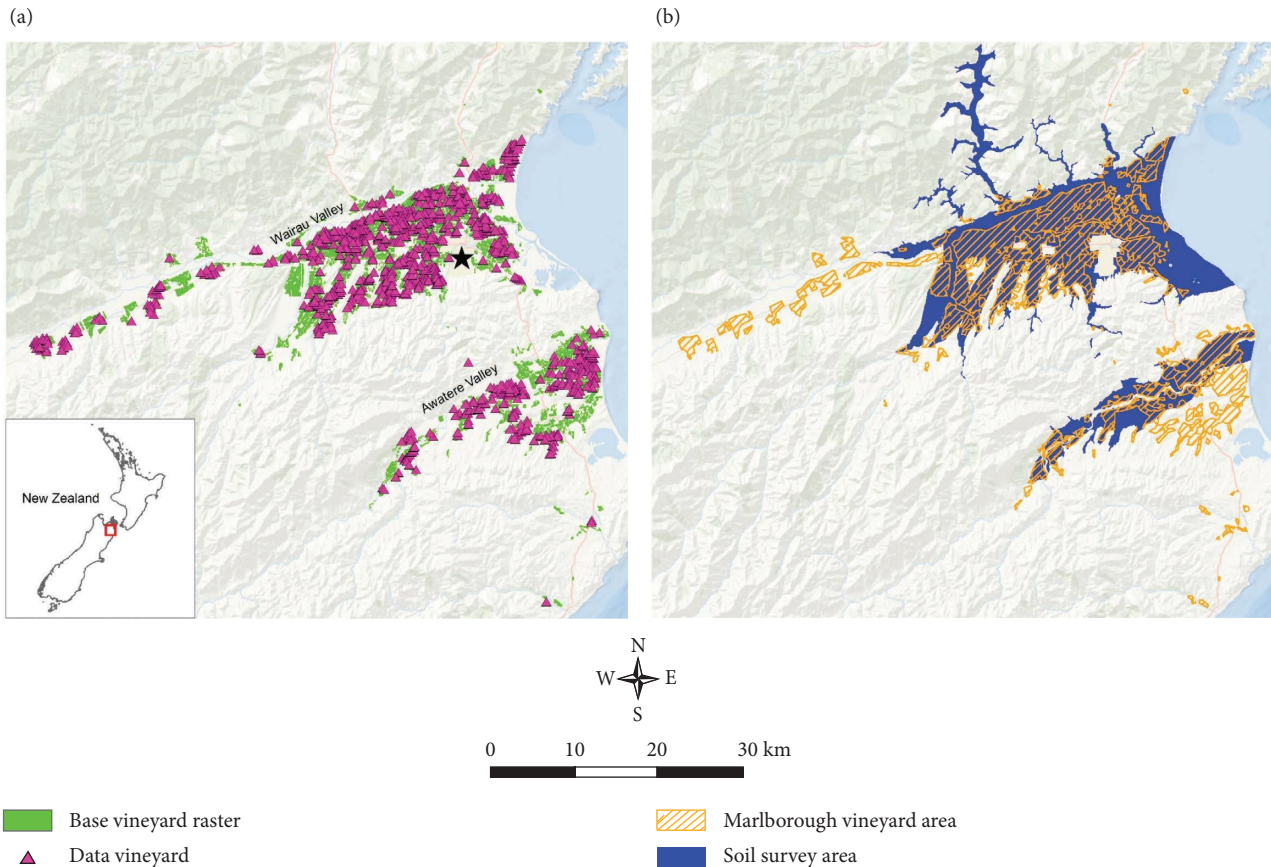


FIGURE 1: The Marlborough winegrowing region, in the northeast of New Zealand’s South Island, comprises the Wairau and Awatere valleys: (a) the locations of the 1083 vineyard blocks planted to Sauvignon Blanc for which yield data were available for the 2019 vintage, and the 1 ha base raster used for map interpolation. This derived from a coverage of land under vineyard (b). Also shown in (b) is the area for which soil survey data were available. The basemap layer was sourced from ESRI and its collaborators through the ArcGIS software. In (a), the star (★) denotes the approximate location of the centre of the town of Blenheim, and the red box in the inset to (a) shows the extent of the map area shown in (a) and (b).

2.1. Vineyard Performance. The methods used for analysis of vineyard performance in the present study are exactly as described by Bramley et al. [22] with the exception that, here we include data for vintage 2019 in addition to 2014–18, and for all years, include data for vineyards additional to those canvassed in the earlier work. Various indices of vineyard performance were acquired, by request and in confidence, from local grape growers and wine companies, with the data collected being those which these entities routinely collect for the purposes of yield estimation, harvest record keeping, and payments to growers. Here, we again focus on yield and harvest date, the attributes for which the greatest amount of data was available. For mapping, reported harvest dates (H_{rep}) were converted to Julian day numbers (where 1 and 32 = 1st January and 1st February). Vines in Marlborough are generally planted in rows with a North:South orientation, with 2.4 to 3.0 m between the rows and 1.8 m within the row and are trimmed to a consistent height and width of about 1.8×0.4 m with a lower fruiting wire at 0.9 m from the soil level. Any effects of different row spacings on the yield per unit area were removed by expressing the data as kg/m, and the effects of seasonal variation were removed by normalising all data on an annual basis to a mean of zero ($\mu = 0$) and standard deviation of one ($\sigma = 1$); the latter normalisation

was also considered useful in protecting the privacy of growers. In any season, only data from blocks planted to Sauvignon Blanc at least three years prior were included, with all data georeferenced to the centroid of the vineyard block from which they derived; that is, the coordinates of the centre of each block were used to define the location of the block from whence the data derived. Regional scale yield and harvest date maps were then interpolated onto the base 1 ha grid using local point kriging in VESPER [32] with an exponential variogram model and a data cloud of 100 data points. Over the 2014–2019 study period, the number of data points available for map interpolation ranged from 618–1083 for yield and 524–851 in the case of harvest date. Figure 1(a) shows the geographical distribution of these data for vintage 2019; the distribution of data in prior vintages was very similar, albeit with generally fewer data points in the earlier vintages.

2.2. Climate and Grapevine Phenology. New Zealand does not have a freely available national gridded climate database such as the one used in the previous Australian work (e.g., [24]). Accordingly, the weather research and forecasting (WRF) model described by Skamarock et al. [33], as used previously in Marlborough by Sturman et al. [34], was run to

simulate weather on a daily timestep at a resolution of 1 km² for the 2013–2019 period; the additional year at the start of the study period was included to ensure the full season leading to vintage 2014. The WRF model has been successfully used and validated in many previous regional climate studies, including other vineyard regions [35]. Validation of WRF model simulations relevant to viticulture has also been undertaken specifically for the Marlborough region [36–38], and the results used to correct any bias in model predictions. The variables modelled here were daily rainfall, from which growing season rainfall (GSR) was calculated, and daily temperature, from which the mean growing season temperature (GST) and season-growing degree days (GDD; base of 10°C) were calculated, with ‘season’ notionally defined as September to April. Note however, that to facilitate alignment to phenological modelling (see below) we used a season start date of 29th August rather than 1st September; 30th April was used as the season end date.

The daily temperature data generated above were used as input to phenological modelling. The dates of flowering (DOF) and of veraison (DOVN) were modelled using the grapevine flowering veraison model of Parker et al. [39] with values of F^* for flowering and veraison of 1282 and 2528, respectively [40]; this model has been shown to perform well in characterising the phenology of Marlborough Sauvignon Blanc [41–43]. The estimated date of harvest (H_{est}), defined for this purpose as the date on which the fruit reached a total soluble solids (TSS) content of 200 g/L, was calculated using the grapevine sugar ripeness model of Parker et al. [44]. A 5 × 5 pixel bilinear smoothing was applied to the 1 km² outputs from both the WRF and phenological models, and these were then resampled to the 1 ha base grid for mapping alongside the other map layers developed. In addition, using simple map algebra in ArcGIS (v. 10.7.1; ESRI, Redlands, CA, USA), we also calculated the duration of the period between flowering and veraison, denoted here as ‘Growth,’ between veraison and harvest (H_{est}), denoted here as ‘Ripen,’ and a ‘harvest error’ (HarvErr), the difference between H_{rep} and H_{est} .

2.3. Soils. Soil property data were provided by New Zealand Landcare Research—Manaaki Whenua. Despite some recent activity in digital soil mapping in New Zealand [45], the available data for the Marlborough region (<https://smap.landcareresearch.co.nz/>) derived from conventional reconnaissance soil survey conducted in the 1980s and 90s. Much of this mapping makes use of categorical, rather than numerical data, and is only available in polygon (i.e., shapefile) rather than raster format. Nonetheless, useful and useable soil data were accessible for soil texture—the contents of sand, silt, and clay in the <2 mm fraction—and also for stone content (i.e., >2 mm). Because soil survey is uncertain, inasmuch that soils are variable over short distances, soil survey in New Zealand has employed a “soil family” and “soil sibling” approach [46] such that each mapped polygon (i.e., each soil mapping unit) may comprise more than one sibling; as such, the published maps have a probabilistic element to them as is also common, for example, in Australian reconnaissance soil survey [31, 47]. For the present

study, we assumed that the soil properties of the dominant soil sibling in each polygon were those of the entire polygon.

The data for soil texture were provided for each ‘functional horizon’ with the depth of these horizons also reported. Accordingly, and notwithstanding the depth basis of soil hydrological properties (see below), we calculated profile weighted mean values for these measures of soil particle size to a maximum depth of 80 cm using the depth and soil property values for each functional horizon. In the case of soils that were deeper than 80 cm, we assumed that the functional horizon which coincided with a depth of 80 cm only reached that depth and that the mean soil property value reported for that functional horizon was appropriate to it being no deeper than 80 cm. For soils shallower than 80 cm, the profile weighted mean soil property values were calculated to the maximum depth of the deepest functional horizon. Of note in this regard is that “mean rooting depth” was also reported, with a sizeable proportion of the soils being listed as having rooting depths of >100 cm. However, most of the soil survey work conducted in Marlborough was done before winegrape production became a dominant land-use in the region. This is important given that the development of Marlborough as a winegrowing region involved minimal land re-forming, and that rooting depth is likely to be crop-specific and is also likely to be affected by the use of irrigation. Anecdotal evidence supports the view that in most locations in Marlborough, irrespective of soil depth, the majority of grapevine roots occur within the top 80 cm of the soil profile [48]. Thus, we calculated profile weighted means over this depth range.

In addition to soil texture, data were also available for the available water capacity (AWC—the amount of water potentially available for plant growth that can be stored in the soil) to 30 and 60 cm depth, with an estimate of profile available water (PAW—i.e., AWC to 100 cm depth or to a physical root barrier if one was present at less than 100 cm) also available. In each case, these were defined as the difference between water holding capacity (%) at –10 kPa and –1500 kPa in the included functional horizons, weighted by their thicknesses. As such, they are consistent with our profile weighted value for soil texture, notwithstanding the different depth ranges. The estimated AWC data used here derived from the approach of McNeil et al. [49] and accounted for the presence of stones. In addition, the categorical “soil drainage status” was available, classified in terms of very poorly, poorly, imperfectly, moderately well, or well drained [50].

Recent soil survey activity in Marlborough (G. Grealish—pers. comm.) suggests that the line work (i.e., polygon boundaries) in the existing soil mapping remains accurate. We therefore assigned the polygon-based soil values for each soil property to each coincident pixel in the base raster which aligned with that polygon. However, as can be seen in Figure 1(b), the area for which soil data were available was somewhat smaller than the area under vine. Accordingly, our soil-based analysis was confined to those parts of the district for which coincident soil and vineyard data were available.

With the exception of drainage status, the soil data were provided as numerical values. However, it was apparent from their distributions that the data were not continuous, a problem that was likely compounded by our method of assigning individual values derived from a polygon of many ha in area to all the coincident 1 ha pixels which aligned with it. In other words, large numbers of pixels could have the same soil property values. Furthermore, for some soil properties (especially the content of stones and silt), there were many pixels containing values of “zero.” For these reasons, for the purposes of clustering the various map layers (see below), the soil data for all soil properties were converted to normal scores [51] prior to cluster analysis. This uses a ranking process to calculate standard normal quantiles of the same size as the original data set. To avoid the introduction of bias in this process, prior to ranking each soil property, the order of all pixels in the dataset was randomised. The results of the cluster analysis were then interpreted in terms of real values by using the normal scores data as a ‘lookup’ table.

2.4. Topography. Elevation data were acquired at 1 m resolution by Land Information New Zealand—Toitu Te Whenua (LINZ) using airborne LiDAR in 2014, 2018, and 2020 (<https://data.linz.govt.nz/search/?q=Marlborough+lidar>) with each dataset covering different parts of the region, albeit with some overlap. These data were used to create a single digital elevation model (DEM) by mosaicing them in ArcGIS (v. 10.7.1; ESRI, Redlands, CA, USA). However, the LINZ dataset did not cover the upstream parts of the grapegrowing area in the Awatere Valley, nor much of the hills separating the Wairau and Awatere valleys. Accordingly, these areas were in-filled using the 8 m resolution DEM available from the Marlborough Regional Council which had been interpolated from a dataset of 20 m contours (<https://data.linz.govt.nz/layer/51768-nz-8m-digital-elevation-model-2012/>).

2.5. Spatial Analysis. From the above, we had a dataset of vineyard performance data (yield, H_{rep}), along with data for climate indices (GSR, GST, and GDD) and estimates of the date of key phenological stages (DOF, DOVN, and H_{est}) and derived phenological data (Growth, Ripen, and HarvErr) across the 2014–19 vintage period. Also available were data for soil attributes (texture, drainage status, AWC, and PAW) and elevation. These data were all either interpolated or sampled to the same 1 ha base raster grid except in the case of soil data for which the areal extent of the raster was matched to the area of data availability. Nonetheless, all map layers had identical alignment. This enabled similarity in patterns of spatial variation amongst these properties and across vintages to be examined using *k*-means clustering in JMP (v.16.0.0, SAS Institute Inc., Cary, NC, USA) with the number of clusters allowed to vary from two to five. The optimum number of clusters was selected using the cubic clustering criterion [52] and when the optimum number was initially identified as five, the analysis was rerun to larger cluster numbers to enable an unconstrained optimum to be

identified. All other spatial analyses, along with map display, were done using the ArcGIS software suite (v. 10.7.1; ESRI, Redlands, CA, USA).

3. Results

3.1. Variation in Vineyard Performance. Consistent with the previous results [22], patterns of variation in both yield (Figure 2) and harvest date (Figure 3) were remarkably stable over the six years of the study, despite the observed differences between their viticultural seasons (Table 1). Thus, some parts of Marlborough can be seen to be inherently lower or higher yielding than others with a notable difference, on average, between the Wairau and Awatere valleys. In both valleys, upstream areas tend to be lower yielding than more central and downstream areas, and a marked band of higher yielding vineyards running NW-SE across the lower Wairau is consistently seen (Figure 2). Similarly, harvest dates in the Awatere Valley are generally later than in the Wairau Valley, with harvest in the Central Wairau Valley, the oldest established winegrowing area, occurring the earliest (Figure 3).

Clustering the map layers for yield and harvest date (Figure 4) emphasises the noted within-region variation and further suggests a distinction between the two valleys. In the case of yield, the optimal number of clusters based on the CCC was four (Figure 4(b)) even though the three-cluster solution, which is very similar to that reported by Bramley et al. [22], shows a more consistent rank order of the clusters (Figure 4(a)). Similarly, in the case of the clustering of harvest dates, where the two-cluster solution (Figure 4(c)) was identified as optimal based on the CCC, the three-cluster solution (Figure 4(d)) is meaningful inasmuch that the rank order of the cluster means is consistent across the six years of the study. These results, along with those for when the yield and harvest date maps are clustered together (Figure 4(e)), support the view that, in general, the Central Wairau Valley, which comprises both lower and higher yielding vineyards, is always harvested earliest, whilst most of the Awatere Valley, along with the upstream parts of the Wairau and tributary valleys are harvested last—even though these are also the lowest yielding. This observation suggests the possible importance of temperature to these patterns of regional variation. On the other hand, if temperatures (and incident sunlight) were constant, one might expect higher yielding areas to ripen later and so be harvested later than lower yielding areas. Figure 4 does not otherwise suggest a clear interaction between yield and harvest date (discussed further below).

Despite the greatly enhanced dataset which underpins the various maps in Figures 2–4 compared to the previous analysis [22], the interaction between the density of data and use of local kriging means that the map confidence intervals do not allow us to identify the statistical significance of the difference between the cluster means based on the median kriging variance [53]. Accordingly, to examine the significance of between-cluster differences, the raw point data for yield and harvest date (e.g. Figure 1(a)) were overlaid on the results of the cluster analysis (Figure 4), and the raw data

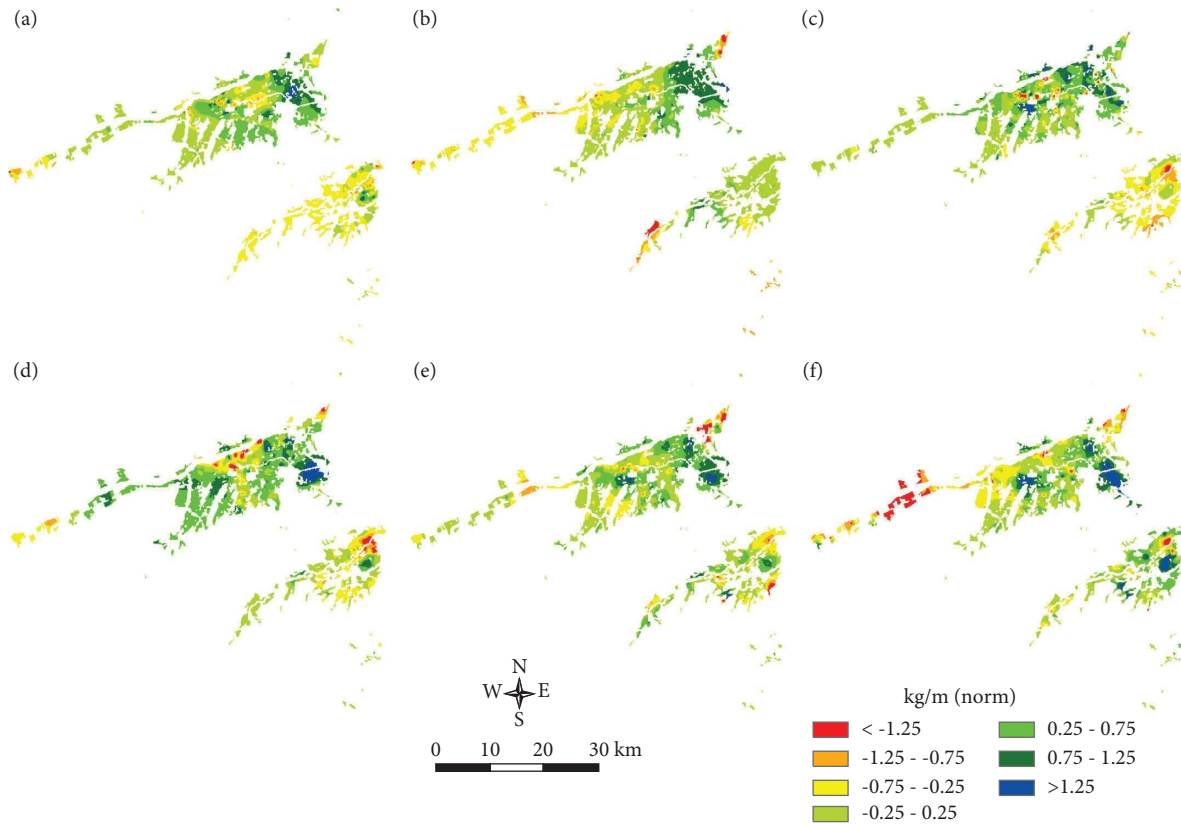


FIGURE 2: Variation in the yield of Sauvignon Blanc in the Marlborough region, 2014–2019. Note that the data (kg/m) have been normalised ($\mu = 0, \sigma = 1$) on a per season basis: (a) vintage 2014, (b) vintage 2015, (c) vintage 2016, (d) vintage 2017, (e) vintage 2018, and (f) vintage 2019.

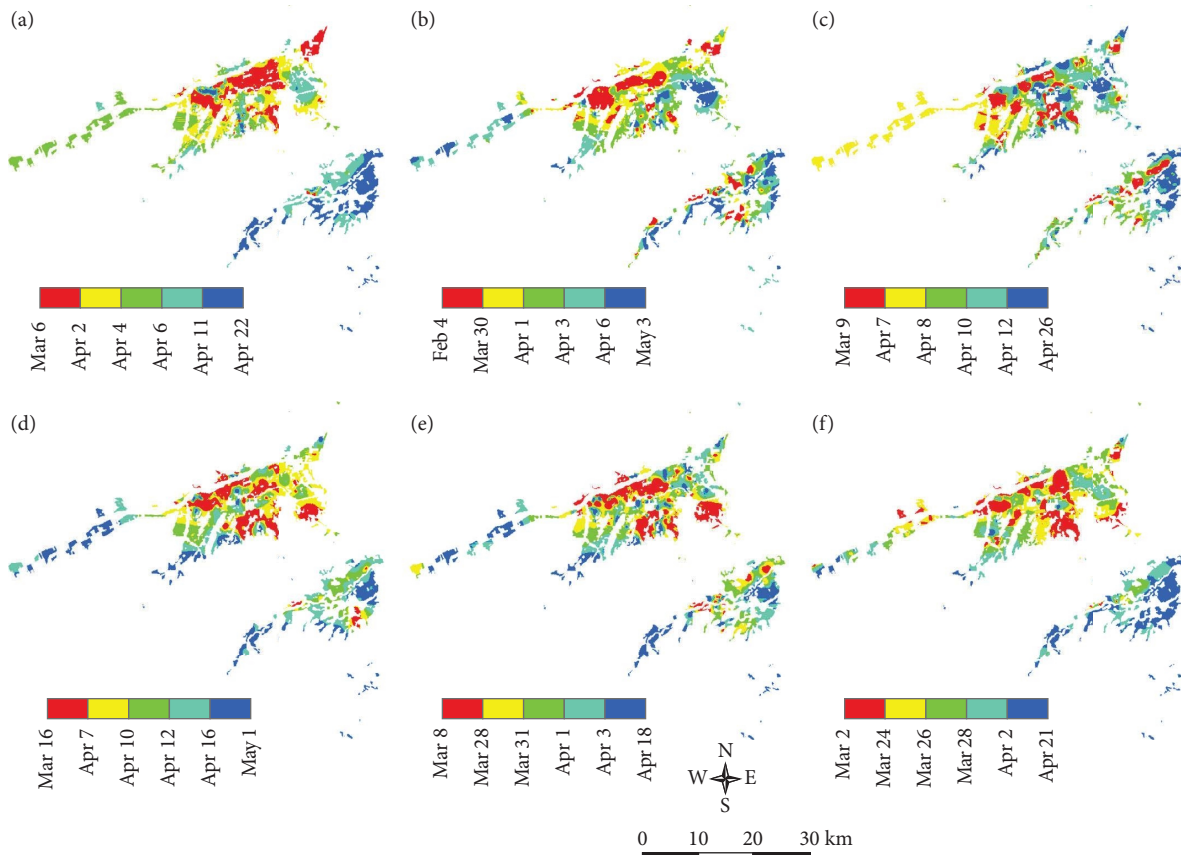


FIGURE 3: Variation in the reported date of harvest (H_{rep}) of Sauvignon Blanc in the Marlborough region, 2014–2019. Note that for each season, the data have been classified in 20th percentiles. The first date in each legend is the date of the earliest harvest recorded in the dataset for that year. The last date listed is the latest date of harvest for that year, whilst the other dates are those that divide the map classes: (a) vintage 2014, (b) vintage 2015, (c) vintage 2016, (d) vintage 2017, (e) vintage 2018, and (f) vintage 2019.

TABLE 1: A simple characterisation of the viticultural seasons in the 2014–19 study period in Marlborough.

Vintage	Notable seasonal features		Yield t/ha ^a
	Temperatures	Rainfall	
2014	Warm initiation and flowering period	January above average (big berries)	15.8
2015	Warm initiation and flowering period	Dry Jan, Feb (small berries)	10.8
2016	Cool flowering period	Jan above average	14.6
2017	Average flowering	Above average Feb and March period	13.2
2018	Above average flowering	Very dry spring, above average Jan, Feb (very high), and Mar	13.1
2019	Warm and dry in Dec-Mar	Very dry Jan and Feb (11.8 mm total), wet March, Small berries at harvest	12.5

^aData obtained from NZ winegrowers vintage surveys and NZ winegrowers vineyard register.

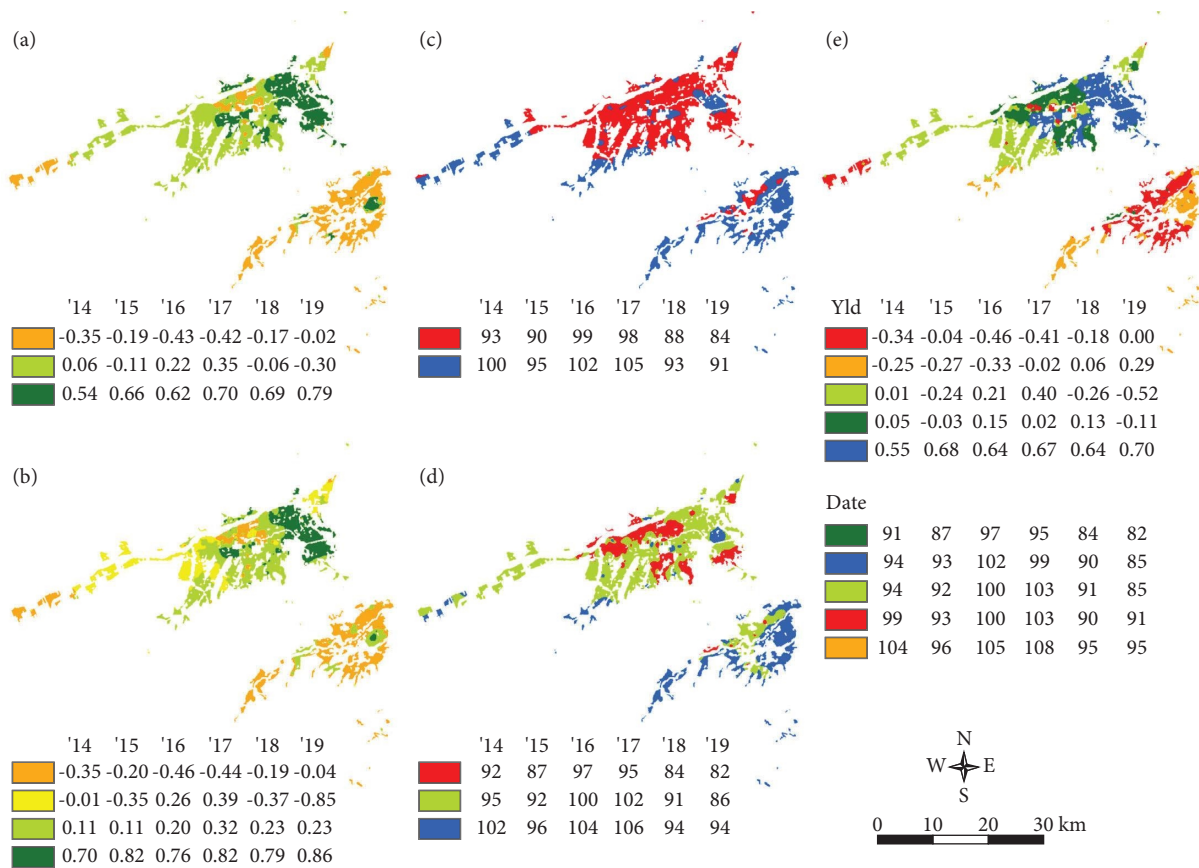


FIGURE 4: Results of clustering: (a, b) the yield maps shown in Figure 2, (c, d) the harvest date maps shown in Figure 3, and (e) all yield and harvest date map layers for the 2014–19 vintage period. The numbers in the legends are cluster means. Based on the cubic clustering criterion, the optimal number of clusters was four in the case of yield (b) and two in the case of harvest date (c) although three-cluster solutions (a, d) were also deemed useful. In (e) the yield and harvest dates are shown in separate legends for ease of interpretation; five clusters were optimal for this combined analysis.

were reanalysed to test for the statistical significance of differences in the means (Tukey–Kramer test) of the identified clusters. The results are presented in Tables 2–4, with a colour coding to assist with matching to the map legends. Note that for this analysis, we only used data from vineyards for which we had both yield and harvest date information; we also used the actual yields (kg/m) rather than normalised data.

Comparison of Table 2 and Figures 4(a) and 4(b) suggests that the different yield clusters identified do reflect the generally statistically significant yield differences in the raw data derived from vineyards located in each cluster. A very similar conclusion may be drawn in terms of the harvest date (Table 3 and Figures 4(b) and 4(c)). When a similar analysis is done for the combined yield and harvest date clusters, the results (Table 4) again mirror those from the cluster analysis

(Figure 4(e)) and, as such, reflect the lack of interaction between the yield and harvest date over the region as a whole; that is, different factors appear to drive yield variation compared to harvest date variation. Of note is the fact that, when a similar analysis is done to test for differences between the Wairau and Awatere valleys (i.e., ignoring the cluster analysis), the two valleys present as clearly different (Table 5).

3.2. Variation in Climate. Consistent with temporal stability in patterns of variation in vineyard performance (Figures 2–4), patterns of spatial variation in both temperature (Figure 5) and rainfall (Figure 6) were also consistent across the six years of the study, even though the absolute values varied from year to year. This was the expected result given the strong reliance of the WRF model at the local level on topographic variation and distance from the sea, coupled to the effects of prevailing weather systems. This is also the reason why we only show GDD in Figure 5 since its patterns of spatial variation were essentially identical to those for GST. Of note is the apparent difference between the patterns of variation in annual rainfall (Figure 6) and those for vineyard performance

(Figures 2–4), in spite of the general observation within both the Wairau and Awatere valleys of a strong S-N rainfall gradient (Figure 6; in the Wairau Valley, rainfall roughly doubles between Blenheim and the north bank of the Wairau River, 10 km due north), and the increase in rainfall with distance upstream (approximately 16 mm/km in the Wairau Valley). On average, the Awatere Valley does not present as markedly cooler than the Wairau Valley (Figure 5) suggesting that, contrary to the comments above, some factors other than temperature accumulation might be responsible for the lower yields in the Awatere Valley.

3.3. Variation in Phenology. Patterns of variation in grapevine phenology closely followed those of temperature. This was the expected result given the dependence of the phenological models of Parker et al. [39, 40, 44] on temperature. Thus, Figure 7 shows mean predicted dates of flowering, veraison, and harvest (i.e., TSS of 200 g/L; H_{est}) across the six study years, whilst Table 6 provides an indication of the interannual variation. Of note is that, whilst the patterns of spatial variation are distinct, the range of variation in DOF, DOVN, and H_{est} is narrow in

TABLE 2: Analysis of differences between yield zones when based on raw vineyard yield data (kg/m) from locations corresponding to the clusters identified in Figures 4(a) and 4(b)^A.

Cluster ^B	2014		2015		2016		2017		2018		2019	
	<i>n</i>	Yield	<i>n</i>	Yield	<i>n</i>	Yield	<i>n</i>	Yield	<i>n</i>	Yield	<i>n</i>	Yield
<i>Three cluster solution (Figure 4(a))</i>												
1	204	3.64c	282	2.63c	299	3.49c	323	2.97c	318	3.24c	334	3.13b
2	190	4.50b	256	2.87b	267	4.55b	274	3.95b	277	3.53b	280	3.26b
3	84	5.31a	122	3.65a	116	4.98a	131	4.69a	177	4.68a	139	4.27a
<i>Four cluster solution (Figure 4(b))</i>												
1	194	3.66c	252	2.60c	266	3.42d	289	2.91c	284	3.19c	302	3.09c
2	52	4.37b	79	2.52c	90	4.75b	83	3.76b	81	3.01c	91	2.75d
3	178	4.53b	255	3.07b	258	4.41c	278	4.05b	289	3.88b	274	3.64b
4	54	5.56a	74	3.83a	68	5.29a	78	4.89a	118	4.82a	86	4.35a

^AFor any individual year, yields marked with different letters are significantly different ($p < 0.05$). *n* denotes the number of data values in each cluster. ^BThe colour coding of cluster numbers matches that in the source figures.

TABLE 3: Analysis of differences between harvest date zones when based on raw vineyard data for harvest date (day; Julian numbers) from locations corresponding to the clusters identified in Figures 4(c) and 4(d)^A.

Cluster ^B	2014		2015		2016		2017		2018		2019	
	<i>n</i>	Day	<i>n</i>	Day	<i>n</i>	Day	<i>n</i>	Day	<i>n</i>	Day	<i>n</i>	Day
<i>Two cluster solution (Figure 4(c))</i>												
1	270	92.3b	371	88.3b	388	97.2b	417	95.6b	451	85.5b	431	82.6b
2	208	102.0a	289	95.7a	294	104.9a	311	106.6a	321	93.5a	322	93.0a
<i>Three cluster solution (Figure 4(d))</i>												
1	177	90.9c	210	85.5c	215	94.5c	243	92.9c	242	81.6c	240	80.3c
2	151	96.4b	247	92.8b	260	100.7b	261	101.2b	306	90.6b	279	86.4b
3	150	103.3a	203	96.4a	207	106.4a	224	107.3a	224	94.1a	234	94.9a

^AFor any individual year, Julian days marked with different letters are significantly different ($p < 0.05$). *n* denotes the number of data values in each cluster. ^BThe colour coding of cluster numbers matches that in the source figures.

TABLE 4: Analysis of differences between yield-harvest date zones when based on raw vineyard data for yield (kg/m) and harvest date (day; Julian numbers) from locations corresponding to the clusters identified in Figure 4(e)^A.

Cluster ^B	2014			2015			2016			2017			2018			2019		
	<i>n</i>	Yield	Day	<i>n</i>	Yield	Day	<i>n</i>	Yield	Day	<i>n</i>	Yield	Day	<i>n</i>	Yield	Day	<i>n</i>	Yield	Day
1	89	3.67d	98.9q	134	2.76bc	94.4pq	142	3.43d	100.1q	159	3.03d	102.1qr	158	3.14d	89.4r	168	3.09c	90.0q
2	88	3.82cd	104.9p	124	2.74bc	95.9p	125	3.80c	107.1p	131	3.48c	108.6p	130	3.77b	95.7p	129	3.65b	96.3p
3	56	4.27bc	94.4rs	103	2.62c	92.2q	113	4.46b	100.6q	107	3.96b	103.4q	112	3.36cd	91.9q	119	3.19c	85.9r
4	172	4.39b	91.3s	202	2.88b	85.4r	208	4.30b	94.9r	226	3.55c	92.6s	220	3.50bc	81.5s	221	3.12c	80.1s
5	73	5.31a	97.5qr	97	3.73a	94.5pq	94	5.05a	104.5p	105	4.70a	100.7r	152	4.64a	90.8qr	116	4.25a	87.2r

^AFor any individual year, yields and Julian days marked with different letters are significantly different ($p < 0.05$). *n* denotes the number of data values in each cluster. ^BThe colour coding of cluster numbers matches that in the source figures.

TABLE 5: Differences between the Wairau and Awatere valleys when assessed using raw vineyard data for yield (kg/m) and harvest date (day; Julian numbers)^A.

Region	2014			2015			2016			2017			2018			2019		
	<i>n</i>	Yield	Day	<i>n</i>	Yield	Day	<i>n</i>	Yield	Day	<i>n</i>	Yield	Day	<i>n</i>	Yield	Day	<i>n</i>	Yield	Day
Wairau	351	4.47a	94.4q	202	2.94a	90.3q	466	4.38a	99.5q	508	3.78a	98.4q	547	3.74a	87.5q	536	3.38a	84.5q
Awatere	127	3.75b	102.4p	456	2.87a	94.2p	214	3.68b	102.6p	218	3.35b	104.6p	223	3.51b	92.0p	216	3.43b	93.5p

^AFor any individual year, yields and Julian days marked with different letters are significantly different ($p < 0.05$). *n* denotes the number of data values from each valley.

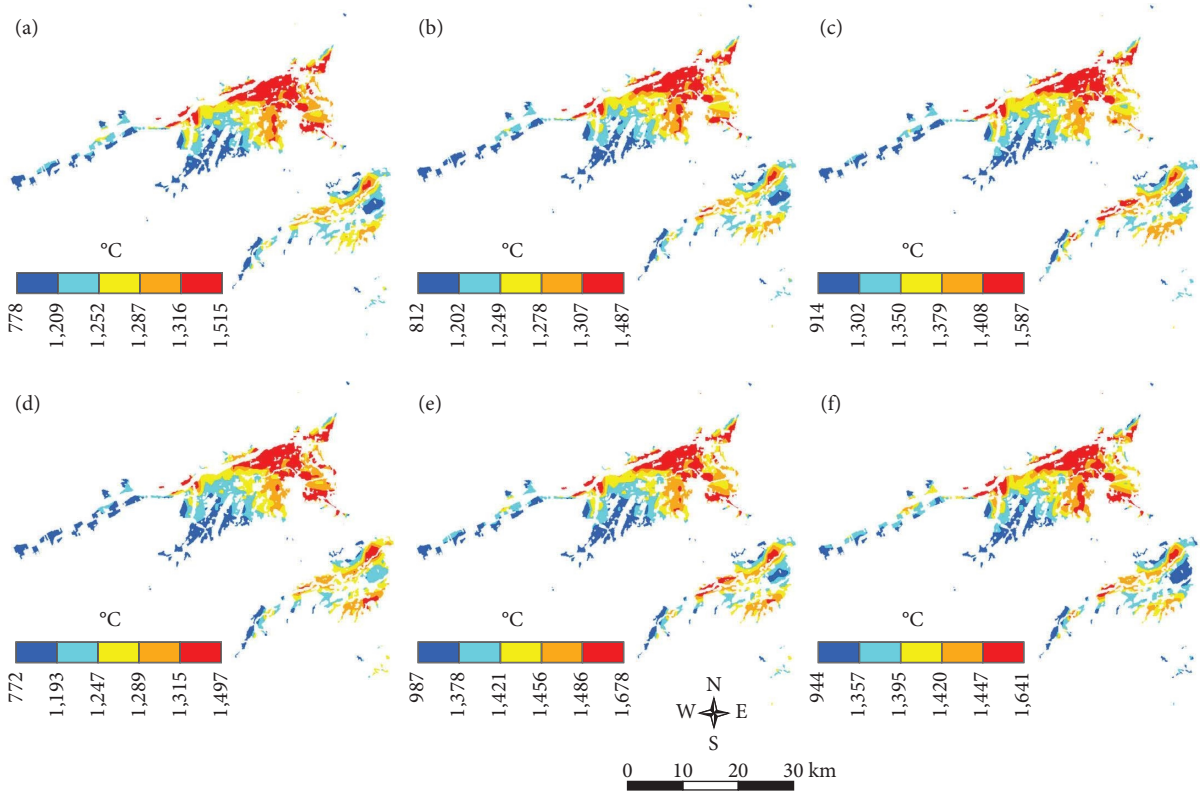


FIGURE 5: Variation in seasonal growing degree days (GDD, base of 10°C) in Marlborough, New Zealand, in the seasons ending with vintage 2014–19, estimated using the WRF model [33]. Note that the season was defined as 29th August to 30th April. The first and last figures in each legend are the lowest and highest values with other values indicating the 20th percentiles: (a) vintage 2014, (b) vintage 2015, (c) vintage 2016, (d) vintage 2017, (e) vintage 2018, and (f) vintage 2019.

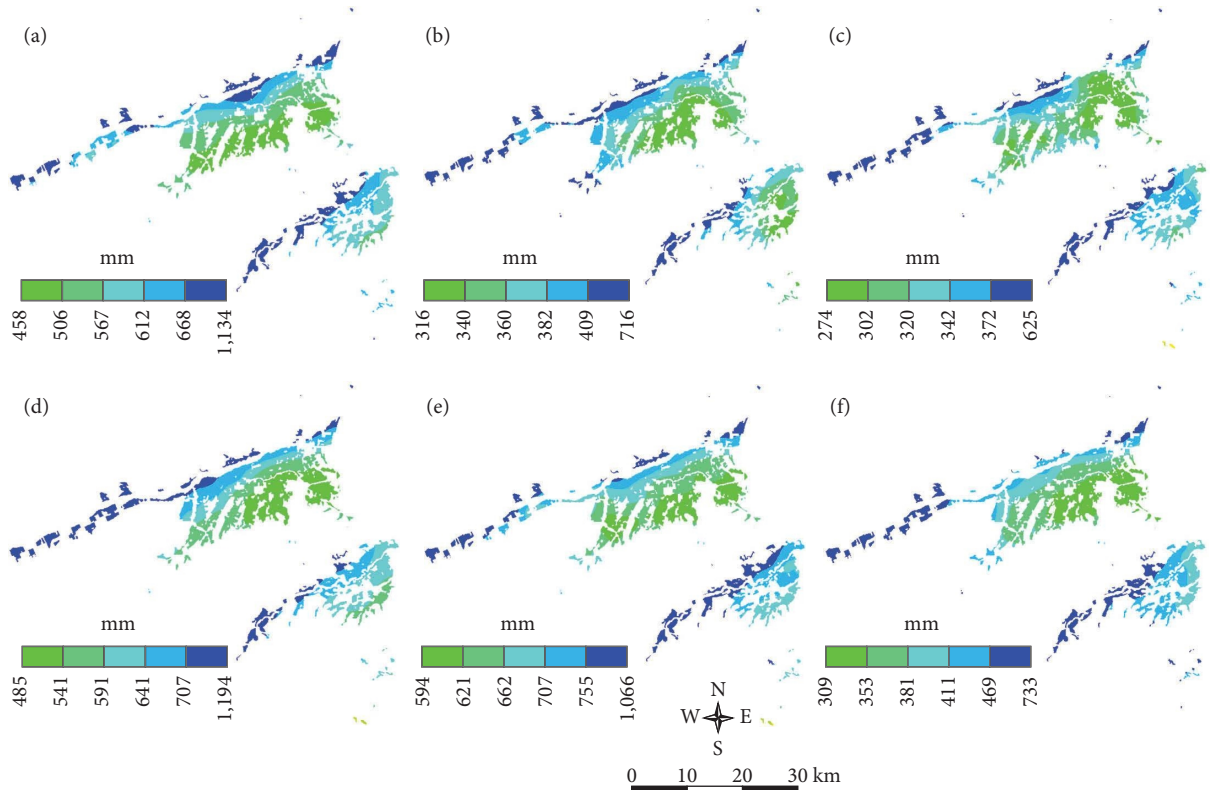


FIGURE 6: Variation in growing season rainfall (29th August to 30th April) in Marlborough, New Zealand, in the seasons ending with vintage 2014–19 estimated using the WRF model [33]. The first and last figures in each legend are the lowest and highest values with other values indicating the 20th percentiles: (a) vintage 2014, (b) vintage 2015, (c) vintage 2016, (d) vintage 2017, (e) vintage 2018, and (f) vintage 2019.

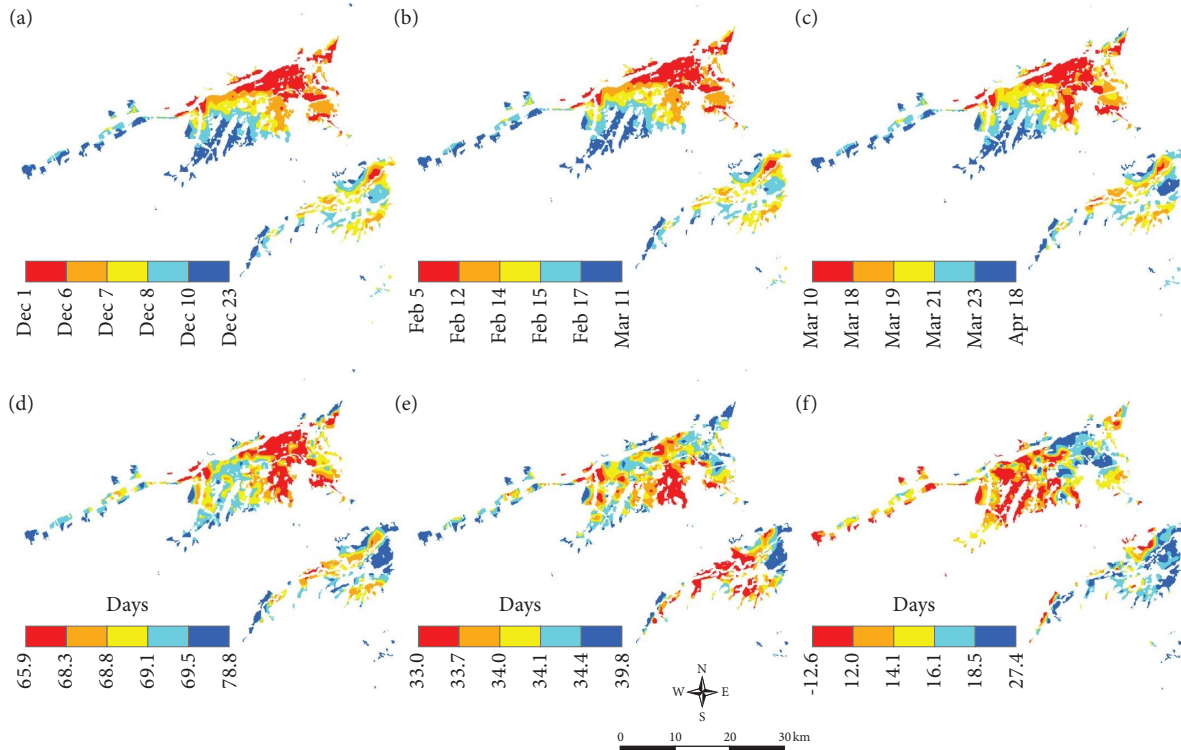


FIGURE 7: Variation in the predicted mean dates of the key phenological stages of (a) flowering, (b) veraison, (c) harvest (TSS of 200 g/L), (d, e) the mean duration of the periods between them (i.e., ‘Growth’ and ‘Ripen’), and (f) the difference between the reported and predicted dates of harvest (i.e., HarvErr) of Sauvignon Blanc in Marlborough, New Zealand. Data are the means calculated from the six seasons which ended with vintage in 2014–19. The first and last figures in each legend are the lowest and highest values with other values indicating the 20th percentiles.

any given year (Table 6). Furthermore, whereas the pattern of spatial variation in the duration of the flowering to veraison growth period (Growth; Figure 7(d)) aligns closely to that of heat accumulation during the whole growing season (GDD; Figure 5), the pattern of spatial variation in the duration of the shorter ‘Ripen’ period between veraison and H_{est} , the date at which fruit reach a TSS of 200 g/L (Figure 7(e)), shows a less organised pattern of variation, in spite of the general temperature dependence of vine phenology (Figures 7(a)–7(c); [39, 44]). This is likely a consequence of the difference in length between the short ‘Ripen’ and much longer ‘Growth’ phenophases, their relative proportions of the length of the overall growing season, and heat summation over the whole season. However, of greater interest in the context of terroir is that the largest values of HarvErr (i.e., $H_{rep} - H_{est}$; Figure 7(f)) occur in the Awatere Valley, and in the high yielding strip in the lower Wairau (Figures 2 and 4); that is, in the Wairau Valley, and contrary to the suggestion (above) of no interaction between the yield and harvest date, the delay in harvest beyond a TSS of 200 g/L appears related to higher yields. Since the patterns of variation in H_{est} across the two valleys (Figure 7(c)) are similar to those of temperature (Figure 5), the delayed harvest in the lower yielding Awatere Valley (Figure 7(f)) cannot be attributed to temperature, as was suggested by Bramley et al. [22].

3.4. Soils. Patterns of variation in available water capacity in Marlborough soils are very similar whether expressed to a depth of 30, 60, or 100 cm (Figures 8(a)–8(c)) and show an inverse relationship to sand content (Figure 8(e)) and stoniness (Figure 8(h)); that is, as is expected, soils with higher contents of sand and stones, such as predominate upstream of the central Wairau Valley, have lower AWC. These soils are also well drained (Figure 8(d)). Conversely, and as is expected in a floodplain, lower Wairau soils have higher contents of silt (Figure 8(f)) and clay (Figure 8(g)) and these areas are also less well drained (Figure 8(d)). An exception occurs in the northeasternmost area of Marlborough around Rarangi where the soils reflect relic beaches and are characterised locally as being composed of ‘pea gravel.’

Consistent with the above, clustering of soil texture data (Figure 9(a)) divided the region into two clusters of soils with either few stones, comparatively low sand contents, and higher silt and clay contents on the one hand, and much sandier, stonier soils on the other. When the soil available water data were clustered (Figure 9(b)), four clusters were identified with a consistent rank order of AWC amongst the clusters irrespective of the soil profile depth increment. When all the soil properties were clustered (not shown), an almost identical delineation resulted as the more parsimonious analysis shown in Figure 9(c) which included just PAW (i.e., AWC to 1 m depth) and the profile weighted

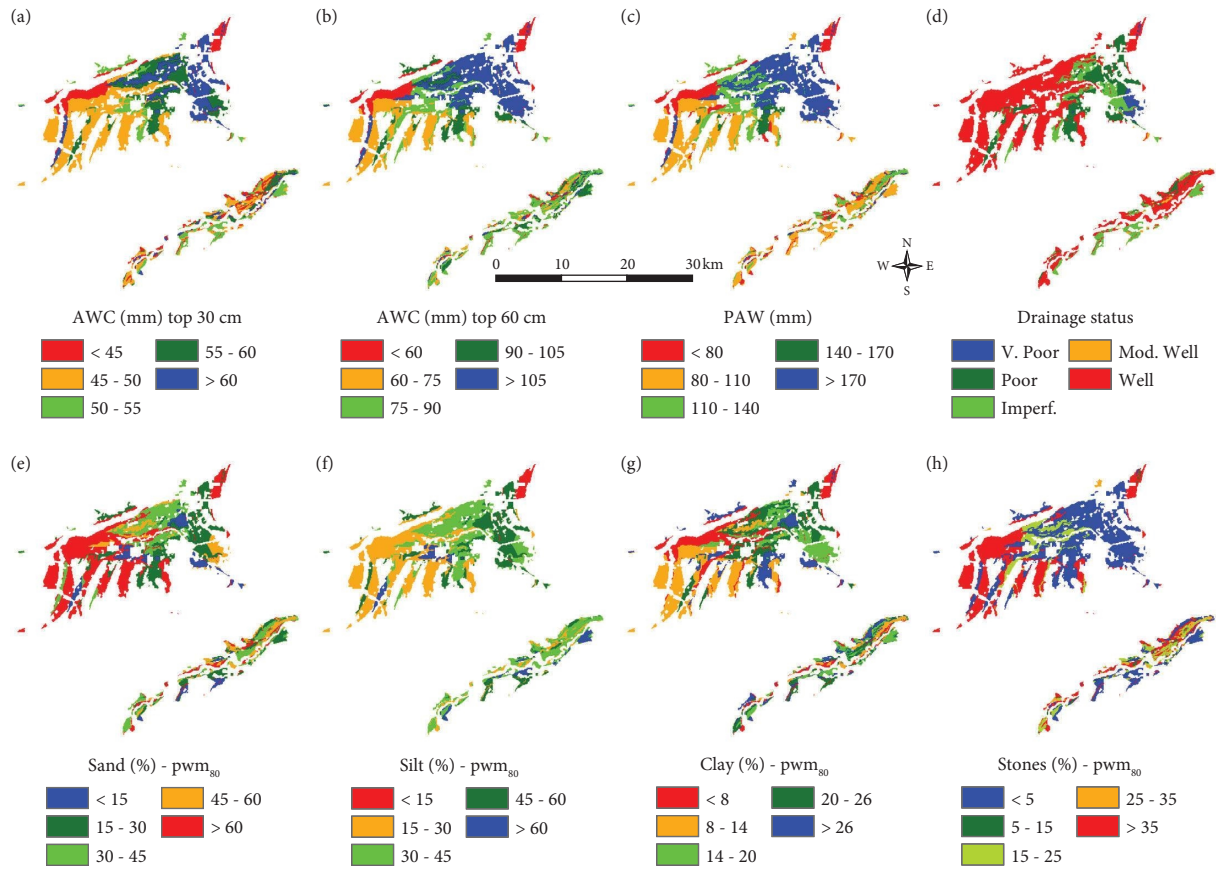


FIGURE 8: Variation in (a–d) soil hydraulic properties and (e–h) soil texture in Marlborough, New Zealand. AWC, available water capacity to either (a) 30 or (b) 60 cm depth; PAW, profile available water, which is the same as AWC to a depth of 1 m. Note that the texture data (e–h) are profile weighted mean values to a depth of 80 cm (pwm_{80}).

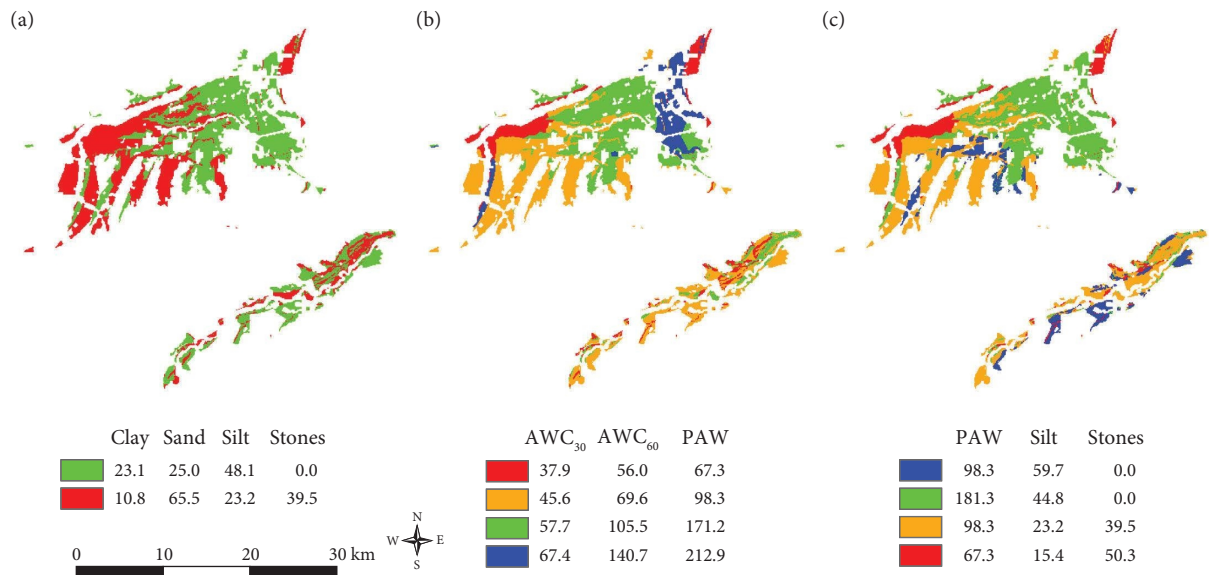


FIGURE 9: Results of clustering indices of (a) soil texture (%), (b) available water (mm), and (c) a combination of these using *k*-means. AWC₃₀ and AWC₆₀ are available water capacity to either 30 or 60 cm depth; PAW, profile available water, which is the same as AWC to a depth of 1 m. Note that the texture data are profile weighted mean values to a depth of 80 cm. This analysis used data that had been transformed to normal scores with the results then converted back to their units of measurements.

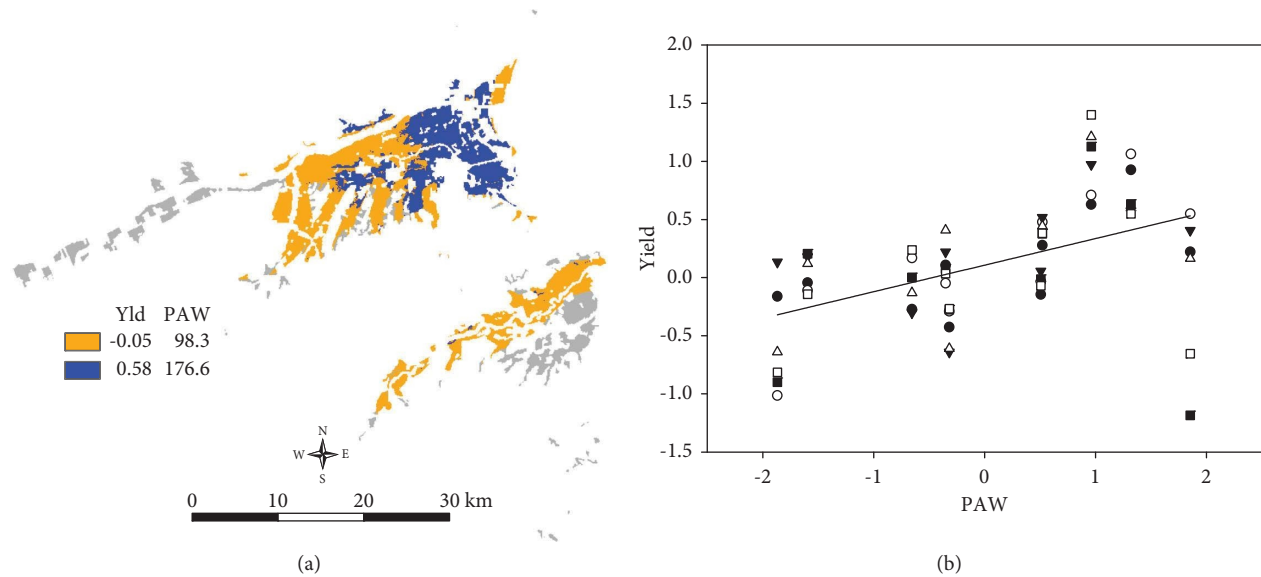


FIGURE 10: The dependence of yield of Marlborough Sauvignon Blanc on profile available water (PAW). In (a), PAW has been clustered with the mean yield achieved over the 2014–2019 period (Figure 2). The numbers in the legends are cluster means. Note that the yield data (kg/m) were normalised ($\mu = 0$, $\sigma = 1$) on a per season basis with PAW data transformed to normal scores with the results then converted back to mm after clustering. In (b), the cluster means (10 cluster solution) for yield and PAW obtained when the individual yield maps (Figure 2) were clustered with PAW and the contents of silt and stones (Figures 8(c), 8(f), and 8(h)) are plotted ($R^2 = 0.24$; $P < 0.0001$). In this case, PAW values have been retained as normal scores: ● 2014, ○ 2015, ▼ 2016, △ 2017, ■ 2018, and □ 2019. The area shaded grey in (a) is the vineyard area for which soil data are not available.

contents of silt and stones to a depth of 80 cm. Comparison of this result with Figure 8(c) suggests that the variation in the available soil properties can be characterised by variation in PAW—which is also the expected result given the dependence of PAW on texture.

3.5. Integrating Variation in Vineyard Performance with Soil and Climate Variation. Clustering a map of mean yield (i.e., the mean of the six maps shown in Figure 2) with PAW using k -means splits the region into two, based on CCC; an above-average yielding area with a mean PAW of 176.6 mm and an area of approximately average district yield ($\mu \approx 0$) with PAW of 98.3 mm (Figure 10(a)). Repeating this analysis with the yield maps for individual years (Figure 2) rather than the mean, gave a very similar result, as did using silt content as the soil property included in the analysis, instead of PAW (not shown). However, when the yield maps for individual years were clustered with PAW and the contents of both silt and stones, no maximum cluster number was reached; that is, even when the clustering was allowed to run to 20 clusters, 20 was the identified optimum number based on the CCC. A possible explanation may be the general trend for yield to increase with increasing PAW (Figure 10(b)). Nonetheless, the results are consistent with the apparent alignment of the pattern of variation in both drainage status (Figure 8(d)) and silt content (Figure 8(f)) with that for yield (Figures 2 and 4). Thus, the higher yielding area in the lower Wairau aligns closely with these poorly drained soils with high silt content—an instance where, contrary to what in other regions might be

‘conventional wisdom,’ poorer drainage promotes higher vine vigour and yield.

Clustering GSR with either yield, harvest date, or both yield and harvest date together did not suggest any impact of regional rainfall distribution on vineyard performance. In both the Wairau and Awatere Valleys, the wettest areas in the upstream parts of the catchments tend to be the lowest yielding and are also harvested later in the season. Including GSR in the cluster analyses otherwise simply tended to reflect the patterns seen in Figure 6 without clear interaction with vineyard performance. Thus, the lower yields and later harvests seen in upstream areas are unlikely to be caused by their wetness and are likely driven more by their lower temperatures (Figure 5). Likewise, including the duration of the modelled ripening period (Ripen) had no effect in separating clusters. In contrast, including HarvErr (the difference between the modelled and actual harvest date) in the cluster analysis did align meaningfully with the patterns seen in many of the other maps (Figure 11). Thus, clustering the mean yield and HarvErr over the 6 seasons, either with or without PAW (Figures 11(a) and 11(b)) delineated two clusters with a familiar pattern. The higher yielding area in the lower Wairau is seen to also have higher values of HarvErr, but because parts of the lower yielding Awatere Valley also align with this higher HarvErr cluster, the mean cluster yield is seen to be lower than in Figures 4(a) and 4(b) or 10(a). When PAW is included in the analysis (Figure 11(b)), the mean yield of the higher yielding, greater HarvErr, and PAW cluster increases by comparison with Figure 11(a), as the

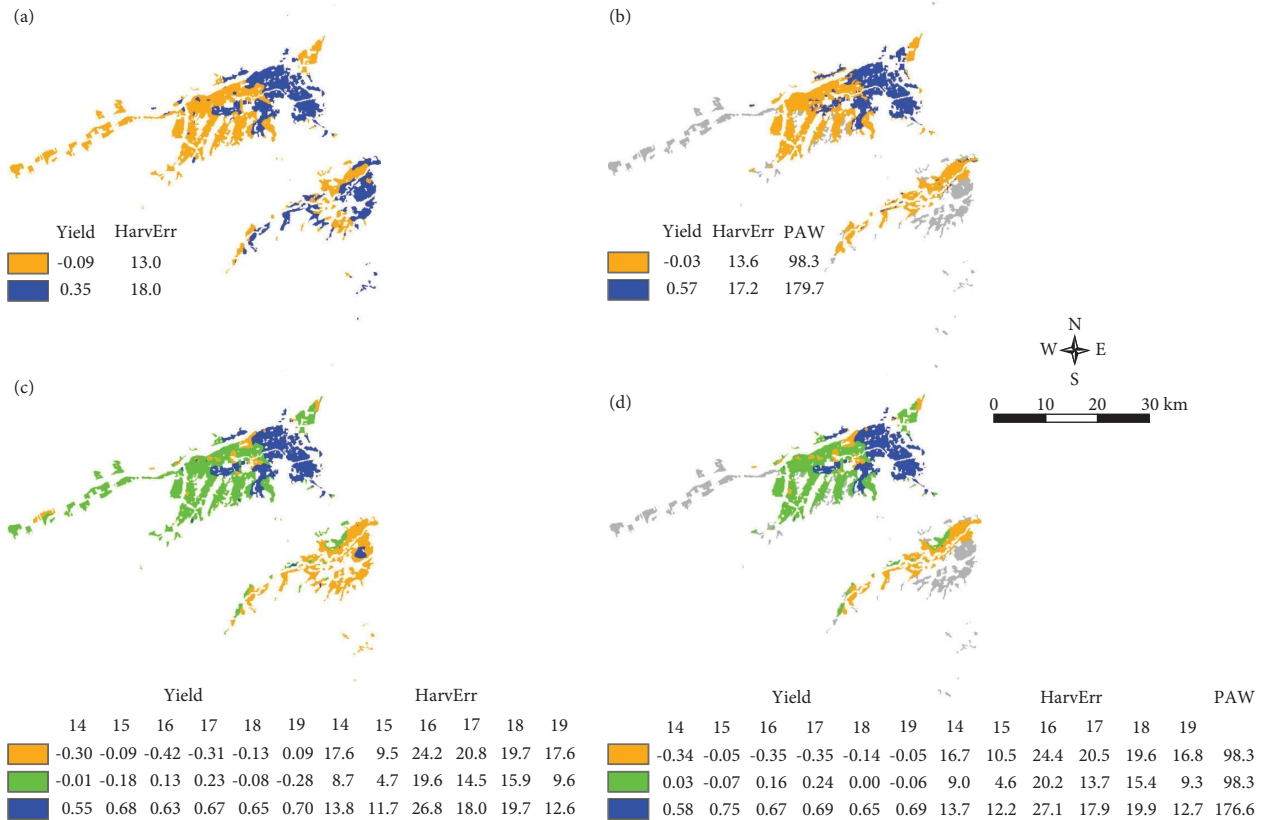


FIGURE 11: Results of clustering yield, the time between fruit reaching a total soluble solids (TSS) of 200 g/L and actual date of harvest (HarvErr), and profile available soil water (PAW). In (a) and (b), mean values of yield and HarvErr were used for the 2014–19 period, whereas in (c) and (d) data for the individual years were used. PAW was only included in the analysis in (b) and (d). Numbers in legends are cluster means. Note that the yield data (kg/m) were normalised ($\mu = 0, \sigma = 1$) on a per season basis with PAW data transformed to normal scores with the results then converted back to mm after clustering. The area shaded grey in (b) and (d) is the vineyard area for which soil data are not available.

Awatere area is no longer included in the analysis given the lack of soil information in that area. When the analysis is expanded to the individual years, three clusters are identified which more explicitly separate the Awatere from the Wairau, in particular highlighting the delay to harvest in the Awatere Valley (Figure 11(c)) and the association between higher yield and PAW and the likely impact of this higher yield in terms of later harvest. Of note is that PAW is not a discriminator between the clusters other than in regard to the high yielding strip in the lower Wairau (Figure 11(d)). Expanding this analysis to also include temperature (GDD) and harvest date (H_{rep} ; Figure 12) provides very similar results, albeit perhaps suggesting that silt content may be a better discriminator between the soils of the different clusters (Figure 12(b), Table 7). Since the patterns seen in Figures 12(b) and 12(c) are essentially the same, it seems clear that soil variation within the Marlborough region is not a primary driver of variation in vineyard performance, other than in terms of the impact of the high PAW and silt / low sand and stone soils of the lower Wairau. Excluding the Awatere Valley from the analysis (Figures 12(d)–12(f)) lends weight to this conclusion, with comparison between Figures 12(b) and 12(e) and

between 12(c) and 12(f) highlighting the distinction between the Wairau and Awatere Valleys.

4. Discussion

Much previous terroir research has focused on the delineation of so-called “homogeneous” terroir zones (e.g., [13, 18, 26]). However, just as research into vineyard variability and precision viticulture [54] has suggested that there is no such thing as a uniform vineyard, comparison of Figures 2, 3, 5, 6, and 8 with Figures 4 and 10–12 supports the view that, similarly, homogenous terroir units do not exist. Recognising the pragmatic need, across scales, to organise and classify variable data in a manner consistent with its intended use, we nevertheless consider the description of zones at any scale as “homogenous” (i.e., invariant) as unhelpful, especially if a part of the objective of the classification is to support process-based understanding of the complex functional relationships between terroir factors and the attributes of wine [26]; such relationships will, of course, be subject to error. Using a technique such as k -means clustering, it is certainly possible to identify clusters or subregions in which the range of variation within the clusters is substantially

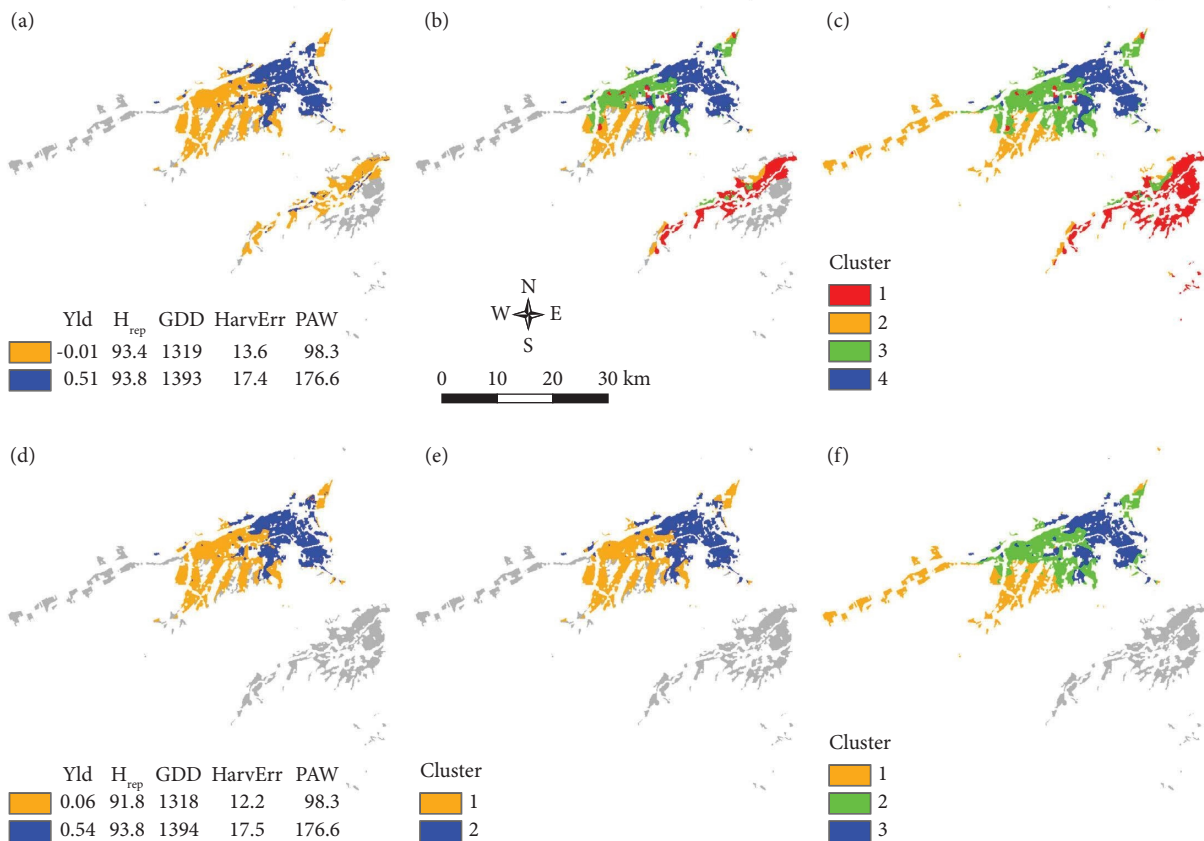


FIGURE 12: Results of clustering yield, harvest date (H_{rep}), season growing degree days (GDD), the time between fruit reaching a total soluble solids (TSS) of 200 g/L and actual date of harvest (HarvErr), and (a, b, d, e) soil properties. In (a–c), results are shown for the Marlborough region as a whole, whilst (d–f) are restricted to the Wairau Valley only. In (a) and (d), mean values of yield and HarvErr were used for the 2014–19 period along with profile available water (PAW), whereas data for the individual years were used in the other maps (b, c, e, f). No soil properties were included in (c, f) but in (b, e), PAW was included along with the contents of silt and stones. Numbers in legends to (a, d) are cluster means; the legends to (b, c, e, f) are presented in Table 7. Note that the yield data (kg/m) were normalised ($\mu = 0$, $\sigma = 1$) on a per season basis with soil property data transformed to normal scores with the results then converted back to mm (PAW) or % (silt, stones) after clustering. The area shaded grey in (a, b) is the vineyard area for which soil data are not available along with the Awatere Valley (d–f).

less than the variation in the region as a whole. This is especially the case in a region like Marlborough, given the observed differences between the Wairau and Awatere valleys (Figures 4, 11, and 12). Similarly, Bramley and Ouzman [24] demonstrated how the soils and climate of the Barossa and Eden Valleys were different, in spite of being part of the same Barossa Zone GI. The important difference between these New Zealand and Australian studies is in the incorporation of vineyard performance metrics in the analysis—something that was not possible in the Barossa example. Of course, neither study was able to incorporate chemical or sensory analysis of wines and it is to be hoped that future work will enable this so that the implications of biophysical variation for final wines might be better understood and relevant functional relationships [26] developed. Nonetheless, both studies speak to variation in terroir at the subregional scale, with the inclusion of vineyard performance metrics lending weight to consideration of the importance of observed biophysical variation in the landscapes in which grapes are grown and wine is made.

Aside from short-range variation, an obvious reason for heterogeneity within the identified terroir zones is variation in the specific production objectives associated with different vineyard blocks and resultant variation in grower management practices, such as trellis design, pruning to particular bud numbers, crop thinning, management of disease risk, irrigation, and the timing of decisions associated with these things. Timing of harvest and its interaction with winery logistics is also a potentially large source of confounding error, as might be vine age. One of the original motivations of this study [22] was to understand whether estimates of yield made in one location could be used to inform estimates needed in other locations, given the practicalities of deploying sensors that might assist with such estimation and/or associated labour to many different vineyards at optimal times. In spite of the constraints imposed by the variation in the nature and timing of grower and winemaker management and the other factors noted above, the fact that a marked and consistent spatial structure in the regional-scale variation in vineyard performance can be noted and interpreted in the context of variation in the

TABLE 7: Legends to Figures 12(b), 12(c), 12(e), and 12(f).

Year	Yield								H_{rep}								GDD (°)				HarvErr				PAW	Silt	Stones				
	'14	'15	'16	'17	'18	'19	'14	'15	'16	'17	'18	'19	'14	'15	'16	'17	'18	'19	'14	'15	'16	'17	'18	'19	'18	'19	(mm)	(%)	(%)		
<i>Figure 12(b)</i>																															
1	-0.37	-0.01	-0.44	-0.37	-0.13	0.00	101.2	95.0	101.5	103.8	91.6	92.2	1268	1263	1371	1275	1446	1408	17.8	10.8	23.9	20.9	19.5	17.7	98.3	40.9	19.8				
2	0.02	-0.16	0.20	0.42	0.04	0.15	94.6	91.5	99.3	103.0	91.5	86.7	1192	1190	1296	1176	1361	1345	7.6	4.1	18.9	14.9	16.6	10.0	98.3	31.2	39.5				
3	0.01	-0.07	0.13	0.07	0.03	-0.16	91.9	87.4	97.4	96.0	85.8	82.4	1291	1284	1383	1277	1455	1430	10.0	4.8	20.9	12.9	14.8	9.2	98.3	23.2	39.5				
4	0.50	0.68	0.58	0.59	0.50	0.53	93.7	93.3	102.3	99.1	89.4	84.8	1334	1319	1418	1331	1496	1461	13.7	12.3	27.4	18.3	20.0	12.7	176.6	44.8	0.0				
<i>Figure 12(c)</i>																															
1	-0.27	-0.06	-0.46	-0.26	-0.10	0.21	102.7	94.5	102.6	104.3	92.3	93.7	1256	1252	1357	1270	1436	1393	18.7	9.6	24.3	21.1	19.5	18.5							
2	-0.11	-0.35	0.06	0.28	-0.17	-0.49	95.5	93.1	99.5	106.1	92.9	87.5	1177	1168	1272	1147	1347	1335	7.4	4.6	18.0	16.7	17.5	10.3							
3	0.05	-0.03	0.18	0.14	0.06	-0.03	92.6	88.2	97.9	97.1	86.9	83.1	1278	1272	1371	1264	1442	1419	9.9	5.0	20.9	13.3	15.3	9.5							
4	0.51	0.68	0.60	0.61	0.56	0.56	93.8	93.5	102.4	99.0	89.3	84.9	1337	1322	1421	1334	1500	1464	14.0	12.6	27.6	18.4	20.1	12.9							
<i>Figure 12(e)</i>																															
1	0.07	-0.11	0.19	0.22	0.01	-0.04	92.6	89.2	98.3	98.8	88.2	84.0	1251	1246	1347	1235	1415	1396	8.7	4.8	20.3	13.7	15.6	9.5	98.3	23.2	39.5				
2	0.46	0.64	0.56	0.57	0.47	0.50	93.5	93.1	102.2	99.0	89.1	84.8	1336	1321	1419	1332	1498	1463	13.6	12.2	27.4	18.2	19.8	12.7	176.6	44.1	0.0				
<i>Figure 12(f)</i>																															
1	-0.04	-0.32	0.13	0.34	-0.18	-0.49	94.5	93.0	99.3	105.4	92.4	86.9	1189	1179	1282	1157	1357	1347	7.2	5.2	18.4	16.5	17.6	10.3							
2	0.08	-0.02	0.21	0.13	0.05	-0.03	92.0	88.2	98.1	96.6	86.4	82.5	1285	1279	1376	1272	1448	1425	9.8	5.5	21.4	13.2	15.2	9.1							
3	0.52	0.68	0.62	0.60	0.57	0.55	94.0	93.5	102.6	99.3	89.6	85.2	1336	1321	1421	1333	1499	1464	14.2	12.6	27.8	18.6	20.4	13.2							

All numbers are cluster means. See Figure 12 for further information.

winegrowing environment is important. It also lends weight to the idea that, given similarities in vineyard characteristics and management, estimates of yield in one vineyard could be useful estimators of yield in other vineyards in the same zone, just as at the within-vineyard scale, zone-based sampling may be useful [29, 55]. Understanding of such variation could also be used to inform winery logistics and associated harvesting decisions, especially when coupled to understanding of variation in fruit quality [56].

Variation in harvest date (Figure 3) is largely a result of variation in temperature-driven vine phenology (Figures 5 and 7). Thus, GDD decreases as one moves upstream in both the Wairau and Awatere valleys and into the southern valleys of the Wairau Plain. Overall, the Awatere Valley is cooler than the Wairau, inasmuch that the warmer areas comprise a proportionally smaller fraction of the grapegrowing area in the Awatere than is the case in the Wairau (Figure 5). However, the differences are arguably not large enough to explain the gross differences in vineyard performance between the two valleys. It is possible that some of the difference can be explained by differences in daily wind run and maximum wind speed observed between the valleys. While the Marlborough region is protected from southerly winds by the inland and seaward Kaikoura Mountains (maximum altitude 2885 m), the western Awatere valley has greater exposure. The Wairau Valley is protected by the Black Birch range of hills (maximum altitude 1500 m). The result is the average daily wind run and maximum daily wind speed are consistently 66 km/day and 5 km/h greater in the Awatere than the Wairau valleys (M. Trought—pers. comm.; <https://www.mrc.org.nz/blenheim-weather-station>, <https://www.mrc.org.nz/awatere-weather-station>), while the predominant wind direction in the Wairau Valley is westerly (at right angles to the canopies), and in the Awatere Valley it is mainly north-westerly or south-easterly, and therefore parallel to the row orientation [57]. Wind flow over grapevine canopies has received little previous attention. While wind direction across rows results in flow similar to a uniform canopy, spatial variability increases as the direction changes to become parallel to the rows, which generates greater turbulent kinetic energy and turbulent flux [58]. Similarly, the effect of wind on grapevines is poorly understood. Using artificial wind breaks, Dry et al. [59] and Bettiga et al. [60] reported increases in Cabernet Franc and Chardonnay yields, largely as a result of better budbreak and heavier bunches under sheltered conditions. Perhaps more wind in the Awatere is a part of the explanation for both its lower yield and later harvest dates? Conversely, variation in yield is associated with soil characteristics, at least in respect of the high yielding band of poorly drained, silty soils in the lower Wairau with higher PAW than in the rest of the region. Trought et al. [61] and Bramley et al. [62] have noted the impact of soil variation at the within-vineyard scale, with narrow silty hollows—a relic of the active Wairau floodplain—promoting higher vigour, but not higher yield [63], with this soil variation also having profound implications for grape and wine quality [56, 61]. At regional scale, the impact of texture was much less clear [64], with neither yield nor location within the Wairau Valley impacting on wine

sensory properties in spite of differences in soil texture; fruit from an Awatere Valley vineyard had a higher methoxypyrazine concentration and herbaceous characteristics than the Wairau wines, when fruit was harvested at the same soluble solids. Conversely, Jouanneau et al. [65] analysed wine aroma compounds in “research-scale” wines made from juices of variable soluble solids collected from seven predetermined subregions within Marlborough and noted a lower methoxypyrazine concentration in Awatere wines. Whilst they noted some subregional differences in wine chemistry, no attempt was made to relate these to fruit ripeness, which influences both thiol and methoxypyrazine concentrations [66], soil properties, or other biophysical attributes. However, the basis for the subregional delineation used by Jouanneau et al. [65] is not clear and is not supported by either the present analysis or the results of Trought et al. [64], which may explain why the distinctiveness of the subregional wines was equivocal. Similarly, the anecdotal local suggestion that Marlborough be divided into the Southern Valleys, Awatere and Wairau Valleys, which seemingly derives largely from the history of Marlborough’s development, does not appear to be otherwise underpinned by data, aside from the presence of more clayey soils in the Southern Valleys (Figure 8(g)). It is also a fact that the original plantings in the Southern Valleys used an E-W row orientation in contrast to the more common N-S orientation in the remainder of the region. However, while the impact of soil properties on higher yields in the lower Wairau is clear, the previous studies, along with the available soil data (Figure 8), have generally supported the view that soil properties are not a major driver of regional-scale terroir variation in Marlborough. Arguably, this might be due to the geologically young and relatively undifferentiated soils in the region—clay contents are generally low throughout (Figure 8(g))—coupled with the need for irrigation to support commercial viticulture.

Comparison of predicted (H_{est}) and actual (H_{rep}) harvest dates (i.e., HarvErr) adds some interesting observations. H_{est} (Figure 7(c)) is temperature-driven and reflects the date of flowering (Figure 7(a)). In contrast, H_{rep} (Figure 3) is more variable with the higher yielding strip in the lower Wairau being harvested relatively late, as indicated by values of HarvErr. Of course, actual harvest dates are influenced by factors other than temperature, such as vineyard management practices. Thus, the time from flowering to veraison is increased as yields increase [67] and the time from veraison to target soluble solids is strongly influenced by yield [68], although presumably due to variation in management practices, this is not evident in comparison of Figure 7(e) with Figures 2 and 4(b). Furthermore, notwithstanding winery requirements for fruit that is fit for intended end-use [66], many harvest management decisions will be influenced by the proximity of the harvester, particularly in wetter vintages when disease risk is an important determinant of quality (A Naylor, Pernod Ricard NZ—pers. comm.). Proximity of the harvester could arguably be one reason for the generally later harvests in the Awatere Valley compared to the Wairau Valley where the majority of the wineries are located.

Finally, it is interesting to note that yields in the Rapaura area of the Central Wairau are lower than adjacent areas with similar soils. This area was the first to be planted within the Marlborough region and so contains the oldest vines with potentially greater numbers succumbing to trunk disease [69] than in other parts of the region.

Previous work has led to differing conclusions as to the importance of elevation and topographic variation to terroir at different scales. In the Margaret River region of Australia, elevation did not contribute usefully to delineation of subregions within the GI [30] because Margaret River vineyards neither occur at locally characteristic elevations nor have locally characteristic slopes or aspects. Similarly, Biss [70] argued that the impact of topography on wine quality in the Chablis region of France was equivocal, yet in more mountainous areas such as the Italian Tyrol, topography may clearly have a major impact [71]. Likewise, in the much less mountainous Barossa Zone GI, topographic variation was seen to play an important role in both delineating the Barossa and Eden Valleys, and also in explaining some of the subregional differentiation within the Barossa Valley [24] and, at property scale, within the Eden Valley [31]. The aforementioned impact of soil property variation at the within-vineyard scale in Marlborough on vine vigour and fruit quality is directly attributable to topographic variation as demonstrated by Bramley et al. [62] and Trought and Bramley [56]. In the Wairau Valley, the active floodplain is characterised by a pattern of silty hollows (Wairau series) dissecting the sandier, more gravelly soils (Rapaura series) that predominate [72]. These soil series represent approximately 3130 ha of the Wairau Plains, but the effects of the silty hollows are not evident at the scale at which the soil property data are available (Figure 8) and the underpinning soil survey was conducted; the 1 ha base raster used for the

present mapping also presents a difficulty in this regard. The hollows run predominantly in an approximately east-west direction, while row orientation is generally north-south. Thus, the full range of within-vineyard variation is commonly expressed in a single row. These scale effects (regional vs. within-vineyard) are likely the reason for the fact that, in the present study, soil properties did not clearly impact on regional-scale variation in vineyard performance beyond the high yielding part of the lower Wairau. Much the same conclusion can be drawn in respect of topographic variation; there is a mismatch between the high resolution (1 m) LINZ DEM and the resolution of other available data which is why, aside from the hills which enclose the Wairau and Awatere Valleys, topography is not evidently a strong driver of regional terroir variation (Figure 13). Further research aimed at understanding how to integrate terroir expression at different scales would therefore be valuable, especially in respect of topography and soils.

Finally, a key reason for Australian interest in sub-regionalisation is the belief that it may promote marketing advantages to wine producers in different parts of Australia's (generally large) GIs through the ability to demonstrate the 'distinctiveness' of their wines and so use their terroir as the basis of the 'story' used to sell them. However, Charters et al. [73] cautioned against the difficulty of promoting "territorial" brands when, understandably, most producers attach primacy to their proprietary brands. Organisations with oversight of the territorial brand are also generally distinct from individual producers. The observation of differences between the Wairau and Awatere Valleys is therefore interesting given that 'Marlborough Sauvignon Blanc' has developed a significant international presence in the wine trade. In other words, for reasons of marketing, Marlborough producers might *not* wish to pursue subregionalisation, even though Table 5 and Figures 4, 11(c), 12(b) and 12(c) present a strong justification as

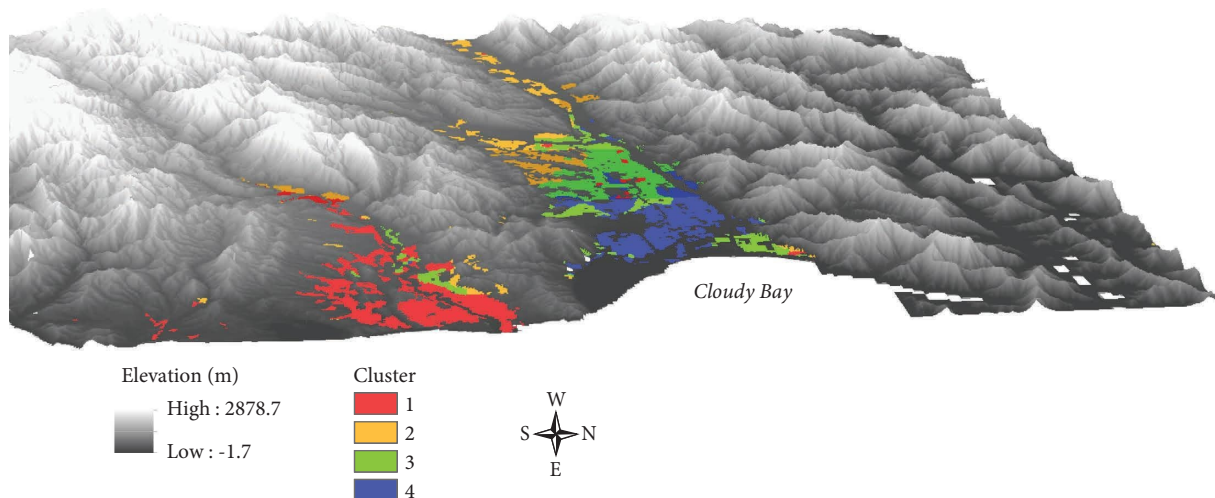


FIGURE 13: Topographic variation in the Marlborough region as seen looking approximately east to west. Also shown is the cluster solution shown in Figure 12(c) derived from annual (2014–19) measurements of the yield and harvest date of Sauvignon Blanc, season-growing degree days and the difference between actual harvest date and the date on which the fruit was predicted to reach Total Soluble Solids of 200 g/L. See Table 7 for the cluster means. Note that the position of the north arrow is approximate only and that elevation has been exaggerated by a factor of 2.5 relative to the horizontal.

to how they could. Conversely, Pinu et al. [74] used a metabolomics approach to assess and compare 400 Sauvignon Blanc juice samples from around New Zealand, 75% of which came from Marlborough. They concluded that seasonal variation was of greater importance than geography in discriminating the characteristics of the samples, although they did not present a within-Marlborough analysis of the Marlborough samples. Nonetheless, perhaps Marlborough presents a case where, contrary to Charters et al. [73], the territorial brand is stronger than, or at least as strong as, its proprietary brands with consistency of style achieved by blending wines from various subregions of Marlborough. If so, the present study lends weight to the idea [25, 31] that understanding terroir has more to offer the optimisation of grape and wine production systems than to being used for marketing objectives.

5. Conclusions

Analytical techniques that have previously been applied to studies of within-vineyard variability and the development of precision viticulture are valuable tools in assessing regional-scale variation in biophysical variation and vineyard performance, which might impact on and reflect a regional/subregional terroir. Their use in the present study strongly suggests that the Marlborough region has a characteristically variable Sauvignon Blanc production with crop phenology and harvest date strongly influenced by variation in temperature, and yield variation impacted by soil properties, albeit less distinctly than is apparent at the within-vineyard scale. A key part of this is the apparent distinction between the Wairau and Awatere Valleys which, hitherto, have been considered together as parts of a single Marlborough region. The results from this study, which to the knowledge of the authors is the first quantitative integration of vineyard performance and biophysical metrics as a means of evaluating terroir, has potentially important implications for the management of both vineyard operations and winery logistics, for wine marketing and potentially, for whole-of-industry planning around expansion or contraction. It also lends weight to the idea that estimates of vineyard performance in some parts of the region may be used to predict performance in others. Accordingly, a coordinated collection of vineyard performance metrics is encouraged for all regions to better understand their terroir—especially as most grapegrowing businesses collect such data as a matter of course.

Data Availability

The vineyard performance data used in this study are confidential and are not available. Details of the soil and climate data used are provided within the article.

Disclosure

The present address of G. J. Grealish is CSIRO, Black Mountain Science and Innovation Park, Canberra, ACT 2601, Australia.

Conflicts of Interest

The authors declare that they have no conflicts of interest.

Acknowledgments

This work was jointly funded by CSIRO, the University of Canterbury, Manaaki Whenua—Landcare Research, New Zealand Plant and Food Research, Innovative Winegrowing, and the New Zealand Ministry of Business Innovation and Employment (MBIE) through an ‘Endeavour grant’ provided to Lincoln Agritech Ltd. (MBIE contract LVLX1601). The authors are most grateful to the Marlborough District Council for providing access to their coverage of vineyard holdings, and in particular, to the following wine companies who contributed data for the work: Babich, Cloudy Bay, Constellation Brands, Delegat, Forrest, Giesen, Indevin, Pernod Ricard, Treasury Wine Estates, The Marlborough Grape Growers Cooperative, The Wine Portfolio, Villa Maria, Weta, Whitehaven, Wither Hills, and Yealands. Soil data were obtained from Manaaki Whenua—Landcare Research. Drs Amber Parker (Lincoln University, New Zealand) and Brent Sams (E&J Gallo Winery, USA) made valuable comments on a previous draft of the manuscript.

References

- [1] G. Seguin, “Terroirs and pedology of wine growing,” *Experientia*, vol. 42, no. 8, pp. 861–873, 1986.
- [2] C. van Leeuwen, P. Friant, X. Choné, O. Tregoat, S. Koundouras, and D. Dubourdieu, “Influence of climate, soil and cultivar on terroir,” *American Journal of Enology and Viticulture*, vol. 55, no. 3, pp. 207–217, 2004.
- [3] C. van Leeuwen, J.-C. Barbe, P. Darriet et al., “Recent advancements in understanding the terroir effect on aromas in grapes and wines,” *Oeno One*, vol. 54, no. 4, pp. 985–1006, 2020.
- [4] C. van Leeuwen, J.-C. Barbe, P. Darriet et al., “Aromatic maturity is a cornerstone of terroir expression in red wine,” *Oeno One*, vol. 56, no. 2, pp. 335–351, 2022.
- [5] C. van Leeuwen and G. Seguin, “The Concept of terroir in viticulture,” *Journal of Wine Research*, vol. 17, pp. 1–10, 2006.
- [6] P. R. Dry, “Understanding the components of terroir,” in *Proceedings of the 16th Australian Wine Industry Conference*, pp. 39–44, Adelaide, South Australia, July, 2016.
- [7] International Organisation of Vine and Wine, “General assembly of the international organisation of vine and wine,” 2010, <https://www.oiv.int/en/technical-standards-and-documents/resolutions-of-the-oiv/viticulture-resolutions>.
- [8] J. Goode, *The Science of Wine: From Vine to Glass*, University of California Press, Berkeley, CA, USA, 2005.
- [9] New Zealand Wine, “Tohu whenua series,” 2019, <https://www.nzwine.com/en/media/our-people/tohu-whenua/>.
- [10] Tohu Wines, “Tūrangawaewae—A place to stand,” 2019, <https://www.tohuwines.co.nz/blog/25/6/2019turangawaewae>.
- [11] C. Pickard, “We are the land and the land is us: indigenous Māori winemakers are guardians of New Zealand terroir,” *Wine Enthusiast magazine*, 2022, <https://www.winemag.com/2022/03/02/indigenous-maori-winemakers-new-zealand/>.
- [12] E. Vaudour, M.-C. Girard, L.-M. Bremond, and L. Lurton, “Spatial terroir characterization and grape composition in the









- Southern Côtes-du-Rhône vineyard (Nyons-Valreas Basin),” *OENO One*, vol. 32, no. 4, pp. 169–182, 1998.
- [13] E. Vaudour, V. A. Carey, and J. M. Gilliot, “Digital zoning of South African viticultural terroirs using bootstrapped decision trees on morphometric data and multitemporal SPOT images,” *Remote Sensing of Environment*, vol. 114, no. 12, pp. 2940–2950, 2010.
- [14] G. V. Jones, N. Snead, and P. Nelson, “Geology and Wine 8. Modelling viticultural landscapes: a GIS analysis of the terroir potential in the Umpqua Valley of Oregon,” *Geoscience Canada*, vol. 31, pp. 167–178, 2004.
- [15] V. A. Carey, E. Archer, G. Barbeau, and D. Saayman, “Viticultural terroirs in Stellenbosch, South Africa. III. Spatialisation of vinicultural and oenological potential for Cabernet-Sauvignon and Sauvignon Blanc by means of a preliminary model,” *OENO One*, vol. 43, pp. 1–12, 2009.
- [16] A. Bonfante, A. Basile, G. Langella, P. Manna, and F. Terribile, “A physically oriented approach to analysis and mapping of terroirs,” *Geoderma*, vol. 167–168, pp. 103–117, 2011.
- [17] A. Bonfante, E. Monaco, G. Langella et al., “A dynamic viticultural zoning to explore the resilience of terroir concept under climate change,” *Science of the Total Environment*, vol. 624, pp. 294–308, 2018.
- [18] H. Fraga, R. Costa, and J. A. Santos, “Multivariate clustering of viticultural terroirs in the Douro winemaking region,” *Ciência e Técnica Vitivinícola*, vol. 32, no. 2, pp. 142–153, 2017.
- [19] M. Lacorde, “Assessing the environmental characteristics of the Margaret River wine region, Australia: potential new geographical indication sub-units,” *International Journal of Applied Geospatial Research*, vol. 10, no. 3, pp. 1–24, 2019.
- [20] J. Robinson and J. Harding, *The Oxford Companion to Wine*, Oxford University Press, Oxford, UK, 4th edition, 2015.
- [21] Council of the European Union, “Council Regulation (EC) No 510/2006 of 20 March 2006,” *On the protection of Geographical Indications and Designations of Origin for Agricultural Products and Foodstuffs*, Council of the European Union, Brussels, Belgium, 2006.
- [22] R. G. V. Bramley, J. Ouzman, and M. C. T. Trought, “Making sense of a sense of place—Precision Viticulture approaches to the analysis of terroir at different scales,” *Oeno One*, vol. 54, no. 4, pp. 903–917, 2020.
- [23] J. Ballester, “In search of the taste of terroir: a challenge for sensory science,” in *Proceedings of the 9th International Terroir Congress*, Reims, France, November, 2020, <https://ives-openscience.eu/6673/>.
- [24] R. G. V. Bramley and J. Ouzman, “Underpinning terroir with data: on what grounds might subregionalisation of the Barossa Zone geographical indication be justified?” *Australian Journal of Grape and Wine Research*, vol. 28, no. 2, pp. 196–207, 2022.
- [25] L. Brillante, A. Bonfante, R. G. V. Bramley, J. Tardaguila, and S. Priori, “Unbiased scientific approaches to the study of terroir are needed,” *Frontiers in Earth Science*, vol. 8, Article ID 539377, 2020.
- [26] A. Bonfante and L. Brillante, “Terroir analysis and its complexity,” *Oeno One*, vol. 56, no. 2, pp. 375–388, 2022.
- [27] R. G. V. Bramley, J. Ouzman, and P. K. Boss, “Variation in vine vigour, grape yield and vineyard soils and topography as indicators of variation in the chemical composition of grapes, wine and wine sensory attributes,” *Australian Journal of Grape and Wine Research*, vol. 17, no. 2, pp. 217–229, 2011.
- [28] R. G. V. Bramley, T. E. Siebert, M. J. Herderich, and M. P. Krstic, “Patterns of within-vineyard spatial variation in the ‘pepper’ compound rotundone are temporally stable from year to year,” *Australian Journal of Grape and Wine Research*, vol. 23, no. 1, pp. 42–47, 2017.
- [29] T. Proffitt, R. Bramley, D. Lamb, and E. Winter, *Precision Viticulture—A new era in Vineyard Management and Wine Production*, Winetitles, Adelaide, Australia, 2006.
- [30] R. G. V. Bramley and P. Gardiner, “Underpinning terroir with data: a quantitative analysis of biophysical variation in the Margaret River region of Western Australia,” *Australian Journal of Grape and Wine Research*, vol. 27, no. 4, pp. 420–430, 2021.
- [31] R. G. V. Bramley, “Vineyard variability and terroir – making sense of a sense of place,” in *Proceedings of the 16th Australian Wine Industry Conference*, K. S. Beames, E. M. C. Robinson, P. R. Dry, and D. L. Johnson, Eds., pp. 45:51, Adelaide, South Australia, July, 2016.
- [32] B. Minasny, A. B. McBratney, and B. M. Whelan, *VESPER Version 1.62*, University of Sydney, Sydney, Australia, 2005, <https://precision-agriculture.sydney.edu.au/resources/software/download-vesper/>.
- [33] W. C. Skamarock, J. B. Klemp, J. Dudhia et al., “A description of the advanced research wrf model version 4.3,” Technical Note 556 (No. NCAR/TN-556+STR), National Center for Atmospheric Research (NCAR), Boulder, CO, USA, 2021.
- [34] A. Sturman, P. Zawar-Reza, I. Soltanzadeh et al., “The application of high-resolution atmospheric modelling to weather and climate variability in vineyard regions,” *Oeno One*, vol. 51, no. 2, pp. 99–105, 2017.
- [35] I. Soltanzadeh, V. Bonnardot, A. Sturman, H. Quénot, and P. Zawar-Reza, “Assessment of the ARW-WRF model over complex terrain: the case of the Stellenbosch Wine of Origin district of South Africa,” *Theoretical and Applied Climatology*, vol. 129, no. 3–4, pp. 1407–1427, 2017.
- [36] R. Le Roux, M. Katurji, P. Zawar-Reza et al., “A fine-scale approach to map bioclimatic indices using and comparing dynamical and geostatistical methods,” in *Proceedings of the 9th International Terroir Congress*, pp. 53–58, Willamette Valley, OR, USA, July 2016.
- [37] R. Le Roux, M. Katurji, P. Zawar-Reza, H. Quénot, and A. Sturman, “Comparison of statistical and dynamical downscaling results from the WRF model,” *Environmental Modelling & Software*, vol. 100, pp. 67–73, 2018.
- [38] R. Le Roux, M. Katurji, P. Zawar-Reza, H. Quénot, and A. Sturman, “Analysis of spatio-temporal bias of Weather Research and Forecasting temperatures based on weather pattern classification,” *International Journal of Climatology*, vol. 39, no. 1, pp. 89–100, 2019.
- [39] A. K. Parker, I. G. De Cortázar-Atauri, C. Van Leeuwen, and I. Chuine, “General phenological model to characterise the timing of flowering and veraison of *Vitis vinifera* L.,” *Australian Journal of Grape and Wine Research*, vol. 17, no. 2, pp. 206–216, 2011.
- [40] A. Parker, I. G. De Cortázar-Atauri, I. Chuine et al., “Classification of varieties for their timing of flowering and veraison using a modelling approach: a case study for the grapevine species *Vitis vinifera* L.,” *Agricultural and Forest Meteorology*, vol. 180, pp. 249–264, 2013.
- [41] A. K. Parker, T. Schulman, A. Sturman et al., “Grapevine phenology of the Marlborough region,” in *Proceedings of the 9th International Terroir Congress*, vol. 2, pp. 105–109, Corvinus University of Budapest, Budapest, Hungary, 2014.
- [42] A. K. Parker, T. Schulmann, A. Sturman et al., “Understanding flowering of Sauvignon blanc in the Marlborough region, New Zealand, using high-resolution weather forecasting and the grapevine flowering véraison model,” in

- Proceedings of the 19th International Meeting of Viticulture GIESCO*, vol. 1, pp. 271–276, Pech Rouge, Montpellier, France, 2015.
- [43] A. K. Parker, I. García de Cortázar-Atauri, M. C. T. Trought et al., “Adaptation to climate change by determining grapevine cultivar differences using temperature-based phenology models,” *Oeno One*, vol. 54, pp. 955–974, 2020.
- [44] A. K. Parker, I. García de Cortázar-Atauri, L. Gény et al., “Temperature-based grapevine sugar ripeness modelling for a wide range of *Vitis vinifera* L. cultivars,” *Agricultural and Forest Meteorology*, vol. 285–286, Article ID 107902, 2020.
- [45] P. Roudier, O. R. Burge, S. J. Richardson, J. K. McCarthy, G. J. Grealish, and A.-G. Ausseil, “National scale 3D mapping of soil pH using a data augmentation approach,” *Remote Sensing*, vol. 12, no. 18, p. 2872, 2020.
- [46] T. H. Webb and L. R. Lilburne, *Criteria for Defining the Soil Family and Soil Sibling: The Fourth and Fifth Categories of the New Zealand Soil Classification*, Manaaki Whenua Press, Lincoln, New Zealand, 2nd edition, 2011.
- [47] J. A. S. Hall, D. J. Maschmedt, and N. B. Billing, “The soils of southern south australia,” in *The South Australian Land and Soil Book Series Geological Survey of South Australia, Bulletin 56*, vol. 1, Government of South Australia, Adelaide, Australia, 2009.
- [48] T. S. Mills, *Relations Among Geology, Soil Type and Sauvignon Blanc Vineyard Variation in Marlborough, New Zealand*, Auckland University, Auckland, New Zealand, 2006.
- [49] S. J. McNeill, L. R. Lilburne, S. Carrick, T. H. Webb, and T. Cuthill, “Pedotransfer functions for the soil water characteristics of New Zealand soils using s-map information,” *Geoderma*, pp. 96–110, 2018.
- [50] J. D. G. Milne, B. Clayden, P. L. Singleton, and A. D. Wilson, *Soil Description Handbook*, Manaaki Whenua Press, Lincoln, New Zealand, 1995.
- [51] L. B. de Guenni, “Normal scores,” in *International Encyclopedia of Statistical Science*, M. Lovric, Ed., Springer, Berlin, Heidelberg, 2011.
- [52] SAS Institute Inc, *Cubic Clustering Criterion*, SAS Technical Report A-108, SAS Institute Inc, Cary, NC, USA, 1983.
- [53] J. A. Taylor, A. B. McBratney, and B. M. Whelan, “Establishing management classes for broadacre agricultural production,” *Agronomy Journal*, vol. 99, no. 5, pp. 1366–1376, 2007.
- [54] R. G. V. Bramley, “Precision Viticulture: managing vineyard variability for improved quality outcomes,” in *Managing Wine Quality*, A. G. Reynolds, Ed., vol. 1, pp. 541–586, Elsevier, Amsterdam, The Netherlands, 2nd edition, 2022.
- [55] M. Araya-Alman, C. Leroux, C. Acevedo-Opazo et al., “A new localized sampling method to improve grape yield estimation of the current season using yield historical data,” *Precision Agriculture*, vol. 20, no. 2, pp. 445–459, 2019.
- [56] M. C. T. Trought and R. G. V. Bramley, “Vineyard variability in Marlborough, New Zealand: characterising spatial and temporal changes in fruit composition and juice quality in the vineyard,” *Australian Journal of Grape and Wine Research*, vol. 17, no. 1, pp. 79–89, 2011.
- [57] P. R. Chappell, “The climate and weather of Marlborough,” *NIWA Science and Technology Series*, vol. 69, National Institute of Water and Atmospheric Research, Auckland, New Zealand, 2nd edition, 2016, <https://docs.niwa.co.nz/library/public/NIWASTs69.pdf>.
- [58] A. Chahine, S. Dupont, C. Sinfort, and Y. Brunet, “Wind-flow dynamics over a vineyard,” *Boundary-Layer Meteorology*, vol. 151, no. 3, pp. 557–577, 2014.
- [59] P. R. Dry, S. Reed, and G. Potter, “The effect of wind on the performance of Cabernet Franc grapevines. Australian temperate fruits review conference,” *Acta Horticulturae*, vol. 240, pp. 143–146, 1988.
- [60] L. J. Bettiga, N. K. Dokoozlian, and L. E. Williams, “Windbreaks improve the growth and yield of Chardonnay grapevines grown in a cool climate,” in *Proceedings of the 4th International Symposium on Cool Climate Viticulture and Enology*, pp. 43–46, Rochester, NY, USA, December 1996.
- [61] M. C. T. Trought, R. Dixon, T. Mills et al., “The impact of differences in soil texture within a vineyard on vine vigour, vine earliness and juice composition,” *OENO One*, vol. 42, no. 2, pp. 67–72, 2008.
- [62] R. G. V. Bramley, M. C. T. Trought, and J.-P. Praat, “Vineyard variability in Marlborough, New Zealand: characterising variation in vineyard performance and options for the implementation of Precision Viticulture,” *Australian Journal of Grape and Wine Research*, vol. 17, no. 1, pp. 72–78, 2011.
- [63] R. G. V. Bramley, J. Ouzman, M. C. T. Trought, S. M. Neal, and J. S. Bennett, “Spatio-temporal variability in vine vigour and yield in a Marlborough Sauvignon Blanc vineyard,” *Australian Journal of Grape and Wine Research*, vol. 25, no. 4, pp. 430–438, 2019.
- [64] M. C. T. Trought, R. A. Agnew, J. Bennett, K. Stronge, W. V. Parr, and M. Greven, “Soils, climate and vine management: their influence on Marlborough Sauvignon Blanc wine style,” in *Proceedings of 8th International Terroir Congress*, Open Science, Soave, Italy, 2010, <https://ives-openscience.eu/9064/>.
- [65] S. Jouanneau, R. J. Weaver, L. Nicolau, M. Herbst-Johnstone, F. Benkwitz, and P. A. Kilmartin, “Subregional survey of aroma compounds in Marlborough Sauvignon Blanc wines,” *Australian Journal of Grape and Wine Research*, vol. 18, no. 3, pp. 329–343, 2012.
- [66] B. Pineau, M. C. T. Trought, K. Stronge, M. K. Beresford, M. W. Wohlers, and S. R. Jaeger, “Influence of fruit ripeness and juice chaptalisation on the sensory properties and degree of typicality expressed by Sauvignon Blanc wines from Marlborough, New Zealand,” *Australian Journal of Grape and Wine Research*, vol. 17, no. 3, pp. 358–367, 2011.
- [67] A. K. Parker, R. W. Hofmann, C. van Leeuwen, A. R. G. McLachlan, and M. C. T. Trought, “Leaf area to fruit mass ratio determines the time of veraison in Sauvignon blanc and Pinot noir grapevines,” *Australian Journal of Grape and Wine Research*, vol. 20, no. 3, pp. 422–431, 2014.
- [68] A. K. Parker, R. W. Hofmann, C. Van Leeuwen, A. R. G. McLachlan, and M. C. T. Trought, “Manipulating the leaf area to fruit mass ratio alters the synchrony of total soluble solids accumulation and titratable acidity of grape berries,” *Australian Journal of Grape and Wine Research*, vol. 21, no. 2, pp. 266–276, 2015.
- [69] M. Sosnowski, D. Mundy, P. Vanga, and M. Ayres, “Practical management of grapevine trunk diseases NZ wine project outcomes,” 2018, <https://www.rd2.co.nz/wp-content/uploads/2018/01/Mark-Sosnowski-Practical-management-of-grapevine-trunk-diseases.pdf>.
- [70] A. J. Biss, “Impact of vineyard topography on the quality of Chablis wine,” *Australian Journal of Grape and Wine Research*, vol. 26, no. 3, pp. 247–258, 2020.
- [71] C. Ferretti, “A new geographical classification for vineyards tested in the South Tyrol wine region, northern Italy, on Pinot Noir and Sauvignon Blanc wines,” *Ecological Indicators*, vol. 108, Article ID 105737, 2020.

- [72] S. N. Rae and C. G. Tozer, *Land and Soil Resources*, Nelson-Marlborough Regional Council, Blenheim, New Zealand, 1990.
- [73] S. Charters, R. Mitchell, and D. Menival, "The territorial brand in wine," in *Proceedings of the 6th International Conference of the Academy of Wine Business Research*, Bordeaux Management School, Bordeaux, France, June 2011.
- [74] F. R. Pinu, S. Tumanov, C. Grose et al., "Juice Index: an integrated Sauvignon Blanc grape and wine metabolomics database shows mainly seasonal differences," *Metabolomics*, vol. 15, no. 1, p. 3, 2019.

Research Article

The Role of Potent Thiols in “Empyreumatic” Flint/Struck-Match/Mineral Odours in Chardonnay Wine

Damian Espinase Nandorfy ^{1,2}, **Tracey Siebert**,¹ **Eleanor Bilogrevic** ¹, **Desireé Likos** ¹, **Flynn Watson**,¹ **Sheridan Barter** ¹, **Lisa Pisaniello**,¹ **Allie Kulcsar**,¹ **Robert A. Shellie** ², **Russell Keast** ², **Leigh Francis** ¹, and **Marlize Bekker** ¹

¹The Australian Wine Research Institute, P.O. Box 197, Glen Osmond, SA 5064, Australia

²CASS Food Research Centre, School of Exercise and Nutrition Sciences, Deakin University, 221 Burwood Highway, Burwood, Vic 3125, Australia

Correspondence should be addressed to Damian Espinase Nandorfy; damian.espinasenandorfy@awri.com.au

Received 17 January 2023; Revised 22 June 2023; Accepted 14 July 2023; Published 31 July 2023

Academic Editor: Anthony Saliba

Copyright © 2023 Damian Espinase Nandorfy et al. This is an open access article distributed under the Creative Commons Attribution License, which permits unrestricted use, distribution, and reproduction in any medium, provided the original work is properly cited.

Background and Aims. A wide range of Chardonnay styles exist on the market, from fruit-forward examples to wines displaying “empyreumatic” aromas such as flint, smoky, mineral, and struck-match. The thiols 2-furylmethanethiol and phenylmethanethiol have been linked to these aromas, and this study aimed to determine the contribution of these compounds to specific sensory properties in Chardonnay wines, as well as the consumer acceptance of wine displaying “empyreumatic” aromas. **Methods and Results.** Twenty-four Australian and New Zealand Chardonnay wines were selected for volatile analysis and quantitative sensory descriptive analysis. Consumer liking of a subset of six wines was also determined, and a further sensory study involving additions of the thiols to a base wine was conducted. Partial least squares regression showed that flint/struck-match/mineral aromas were related to 2-furylmethanethiol concentration with phenylmethanethiol less well associated. The odorant addition study confirmed that 2-furylmethanethiol directed flint/struck-match/mineral aromas and exerted strong suppression of other aromas while phenylmethanethiol played a lesser role. Consumer acceptance ($n = 92$) was overall lower for wines displaying high flint/struck-match/mineral aromas, although cluster analysis of the liking scores identified a sizeable consumer group (33%) who preferred wines with this attribute. **Conclusions.** The potent thiol 2-furylmethanethiol was indicated to be the primary contributor to flint/struck-match/mineral aromas in Chardonnay wines, with phenylmethanethiol playing a subordinate role. **Significance of the Study.** Increased concentration of 2-furylmethanethiol and the conferred “empyreumatic” odours should be carefully considered when producing wine styles to appeal to consumers.

1. Introduction

Australian wines made from the Chardonnay cultivar represent a high proportion of domestic and exported white wines. They are produced in most regions with varied winemaking techniques and can display a wide range of sensory properties. Of these styles, so-called “empyreumatic” aromas are common for some Chardonnay styles, particularly for barrel-aged or barrel-fermented Chardonnay. The odour category of empyreumatic was introduced to the fragrance lexicon by Dutch scientist H. Zwaardemaker to

describe smoky and burnt odours [1]. Although this category is not commonly used in wine science literature outside of Europe, it has been used to describe wines, often oaked white wines, which display aromas reminiscent of smoke, gun-powder/gun flint, minerals, roasted coffee, toast, brioche, or the smoky/sulfidic odour of a struck-match [2, 3].

Links between Chardonnay chemical composition and specific sensory properties have been reported for several compounds: thiols with tropical aromas [4]; acetate esters and terpenes with fruity and floral notes; volatile phenols with oaky nuances [5]; pyrroles and pyrrolemethanethiols

with hazelnut-like aromas [6]; fatty acid ethyl and acetate esters as well as lactones with stone fruit aromas [7, 8]; higher alcohols and floral notes [9]; aldehydes and oxidation related flavour deterioration [10]. Although these studies have shown evidence of relationships using winemaking experiments, correlation tests, or regression approaches, wine compounds are in many cases ubiquitous and co-correlated, and these associations do not definitively imply chemical cause and sensory effect.

Regarding “empyreumatic” odours, two polyfunctional thiols have been linked to this aroma category, phenylmethanethiol (benzenemethanethiol and benzyl mercaptan) [2] and 2-furylmethanethiol (furan-2-ylmethanethiol, 2-furanmethanethiol, or furfuryl thiol) [3], in both still Chardonnay table wines and Champagne wines.

Sensory detection threshold testing of compounds likely to be important to Chardonnay has been conducted with 2-furylmethanethiol [11] and phenylmethanethiol [2], as well as for 4-methyl-4-sulfanylpentan-2-one [12], stereoisomers of oak lactone [13], 1-methylpyrrole-2-methanethiol, and 1-ethylpyrrole-2-methanethiol [6] which allow for the comparison of the potency of aroma compounds. Knowledge of the sensory detection threshold of a particular compound has been invaluable to gauge if a compound is likely to contribute to wine aroma and flavour at the concentration range found naturally, but again these values lack the ability to characterise the particular odour quality or intensity in a wine. Beyond “impact odorants,” the demonstration of causation is further complicated by complex interactions which may occur at the chemical, sensory receptor, and cognitive levels to suppress, augment, or otherwise alter sensory perception.

Other approaches exploring perceptual interactions by capturing changes in sensory quality and intensity are robust sensory methods such as quantitative descriptive analysis (QDA) [14] coupled with tests such as reconstitution/omission and odorant spiking experiments [15].

The steps of analytical identification, correlation of chemical concentration with sensory properties followed by causally qualifying sensory effects, together contribute in explaining observed phenomena within a product such as wine. These types of experimentation, however, cannot determine if a particular sensory character, directed by a particular compound, might be important in influencing consumer acceptance or purchase behaviour. Often this question is left unresolved; however, wine is a consumer product and presumably, a wine’s aroma, taste, and mouthfeel contribute strongly to acceptance and purchase behaviour, alongside important marketing cues such as price, packaging, labelling, and advertising. Consumer blind testing can involve investigation of the influence of a particular compound, such as “consumer rejection threshold” methodology reported for 2,4,6-trichloroanisole (TCA) [16], 1,3,3-trimethyl-2-oxabicyclo[2.2.2]octane (1,8-cineole) [17], and 1,1,6-trimethyl-1,2-dihydronaphthalene (TDN) [18]. Consumer acceptance testing, however, can also evaluate the wine styles on the market such as the previous study by Saliba et al. [19] which identified an overall preference of Australian consumers for fruity Chardonnay styles with

negligible oak influence. In contrast to “empyreumatic” wine styles, these more fruit-forward Chardonnay styles, preferred by consumers, were found to display “peach” aromas with some sweetness. Using odour addition studies, the ethyl esters conferring “peach” aroma in Chardonnay have only recently been demonstrated [20], while the source of “sweetness” in sugar dry white wines is not well understood. In dry red wines, the residual amino acid proline has been shown to increase “sweetness,” “viscosity,” and fruit flavours [21].

Only a few studies have investigated the consumer response to wines displaying empyreumatic aromas such as those reminiscent of “smoky,” “struck-match,” or “flint.” Smoke-related compounds such as guaiacol, cresols, and their glycoconjugates have been demonstrated to cause the “smoky” aroma and flavour of wines affected by bushfires [22]. Of these, guaiacol at high and low concentration has been reported to detract from overall consumer acceptance scores, but some consumer segmentation in preference was also reported [23]. Regarding “struck-match” or “flint” aromas, Capone et al. [4] found “flint” aroma was most strongly associated with phenylmethanethiol and weakly negatively related to liking; however, these were unoaked wines produced with standardised winemaking. No study to date has assessed the contribution of 2-furylmethanethiol to consumer acceptance of white wine. Anecdotally, empyreumatic aromas are observed to be more common with barrel-fermented white wines, particularly Chardonnay.

The concept of “minerality” in wines has been found to be ill-defined among experts [24]; however, it has been associated with empyreumatic aromas such as flint, match smoke, kerosene, slate, granite, limestone, tar, charcoal, graphite, rock dust, wet stones, metallic, steel, and ferrous [25]. In the same study relating chemical composition to “mineral” aroma and flavour ratings, phenylmethanethiol and tartaric acid were found to have the highest correlation coefficients. A sensory study investigating “minerality” by comparing wine industry professional’s projective maps with flavour profiles for a trained QDA panel found minerality to be positively correlated with reduced, chalky, and grassy aromas and bitter taste [14]. Malic acid, tartaric acid, and the titratable acidity of the wines were highly associated with minerality. In this study, a series of experiments were used to better understand “empyreumatic” odours sometimes found in Chardonnay wines. A survey of the occurrence of the thiols phenylmethanethiol (PMT) and 2-furylmethanethiol (2FMT) was conducted in commercially produced Chardonnay wines from Australia, New Zealand, and France, followed by detailed chemical and formal sensory evaluations of a subset of 24 wines. Consumer testing was then completed on six wines. Finally, a follow-up odorant addition study was conducted to understand the causal effects of candidate compounds associated with wines displaying “empyreumatic” aroma nuances.

The main aim of this work was to assess the sensory significance of PMT and 2FMT in commercially produced Chardonnay wines. We hypothesised that PMT, as identified by Tominaga et al. [2] and Capone et al. [4], would play the major role in directing these smoky/mineral-like aromas and

would contribute positively to consumer acceptance. A secondary objective was to assess the relative importance of ester compounds and residual proline concentration identified by Espinase Nandorfy et al. [20] and Espinase Nandorfy et al. [21], respectively, in conferring peach/stone fruit aroma, sweetness, and viscosity in Chardonnay.

2. Materials and Methods

2.1. Wine Samples. A convenience sample of 71 commercially produced white wines (2016–2020 vintages, \$11–150), described as having a flint-like and/or stone fruit-like aromas by the winery or wine critic review, were purchased. The Australian wines ($n=61$) were sourced from a wide range of regions including South-Eastern Australian blends, while eight were from New Zealand (across five regions) and two from France (Chablis, Burgundy). Each wine underwent preliminary informal tasting by AWRI staff from the sensory and research teams, and was subjected to analytical testing for thiol concentrations. 24 Chardonnay wines were selected for the commercial wine QDA, regional and basic chemical composition, and oak usage information available in Table 1, and of these, six wines were further used for consumer testing.

2.2. QDA Panels. Two sensory panels were convened to complete the formal QDA studies of this work. The first panel of eleven assessors (ten females) with an average age of 51 years ($SD=8.4$) evaluated the commercial Chardonnay wines. The second panel consisting of eleven assessors (ten females, average age of 53 years, $SD=6.9$), including six of the original participants, was then convened to assess the aroma of the odorant spiking samples. All panellists were part of the external AWRI trained descriptive analysis panel and had extensive experience in wine sensory descriptive analysis. All assessors provided informed consent to participate, and this work was conducted in accordance with Deakin University's ethics policy (HEAG-H 169_2019) with the evaluations conducted at the AWRI in Adelaide, South Australia.

2.3. Sensory Evaluation of Commercial Chardonnay Wines. A series of four preliminary sensory evaluations by a panel ($n=12$) of expert technical wine assessors (four females) with an average age of 40 years ($SD=10.9$), were conducted to select 24 wines, from the 71 wines surveyed. Wines were selected that displayed a range of intensities of “empyreumatic” and stone fruit aromas, excluding wines with dominant off-flavours or winemaking artefacts. After the QDA of the commercial wine set, this panel was reconvened to confirm a subselection of wines deemed appropriate for further consumer testing and the odorant addition QDA.

Wines were formally evaluated using the generic QDA method as described in Heymann et al. [14]. To evaluate the 24 commercial wines, assessors attended six two-hour training sessions to determine appropriate descriptors for rating in the formal sessions. All the wines from the study were progressively used during training sessions to generate and refine appropriate descriptive attributes and definitions through a consensus-based approach.

Wines were assessed by appearance, aroma, and flavour. In the third session, standards for attributes were presented and discussed and these standards were also available during subsequent training sessions, the booth practice session, and the formal assessment sessions. As a familiarisation exercise, assessors revisited these aroma and flavour standards as well as at least one “warm-up” sample from the wine set at the beginning of each formal assessment session.

Following the fourth training session, assessors participated in two practice sessions in the sensory booths under the same conditions as those for the formal sessions. After the practice sessions, any terms which needed adjustment were discussed and the final list of terms and standards were determined. For the formal sessions, this list was refined to include one appearance term, fourteen aroma terms (thirteen defined and one “other” term) and fourteen palate terms (thirteen defined and one “other” term). The final list of attributes, definitions/synonyms, and reference standards are shown in Table 2.

2.4. Evaluation. The wines were presented to assessors in 30 mL aliquots in 3-digit-coded, covered, and ISO standard wine glasses at 22–24°C in isolated booths under daylight-type fluorescent lighting. Randomised presentation order across assessors was followed except in the practice sessions when there was a constant presentation order. All samples were expectorated. In the formal booth sessions, the assessors were presented with four trays of three samples per tray, per day. The assessors were forced to have a 60-second rest between samples and were encouraged to rinse with water, and a minimum ten-minute rest between the trays. During the ten-minute break, they were requested to leave the booths. Formal evaluation was completed in six two-hour sessions on separate days. A new bottle was used for each of the presentation days. The 24 commercial wines were presented to assessors three times, in a Williams Latin Square random block design generated by using Compusense20 sensory evaluation software (Compusense Inc., Guelph, Canada). The intensity of each attribute listed in Table 2 was rated using an unstructured 15 cm line scale (numericized 0 to 10), with indented anchor points of “low” and “high” placed at 10% and 90%, respectively. Data were acquired using Compusense20 sensory evaluation software.

2.5. Sample Preparation for Odorant Addition Study. A single, fruity commercial Chardonnay wine (South Australia, 2021 vintage) was used as the base wine with compounds PMT and 2FMT (Sigma-Aldrich, Castle Hill, NSW, Australia) added in a 5^2 full factorial design (two compounds, each added at five concentrations) that generated 25 permutation samples, with each of the five concentration levels increasing by a factor of 2.5. The concentration range chosen represented the minimum-maximum measured in commercial samples previously tested. Appropriate aliquots of PMT (100.0 $\mu\text{g/L}$) and 2FMT (100.9 $\mu\text{g/L}$) solutions in ethanol (food grade—ultra premium, Tarac Technologies, Nuriootpa, SA, Australia) were added volumetrically to the homogenized volume of base wine targeting 0, 2.6, 6.3, 16.3, and 40.6 ng/L of PMT and 0, 10, 25, 62.5, and 156.5 ng/L of 2FMT as well as all design combinations. The small amount of ethanol added from the stock

TABLE 1: Basic compositional data and oak usage for the 24 commercial Chardonnay wine samples from Australia and New Zealand (NZ) assessed in the commercial wine QDA study.

Code	Region	Year	Alcohol (% v/v)	Glucose + fructose (g/L)	pH	Titratable acidity (g/L)	Volatile acidity (g/L)	Malic acid (g/L)	SO ₂ free (mg/L)	SO ₂ total (mg/L)	Oak usage
AH 1 [†]	Adelaide Hills, SA	2017	12.8	1.1	3.18	6.2	0.47	<0.40	22	72	Major
AH 2	Adelaide Hills, SA	2017	12.8	1.7	3.20	6.6	0.35	2.07	22	117	Major
AH 3	Adelaide Hills, SA	2018	12.9	1.0	3.24	6.6	0.45	0.93	28	105	Major
AH 4	Adelaide Hills, SA	2019	14.0	1.2	3.24	6.3	0.28	1.41	22	116	Partial
AH 5	Adelaide Hills, SA	2019	11.9	2.4	3.05	6.7	<0.25	1.75	12	101	None
AH 6 [†]	Adelaide Hills, SA	2019	12.5	1.4	3.33	6.6	0.49	1.59	33	123	Major
AH 7	Adelaide Hills, SA	2019	12.2	1.7	3.00	7.9	0.47	1.48	9	75	Major
AH 8	Adelaide Hills, SA	2019	13.4	2.3	3.20	6.4	0.41	1.35	18	112	Major
AH 9 [†]	Adelaide Hills, SA	2020	12.9	1.0	3.28	7.0	0.43	1.85	21	101	Major
TAS [†]	Coal River Valley, Tas	2019	12.5	0.8	3.17	7.2	0.55	<0.40	37	112	Major
HV	Hunter Valley, NSW	2018	12.7	0.7	3.23	5.8	0.31	1.32	25	115	Major
KR	Kumeu River, NZ	2019	13.3	2.3	3.35	5.4	0.40	<0.40	24	94	Partial
MRS	Macedon Ranges Vic	2018	13.6	3.2	3.35	5.5	0.45	0.41	16	78	Major
MR 1	Margaret River, WA	2019	12.8	0.9	3.09	7.6	0.42	1.48	23	82	Major
MR 2	Margaret River, WA	2020	13.0	1.6	3.26	6.2	0.33	0.96	23	90	Major
MBH 1	Marlborough, NZ	2016	14.0	1.3	3.34	6.3	0.65	<0.40	25	155	Major
MBH 2	Marlborough, NZ	2017	13.3	0.6	3.22	7.1	0.65	<0.40	18	108	Major
MBH 3	Marlborough, NZ	2018	13.5	3.5	3.49	5.1	0.58	<0.40	22	65	Major
MV	McLaren Vale, SA	2020	12.1	0.6	3.36	5.9	0.26	1.60	30	111	None
MP [†]	Mornington Peninsula, Vic	2019	13.4	1.4	3.21	6.4	0.62	<0.40	24	66	Major
TBA 1	Tumbarumba, NSW	2017	13.1	1.3	3.36	6.2	0.42	1.28	21	93	Major
TBA 2	Tumbarumba, NSW	2019	13.4	1.3	3.46	5.3	0.62	<0.40	14	44	Major
YV 1 [†]	Yarra Valley, Vic	2018	12.8	1.2	3.21	7.0	0.39	1.71	18	89	Partial
YV 2	Yarra Valley, Vic	2019	14.4	2.2	3.19	7.1	0.50	1.10	27	105	Partial

Note: [†]Samples selected for consumer test. Oak usage data were collated from the wine labels and wine company tasting notes. Major, most or all of the wine was fermented or matured in oak vessels. Partial, a portion of the wine was fermented or matured in oak vessels. None, the wine was neither fermented nor matured in oak vessels.

TABLE 2: Sensory attributes, synonyms/definitions, and composition of reference standards evaluated by sensory panels during the QDA studies of commercial wines and odorant addition samples.

Study	Attribute	Definition/synonyms	Standard
Commercial wine study	<i>Appearance</i> Yellow colour intensity	The degree of colour of the sample (colour intensity)	Conceptual standard
	<i>Aroma</i>		
Both studies	Pungency	The intensity of the warming alcohol and tingling sensation	12% v/v of 95% food grade ethanol (Rowe Scientific) and 0.2 mg potassium metabisulfite (Sigma-Aldrich) Standard 1. 20 µL of 1.6 mg/L phenylmethanethiol
	Flint	Intensity of the aroma of flint, mineral, and struck-match	Standard 2. A chardonnay wine displaying a pronounced struck-match aroma according to the assessors
	Peach	Intensity of the aroma of peach and stone fruit	Standard 1. 3 × chopped fuzzy peach confectionary (Maynards) not in wine
	Pineapple	Intensity of the aroma of pineapple	Standard 2. 10 mL Crème de Peche liqueur (Massenez)
	Citrus	Intensity of the aroma of lemon and lime	3 × cubes of tinned pineapple (Golden Circle) 10 mL lemon and 10 mL lime cordial (Bickford's)
	Toasty	The intensity of the aroma of toasted bread and brioche	Standard 1. Small portion of warmed toast and croissant not in wine Standard 2. 1 g dried yeast (Lallemand)
	Apple/pear	The intensity of the aroma of fresh pears and red or green apples	30 mL apple cordial and 1 × slice of fresh packham pear
	Passionfruit/grapefruit	Intensity of the aroma of passionfruit, grapefruit, box hedge, cat pee, and sweat	Standard 1. 30 mL canned passionfruit pulp (John West) and 20 µL of 14.3 mg/L 3-sulfanylhethyl acetate
	Floral	Intensity of the aroma of orange blossom and mixed florals	Standard 2. 3 mL grapefruit cordial (Bickford's)
	Natural gas	Intensity of the aroma of drain, sewage, and natural gas	1 mL each of orange blossom water (Aoun), rosewater (Aoun), and Crème de Violette (Massenez)
Commercial wine study	Woody/vanilla	Intensity of the aroma of oak, vanilla, toasted coconut, and coconut shavings	5 g of wood ash (mixed fresh each day with wine to release sulfidic aroma) 2 g toasted American oak chips, 1.25 mL vanilla pod paste (Queen) 10 µL of 0.97 g/L oak lactone, and pinch of toasted coconut shavings (McKenzie's)
	Tinned vegetables	Intensity of the aroma of cooked and tinned vegetables	50 µL of 0.1% dimethyl sulfide
	Cheesy	Intensity of the aroma of cheese and rancid dairy	100 µL of 10% butanoic acid
	<i>Palate</i>		
	Sourness	Intensity of the perceived sour and acidic taste	1 g/L L-(+)-tartaric acid (ChemSupply) in water
	Bitterness	Intensity of the perceived bitter taste	15 mg/L quinine sulfate (Sigma-Aldrich) in water
	Viscosity	Intensity of thickness and slipperiness in the mouth	1.5 g/L carboxymethylcellulose sodium salt (Sigma-Aldrich) in water
	Hotness	Intensity of the alcohol burning sensation, including aftertaste	12% v/v of 95% food grade ethanol (Tarac Technologies) in water
	Sweetness	Intensity of the sweet taste	5 g/L sucrose (Foodland SA) in water
	Astringency	Intensity of the drying sensation in the mouth	0.5 g/L aluminium sulfate (Ajax Fine Chem Supply Pty Ltd) in water
Commercial wine study	Citrus	Intensity of the flavour of lemon and lime	Conceptual standard
	Stone fruit	Intensity of the flavour of peaches, nectarines, and apricots	Conceptual standard
	Tropical	Intensity of the flavour of pineapple, melon, and mango	Conceptual standard
	Mineral	Intensity of the flavour of flint, mineral, and struck-match	Conceptual standard
	Apple/pear	Intensity of the flavour of fresh apples and pears	Conceptual standard
	Toasty	Intensity of the flavour of toast, bread, and brioche	Conceptual standard
	Woody/vanilla	Intensity of the flavour of oak, vanilla, toasted coconut, and coconut shavings	Conceptual standard

All standards were added to 100 mL of 2019 Yalumba premium selection bag-in-box unoaked Chardonnay (2L, Angaston, SA) unless otherwise noted.

solutions was equalized for all samples including the base wine control. Addition samples were prepared freshly each day. The Chardonnay wine used as the base wine for the addition experiment was approximately 18 months old, bottled (750 mL) with screw-cap closure, 13.2% v/v ethanol, pH 3.33, titratable acidity (TA) = 5.7 g/L, SO₂ (free) = 20 mg/L, and SO₂ (total) = 100 mg/L. A preliminary informal tasting by AWRI staff from the sensory and research teams assessed the base wine as having subtle oak characters but no struck-flint-like aroma. The concentrations of PMT and 2FMT in this base wine were 1.1 ng/L and 2.6 ng/L, respectively.

2.6. Sensory Evaluation of Confirmatory Odorant Addition Study. Very similar training and evaluation conditions as described above were used for the follow-up confirmatory study investigating the aroma contribution of PMT and 2FMT to a fruity base Chardonnay wine with the following changes. Assessors participated in three days of training where each sample was presented at least once, followed by three formal evaluation days. All samples were evaluated by aroma only with the rated attributes listed in Table 2. The 25 combinations of the experimental design were presented to assessors in triplicate, with five trays of five samples per tray presented on each of the three formal evaluation days. Assessors took 30-second breaks between each sample.

2.7. Consumer Test Participants and Evaluation Conditions. A hedonic consumer test involving 92 regular white wine drinkers took place at the AWRI sensory laboratory located in Adelaide, South Australia. The sample of consumers was screened and selected based on their drinking preferences and habits, aimed to be balanced for age and gender as practically as possible. Consumers who drink Chardonnay wine at least once or twice per year, were not pregnant and were between 18 and 65 years of age participated in the assessment. Consumer demographic details can be found in Table S1. Each consumer attended a single session to taste six Chardonnay wines selected to broadly represent the range of attributes differentiating the samples from the statistical analysis of QDA data as well as having similar basic chemical compositions. Consumers gave informed consent, completed a demographic questionnaire, and were briefed on the hedonic task which lasted less than 1 hour.

The wines were presented to respondents monadically following a Williams Latin Square random block design, presented in 3-digit-coded ISO wine tasting glasses containing 30 mL aliquots of wine at $10.5 \pm 0.8^\circ\text{C}$. Tasting took place in isolated sensory booths under daylight-type lighting. A 2-minute break between the samples was enforced where participants were encouraged to drink water between the samples. Tasters could choose if they wanted to drink or expectorate the samples into the sink available in each booth. Each wine was first rated by the consumers using a nine-point hedonic scale labelled from “dislike extremely” to “like extremely” [26], then purchase intent was collected using

a five-point scale labelled from “definitely would not buy” to “definitely would buy.” A few questions relating to wine use and attitudes were administered after the tasting, with participants receiving a \$30 gift coupon as a reward for their time.

2.8. Statistical Analysis and Interpretation. Trained panel performance was assessed using Compusense20 software and R with the SensomineR (sensominer.free.fr/) and FactomineR (factominer.free.fr/) packages. The performance assessment included analysis of variance for the effect of assessor, wine and presentation replicate and their interactions, degree of agreement with the panel mean, degree of discrimination across samples, and the residual standard deviation of each assessor by attribute. All assessors were found to be performing at an acceptable standard.

Analysis of variance (ANOVA) for the QDA data was carried out using Minitab 20 (Minitab Inc., Sydney, NSW) for the effects of wine, assessor, presentation replicate, and all their two-way interactions. A Fisher's protected least significant difference (LSD) value was calculated at a 95% confidence level using the mean sum of squares value from the assessor by treatment interaction effect. Principal component analysis (PCA) was conducted for the means of the samples of the attributes using the correlation matrix, calculated by using XLSTAT 2020 (Addinsoft, France). For the odorant addition study response surface regression modelling (RSM), ANOVA and visualisations were completed with STAT-EASE 360 (MN, USA) treating presentation replicates as blocks.

For the consumer test data, ANOVA was calculated for the effects of wine and assessor, treating consumers as a random effect. Agglomerative hierarchical clustering (AHC) of raw liking scores was then calculated, as recommended in MacFie [27], by transforming to (dis)similarity matrix and using Pearson correlation coefficient index with average linkage (unweighted pair groups), and used inspection to the level of 0.58 to truncate clusters. A Fisher's protected LSD value was calculated at a 95% confidence level for each of the consumer groups.

To explore relationships between wine chemical composition, sensory profiles, and consumer responses, partial least squares regression (PLS-R) models were generated using the NIPALS algorithm (30,000 iterations) and standardisation. Models first linked chemical composition (x) to sensory attributes (y); then, another model was generated which associated sensory attributes (x) with mean consumer liking and consumer clusters mean liking scores (y). Wine chemical compounds important to sensory attributes and sensory terms identified as important to consumer response were identified by statistical jack-knifing and considering the size of regression coefficients as recommended in [28].

Due to the relatively small sample sizes practicable in wine research, less emphasis was placed on arbitrary P value significance levels, instead attention was given to the level of statistical evidence (P value), magnitude of effect size (F

value) and absolute effect value (sample mean values) to interpret and draw conclusions about effects of sensory significance [29, 30]. Statements ascribing the level of statistical evidence in this work are as follows: $P \geq 0.10$ “virtually no evidence,” $P \leq 0.10$ “weak evidence” (\ddagger), $P \leq 0.05$ “evidence” (*), $P \leq 0.01$ “strong evidence” (**), and $P \leq 0.005$ “very strong evidence” (***).

2.9. Chemical Analysis. Targeted volatile compounds were quantified using previously published methods by Siebert et al. [7] and updated by Espinase Nandorfy et al. [20] that are routinely used in-house and are described briefly below. Furthermore, two new methods developed to quantify *n*-alkyl γ -lactones and benzyl compounds are described in detail. All analytical methods for volatile compounds used deuterated analogues as the internal standards, and MS in selected ion monitoring mode or MS/MS with multiple reaction monitoring except the method using a GC/sulfur chemiluminescence detector (SCD) which instead used two chemically similar compounds to the analytes.

The set of 71 survey wines, including the subset of 24 wines were analysed for polyfunctional thiols (including PMT and 2FMT) by HPLC/MS/MS after derivatisation with 4,4'-dithiodipyridine (Acros Thermo Fisher Scientific, Thebarton, SA, Australia) and SPE as described by Capone et al. [31] and Cordente et al. [32] using an Exion UHPLC coupled to a 6500 QTrap+ (Sciex, Mulgrave, Vic., Australia).

The following analyses were only conducted on the subset of 24 wines. Fermentation-derived aroma compounds were analysed by headspace (HS)-solid phase micro-extraction (SPME)-GC/MS as described by Siebert et al. [33] except using a polyacrylate (PA, white) 85 μm SPME fibre (Supelco, Sigma-Aldrich), a VF-624 ms (30 m \times 0.25 mm \times 1.4 μm ; Agilent) GC column, and an Agilent 7890A GC (Agilent Technologies Australia, Mulgrave, Vic., Australia) coupled to an Agilent 5975C MS and equipped with a Gerstel MPS2 multipurpose sampler (Lasersan Australasia, Tanunda, SA, Australia). Monoterpenes and C13-norisoprenoids were analysed according to Pisaniello et al. [34] using membrane-assisted solvent extraction (MASE)-GC/MS on an Agilent 7890B GC, coupled to an Agilent 5977B MS and equipped with a Gerstel MPS Robotic Pro (Lasersan). The MASE membrane bags were supplied by Lasersan. Oak-derived aroma compounds were quantified according to Pollnitz et al. [35]; all compounds were analysed by liquid-liquid extraction-GC/MS using an Agilent 6890 GC, coupled to an Agilent 5973 MS and equipped with a Gerstel MPS2. Volatile sulfur compounds were analysed according to Siebert et al. [36] and Cordente et al. [32] utilising static HS-GC/SCD on an Agilent 7890B GC, coupled to an Agilent 8355 SCD and equipped with a Gerstel MPS2 XL (Lasersan).

n-Alkyl γ -lactones were quantified by direct-immersion (DI)-SPME-GC-MS/MS similar to that described for (*Z*)-6-dodeceno- γ -lactone [37] using an Agilent 7000C Triple Quadrupole GC-MS/MS system (version 7.03) equipped with a Gerstel MPS2-XL (Lasersan). γ -Octa-, -nona-, -deca-, and -dodecalactone, were purchased from Sigma-Aldrich.

(*Z*)-6-Dodeceno- γ -lactone was kindly donated by Symrise (Holzminden, Germany), and γ -methyldecalactone was kindly donated by Pyrazine Specialties. (*Z*)-7-Decen-5-olide was supplied by Penta International (Livingston, NJ), and 6-pentyl- α -pyrone was supplied by Pyrazine Specialties (Ellenwood, GA). *n*-Alkyl d_7 - γ -lactones (C8–C12) had been synthesized in-house [38]. Stock solutions and dilutions of *n*-alkyl γ -lactones were prepared in ethanol (gradient grade for LC, Merck, Bayswater Vic, Australia). Samples were prepared by diluting wine (5 mL) with water (4 mL) and adding internal standard (25 μL) into a 10 mL vial (Agilent). Analytes were then extracted with DI-SPME using a 65 μm DVB/PDMS (blue) fibre (Supelco, Sigma-Aldrich) for 40 minutes at 30°C with agitation at 250 rpm. The fibre was then washed in a 20 mL vial containing water for 1 minute prior to desorption to decrease the amount of inlet contamination due to sugars and other nonvolatiles. Volatiles were desorbed at 260°C onto a VF-200 ms (30 m \times 0.25 mm \times 0.25 μm ; Agilent) which was held at a constant flow of 1 mL/min. During injection, the inlet was splitless for 2 minutes followed by inlet purging at 50 mL/min. To enable back-flushing, the analytical column was connected to a Deans switch, where, during analysis, compounds were transferred to the MS using 1.5 m \times 0.15 mm fused silica held at a constant flow of 1.2 mL/min. The temperature program for the oven was: 40°C for 1 minute, ramped to 120°C at 20°C/min, and then ramped to 180°C at 2°C/min. The analytical column was then backflushed for 5 minutes (2 column volumes) at 260°C. The MS transfer line was held constant at 240°C for the duration of the analysis. Method linearity was determined using ten calibration levels, each in duplicate, over the concentration range of 0.1–100 $\mu\text{g/L}$ of all listed lactones except for (*Z*)-6-dodeceno- γ -lactone at 1–1000 ng/L, and included control wine samples without any addition of analytes. The limit of detection (LOD) was calculated as $S/N = 3$ and the limit of quantification (LOQ) was calculated as $2 \times \text{LOD}$. Method precision and recovery were determined using seven replicate samples spiked at low and high concentrations (1 and 10 $\mu\text{g/L}$ for all lactones except 10 and 100 ng/L for (*Z*)-6-dodeceno- γ -lactone). See Table S2 for calibration and validation data. To check the accuracy of the analysis, at least one in every six wines was analysed in duplicate.

Benzyl compounds were quantified by HS-SPME-GC/MS using an Agilent 7890A GC coupled to an Agilent 5975C MS and equipped with a Gerstel MPS2-XL. Benzaldehyde, benzyl alcohol, and benzyl acetate were supplied by Sigma-Aldrich, d_6 -benzaldehyde by Cambridge Isotopes (Novachem, Collingwood, Vic, Australia), and d_5 -benzyl acetate and d_5 -benzyl alcohol by CDN Isotopes (SciVac, Hornsby, NSW). Stock solutions of benzaldehyde, benzyl alcohol, and benzyl acetate, and mixed dilutions were prepared in ethanol (LC grade, Merck). The GC was fitted with a Deans switch (Agilent) to utilise a postrun backflush program. The analytical column used was a VF-624 ms (60 m \times 0.25 mm \times 1.4 μm ; Agilent) and the restrictor column was deactivated fused silica 1.0 m \times 0.10 mm; Agilent). The carrier gas was helium (ultrahigh purity, BOC, Adelaide, SA, Australia) in constant flow mode: analytical column

1.75 mL/min (initial pressure 273 kPa) and restrictor column 1.85 mL/min (initial pressure 137 kPa). A polyacrylate (PA, white) 85 μm SPME fibre (Supelco, Sigma-Aldrich) was exposed to the headspace (20 mins at 45°C) with agitation (250 rpm). The SPME fibre was desorbed in splitless mode and left in the injector for 10 min. The splitter, at 29:1, was opened after 2 min. The injector temperature was held at 250°C. The oven temperature was started at 50°C, held for 1 min, raised to 140°C at 20°C/min, and then further raised to 235°C at 5°C/min. Subsequently, the inlet pressure was reduced to 7 kPa, the reversed flow through the analytical column at -4.5 mL/min via the Deans switch, and the oven heated to 280°C and held for 5 min. The temperature of the transfer line was 240°C. The mass spectrometer was operated in electron (EI+) ionization mode at 70 eV and utilising simultaneous scan/SIM mode. The wine samples were prepared for HS-SPME; sampling was as follows: a 5 mL aliquot of wine, 50 μL of internal standard mixed solution d_6 -benzaldehyde, d_5 -benzyl acetate, and d_5 -benzyl alcohol (each at 20 mg/L), a 5 mL aliquot of tartrate buffer (pH 3.20), and sodium chloride (2 g; Merck) was added to a 20 mL screw-cap vial (magnetic, Teflon lined silicone septum; Agilent). Method precision and calibration linearity were validated by a series of standard addition experiments to white wine diluted 1:1 with model wine (12% v/v ethanol, pH 3.20). Method linearity was determined using ten calibration levels, each in duplicate, over the concentration range of 2–2000 $\mu\text{g/L}$ of benzaldehyde, benzyl alcohol, and benzyl acetate and included control wine samples without any addition of analytes. The LOD was calculated as $S/N = 3$ and the LOQ was calculated as $3 \times \text{LOD}$. Method precision was determined using seven replicate samples spiked at low and high concentrations (50 and 500 $\mu\text{g/L}$). See Table S3 for calibration and validation data. To check the accuracy of the analysis, at least one in every six wines was analysed in duplicate. To check the recovery, a master mix of all samples was spiked with 50 $\mu\text{g/L}$ and 500 $\mu\text{g/L}$ of the analytes in duplicate.

The concentration of proline was quantified using ^1H NMR. Analysis was performed on a Bruker Avance Neo operating at 400 MHz (Bruker, Sydney, Australia). Samples were prepared as follows: 900 μL of wine was buffered with Bruker “Buffer C,” and then automatically titrated with 1.0 M HCl or 1.0 M NaOH to pH 3.10 using a microtitrator (Bruker). A 600 μL aliquot of the titrated wine was then transferred to a 5 mm tube (Duran Wheaton Kimble, Economic, ASIS Scientific, Adelaide, Australia) and submitted for acquisition. Experiments, including tuning, matching, locking, shimming, and pulse calibration, were performed automatically according to the Bruker FoodScreener module [39]. Proline was then quantified from the water and ethanol suppressed *noesygpps* spectrum (ds 4, ns 32, TD 64k, sw 20 ppm, rg 16) using an in-house workflow (Python3.9, <https://github.com/AWRIMetabolomics/prommr-quant>), where the area under the curve (AUC) of the multiplet at ~2.3 ppm was obtained and regressed against a calibration function. The ppm coordinates were identified as a range containing a clean signal specific to proline, relatively free of other compounds in wine.

The subset of 24 wines was analysed by Affinity Labs for their basic composition using a Foss WineScan FT 2 as described by the manufacturer (Foss, Hillerød, Denmark), and the free and total sulfur dioxide (F/T SO_2) were measured using a Gallery discrete analyser (Thermo Fisher Scientific, Thebarton, SA, Australia).

3. Results and Discussion

3.1. Chardonnay Survey of the Occurrence of 2FMT and PMT. A total of 71 white wines (66 Chardonnay) were analysed for the concentration of 2FMT and PMT, with the results shown in Figure 1. The range of 2FMT in the wines was approximately 0.2–164.5 ng/L, with a mean of 15.1 ng/L and median value of 3.5 ng/L. For PMT, the range was 0.2–7.8 ng/L, with a mean of 1.7 ng/L and a median value of 1.4 ng/L. 2FMT and PMT were significantly correlated ($P < 0.0001$, $r = 0.47$, $n = 71$), but differed in their distribution, with PMT following a normal distribution while 2FMT was strongly right skewed with many values in the low range and a few high concentrations. The concentration of both compounds was above the reported aroma detection thresholds (0.4 ng/L and 0.3 ng/L) for almost all wines. The concentration range of 2FMT measured here was much higher than the eight white wines reported by [40] or the nine Spanish Chardonnays reported in [41] (2–19 ng/L) but below the range reported in some aged Champagnes [3] (up to 5500 ng/L). The maximum concentration of PMT measured in this study was approximately five times lower than the maximum non-Sauvignon Blanc white wines reported in [41] (36 ng/L) and lower than the values reported in [4] (up to 40 ng/L).

3.2. Sensory Descriptive Analysis of Commercial Chardonnay Wines. The attributes rated by the trained panel were generated by a consensus-based approach during training sessions. The attributes (Table 2) consisted of one colour attribute, one nasal sensation (pungency), twelve aromas, three tastes, three mouthfeel terms, and seven flavour attributes.

From the ANOVA, very strong evidence was found that all the attributes rated by the panel differed between the 24 commercial wines except for toasty aroma (Table 3). The largest differences, indicated by the largest F values, between the wines were the degree of yellow colour intensity, flint aroma, and mineral/flint flavour.

As a visual overview of the sensory properties of the 24 Chardonnay samples, a PCA (Figure 2) was conducted on the mean values of the sensory attributes (Tables S4 and S5). Principal components 1 and 2 explained 63.4% of the variation in the sensory data. PCs 3, 4, and 5 were also found to have eigenvalues above 1 and explained a further 8.8%, 6.8%, and 5.2% of the variation in the data. However, these PCs are mainly related to the intensity of cheesy aroma. The horizontal separation of the wines along PC1 related to the intensity of nonfruit sensory attributes pungency, natural gas aroma, flint aroma, mineral/flint flavour, tinned vegetable aroma, and woody/vanilla aroma and flavour, which

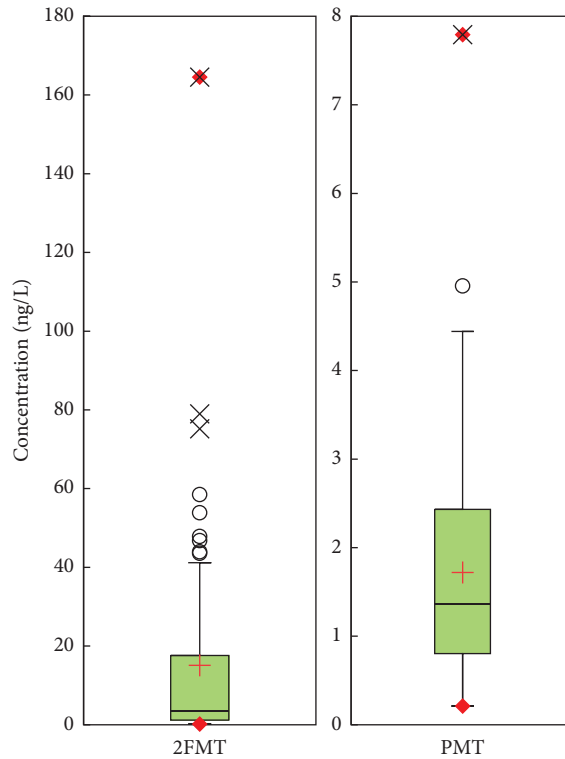


FIGURE 1: Box plots visualising the distribution of 2FMT and PMT from a survey of 71 white wines from Australia, New Zealand, and France, including 66 Chardonnay samples. The inclusive median quartile occurs within the box are shown with vertical whiskers corresponding to minimum and maximum values within a range limit and absolute maximum and minimum indicated by (◆) and mean by (+). Outlier point wines fall beyond the upper whisker with those values beyond 2.5 standard deviations marked (○) and 3 standard deviations marked (×).

TABLE 3: *F* ratios, probability values[†], degrees of freedom (df), and mean square error (MSE) from the analysis of variance of QDA data.

Attribute	Wine (W)	Assessor (A)	Rep (R)	W * A	R * W	R * A	MSE
Yellow colour	22.12***	104.79***	0.50	1.83***	1.12	5.27***	0.182
Pungency A	3.99***	68.80***	0.45	1.19	2.08***	4.18***	0.285
Flint A	19.4***	8.37***	0.89	1.74***	1.16	1.51	2.268
Peach A	3.74***	30.82***	2.29	1.89***	1.27	0.78	1.600
Passionfruit/grapefruit A	2.84***	8.73***	0.01	1.63***	0.94	2.56***	1.819
Pineapple A	4.91***	20.15***	2.71	1.95***	1.35	1.72*	1.488
Citrus A	2.18***	40.73***	1.82	1.28*	1.22	6.90***	0.436
Natural gas A	4.75***	5.68***	1.16	1.62***	1.36	1.99**	0.453
Woody/vanilla A	4.79***	24.79***	1.15	1.81***	1.46*	0.61	1.350
Toasty A	1.37	68.22***	0.19	1.33***	1.17	1.56	0.841
Apple/pear A	4.79***	15.17***	1.05	1.80***	1.30	6.60***	0.876
Tinned vegetables A	3.44***	10.86***	0.75	1.19	1.13	2.40***	1.005
Cheesy A	4.12***	5.24***	0.25	2.00***	0.75	2.19***	1.150
Floral A	5.92***	15.60***	0.59	1.70***	0.71	2.28***	1.800
Sourness T	3.98***	46.81***	0.68	1.29*	1.06	3.53***	0.468
Bitterness T	1.90**	41.34***	0.84	1.39***	1.43*	7.18***	0.422
Viscosity MF	1.65*	258.86***	1.10	1.32**	0.78	1.76*	0.313
Hotness MF	3.47***	58.89***	5.31*	0.93	0.63	3.39***	0.535
Sweetness T	3.19***	93.26***	2.47	1.09	0.99	1.25	0.766
Astringency MF	3.20***	26.61***	1.04	1.49***	0.99	9.57***	0.378
Citrus F	3.28***	113.87***	4.04*	1.27*	0.76	2.74***	0.466
Stone fruit F	2.30***	34.78***	2.23	1.71***	1.36	2.34***	0.965
Tropical F	2.59***	48.53***	5.33*	1.55***	0.97	1.35	1.186
Mineral/flint F	7.35***	15.13***	0.19	1.76***	1.26	1.16	1.325
Apple/pear F	3.58***	28.63***	0.71	1.99***	1.36	3.14***	0.823
Toasty F	1.66*	81.22***	0.54	1.39***	1.20	1.44	0.792
Woody/vanilla F	5.44***	23.17***	0.08	1.43***	0.73	2.15***	1.444
df	23	10	2	230	46	20	460

Note: A: aroma, F: flavour, T: taste, MF: mouthfeel, Rep: presentation replicate. [†]Significance levels are as follows: **P* < 0.05; ***P* < 0.01; ****P* < 0.005; and [‡]*P* < 0.10. df = degrees of freedom.

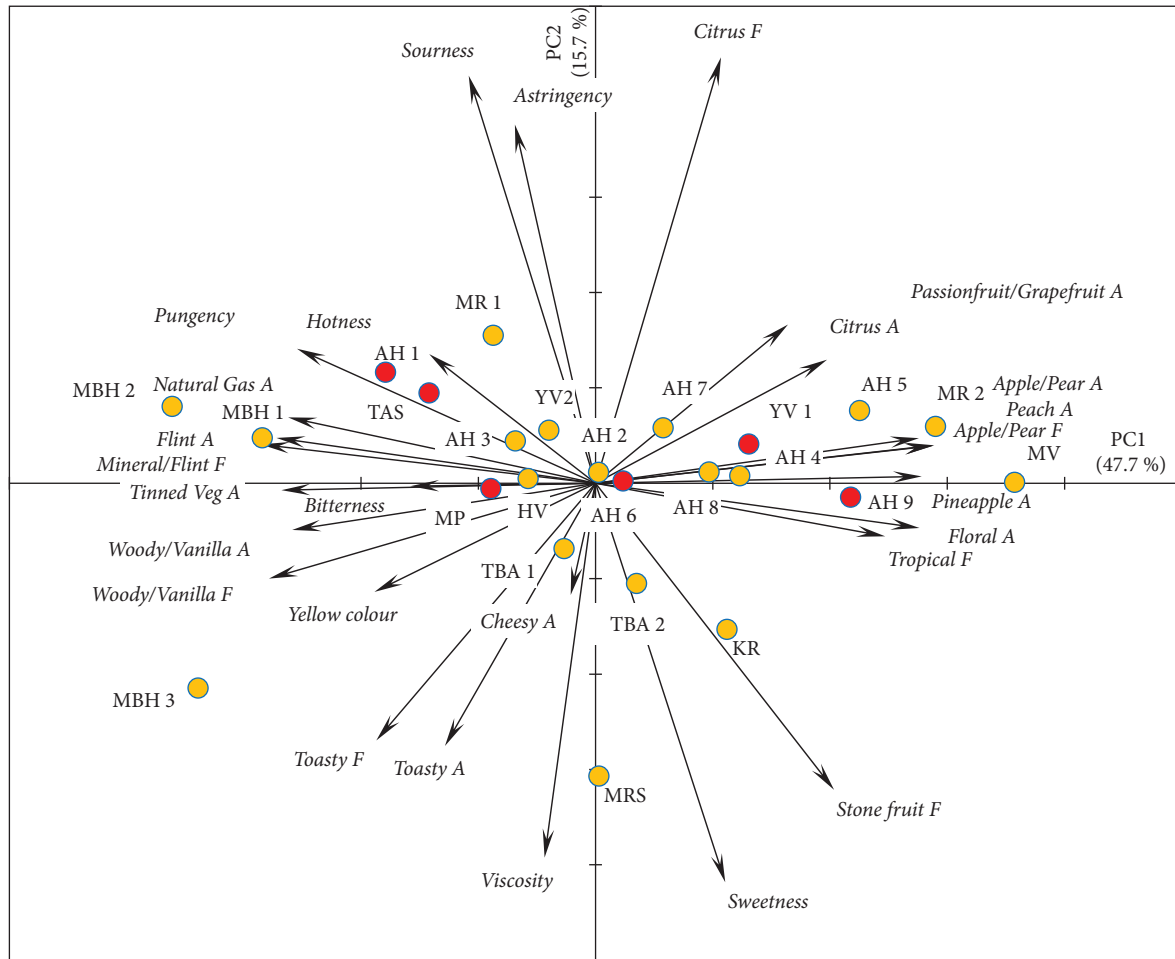


FIGURE 2: Biplot of principal component analysis PC1 and PC2 of all the wine sensory attributes and the scores for the 24 Chardonnay wines assessed by quantitative descriptive analysis. Wines selected for consumer testing are highlighted (●).

were heavily negatively loaded on PC1 with wines from Marlborough (MBH1, MBH2, and MBH3) as well as samples AH1 and TAS rated higher in these attributes. Conversely, fruity attributes passionfruit/grapefruit aroma, citrus aroma, apple/pear aroma and flavour, peach aroma, pineapple aroma, tropical flavour, as well as floral aroma were positively loaded on PC1 with wines MV, MR2, AH9, and AH5 rated the highest in these attributes. The vertical separation along the PC2 was driven by the ratings of sourness, astringency, citrus flavour, as well as toasty aroma (ns) and flavour, viscosity, sweetness, and stone fruit flavour. Generally, the retail price of the wines was higher for those to the left of Figure 2, with price positively and significantly ($P < 0.05$) correlated with flint aroma ($r = 0.45$), woody/vanilla aroma ($r = 0.55$) and flavour ($r = 0.52$) and pungency ($r = 0.42$). Overall, the wines selected showed a range of “empyreumatic” aroma and flavour intensities.

3.3. Assessing the Association of PMT and 2FMT with Smoky/Burnt Sensory Characteristics Using PLS-R. Basic chemical composition for the 24 wines is shown in Table 1, and Table S6 lists the volatile compounds quantified in the wines,

together with their CAS numbers; abbreviation codes; published aroma detection thresholds; and mean, minimum, and maximum concentrations.

To link chemical composition and sensory response using PLS-R, a five-factor model was used that explained 72% of the total sensory response variance from the chemical compositional data. Visualisation of the scores and loadings for factors 1 and 5 from this model can be seen in Figure S1. Chemical compounds (X 's) and sensory attributes (Y 's) located together in Figure S1 are generally positively associated, and those towards the outside of the plots are considered well modelled. Compounds of sensory significance were identified by considering both the size of their regression coefficients (Figure 3) and statistical importance as determined by a jack-knife resampling test. Significant compounds most strongly and positively associated with flint aroma were 2FMT, acetic acid, the oak compounds 4-methyl guaiacol, eugenol, guaiacol, and *trans*-oak lactone, while β -damascenone was significantly negatively associated with this attribute and positively related to several of the fruity attributes. In addition to those identified as significant, the compounds PMT, ethyl thioacetate, and ethanethiol had

relatively high and positive regression coefficients for flint aroma intensity. The model was strong (R^2 calibration predicted vs measured = 0.91 and R^2 validation predicted vs. measured = 0.70). Similar compounds were also identified as important to mineral/flint flavour, and β -citronellol and 3-sulfanylhexanol were additionally implicated, again with a strong model. Linear regression tests of PMT ($R^2 = 0.102$, $P = 0.128$) and 2FMT ($R^2 = 0.589$, $P < 0.0001$) with flint/struck-match/mineral aroma intensity confirmed 2FMT was much more strongly correlated than PMT. Previous studies implicated PMT with “flint” aroma in research Chardonnay wines [4] and other white wines [2]; however, the stronger association uncovered for 2FMT was unexpected.

As a secondary objective of this work, we sought to determine the role of ethyl esters which had been identified in a recent association study and multistep screening reconstitution study as conferring peach aroma to model wine samples [20]. For the peach aroma attribute in the present study, 3-sulfanylhexyl acetate, 2-methylbutyl acetate, β -damascenone, 3-methylbutyl acetate, and 2-phenylethyl acetate were all identified as significant and had high positive regression coefficients (Figure 3). Ethyl octanoate and ethyl hexanoate had small negative regression coefficients for the five-factor model, with a small positive regression coefficient for a one-factor model. Ethyl octanoate was present in a much narrower concentration range in these wines (933–1560 $\mu\text{g/L}$, Table S6) than previously tested with reconstitution experiments (0–1500 $\mu\text{g/L}$). The importance of ethyl esters of fatty acids to fruity aromas was thus not confirmed here, likely due to masking effects on fruity odorants making a statistical association difficult to be uncovered. Even though monoterpenes were found at relatively low concentrations, as is commonly reported for Chardonnay wines [42], linalool (0–5 $\mu\text{g/L}$) was also significant and positive to peach aroma, while α -terpineol (3–12 $\mu\text{g/L}$) had a high positive regression coefficient for stone fruit flavour. Monoterpenes were also found to be linked to fruity attributes in an earlier study [4].

Compounds understood to be related to odours resulting from reductive fermentations and oak maturation were generally strongly and negatively associated with fruity attributes, likely due to masking effects. For natural gas aroma, an attribute denoting reductive off-odour, compounds methanethiol and ethanethiol had the highest regression coefficients along with 2FMT and PMT; however, none were significant by the jack-knifing test. For the oak-related aroma attribute woody/vanilla, 4-methyl guaiacol, *cis*- and *trans*-oak lactone, eugenol, guaiacol, and vanillin all had significantly high regression coefficients, with PMT and 2FMT relatively high but nonsignificant, while passionfruit/grapefruit aroma was most significantly and positively associated with 3-sulfanylhexyl acetate, linalool, 2-phenylethyl acetate, hexyl acetate, and 2- and 3-methylbutyl acetate (Figure 3).

Recently, Espinase Nandorfy et al. [21] demonstrated the sensory influence of the residual amino acid proline in dry red wine, which increased perceived sweetness, fruit flavour, and viscous mouthfeel, while diminishing bitterness and astringency. Although the proline concentration is reported

to be lower in white wines (0.025–1.4 g/L) compared to red wines (0.018–4.4 g/L) as reviewed by Gutiérrez-Gamboa et al. [43], the range can span across the sensory detection threshold reported in water of approximately 2 g/L [44] and has been linked to wine “body” previously [45]. In this study, the range of proline measured was 0.6–1.4 g/L and had modest, but not significant regression coefficients from the PLS model, relating positively to viscosity (0.0346) and negatively to astringency (–0.0298). Stronger and significant associations, however, with taste and mouthfeel terms were found for pH and titratable acidity (TA) in agreement with the previous findings [46].

3.4. Aroma QDA of a Chardonnay Wine with Added PMT and 2FMT. From the sensory evaluation of the 25 wines created by adding PMT and 2FMT to a fruity and lightly oaked base Chardonnay wine in a full factorial design, nine aroma attributes were generated to describe their sensory properties by a consensus-based approach. Nearly identical definitions and standards as those used during the QDA of the commercial Chardonnay wines were agreed to by the sensory panel.

From the response surface regression models summary presented in Table 4, very strong evidence was found that wines differed in their aroma intensity of all attributes with the addition of PMT and 2FMT. The largest linear effect observed was for 2FMT to increase the intensity of flint aroma while added PMT also imparted this aroma, albeit with an effect size 22 times smaller. It is noteworthy that the maximum concentration of 2FMT was nearly four-fold higher than that of PMT in the addition samples, which was aimed to better represent the observed maximum found naturally in Chardonnay wines. Therefore, it is feasible, that PMT could be as potent as 2FMT in white wine if ever found at similar concentrations. From a practical perspective, the concentration of 2FMT was found to be 21-fold higher than that of PMT in this survey, suggesting the influence of PMT is naturally limited. Weak evidence ($P = 0.052$) of an interactive effect between PMT and 2FMT was also found to result in slight mutual suppression for this attribute. These effects on flint aroma can be visualised in Figure 4. The other attributes (Table 4) were all found to be suppressed by the two compounds, with 2FMT exerting stronger suppression on peach, apple/pear, and floral attributes than PMT, as indicated by the effect size values.

Overall, the results of this study have clarified the role of 2FMT and PMT in “empyreumatic” aromas, including smoky, gun smoke, flint, or struck-match characters, in Chardonnay wines. From the commercial wines QDA, flint/struck-match/mineral aroma was only modestly related to PMT, as previously reported by Tominaga et al. [2, 3] with more evidence found supporting a link to 2FMT. Although 2FMT is reported to contribute a roasted coffee aroma to certain wines [11], no evidence of this was found during either sensory studies conducted here. Both sensory panels described and rated wines high in 2FMT (and PMT) as high in flint/struck-match/mineral aroma rather than any roasted coffee-related attribute, suggesting the context set by other red or white wine volatiles

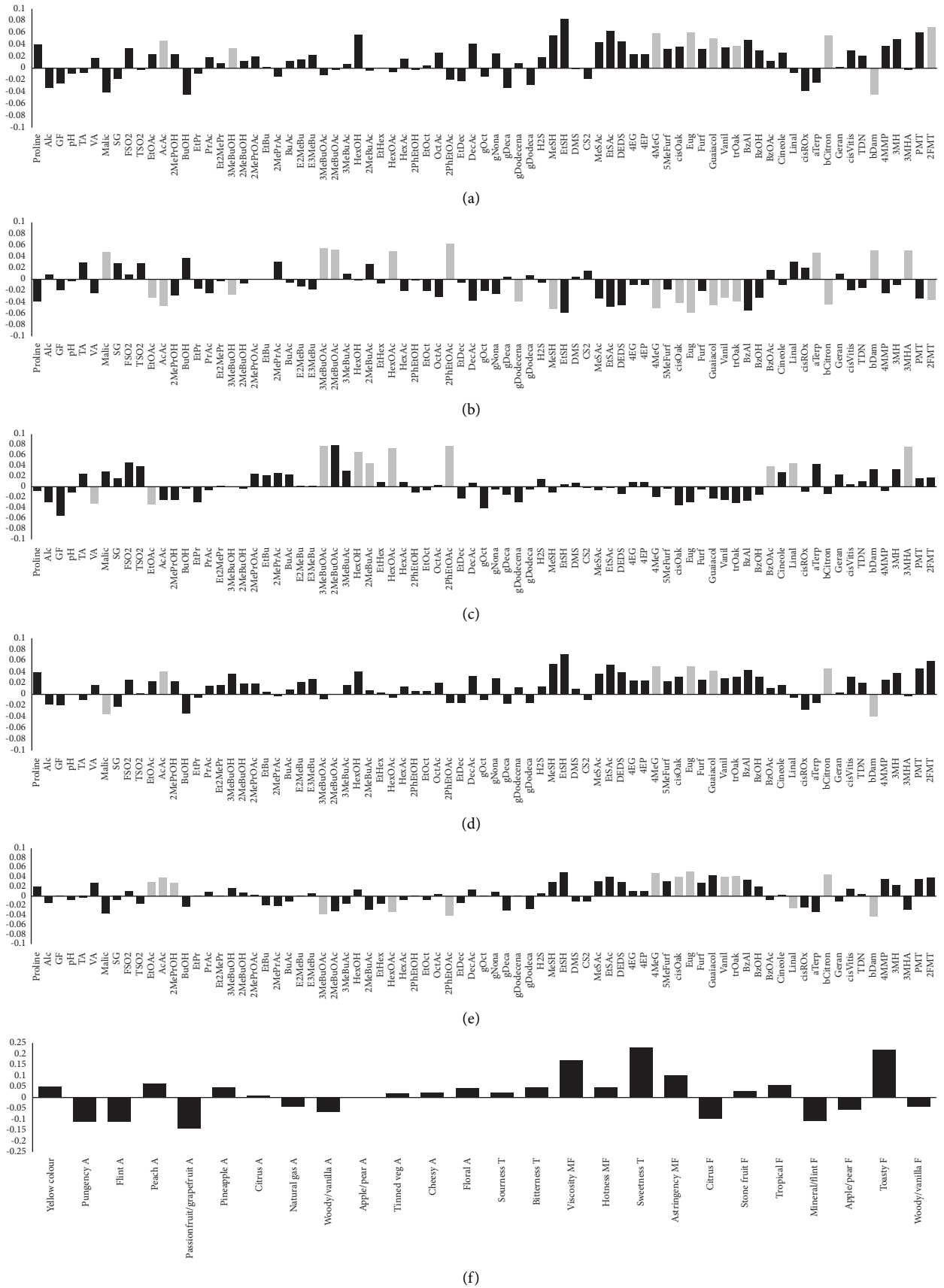


FIGURE 3: Continued.

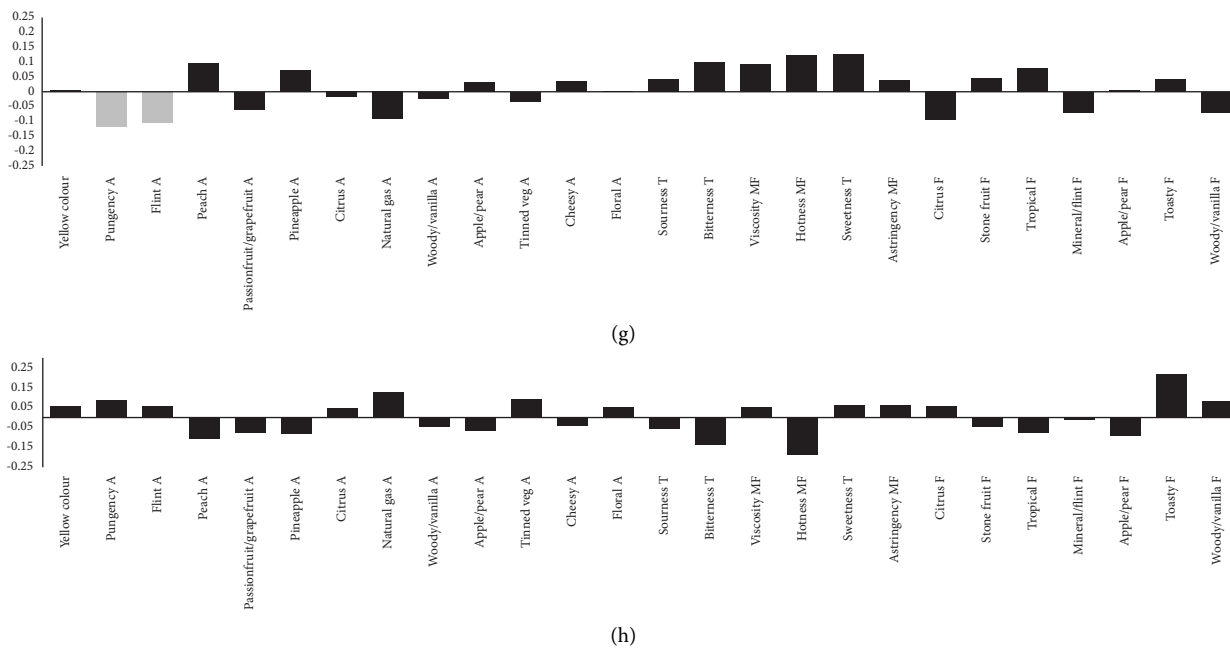


FIGURE 3: Regression coefficients from partial least squares models generated to relate the chemical composition of the 24 commercial Chardonnay wines with aromas (a) flint, (b) peach, (c) passionfruit/grapefruit, (d) natural gas, (e) woody/vanilla, as well as sensory attributes related to (f) overall consumer liking ($n = 92$), (g) consumer cluster 1 ($n = 62$), and (h) consumer cluster 2 ($n = 30$) liking scores. Significant variables shaded grey (■), not significant shaded in black (■). Abbreviations of chemical compounds can be found in Table S6.

TABLE 4: F ratios, probability values[†], degrees of freedom (df), and mean square error (MSE) from the response surface model of quantitative descriptive analysis aroma data from the individual PMT and 2FMT addition samples blocked by presentation replicate.

Attribute	Factors and interaction				MSE
	Model	PMT	2FMT	PMT * 2FMT	
Citrus	6.08***	1.53	13.90***	0.02	0.085
Peach	21.01***	8.18**	39.81***	0.14	0.225
Flint	78.11***	7.01**	152.70***	3.90 [‡]	0.309
Apple/pear	21.35***	0.083	41.63***	2.09	0.108
Pineapple	8.25***	3.51 [‡]	14.65***	0.13	0.147
Floral	15.63***	3.69 [‡]	34.90***	0.01	0.223
Toasty	2.51 [‡]	3.25 [‡]	5.48*	1.53	0.219
Sweaty	4.62***	1.36	10.33***	0.02	0.202
Pungency	3.82*	2.65	0.2	7.83**	0.024
DF	3	1	1	1	69

Note: [†]Significance levels are as follows: * $P < 0.05$; ** $P < 0.01$; *** $P < 0.005$; and [‡] $P < 0.10$. df = degrees of freedom.

may affect the odour percept conferred. Ferreira [47] stated PMT together with 2FMT can impart empyreumatic aromas to some aged wines including Chardonnay, but also young wines, based on the studies of Mateo-Vivaracho et al. [41] and Tominaga et al. [2, 3], which is in some degree of agreement with the results presented here for high concentration ranges, although our results provide evidence for a greater role of 2FMT. The addition studies reported by Mateo-Vivaracho et al. [41] indicated that the low concentrations of 2FMT were described (by free choice notes) as increasing fruitiness and pineapple character, while contributing toasty and coffee nuances above 5.3 ng/L. Our study did not find any evidence that 2FMT at low levels contributed to fruity nuances; however, the first addition step of 10 ng/L was higher than their study. Conversely, for PMT, very low concentrations were reported in

the same study to impart toasty, burnt, and empyreumatic notes at levels of 0.7 and 1.4 ng/L. Our concentration range of PMT (2.6–40.6 ng/L) was again higher than that of Mateo-Vivaracho et al. [41] and the effect was less pronounced compared to 2FMT. These differences may also be explained by the use of a de-aromatized wine in the 2010 report rather than a wine with all other aroma compounds still present.

3.5. Consumer Acceptance and Associations with Sensory Properties. A selection of six of the wines from the QDA was assessed for consumer liking. The wines were selected to represent the range of sensory properties heavily loaded on PC1 from the QDA (Figure 2), particularly targeting the range of flint aroma intensity while attempting to have basic chemical composition measures such as alcohol and

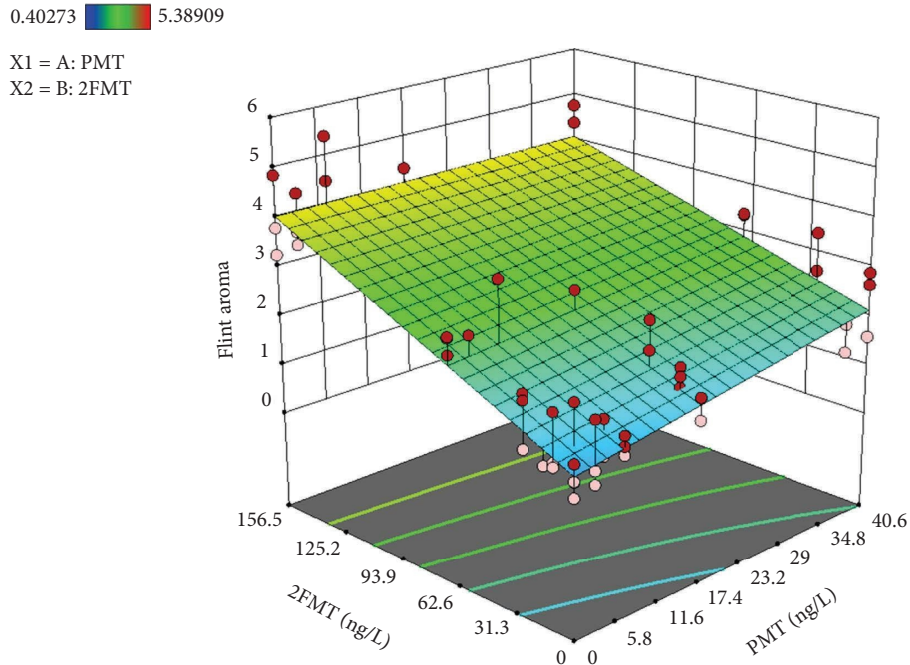


FIGURE 4: Response surface relating the intensity of flint aroma to the concentration of added 2-furylmethanethiol (2FMT) and phenylmethanethiol (PMT) in Chardonnay base wine from the confirmatory odorant addition quantitative descriptive analysis. Presentation replicated mean values of design points are displayed with those above (●) and below (○) the response surface indicated.

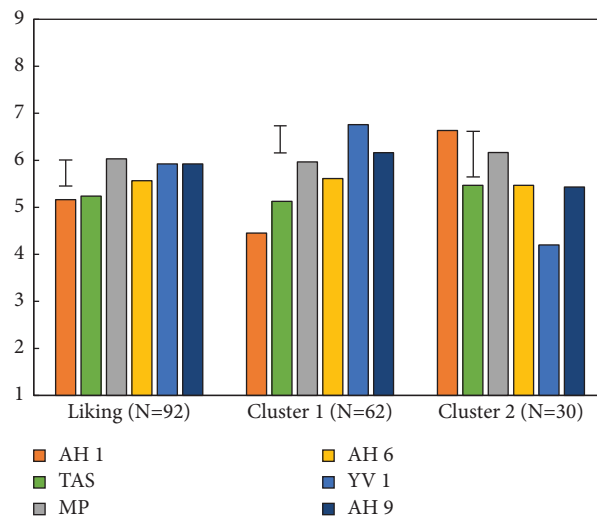


FIGURE 5: Mean liking scores for the total consumer sample as well as for two clusters of consumers for the six Australian Chardonnay wines, AH1 (■), TAS (■), MP (■), AH6 (■), YV1 (■), and AH9 (■) with varied intensity of flint/struck-match/mineral aroma. Fisher's LSD value for each consumer group (black bar).

titratable acidity as similar as practicable. Wines with other characters such as overt bitterness or sweetness were not included in the consumer test.

From the ANOVA of the consumer liking scores, strong evidence was found ($P = 0.002$, $F = 3.78$) supporting a difference across the wines. The mean liking scores ($n = 92$) are shown in Figure 5. Wines AH1 and TAS were high in flint aroma intensity (mean values of 4.4 and 3.6), MP and AH6 were scored moderately (mean values

of 2.4), while wines YV1 and AH 9 were the lowest (mean values of 1.1 and 1.0). The wines MP, YV1, and AH9 were most well liked, with the high flint wines AH1 and TAS liked the least. From the PLS-R (Figure S2), mean liking scores were positively related to sweetness, viscosity, and toasty flavour, with the model having a high calibration predicted versus measured R^2 value of 0.98, although the validation R^2 was relatively low (0.41) and the MP wine was especially poorly predicted.

There was evidence for two clusters of consumers based on the liking scores (Figures 5 and S2). For cluster 1 (67% of the consumers) the pattern of liking scores was similar to that of the total sample of consumers, with the two high flint wines (AH1 and TAS) not well liked. For cluster 2 (33% of the consumers), the AH1 wine was the most well liked, while the lowest flint intensity wine YV1 was liked the least, and the PLS-R indicated that the toasty flavour was most strongly and positively associated with liking for this cluster, flint aroma being only moderately associated, while hotness was strongly negatively associated.

This finding expands on the consumer test conducted by Capone et al. [4] with unwooded research wines which also found a consumer group who responded negatively to samples with higher flint aroma. Overall wines with low to moderate flint aroma were well accepted, while those with high flint intensity could be considered polarizing to consumers. There was no difference found in demographics or usage and attitudes between the two clusters.

4. Conclusion

This study showed that the potent thiols, 2FMT and PMT, are at concentrations of sensory significance in most commercially produced Chardonnay wines from Australia. PMT and 2FMT were confirmed to be associated with “empyreumatic” nuances with 2FMT most strongly related to flint/struck-match/mineral aroma. Challenging our original hypothesis, the role of 2FMT is newly highlighted as a major contributor to this character in Chardonnay, rather than roasted coffee as suggested by previous reports [11]. The flint/struck-match/mineral note was found to be polarizing to consumer acceptance, with the largest proportion of consumers responding negatively to wines high in this character. Further work should assess the winemaking practices responsible for the occurrence of PMT and 2FMT. The odorant addition study demonstrated that different volatile compounds can, when present in a complex natural mixture such as wine, contribute to the same odour quality, even if in isolation (such as assessed in water or on a smelling strip) they are aromatically distinct. These findings emphasise the importance of pairing analytical quantification with robust sensory evaluation such as QDA and the need for confirmatory experiments when attempting to draw conclusions from associational tests with commercial samples. The inclusion of formal consumer testing can also provide an extra layer of practical insight into the flavour research.

Data Availability

The data used in this study are included in the manuscript or supporting information attached.

Conflicts of Interest

The authors declare that they have no conflicts of interest.

Authors' Contributions

Damian Espinase Nandorfy and Tracey Siebert contributed equally to this original research article.

Acknowledgments

DEN, TS, EB, DL, FW, SB, LP, AK, LF, and MB were supported by Australian grapegrowers and winemakers through their investment body, Wine Australia, with matching funds from the Australian government. RS and RK acknowledge the financial support from Deakin University. This work was supported by Wine Australia with levies from Australia's grapegrowers and winemakers and matching funds from the Australian Government. The AWRI is a member of the Wine Innovation Cluster in Adelaide, SA. Special thanks to Professor John Bekkers from the Eccles Institute of Neuroscience at the Australian National University for advice. The authors thank the members of the AWRI descriptive, technical quality, and survey sensory panels as well as Don Teng (SA node of Metabolomics Australia) for technical assistance and Dr Simon Schmidt (AWRI) for assistance with figure visualisations, and Affinity Labs is gratefully acknowledged.

Supplementary Materials

Table S1: summary of the self-reported demographic data collected from all participating consumers. Table S2: white wine calibration and validation data quantifying for *n*-alkyl γ -lactones using direct-immersion (DI)-SPME-GC-MSMS method, as determined in duplicate in commercially available Chardonnay wine (13.0% alcohol). Table S3: calibration and validation data for the quantification of benzyl compounds in white wine using HS-SPME-GC/MS in SIM mode. Table S4: mean sensory scores for the appearance and aroma attributes of the 24 commercial Chardonnay wines. Table S5: mean sensory scores for the taste, mouthfeel, and flavour attributes of the 24 commercial Chardonnay wines. Table S6: summary of the aroma compounds quantified in the 24 commercial Chardonnay wines. Figure S1: factors 1 and 5 of the scores and loadings plots from the PLS regression model. Plots were generated using sensory terms (*Y* variables) and compositional compounds (*X* variables) supported by statistical evidence ($P < 0.05$) to have differed among the wines. Figure S2: factors 1 and 3 of scores and loadings plots from the PLS regression model. Plots were generated using consumer response (*Y* variables) and sensory attributes (*X* variables) supported by statistical evidence ($P < 0.05$) to have differed among the wines. (*Supplementary Materials*)

References

- [1] H. Zwaardemaker, A. J. von Langeegg, and F. A. J. von Langeegg, *Die physiologie des geruchs*, W. Engelmann, Germany, 1895.
- [2] T. Tominaga, G. Guimbertau, and D. Dubourdieu, “Contribution of benzenemethanethiol to smoky aroma of certain *Vitis vinifera* L. wines,” *Journal of Agricultural and Food Chemistry*, vol. 51, no. 5, pp. 1373–1376, 2003.

- [3] T. Tominaga, G. Guimbertau, and D. Dubourdiou, "Role of certain volatile thiols in the bouquet of aged Champagne wines," *Journal of Agricultural and Food Chemistry*, vol. 51, no. 4, pp. 1016–1020, 2003.
- [4] D. L. Capone, A. Barker, P. O. Williamson, and I. L. Francis, "The role of potent thiols in Chardonnay wine aroma," *Australian Journal of Grape and Wine Research*, vol. 24, no. 1, pp. 38–50, 2018.
- [5] S. J. Lee and A. C. Noble, "Characterization of odor-active compounds in Californian Chardonnay wines using GC-olfactometry and GC-mass spectrometry," *Journal of Agricultural and Food Chemistry*, vol. 51, no. 27, pp. 8036–8044, 2003.
- [6] J. Gros, V. Lavigne, F. Thibaud et al., "Toward a molecular understanding of the typicality of Chardonnay wines: identification of powerful aromatic compounds reminiscent of hazelnut," *Journal of Agricultural and Food Chemistry*, vol. 65, no. 5, pp. 1058–1069, 2017.
- [7] T. E. Siebert, A. Barker, W. Pearson et al., "Volatile compounds related to 'stone fruit' aroma attributes in Viognier and Chardonnay wines," *Journal of Agricultural and Food Chemistry*, vol. 66, no. 11, pp. 2838–2850, 2018b.
- [8] T. E. Siebert, S. R. Barter, M. A. de Barros Lopes, M. J. Herderich, and I. L. Francis, "Investigation of 'stone fruit' aroma in Chardonnay, Viognier and botrytis Semillon wines," *Food Chemistry*, vol. 256, pp. 286–296, 2018c.
- [9] A. G. Cordente, D. Espinase Nandorfy, M. Solomon et al., "Aromatic higher alcohols in wine: implication on aroma and palate attributes during Chardonnay aging," *Molecules*, vol. 26, no. 16, p. 4979, 2021.
- [10] L. Culleré, J. Cacho, and V. Ferreira, "An assessment of the role played by some oxidation-related aldehydes in wine aroma," *Journal of Agricultural and Food Chemistry*, vol. 55, no. 3, pp. 876–881, 2007.
- [11] T. Tominaga, L. Blanchard, P. Darriet, and D. Dubourdiou, "A powerful aromatic volatile thiol, 2-furanmethanethiol, exhibiting roast coffee aroma in wines made from several *Vitis vinifera* grape varieties," *Journal of Agricultural and Food Chemistry*, vol. 48, no. 5, pp. 1799–1802, 2000.
- [12] P. Darriet, T. Tominaga, V. Lavigne, J.-N. Boidron, and D. Dubourdiou, "Identification of a powerful aromatic component of *Vitis vinifera* L. var. Sauvignon wines: 4-mercapto-4-methylpentan-2-one," *Flavour and Fragrance Journal*, vol. 10, no. 6, pp. 385–392, 1995.
- [13] R. C. Brown, M. A. Sefton, D. K. Taylor, and G. M. Elsey, "An odour detection threshold determination of all four possible stereoisomers of oak lactone in a white and a red wine," *Australian Journal of Grape and Wine Research*, vol. 12, no. 2, pp. 115–118, 2006.
- [14] H. Heymann, H. Hopfer, and D. Bershaw, "An exploration of the perception of minerality in white wines by projective mapping and descriptive analysis," *Journal of Sensory Studies*, vol. 29, pp. 1–13, 2014.
- [15] H. Guth, "Quantitation and sensory studies of character impact odorants of different white wine varieties," *Journal of Agricultural and Food Chemistry*, vol. 45, no. 8, pp. 3027–3032, 1997.
- [16] J. Prescott, L. Norris, M. Kunst, and S. Kim, "Estimating a 'consumer rejection threshold' for cork taint in white wine," *Food Quality and Preference*, vol. 16, no. 4, pp. 345–349, 2005.
- [17] A. J. Saliba, J. Bullock, and W. J. Hardie, "Consumer rejection threshold for 1,8-cineole (eucalyptol) in Australian red wine," *Food Quality and Preference*, vol. 20, no. 7, pp. 500–504, 2009.
- [18] A. Tarasov, N. Giuliani, A. Dobrydnev et al., "1,1,6-Trimethyl-1,2-dihydronaphthalene (TDN) sensory thresholds in Riesling wine," *Foods*, vol. 9, no. 5, p. 606, 2020.
- [19] A. J. Saliba, H. Heymann, J. W. Blackman, and J. B. MacDonald, "Consumer-sensory evaluation of Australian Chardonnay [online]," *Wine & Viticulture Journal*, vol. 28, pp. 64–66, 2013.
- [20] D. E. Nandorfy, T. Siebert, F. Watson, R. Keast, and I. L. Francis, "Understanding the interactive effects of volatile compounds contributing to 'stone fruit' aroma nuances in white wines," *Australian Journal of Grape and Wine Research*, vol. 28, no. 3, pp. 424–438, 2022.
- [21] D. E. Nandorfy, F. Watson, D. Likos et al., "Influence of amino acids, and their interaction with volatiles and polyphenols, on the sensory properties of red wine," *Australian Journal of Grape and Wine Research*, vol. 28, no. 4, pp. 621–637, 2022.
- [22] M. Parker, P. Osidacz, G. A. Baldock et al., "Contribution of several volatile phenols and their glycoconjugates to smoke-related sensory properties of red wine," *Journal of Agricultural and Food Chemistry*, vol. 60, no. 10, pp. 2629–2637, 2012.
- [23] M. J. Herderich, T. E. Siebert, M. Parker et al., "Spice up your life: analysis of key aroma compounds in Shiraz," in *Flavor Chemistry of Wine and Other Alcoholic Beverages*, pp. 3–13, American Chemical Society, Washington, DC, USA, 2012.
- [24] J. Ballester, M. Mihnea, D. Peyron, and D. Valentin, "Exploring minerality of Burgundy Chardonnay wines: a sensory approach with wine experts and trained panellists," *Australian Journal of Grape and Wine Research*, vol. 19, no. 2, pp. 140–152, 2013.
- [25] E. Zaldívar Santamaría, D. Molina Dagá, and A. T. Palacios García, "Statistical modelization of the descriptor 'minerality' based on the sensory properties and chemical composition of wine," *Beverages*, vol. 5, no. 4, p. 66, 2019.
- [26] D. R. Peryam and F. J. Pilgrim, "Hedonic scale method of measuring food preferences," *Food Technology*, vol. 11, 1957.
- [27] H. MacFie, "23- Preference mapping and food product development," in *Consumer-Led Food Product Development*, H. MacFie, Ed., pp. 551–592, Woodhead Publishing, Cambridge, UK, 2007.
- [28] K. H. Esbensen, D. Guyot, F. Westad, and L. P. Houmoller, *Multivariate Data Analysis: In Practice: An Introduction to Multivariate Data Analysis and Experimental Design*, Multivariate Data Analysis, Oslo, Norway, 2002.
- [29] G. M. Sullivan and R. Feinn, "Using effect size—or why the P value is not enough," *Journal of Graduate Medical Education*, vol. 4, no. 3, pp. 279–282, 2012.
- [30] R. L. Wasserstein, A. L. Schirm, and N. A. Lazar, "Moving to a world beyond 'p < 0.05'," *The American Statistician*, vol. 73, no. 1, pp. 1–19, 2019.
- [31] D. L. Capone, R. Ristic, K. H. Pardon, and D. W. Jeffery, "Simple quantitative determination of potent thiols at ultratrace levels in wine by derivatization and high-performance liquid chromatography–tandem mass spectrometry (HPLC-MS/MS) analysis," *Analytical Chemistry*, vol. 87, no. 2, pp. 1226–1231, 2015.
- [32] A. G. Cordente, C. D. Curtin, M. Solomon et al., "Modulation of volatile thiol release during fermentation of red musts by wine yeast," *Processes*, vol. 10, no. 3, p. 502, 2022.
- [33] T. E. Siebert, H. Smyth, D. Capone et al., "Stable isotope dilution analysis of wine fermentation products by HS-SPME-GC-MS," *Analytical and Bioanalytical Chemistry*, vol. 381, no. 4, pp. 937–947, 2005.
- [34] L. Pisaniello, F. Watson, T. Siebert, L. Francis, and J. L. Hixson, "The varietal influence of flavour precursors from

- grape marc on monoterpene and C13-norisoprenoid profiles in wine as determined by membrane-assisted solvent extraction (MASE) GC-MS," *Molecules*, vol. 27, no. 7, p. 2046, 2022.
- [35] A. P. Pollnitz, K. H. Pardon, M. Sykes, and M. A. Sefton, "The effects of sample preparation and gas chromatograph injection techniques on the accuracy of measuring guaiacol, 4-methylguaiacol and other volatile oak compounds in oak extracts by stable isotope dilution analyses," *Journal of Agricultural and Food Chemistry*, vol. 52, no. 11, pp. 3244–3252, 2004.
- [36] T. E. Siebert, M. R. Solomon, A. P. Pollnitz, and D. W. Jeffery, "Selective determination of volatile sulfur compounds in wine by gas chromatography with sulfur chemiluminescence detection," *Journal of Agricultural and Food Chemistry*, vol. 58, no. 17, pp. 9454–9462, 2010.
- [37] T. E. Siebert, A. Barker, S. R. Barter, M. A. de Barros Lopes, M. J. Herderich, and I. L. Francis, "Analysis, potency and occurrence of (Z)-6-dodeceno- γ -lactone in white wine," *Food Chemistry*, vol. 256, pp. 85–90, 2018a.
- [38] R. C. Cooke, D. L. Capone, K. A. van Leeuwen, G. M. Elsey, and M. A. Sefton, "Quantification of several 4-alkyl substituted γ -lactones in Australian wines," *Journal of Agricultural and Food Chemistry*, vol. 57, no. 2, pp. 348–352, 2009.
- [39] M. Spraul, M. Link, H. Schaefer, F. Fang, and B. Schuetz, "Wine analysis to check quality and authenticity by fully-automated 1H-NMR," *BIO Web of Conferences*, vol. 5, p. 2022, 2015.
- [40] T. Tominaga and D. Dubourdieu, "A novel method for quantification of 2-methyl-3-furanthiol and 2-furanmethanethiol in wines made from *Vitis vinifera* grape varieties," *Journal of Agricultural and Food Chemistry*, vol. 54, no. 1, pp. 29–33, 2006.
- [41] L. Mateo-Vivaracho, J. Zapata, J. Cacho, and V. Ferreira, "Analysis, occurrence, and potential sensory significance of five polyfunctional mercaptans in white wines," *Journal of Agricultural and Food Chemistry*, vol. 58, no. 18, pp. 10184–10194, 2010.
- [42] C. A. Black, M. Parker, T. E. Siebert, D. L. Capone, and I. L. Francis, "Terpenoids and their role in wine flavour: recent advances," *Australian Journal of Grape and Wine Research*, vol. 21, pp. 582–600, 2015.
- [43] G. Gutiérrez-Gamboa, T. Garde-Cerdán, Y. Moreno-Simunovic, and E. P. Pérez-Álvarez, "10- Amino acid composition of grape juice and wine: principal factors that determine its content and contribution to the human diet," in *Nutrients in Beverages*, A. M. Grumezescu and A. M. Holban, Eds., pp. 369–391, Academic Press, Cambridge, MA, USA, 2019.
- [44] L. J. Van Gemert, *Flavour Thresholds. Compilations of Flavour Threshold Values in Water and Other media*, Oliemans Punter and Partner, Utrecht, Netherlands, 2nd edition, 2011.
- [45] K. Skogerson, R. Runnebaum, G. Wohlgemuth, J. de Ropp, H. Heymann, and O. Fiehn, "Comparison of gas chromatography-coupled time-of-flight mass spectrometry and 1H nuclear magnetic resonance spectroscopy metabolite identification in white wines from a sensory study investigating wine body," *Journal of Agricultural and Food Chemistry*, vol. 57, no. 15, pp. 6899–6907, 2009.
- [46] R. Gawel, P. A. Smith, S. Cicerale, and R. Keast, "The mouthfeel of white wine," *Critical Reviews in Food Science and Nutrition*, vol. 58, no. 17, pp. 2939–2956, 2018.
- [47] V. Ferreira, "1- Volatile aroma compounds and wine sensory attributes," in *Managing Wine Quality*, A. G. Reynolds, Ed., pp. 3–28, Woodhead Publishing, Cambridge, UK, 2010.

Research Article

The Genome Assembly of *Vitis vinifera* cv. Shiraz

Cristobal A. Onetto ¹, Christopher M. Ward ¹, and Anthony R. Borneman ^{1,2}

¹The Australian Wine Research Institute, Glen Osmond, Urrbrae, South Australia 5064, Australia

²School of Agriculture, Food and Wine, The University of Adelaide, Adelaide, South Australia 5005, Australia

Correspondence should be addressed to Anthony R. Borneman; anthony.borneman@awri.com.au

Received 12 December 2022; Revised 15 March 2023; Accepted 29 April 2023; Published 11 May 2023

Academic Editor: Amber Parker

Copyright © 2023 Cristobal A. Onetto et al. This is an open access article distributed under the Creative Commons Attribution License, which permits unrestricted use, distribution, and reproduction in any medium, provided the original work is properly cited.

Background and Aims. Shiraz (Syrah) is a dark-skinned cultivar of the wine grape *Vitis vinifera* that forms the basis of some of the world's most iconic wines. Worldwide, Shiraz is the fourth most planted grapevine cultivar; however, it represents the most planted cultivar in Australia. Given the importance of Shiraz to worldwide wine production, this study aimed to produce a reference genome for this cultivar while investigating the unique genetic variants and ancestral origins of this iconic variety. **Methods and Results.** Long-read ONT data were selected to produce a highly contiguous genome assembly for Shiraz. Phylogenetic reconstruction using high-quality genome assemblies for wine grape cultivars provided further support of a kinship between Shiraz and Pinot Noir. Harnessing long-read data, transposable element insertions potentially affecting gene function were characterized in Shiraz and assessed relative to other cultivars. This revealed a heterogeneous landscape of transposon insertion points across cultivars and uncovered a specific combination of allelic variants at the *VviTPS24* terpene synthase locus. **Conclusions.** This establishment of a Shiraz genome provides a detailed view of the genetics that underpin this cultivar, including the discovery of a specific combination of *VviTPS24* variants, which when combined with appropriate environmental triggers may allow Shiraz to produce high levels of rotundone, the aroma compound responsible for the distinctive peppery characteristics of this cultivar. **Significance of the Study.** The availability of a reference genome for Shiraz expands the pool of genomes available for wine grapes while providing a foundation resource for whole-genome studies involving this iconic cultivar, including intracultivar variant identification and transcriptomic studies using a matching reference genome.

1. Introduction

Shiraz (Syrah) is a dark-skinned cultivar of the wine grape *Vitis vinifera*, which is used to create some of the world's most iconic red wines. There have been many theories surrounding the history of Shiraz, including a potential origin in the city of Shiraz in ancient Persia (now a part of Iraq). However, previous DNA-based marker analysis has identified Shiraz as the offspring of the grape cultivars Dureza (dark-skinned) and Mondeuse Blanche (white-skinned), two-cultivars that are considered native to the northern Rhône in the south-east of France [1]. It is therefore likely that Shiraz also originated in this geographic location through a natural outcrossing event, which may date back to Roman times.

Globally, Shiraz is the fourth-most planted grapevine cultivar in the world. France contains the largest plantings of Shiraz, where it represents the third most commonly planted wine grape. In Australia, Shiraz is the most widely planted cultivar, with 40,000 hectares of vines, positioning the country as second only to France in worldwide plantings of Shiraz. Australia is also home to many of the oldest Shiraz vineyards in the world, with many vines that predate the devastation of grapevine phylloxera on European vineyards in the 1800s.

One of the trademark flavours of Shiraz, and especially of Shiraz grapes grown in cool climates, is black pepper [2]. These peppery notes have been attributed to the presence of the highly-potent sesquiterpene rotundone, with reported detection thresholds as low as 16 ng/L in red wine and 8 ng/L in water [3]. Although being reported in comparatively

higher concentrations in Shiraz, rotundone has also been detected in several other cultivars, with Duras, Vespolina, and Grüner Veltliner also displaying relatively high concentrations of this compound [4]. While the complete biosynthetic pathway of rotundone has not been elucidated, it has been shown that the sesquiterpene synthase *VviTPS24* is responsible for the biosynthesis of the precursor of rotundone, α -guaiene [5]. Rotundone can then be formed from α -guaiene either by simple oxidation or enzymatically through the cytochrome P450 α -guaiene 2-oxidase [6, 7].

There are thousands of distinct cultivars of *V. vinifera* that are used for wine production, which display extensive phenotypic diversity. Given the economic importance of this species, genome sequencing is being used to determine the genetic differences that separate the various types of wine grapes. Early efforts in the production of reference genomes for *V. vinifera* were confounded by high levels of heterozygosity and hemizygoty [8], such that inbreeding was used to produce a homozygous line derived from Pinot Noir for initial attempts at assembling a complete grapevine genome [9]. Advances in “long-read” sequencing and phased genome assembly algorithms have now allowed for the production of highly-contiguous assemblies for the grapevine cultivars Chardonnay [10, 11], Cabernet Sauvignon [12], Carménère [13], Zinfandel (syn Primativo) [14], Nebbiolo [15], Cabernet Franc [16], Riesling [17], and Merlot [18]. These studies have expanded the knowledge on the mechanisms of genome evolution in this species, highlighting the importance of structural variants and repetitive elements as drivers of cultivar and clonal phenotypic diversity.

Given the importance of Shiraz to worldwide wine production, a reference genome assembly for this cultivar is required. Long-read data were selected to produce a highly contiguous diploid genome assembly for Shiraz, which could provide the basis for detailed phylogenetic investigations and to compare structural variations across Shiraz and other cultivars for which high-quality, phased genomes were available. Overall, this study aims to provide a resource for future comparative genomics of grapes with implications for diploid genome evolution, the determination of clonal variation, and historical provenance of *V. vinifera* L. varieties.

2. Materials and Methods

2.1. Sampling, DNA Extraction, and Whole Genome Sequencing. DNA was extracted from early-season *V. vinifera* Shiraz clone 1654 leaves taken from field-grown plants at the Coombe Vineyard (Waite Campus, University of Adelaide, Adelaide, Australia). Samples were immediately frozen and ground to powder in liquid nitrogen. Approximately 100 mg of plant material was used for DNA extraction using a DNeasy Plant Mini Kit (QIAGEN, Australia), following the manufacturer’s instructions. Prior to Oxford Nanopore Technologies (ONT) sequencing library preparation, high-molecular weight DNA >10 kb was enriched using a Short Read Elimination Kit SRE XS (Pacific Biosciences, CA, USA). Sequencing libraries were prepared using the SQK-LSK110 kit and loaded into two FLO-

MIN106 and one FLO-MIN111 flow cells. Fast5 files were base-called using Guppy v. 5.0.16 (Oxford Nanopore Technologies, Oxford, UK) with the “sup” model and a minimum quality score filtering of 7. A total sequencing yield of 30,663 Mb was obtained (63-fold coverage) with an N_{50} length of 21.8 kb. For short-read sequencing, genomic libraries were prepared using the Illumina DNA Prep library kit and sequenced on a Novaseq 6000 instrument using an S4 flow cell and 2×150 bp chemistry (Ramaciotti Centre for Genomics, NSW, Australia). A total of 97 million read-pairs were obtained (64-fold coverage).

For cultivar Sauvignon Blanc, DNA was extracted from early-season leaves taken from a field-grown plant of clone F4V6 located at the South Australian Research and Development Institute Nuriootpa Research Centre (Nuriootpa, Barossa Valley, Australia). Samples were ground to powder in liquid nitrogen, and nuclei were isolated following protocol 102-574-800 (Pacific Biosciences, CA, USA). DNA was extracted from nuclei using the Nanobind plant nuclei kit (Pacific Biosciences, CA, USA), following the manufacturer’s instructions. High-molecular weight DNA >10 kb was enriched using a Short Read Elimination Kit SRE XS (Pacific Biosciences, CA, USA). Sequencing libraries were prepared using the SQK-LSK112 kit and loaded into two FLO-MIN112 flow cells. Fast5 files were base-called using Guppy v. 6.4.2 (Oxford Nanopore Technologies, Oxford, UK) with the “sup” model and a minimum quality score filtering of 7. A total sequencing yield of 19,655 Mb was obtained (43-fold coverage). For short-read sequencing, genomic libraries were prepared using DNA from clone F4V6 with the Illumina DNA Prep library kit and sequenced on a Novaseq 6000 instrument using an S4 flow cell and 2×150 bp chemistry (Ramaciotti Centre for Genomics, NSW, Australia).

2.2. Genome Assembly and Annotation. Preliminary assemblies for Shiraz were performed using Canu v. 2.1.1 [19] and Flye v. 2.8.3 [20] and then polished with ONT reads using Medaka v. 1.5.0 (<https://github.com/nanoporetech/medaka>). Both assemblies were then combined using quickmerge v. 0.3 [21] with the Canu assembly as reference and a minimum overlap of 20 kb, and polished twice using short-reads and Pilon v. 1.24 [22]. Lastly, allelic contig reassignment was performed using Purge Haplotigs v. 1.1.2 [23] and assessed with BUSCO v. 5.3.2 [24] using the embryophyta ODB v10 database. The same methodology was applied for the genome assembly of the cultivar Sauvignon Blanc using the assemblers Canu v. 2.1.1 [19] and SMARTdenovo [25]. A scaffolded version of the Shiraz primary assembly was created for visualization purposes using the *V. vinifera* reference genome (accession GCA_000003745.2) and RagTag v. 2.1.0 [26].

A custom repeat library was built for Shiraz using RepeatModeler v. 2.0.3 [27] and the LTR pipeline extension, which applies LtrHarvest and Ltr_retriever [28] during *de novo* repeat identification. Identification of miniature inverted-repeat transposable elements (MITEs) was performed using MITE-Tracker [29]. The custom repeat

sequences were combined into a single library and used for repeat annotation using RepeatMasker v. 4.1.2 [30]. Gene prediction was performed following the funannotate pipeline v. 1.8.13 [31], including Genemark-ES v. 4.68 [32], SNAP [33], Augustus v. 3.3.3 [34], and Glimmerhmm v. 3.0.4 [35] annotations, allowing a maximum intron length of 10 kb. Previously published RNA-seq data for Shiraz ([36], Table S1) and the protein data of the *V. vinifera* reference genome (accession GCA_000003745.2) were provided as evidence for gene model prediction.

Homo and hemizygous regions were investigated by mapping short-read data to the primary assembly. Heterozygous SNPs were called using VarScan v. 2.3 [37] and read-depth and SNP density calculated in 50 kb windows (25 kb steps) using BEDTools v. 2.30.0 [38].

2.3. Phylogenetics and Identity by Descent (IBD). Single-copy orthologs (SCOs) were identified in Nebbiolo, Chardonnay, Carménère, Zinfandel, Cabernet Sauvignon, Cabernet Franc, Riesling, and Merlot along with *V. vinifera sylvestris* and *V. rotundifolia*, using the BUSCO eudicot dataset. Alignment was then carried out using MUSCLE [39]. To ensure that errors in annotation do not bias phylogenetic reconstruction, each alignment was manually investigated and trimmed to remove mis-annotated exons between transcripts through the excision of regions representing insertions and/or deletions that were not present in any other sample or sequences that represented unaligned extensions to the start or end of the gene. Each gene alignment was imported into BEAST2 [40] with unlinked Hasegawa-Kishino-Yano site and relaxed log normal clock [41] model priors. A MCMC chain was then run across 1×10^8 samples with a yule tree prior. Tracer was used to identify when the model began to mix and select an appropriate burn-in (48%).

Previously published RAD-Seq Illumina paired-end reads from cultivars Dureza and Mondeuse Blanche [42] were mapped to the Shiraz primary assembly using Mini-map2 v. 2.24 [43]. Mapped reads had their variants called (MQ > 20) and were filtered (DP > 5, GQ > 20, F_MISS = 0) using BCFtools v. 1.16 [44]. Heterozygous sites in Shiraz were further filtered to remove any sites where allele depth did not fit a binomial distribution, thereby removing somatic mutations developed after the cross event between Dureza and Mondeuse blanche. Putative alleles that suffered from dropout due to mutations in the RADtag cut site were identified by inspecting the first four base pairs of both the forward and reverse reads for mutations within Shiraz with geaR v. 0.1 [45]. Any tags that contained mutations were removed from the analysis space. Filtered variants were converted to the GDS format and IBD calculated using SNPrelate v. 1.32 [46].

2.4. Characterization of TE Content and Comparative Genomics. Read depth and structural variant information were leveraged using plyranges v. 1.18 [47] and geaR v. 0.1 [45] to collapse fragmented transposable element annotations into a single record. First, read depth was calculated

against the Shiraz primary assembly across the middle 10 bp of a TE annotation using SAMtools v. 1.16.1 [44]. This was then compared to the median read depth observed across surrounding coding regions and overlapped with structural variants called from long-read nanopore data using Sniffles v. 2.0.2 [48] to determine zygosity. Homozygous annotations were then conditionally merged if adjacent annotations from the same class were both contained within the same read and were also homozygous. Heterozygous annotations were then compared to overlapping heterozygous structural variants. Adjacent transposable element annotations that were both heterozygous and contained within a single structural variant were merged into one record.

Transposable element annotations within introns and 1 kb of an orthologs TSS or stop codon were extracted and intersected to identify putative genic TE insertions. Exonic insertion points were identified by first extracting gene and CDS features from the Pinot Noir reference [9] genome and annotation sourced from Ensemble Plants (PN40024.v4).

Putative genic TEs were then leveraged against Nebbiolo, Chardonnay, Carménère, Zinfandel, Cabernet Sauvignon, Sauvignon Blanc, Riesling, and Merlot long-read data (see Table S1 accession number) structural variants using Sniffles v. 2.0.2 [48].

Publicly available short-read data from 23 common cultivars (see Table S1 for accession number) was used to determine if the TE insertion in *VviTPS24* is present in other cultivars. Data was first inspected for quality using ngsReports v. 2.0.1 [49], mapped to the Shiraz primary assembly using BWA-mem v. 0.7.17 [50], and filtered to remove any reads with MQ below 20 using SAMtools v. 1.16.1 [44]. Both the upstream and downstream breakpoints of the TE insertion were manually inspected for reads that contained both the *VviTPS24* coding region and TE sequence and for paired reads whose insert spanned the TE insertion point (i.e. reads that mapped to *VviTPS24* exon 5 whose mate mapped to the TE). For a sample to be considered to contain the TE, evidence must have been found at both the upstream and downstream breakpoints. The zygosity of the TE in each variety was then confirmed using sliding 31 mers of each breakpoint and the reconstructed functional allele with Jellyfish v. 2.3 [51].

3. Results and Discussion

3.1. Haplotype Phased Assembly of the Cultivar Shiraz. Recent advances in long-read DNA sequencing technologies have enabled the creation of high-quality, diploid genome assemblies for repeat-rich and highly heterozygous plant species such as *V. vinifera* [12]. Haplotype-phased genome assemblies have been produced for a handful of the most widely planted cultivars, including Cabernet Sauvignon [12], Merlot [18], and Chardonnay [10, 11]; however, there is no publicly available reference genome for Shiraz to date, despite it representing the fourth-most planted cultivar in the world. To address this knowledge gap, a reference genome for the cultivar Shiraz was produced using a hybrid sequencing approach that included 63-fold coverage of ONT long reads and 64-fold coverage of Illumina short-reads.

Clone 1654 was selected as the sourced plant material due to its widespread use in the Australian wine industry.

After assembly, polishing, and haplotype phasing, a 476 Mb primary assembly with an N_{50} of 1.9 Mb was obtained, falling well within the expected haploid size for *V. vinifera* and only 2% smaller than the inbred Pinot Noir reference genome (PN40024). While larger primary assemblies have been obtained for other wine cultivars (Cabernet Sauvignon: 590 Mb, Cabernet Franc: 570 Mb, Merlot: 606 Mb, Chardonnay: 490 Mb, Carménère: 623 Mb, Nebbiolo: 561 Mb, and Zinfandel: 591 Mb), not all of the reported grapevine assemblies have been processed with tools to optimize the reassignment of allelic contigs, and the larger sizes are likely due to the retention of both copies of highly heterozygous regions within the primary assembly contig pool.

Haplotype phasing generated a total of 356 Mb of associated haplotigs with an N_{50} of 199 kb (Table 1). The primary assembly included 95.1% of BUSCO orthologues and contained 56.1% repetitive content, which was represented primarily by gypsy and copia LTR retroelements (Table 1). After removal of repeat-associated gene models a total of 32,333 protein-coding genes were retained (Table 1).

To assess the degree and distribution of hemizyosity and homozygosity across the Shiraz genome, information from read-depth and heterozygous variant density were assessed across both the primary and scaffolded assemblies (Figure 1). Selection of regions characterized by half the median read-depth and low heterozygous variant density highlighted 54 Mb (10.5%) of the Shiraz assembly as hemizygous, with these regions predicted to encode 3017 genes (Figure 1). Similar genome wide hemizyosity levels have been reported in distantly-related cultivars such as Cabernet Sauvignon (15.5% of genes in primary assembly) and Chardonnay (14.6% of genes in primary assembly) [11], suggesting a basal level of hemizyosity that separates pairs of parental alleles in *V. vinifera*.

The functional consequences of hemizygous regions were assessed through gene ontology functional enrichment. This revealed an overrepresentation of several functional classes, including chitinases that form part of the systemic acquired resistance mechanism of *V. vinifera* [52] and terpene synthases (Table S2). This is not surprising as previous comparative genomic studies have suggested that hemizyosity and variation in gene content have a potential contribution towards the phenotypic differences between cultivars [11, 15].

Homozygous regions, which were categorized as areas of median read-depth and low heterozygous variant density, comprised 11.7% of the primary assembly. The longest run of homozygosity was a stretch of 4.8 Mb located at one end of chromosome 9 (Figure 1). In comparison, Chardonnay, which has been suggested to be a naturally inbred cultivar [10], was shown to contain twice the levels of homozygosity (22.4%) as Shiraz, providing support that the parental cultivars of Shiraz do not share a recent common ancestor.

TABLE 1: Shiraz assembly statistics.

	Primary assembly	Haplotigs
Assembly size (bp)	476,422,955	356,328,851
Contigs	435	2,408
N_{50}	1,969,387	199,587
Largest contig	7,765,998	2,855,789
Predicted proteins	32,333	22,725
Repetitive content (%)	56.1	62.3
Predicted hemizygous (bp)	50,426,450	
Predicted hemizygous genes	3,017	
Predicted homozygous (bp)	55,847,349	
Complete BUSCOs	1536 (95.1%)	
Complete and single-copy BUSCOs	1466 (90.8%)	
Complete and duplicated BUSCOs	70 (4.3%)	

The density of genes (Figure 1(c)) and LTR retrotransposons (Figure 1(d)) displayed a distinctive pattern whereby gene density decreased, with a concomitant increase in LTR density surrounding centromeric regions. However, a clear spike in LTR density was also observed outside of the centromeric region on Chr 10 (Figure 1(d)), suggesting a nested transposable element insertion region. Detailed annotation of this LTR repeat domain rich region on Chr 10 identified 29 separate LTR repeat domains and 127 internal domains, which were distributed across an 88 kb region (Figure S1). Long-terminal repeat insertions appeared to be nested within the internal domains, with multiple LTR domains occurring within small (<2 kb) windows. Analysis of the mapped reads (Figure S2) showed no indication of a mis-assembly across the region, with long reads spanning multiple nested LTR domains.

3.2. Phylogenetic Reconstruction and Parentage of Shiraz.

The availability of several long-read grapevine genomes offered the ability to assess phylogenetic relatedness that encompassed information inherent within both phased alleles across the diploid genome. SCOs were identified across the ten long-read *V. vinifera* genomes, in addition to *V. vinifera sylvestris* and *V. rotundifolia* as outgroups. Phylogenetic reconstruction using these 437 SCOs revealed Pinot Noir as the closest relative of Shiraz (Figure 2), providing further support for their proposed kinship [53]. Cabernet Franc and its offspring Cabernet Sauvignon, Carménère, and Merlot (Figure 2) were closely related, yet clade branching placed Cabernet Franc as the most derived and Merlot as more closely related to Riesling than the Cabernet clade. This suggests Merlot and Riesling may share a close relative as alleles from the non-Cabernet Franc parental haplotype may be influencing the topology. The observed topology is likely due to the “primary” assembly of each of the cultivars containing the most contiguous reference allele, producing pseudohaplotypes that represent a random blending of the two true parental haplotypes. Therefore, care should be taken in future studies when interpreting the trees containing closely related crop plants

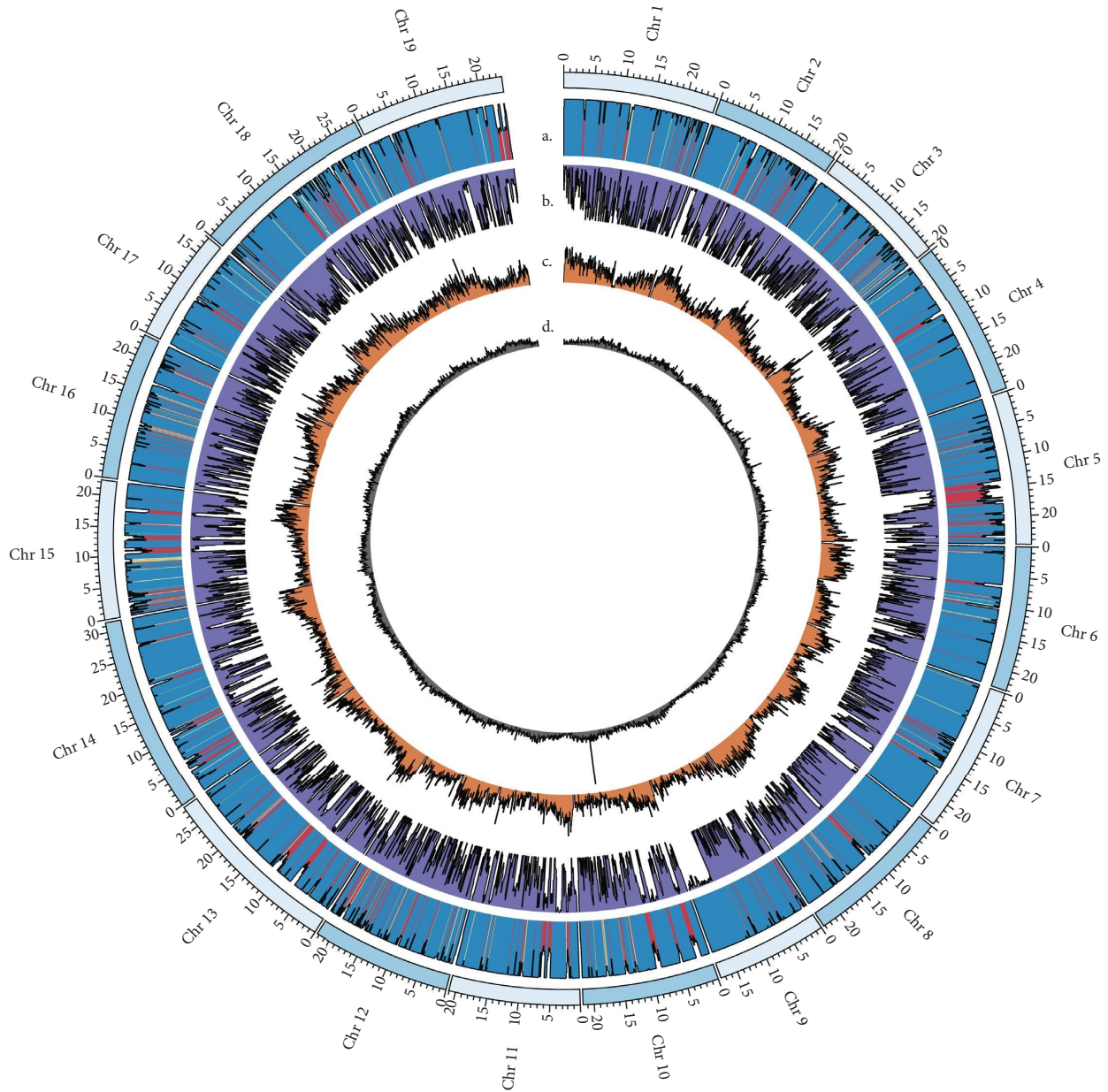


FIGURE 1: Genome assembly of *V. vinifera* cv. Shiraz. Circos plot depicts chromosome-scaffolded primary assembly using the Pinot Noir 12X reference genome (accession GCF_000003745.3). (a) Read-depth of Illumina reads mapped to the primary assembly with color scale ranging from \geq median read-depth (blue) to half median read-depth (red), (b) heterozygous variants, (c) gene, and (d) LTR retrotransposon density.

with mixed ancestry unless true haplotypes can be resolved and not relying in algorithmic phasing.

As SSR data was previously used to suggest that Mondeuse Blanche and Dureza comprise the parents of Shiraz [1], existing RAD-Seq data from these two cultivars [42] was utilized to provide further support to their relationship to Shiraz. Whole genome variant calling was performed using the RAD-Seq data of Mondeuse Blanche and Dureza against the Shiraz genome sequence, producing a space of 81,551 variants for analysis. Quality filtering, removing calls within annotated repeats, and RAD allele dropout decreased the total number of useable

genotypes to 22,358 for kinship estimation. During filtering, allelic ratio was used to calculate a binomial probability ($np = 0.5$) at each heterozygous Shiraz variant to remove variants that may be somatic from the Shiraz genotypes. Kinship estimation and identity by descent (IBD) calculation was then carried out using the MOM method. A kinship matrix consistent with a parent-offspring relationship was calculated for Dureza and Shiraz ($IBD = 0.25$, $(k_0 0, k_1 1)$). However, values that would be considered consistent with a true parent-offspring relationship were not recovered for Mondeuse Blanche ($IBD = 0.192$, $(k_0 0.23, k_1 0.77)$). This suggests that

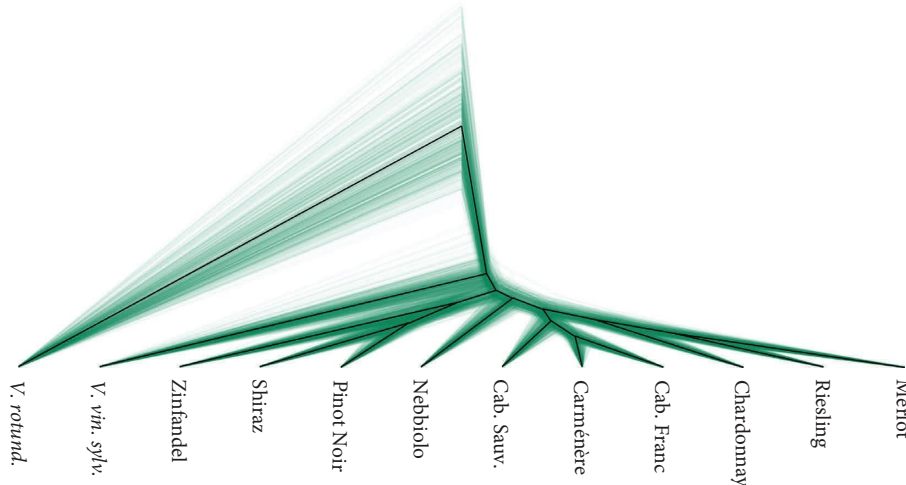


FIGURE 2: Bayesian phylogeny of Shiraz and other common cultivars with *Vitis vinifera sylvatica* (*V. vin. sylv.*) and *Vitis rotundifolia* (*V. rotund.*) used as outgroups. Cab. Sauv.: Cabernet Sauvignon, Cab. Franc: Cabernet Franc.

the relationship between Mondeuse Blanche and Shiraz may be more complex than previously estimated using SSR markers.

3.3. Repeat Characterization in Shiraz Reveals TEs near Genes Absent from Other Cultivars. Somatic variation and specifically transposable element (TE) insertions have been shown to drive adaptation [54, 55] and to provide an important source of genetic diversity for trait selection and breeding in clonally propagated crop plants [56, 57]. Disruption of proper gene function via the insertion of TEs can either occur directly through disruption of the open reading frame or indirectly through influencing transcription by insertion into regulatory regions or through chromatin availability and epigenetic silencing [58–60]. In *V. vinifera*, TE insertions have been identified as the causative mutation that underpins important phenotypes such as differences in berry color [61], which have convergently occurred across multiple lineages [61, 62] through insertion of the Gret1 LTR into the promoter region of *VviMYBA1* [61, 63].

Genome-wide characterization of TE content identified 125,736 TE annotations in the Shiraz primary assembly (Figure 3(a)). Long terminal repeats (LTR) comprised the most frequent TE class, with Copia and Gypsy LTRs representing 50.6% of all annotated TEs. LINE elements (17.8%) were the third most common class, followed by MITEs (14%) (Figure 3(a)).

As TE insertions within genic regions can impact gene function, these were mapped across the Shiraz genome and compared to those in other cultivars. First, the Shiraz gene and repeat annotations were utilized to identify TEs within 1 kb of either the 5' or 3' termini of each gene model, in addition to those within intronic regions. This identified 10,570 TE annotations upstream (Table S3) and 10,223 annotations downstream (Table S3), which may affect gene regulation (Figure 3(b)). In contrast to the genome-wide data, in which LTR elements are the most frequent TE across the genome, MITE elements were most commonly observed

upstream (24.2%) and downstream (21.6%) of genes, agreeing with past studies [58, 64]. LINE insertions were the most frequently observed TE within intronic regions, comprising 52.9% of the 24,721 intronic TEs (Table S3).

Insertions of TEs within exons would evade detection by the previous methodology, as it is likely that exonic insertion would interfere with correct gene annotation within Shiraz. To overcome this limitation, a secondary methodology was applied in which gene annotations were extracted from the Ensembl Pinot Noir reference genome entry and mapped to the Shiraz primary assembly. This identified a total of 31,839 putative gene annotations, which were then overlapped with the Shiraz TE annotations, revealing 83 potential exonic insertions in Shiraz (Table S3) (Figure 3(b)).

To identify genic TE insertions that are variable between cultivars or specific to Shiraz, structural variants called from long-read data of Cabernet Sauvignon, Chardonnay, Carménère, Merlot, Nebbiolo, Riesling, Shiraz, Sauvignon Blanc, and Zinfandel were cross-referenced against the set of putative genic TEs. This identified 4,554 genic TE insertions variable between these cultivars (Table S4), which may contribute to their phenotypic diversity. Shiraz-specific TE insertions were also identified (Table S5), 34 upstream (LTR: 82.3%; MITE: 11.8%; and LINE: 5.9%) (Figure 3(c) (i)), 28 downstream (LTR: 92.9% and MITE: 7.1%) (Figure 3(c) (ii)), 45 intronic (LTR: 55.6%; MITE: 2.2%; and LINE: 42.2%) (Figure 3(c) (iii)), and 6 exonic (LTR: 100%) (Figure 3(c) (iv)). Furthermore, the majority of Shiraz-specific TEs were in the heterozygous state (88.6%).

3.4. The *VviTPS24* Locus Comprises a Distinct Genotype in the Cultivar Shiraz. From the few characterized enzymes involved in the production of aroma compounds or their precursors, terpene synthases have received particular attention due to their role in the biosynthesis of volatile terpenoids that define the varietal characters of several grape cultivars [65, 66]. The potent bicyclic sesquiterpene

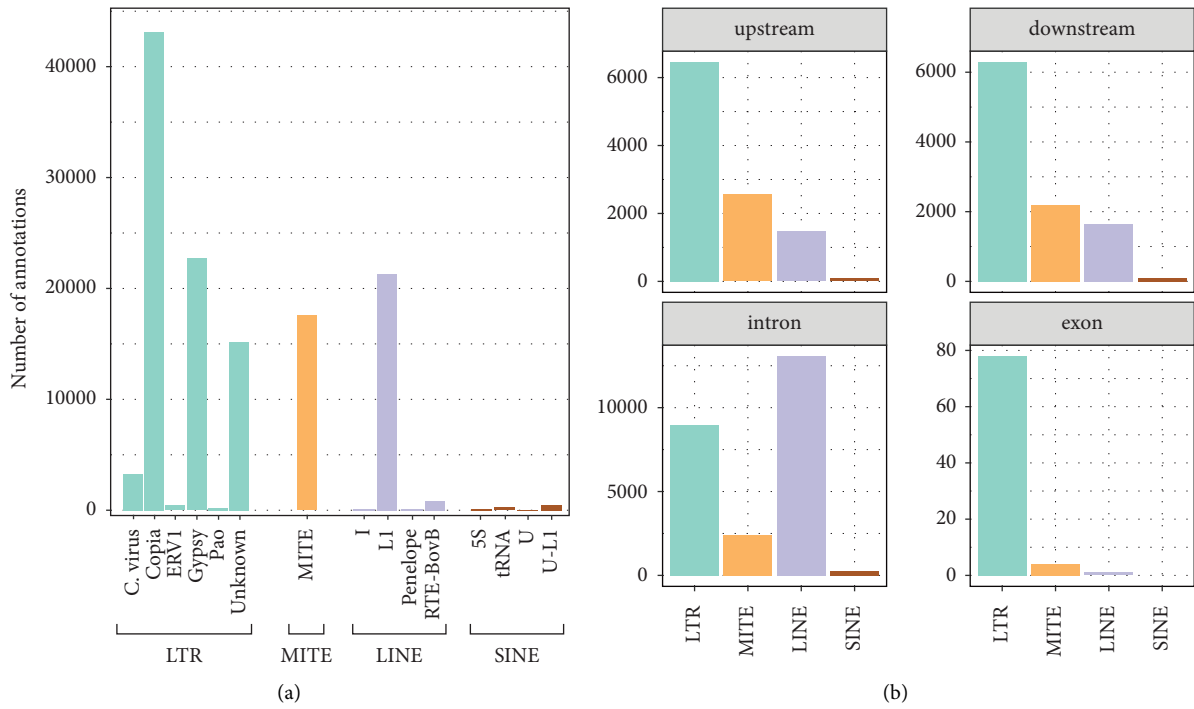


FIGURE 3: Continued.

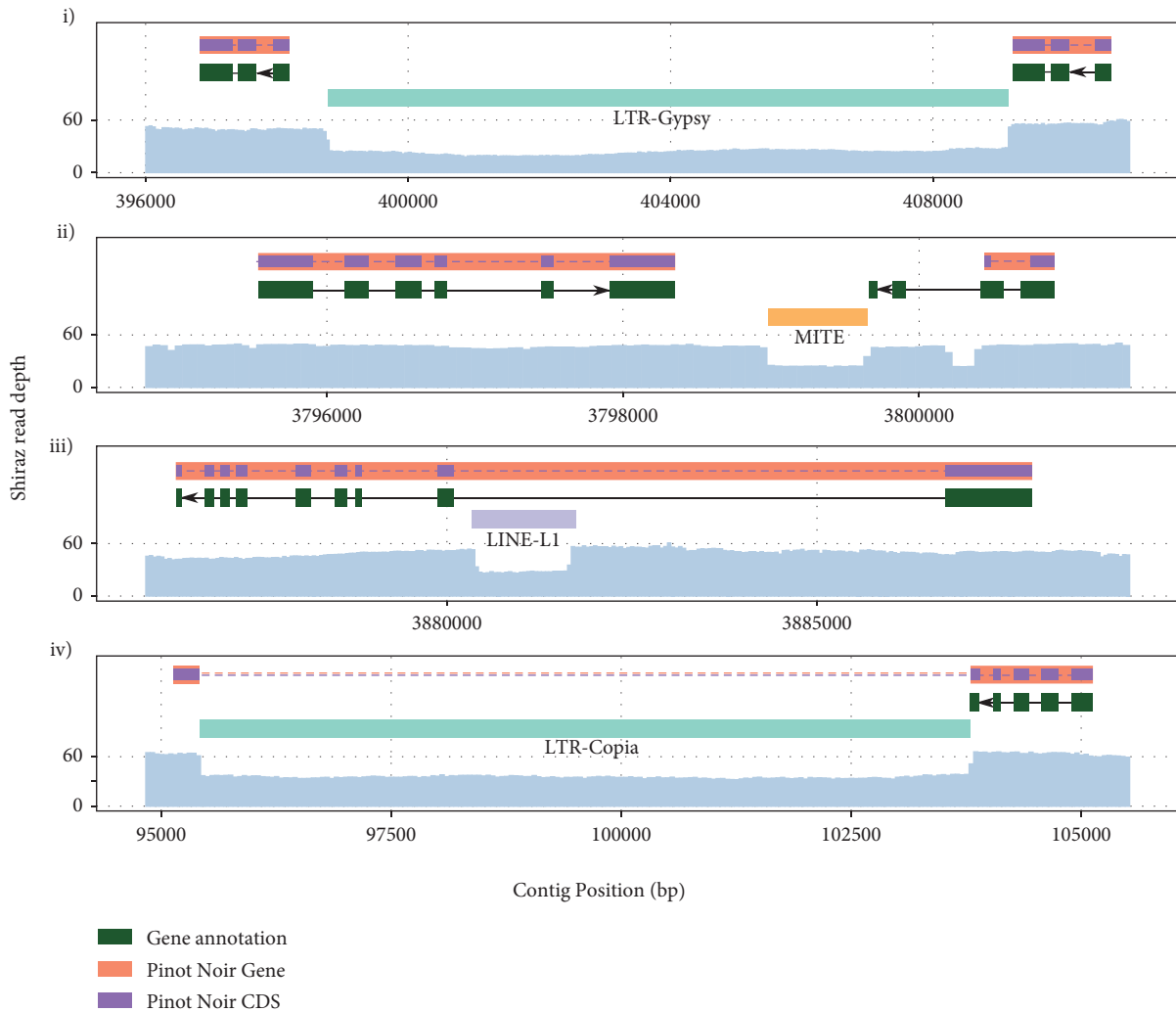


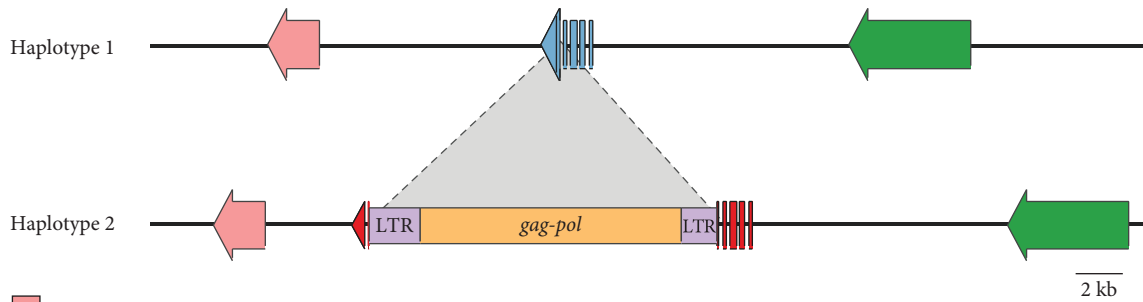
FIGURE 3: Repeat structure of *V. vinifera* Shiraz clone 1654. (a) Genome wide classification of transposable elements (TEs) annotated in the Shiraz primary assembly. LTR, MITE, LINE, RC, and SINE TEs are broken down into subclasses and colored according to their class. (b) Classification of TEs that are annotated 1 kb upstream, downstream, and intronic of an annotated gene or exonic of a Pinot Noir gene/CDS combo. Gaps in Pinot Noir gene/CDS alignments to the Shiraz reference are depicted as dashed lines. (c) TEs that are specific to Shiraz after overlapping genic TEs with structural variants from Nebbiolo, Chardonnay, Carménère, Zinfandel, Cabernet Sauvignon, Sauvignon Blanc, Riesling, and merlot long-read data: (i) upstream, (ii) downstream, (iii) intronic, and (iv) exonic.

rotundone is characterized by a peppery aroma and is responsible for one of the key varietal characteristics of Shiraz [2]. The biosynthesis of rotundone involves a two-step process, involving the production of the precursor α -guaiene from farnesyl pyrophosphate by an allele of the sesquiterpene synthase *VviTPS24* [5] and the subsequent oxidation of α -guaiene into rotundone [6, 7]. Wildtype *VviTPS24* produces an array of sesquiterpenes, of which only a minor fraction is α -guaiene [66]. However, a high α -guaiene producing variant of *VviTPS24* has been recently reported in Shiraz, which contains two polymorphisms in the active site of the protein [5]. This is likely to be linked to the ability to synthesize high levels of rotundone, although it remains to be determined if this variant is present in other cultivars.

Investigation of the *VviTPS24* locus in the diploid genome assembly of Shiraz revealed a single predicted gene model (Gene ID 002051) with 98.9% protein similarity to the *VviTPS24* ortholog from Pinot Noir (NCBI accession XP_002282488) that was present in the haplotig pool. The protein predicted by this gene annotation in Shiraz contained both the T414S and V530M substitutions that have been previously associated with higher production of α -guaiene [5] (Figure S3).

Given the diploid nature of the Shiraz assembly, a second allele of *VviTPS24* would also be expected to be present in the primary contigs of the genome assembly. To determine if this second allele was present, but missing from the initial annotation, splice-aware mapping of the CDS of *VviTPS24* was performed against the primary assembly. Results

Chromosome 19
V. vinifera
 Shiraz



- IPR001906-Terpene synthase
- VvGuaS* IPR001906-Terpene synthase
- VvTPS24* IPR001906-Terpene synthase
- IPR002942-RNA-binding S4 domain

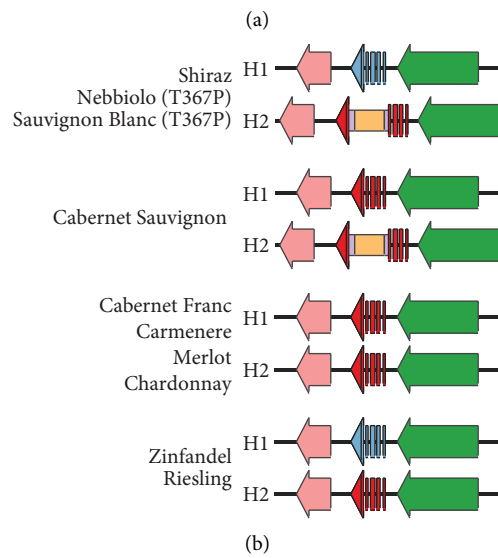


FIGURE 4: Continued.

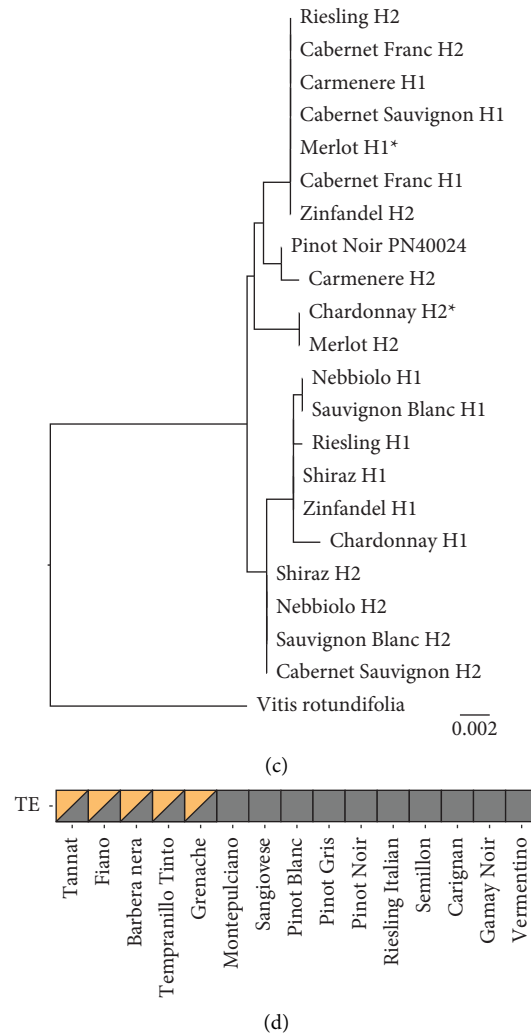


FIGURE 4: The *VviTPS24* locus in *V. vinifera*. (a) Functional annotation of the *VviTPS24* locus in the haplotypes of *V. vinifera* Shiraz. *VviGuaS* (blue) represents the polymorphic variant of *VviTPS24* containing the T414S and V530M amino acid substitutions previously reported [5]. *VviTPS24* (red) represents an allele without the T414S and V530M amino acid substitutions. Dotted lines depict the insertion point of a transposable element within exon 5 of *VviTPS24*. (b) Schematic representation of the *VviTPS24* locus in the haplotype phased assemblies of nine additional *V. vinifera* cultivars. (c) Maximum likelihood phylogenetic tree predicted from the CDS of *VviTPS24* for nine *V. vinifera* cultivars with *V. rotundifolia* as an outgroup. The CDS for all alleles including retroelement disrupted variants were manually predicted using the *VviTPS24* CDS of the pinot noir PN40024 reference genome. Cultivars denoted with an asterisk (*) contain an insertion/deletion within the CDS of *VviTPS24*. (d) Presence (orange) and absence (grey) of a retroelement within *VviTPS24* for 15 *V. vinifera* cultivars predicted using publicly available short-read data (Table S1).

showed the presence of a second putative allele of *VviTPS24* that contained a large, 15 kb insertion within exon 5 (Figure 4(a)). Annotation of this large insertion using the RepBase database revealed the insertion to be a Ty3-gypsy-type retrotransposon with high similarity to the Gypsy18 LTR of grapevine (NCBI accession AM476928) [67]. Manual annotation of this presumably inactivated allele of *VviTPS24* indicated that, in the absence of the LTR insertion, the protein sequence of the second allele would have 99.5% similarity to the Pinot Noir *VviTPS24* and only contain the T414S substitution (Figure S3). Overall, these results indicate that due to this unique combination of SNP and structural variation in Shiraz, the main product of the *VviTPS24* locus would be α -guaiene.

To obtain a broader understanding of the potential metabolic pathways underpinning rotundone biosynthesis in other cultivars, the *VviTPS24*, *VviFPPS* (farnesyl diphosphate synthase) [68], and *VviSTO2* (α -guaiene 2-oxidase) [7] loci, which have all been linked to the biosynthesis of rotundone, were genotyped across the eight *V. vinifera* cultivars with available haplotype phased assemblies (Figure 4(b)). No structural differences were observed for either the *VviFPPS* or *VviSTO2* genes (data not shown); however, an allele of *VviTPS24* with a LTR retrotransposon inserted within exon 5 was observed in the cultivars Nebbiolo and Cabernet Sauvignon (Figure 4(b)). Alignment of the theoretical *VviTPS24* proteins indicated that, such as Shiraz, the *V. vinifera* cultivars Zinfandel, Riesling,

Nebbiolo, and Sauvignon Blanc also carry a copy of *VviTPS24* containing the T414S and V530M substitutions (Figure 4(b), Figure S3). An additional amino acid substitution (T367P) relative to the *VviTPS24* of Shiraz was also observed in the H1 haplotype of Nebbiolo and Sauvignon Blanc (Figure S3). Highly variable rotundone concentrations in grapes have been linked with environmental conditions and phenological stages of grape ripening [69–71]; however, these results also suggest a molecular basis may prime an inherent variability of rotundone concentrations between cultivars of *V. vinifera* [4, 72].

Phylogenetic reconstruction of *VviTPS24* annotations revealed that the alleles specifying the T414S and V530M amino acid substitutions share an evolutionary origin (Figure 4(c)). The topology of the gene tree was largely congruent with the species tree (Figure 2), with the lineages derived from Cabernet Franc being monophyletic in at least one allele. The H2 allele of Chardonnay and Merlot were also shown to be closely related (Figure 4(c)), providing additional support for the shared ancestry suggested by the species tree (Figure 2). After excising the TE insertion from exon 5, all alleles containing the TE were found to be monophyletic (Figure 4(c)), indicating that Shiraz inherited both the inactivated and high α -guaiene producing alleles of *VviTPS24* through an ancestral outcrossing event. Short-read data from a further 15 cultivars was mapped to the Shiraz primary, assembly identifying the TE insertion in exon 5 of *VviTPS24* in a further five cultivars (Figure 4(d)). While these results might suggest these cultivars share an ancestry with Shiraz, long-read sequencing data will be required to confirm the genotype of the putative functional copy of *VviTPS24* in these cultivars. The correlation of these results with measured rotundone levels in other cultivars might provide further insights into the relevance of the detected allelic differences in the *VviTPS24* locus once the environmental triggers of sesquiterpene biosynthesis are more thoroughly understood.

4. Conclusions

The availability of a reference genome for Shiraz expands the pool of genomes available for wine grapes while providing a foundation resource for whole-genome studies involving this iconic cultivar, including intracultivar variant identification and transcriptomic studies using a matching reference genome, rather than a disparate proxy. The identification of a pair of specific genomic variants involving the *VviTPS24* gene, outline a potential genetic basis for the propensity of Shiraz (and other cultivars) to be primed for the formation of α -guaiene-type sesquiterpenes, such as rotundone, when exposed to appropriate environmental triggers. Following appropriate confirmation, this study could provide a genetic marker for the production of cool climate-associated peppery characters in future grape breeding strategies.

Data Availability

The sequencing data and genome assembly of the cultivar Shiraz and Sauvignon Blanc are publicly available at NCBI

under BioProjects PRJNA907382 and PRJNA939136. The GFF files with the gene annotations are included in the supplementary data.

Disclosure

This article has been previously published as a preprint at bioRxiv [73].

Conflicts of Interest

The authors declare that they have no conflicts of interest.

Authors' Contributions

C.A.O. and C. M.W. performed the sequencing, data analysis, and drafting of the manuscript. A.R.B supervised and provided guidance through the project and drafted the manuscript. Cristobal A. Onetto and Christopher M. Ward contributed equally to this work.

Acknowledgments

This work was supported by the Wine Australia, with levies from Australia's grapegrowers and winemakers and matching funds from the Australian Government. Support for DNA sequencing was provided by Bioplatforms Australia as part of the National Collaborative Research Infrastructure Strategy, an initiative of the Australian Government. The AWRI is a member of the Wine Innovation Cluster (WIC) in Adelaide. The authors would like to thank AWITC for the invitation to publish our research in this special issue. The authors would also like to thank Benjamin Pike for providing access to the Coombe Vineyard and Darren Graetz for collecting the samples of the cultivar Sauvignon Blanc.

Supplementary Materials

Supplementary_figures.pdf: Figures S1–S3. Tables_S1.txt: SRA accessions included in this study. Tables_S2.txt: GO molecular function enrichment analysis of hemizygous genes predicted in the assembly of Shiraz. Tables_S3.txt: Genic transposable element insertions in the Shiraz genome. Tables_S4.txt: Variable transposable element (TE) insertions between cultivars of *V. vinifera*. Tables_S5.txt: Shiraz specific transposable element (TE) insertions. SHZ_1654_primary_annotation.txt: Gene annotations in GFF3 format of the primary assembly of Shiraz. SHZ_1654_haplotigs_annotation.txt: Gene annotations in GFF3 format of the haplotigs of the genome assembly of Shiraz. (*Supplementary Materials*)

References

- [1] J. E. Bowers, R. Siret, C. P. Meredith, P. This, and J.-M. Boursiquot, "A single pair of parents proposed for a group of grapevine varieties in Northeastern France," *Acta Horticulturae*, no. 528, pp. 129–132, 2000.
- [2] C. A. Black, M. Parker, T. E. Siebert, D. L. Capone, and I. L. Francis, "Terpenoids and their role in wine flavour: recent

- advances: terpenoids: role in wine flavour,” *Australian Journal of Grape and Wine Research*, vol. 21, pp. 582–600, 2015.
- [3] C. Wood, T. E. Siebert, M. Parker et al., “From Wine to pepper: rotundone, an obscure sesquiterpene, is a potent spicy aroma compound,” *Journal of Agricultural and Food Chemistry*, vol. 56, no. 10, pp. 3738–3744, 2008.
 - [4] O. Geffroy, D. Kleiber, and A. Jacques, “May peppery wines be the spice of life? A review of research on the ‘pepper’ aroma and the sesquiterpenoid rotundone,” *OENO One*, vol. 54, no. 2, 2020.
 - [5] D. P. Drew, T. B. Andersen, C. Sweetman, B. L. Møller, C. Ford, and H. T. Simonsen, “Two key polymorphisms in a newly discovered allele of the *Vitis vinifera* TPS24 gene are responsible for the production of the rotundone precursor α -guaiene,” *EXBOTJ*, vol. 67, no. 3, pp. 799–808, 2016.
 - [6] A.-C. Huang, S. Burrett, M. A. Sefton, and D. K. Taylor, “Production of the pepper aroma compound (–)-Rotundone, by aerial oxidation of α -guaiene,” *Journal of Agricultural and Food Chemistry*, vol. 62, no. 44, Article ID 10809, 2014.
 - [7] H. Takase, K. Sasaki, H. Shinmori et al., “Cytochrome P450 CYP71BE5 in grapevine (*Vitis vinifera*) catalyzes the formation of the spicy aroma compound (–)-rotundone,” *EXBOTJ*, vol. 67, no. 3, pp. 787–798, 2016.
 - [8] R. Velasco, A. Zharkikh, M. Troggo et al., “A high quality draft consensus sequence of the genome of a heterozygous grapevine variety,” *PLoS One*, vol. 2, no. 12, p. 1326, 2007.
 - [9] The French–Italian Public Consortium for Grapevine Genome Characterization, J.-M. Aury, B. Noel, A. Policriti, C. Clepet, and A. Casagrande, “The grapevine genome sequence suggests ancestral hexaploidization in major angiosperm phyla,” *Nature*, vol. 449, no. 7161, pp. 463–467, 2007.
 - [10] M. J. Roach, D. L. Johnson, J. Bohlmann et al., “Population sequencing reveals clonal diversity and ancestral inbreeding in the grapevine cultivar Chardonnay,” *PLoS Genetics*, vol. 14, no. 11, Article ID e1007807, 2018.
 - [11] Y. Zhou, A. Minio, M. Massonnet et al., “The population genetics of structural variants in grapevine domestication,” *Native Plants*, vol. 5, no. 9, pp. 965–979, 2019.
 - [12] C.-S. Chin, P. Peluso, F. J. Sedlazeck et al., “Phased diploid genome assembly with single-molecule real-time sequencing,” *Nature Methods*, vol. 13, no. 12, pp. 1050–1054, 2016.
 - [13] A. Minio, M. Massonnet, R. Figueroa-Balderas, A. Castro, and D. Cantu, “Diploid genome assembly of the wine grape Carménère,” *G3 Genes Genomes Genetics*, vol. 9, no. 5, pp. 1331–1337, 2019.
 - [14] A. M. Vondras, A. Minio, B. Blanco-Ulate et al., “The genomic diversification of grapevine clones,” *BMC Genomics*, vol. 20, no. 1, p. 972, 2019.
 - [15] S. Maestri, G. Gambino, G. Lopatriello et al., “Nebbiolo” genome assembly allows surveying the occurrence and functional implications of genomic structural variations in grapevines (*Vitis vinifera* L.),” *BMC Genomics*, vol. 23, no. 1, p. 159, 2022.
 - [16] A. M. Vondras, L. Lerno, M. Massonnet et al., “Rootstock influences the effect of grapevine leafroll-associated viruses on berry development and metabolism via abscisic acid signaling,” *Molecular Plant Pathology*, vol. 22, no. 8, pp. 984–1005, 2021.
 - [17] C. Zou, M. Massonnet, A. Minio et al., “Multiple independent recombinations led to hermaphroditism in grapevine,” *Proceedings of the National Academy of Sciences of the U S A*, vol. 118, no. 15, Article ID e2023548118, 2021.
 - [18] M. Massonnet, N. Cochetel, A. Minio et al., “The genetic basis of sex determination in grapes,” *Nature Communications*, vol. 11, no. 1, p. 2902, 2020.
 - [19] S. Koren, B. P. Walenz, K. Berlin, J. R. Miller, N. H. Bergman, and A. M. Phillippy, “Canu: scalable and accurate long-read assembly via adaptive k-mer weighting and repeat separation,” *Genome Research*, vol. 27, no. 5, pp. 722–736, 2017.
 - [20] M. Kolmogorov, J. Yuan, Y. Lin, and P. A. Pevzner, “Assembly of long, error-prone reads using repeat graphs,” *Nature Biotechnology*, vol. 37, no. 5, pp. 540–546, 2019.
 - [21] M. Chakraborty, J. G. Baldwin-Brown, A. D. Long, and J. J. Emerson, “Contiguous and accurate *de novo* assembly of metazoan genomes with modest long read coverage,” *Nucleic Acids Research*, vol. 44, no. 19, p. e147, 2016.
 - [22] B. J. Walker, T. Abeel, T. Shea et al., “Pilon: an integrated tool for comprehensive microbial variant detection and genome assembly improvement,” *PLoS One*, vol. 9, no. 11, Article ID e112963, 2014.
 - [23] M. J. Roach, S. A. Schmidt, and A. R. Borneman, “Purge Haplotigs: allelic contig reassignment for third-gen diploid genome assemblies,” *BMC Bioinformatics*, vol. 19, no. 1, p. 460, 2018.
 - [24] M. Manni, M. R. Berkeley, M. Seppey, F. A. Simão, and E. M. Zdobnov, “BUSCO update: novel and streamlined workflows along with broader and deeper phylogenetic coverage for scoring of eukaryotic, prokaryotic, and viral genomes,” *Molecular Biology and Evolution*, vol. 38, no. 10, pp. 4647–4654, 2021.
 - [25] H. Liu, S. Wu, A. Li, and J. Ruan, “SMARTdenovo: a *de novo* assembler using long noisy reads,” *Gigabyte*, vol. 2021, pp. 1–9, 2021.
 - [26] M. Alonge, S. Soyk, S. Ramakrishnan et al., “RaGOO: fast and accurate reference-guided scaffolding of draft genomes,” *Genome Biology*, vol. 20, no. 1, p. 224, 2019.
 - [27] J. M. Flynn, R. Hubley, C. Goubert et al., “RepeatModeler2 for automated genomic discovery of transposable element families,” *Proceedings of the National Academy of Sciences of the United States of America*, vol. 117, no. 17, pp. 9451–9457, 2020.
 - [28] S. Ou and N. Jiang, “LTR_retriever: a highly accurate and sensitive program for identification of long terminal repeat retrotransposons,” *Plant Physiology*, vol. 176, no. 2, pp. 1410–1422, 2018.
 - [29] J. M. Crescente, D. Zavallo, M. Helguera, and L. S. Vanzetti, “MITE Tracker: an accurate approach to identify miniature inverted-repeat transposable elements in large genomes,” *BMC Bioinformatics*, vol. 19, no. 1, p. 348, 2018.
 - [30] A. F. A. Smit, R. Hubley, and P. Green, “RepeatMasker open-4.0. 2013–2015,” 2015, <https://www.repeatmasker.org/>.
 - [31] J. Palmer and J. Stajich, *Nextgenusfs/Funannotate: Funannotate v1.5.3*, Zenodo, Geneva, Switzerland, 2019.
 - [32] V. Ter-Hovhannisyan, A. Lomsadze, Y. O. Chernoff, and M. Borodovsky, “Gene prediction in novel fungal genomes using an *ab initio* algorithm with unsupervised training,” *Genome Research*, vol. 18, no. 12, pp. 1979–1990, 2008.
 - [33] I. Korf, “Gene finding in novel genomes,” *BMC Bioinformatics*, vol. 5, no. 1, p. 59, 2004.
 - [34] M. Stanke and B. Morgenstern, “AUGUSTUS: a web server for gene prediction in eukaryotes that allows user-defined constraints,” *Nucleic Acids Research*, vol. 33, pp. W465–W467, 2005.
 - [35] A. Delcher, “Improved microbial gene identification with GLIMMER,” *Nucleic Acids Research*, vol. 27, no. 23, pp. 4636–4641, 1999.

- [36] P. J. Fabres, L. Anand, N. Sai et al., “Tissue and regional expression patterns of dicistronic tRNA–mRNA transcripts in grapevine (*Vitis vinifera*) and their evolutionary co-appearance with vasculature in land plants,” *Horticultural Research*, vol. 8, no. 1, p. 137, 2021.
- [37] D. C. Koboldt, Q. Zhang, D. E. Larson et al., “VarScan 2: somatic mutation and copy number alteration discovery in cancer by exome sequencing,” *Genome Research*, vol. 22, no. 3, pp. 568–576, 2012.
- [38] A. R. Quinlan and I. M. Hall, “BEDTools: a flexible suite of utilities for comparing genomic features,” *Bioinformatics*, vol. 26, no. 6, pp. 841–842, 2010.
- [39] R. C. Edgar, “MUSCLE: multiple sequence alignment with high accuracy and high throughput,” *Nucleic Acids Research*, vol. 32, no. 5, pp. 1792–1797, 2004.
- [40] R. Bouckaert, J. Heled, D. Kühnert et al., “Beast 2: a software platform for Bayesian evolutionary analysis,” *PLoS Computational Biology*, vol. 10, no. 4, Article ID e1003537, 2014.
- [41] A. J. Drummond, S. Y. W. Ho, M. J. Phillips, and A. Rambaut, “Relaxed Phylogenetics and dating with confidence,” *PLoS Biology*, vol. 4, no. 5, p. 88, 2006.
- [42] T. Flutre, L. Le Cunff, A. Fodor et al., “A genome-wide association and prediction study in grapevine deciphers the genetic architecture of multiple traits and identifies genes under many new QTLs,” *G3 Bethesda Md*, vol. 12, no. 7, Article ID jkac103, 2022.
- [43] H. Li, “Minimap2: pairwise alignment for nucleotide sequences,” *Bioinformatics*, vol. 34, no. 18, pp. 3094–3100, 2018.
- [44] H. Li, B. Handsaker, A. Wysoker et al., “The sequence alignment/map format and SAMtools,” *Bioinformatics*, vol. 25, no. 16, pp. 2078–2079, 2009.
- [45] C. M. Ward, A. J. Ludington, J. Breen, and S. W. Baxter, *Genomic Evolutionary Analysis in R with geaR*, Cold Spring Harbor Laboratory, Laurel Hollow, New York, 2020.
- [46] X. Zheng, D. Levine, J. Shen, S. M. Gogarten, C. Laurie, and B. S. Weir, “A high-performance computing toolset for relatedness and principal component analysis of SNP data,” *Bioinformatics*, vol. 28, no. 24, pp. 3326–3328, 2012.
- [47] S. Lee, D. Cook, and M. Lawrence, “Plyranges: a grammar of genomic data transformation,” *Genome Biology*, vol. 20, no. 1, p. 4, 2019.
- [48] F. J. Sedlazeck, P. Rescheneder, M. Smolka et al., “Accurate detection of complex structural variations using single-molecule sequencing,” *Nature Methods*, vol. 15, no. 6, pp. 461–468, 2018.
- [49] C. M. Ward, T.-H. To, and S. M. Pederson, “ngsReports: a Bioconductor package for managing FastQC reports and other NGS related log files,” *Bioinformatics*, vol. 36, no. 8, pp. 2587–2588, 2020.
- [50] H. Li, “Aligning sequence reads, clone sequences and assembly contigs with BWA-MEM,” 2013, <https://arxiv.org/abs/1303.3997>.
- [51] G. Marçais and C. Kingsford, “A fast, lock-free approach for efficient parallel counting of occurrences of k-mers,” *Bioinformatics*, vol. 27, no. 6, pp. 764–770, 2011.
- [52] G. Busam, H. Kassemeyer, and U. Matern, “Differential of in *Vitis vinifera* L. To or,” *Plant Physiology*, vol. 115, no. 3, pp. 1029–1038, 1997.
- [53] J. F. Vouillamoz and M. S. Grando, “Genealogy of wine grape cultivars: ‘Pinot’ is related to ‘Syrah,” *Heredity*, vol. 97, no. 2, pp. 102–110, 2006.
- [54] J. González and D. A. Petrov, “The adaptive role of transposable elements in the *Drosophila* genome,” *Gene*, vol. 448, no. 2, pp. 124–133, 2009.
- [55] X.-M. Niu, Y.-C. Xu, Z.-W. Li et al., “Transposable elements drive rapid phenotypic variation in *Capsella rubella*,” *Proceedings of the National Academy of Sciences of the United States of America*, vol. 116, no. 14, pp. 6908–6913, 2019.
- [56] D. McKey, M. Elias, B. Pujol, and A. Duputié, “The evolutionary ecology of clonally propagated domesticated plants,” *New Phytologist*, vol. 186, no. 2, pp. 318–332, 2010.
- [57] L. Wang, Y. Huang, Z. Liu et al., “Somatic variations led to the selection of acidic and acidless orange cultivars,” *Native Plants*, vol. 7, pp. 954–965, 2021.
- [58] Q. H. Le, S. Wright, Z. Yu, and T. Bureau, “Transposon diversity in *Arabidopsis thaliana*,” *Proceedings of the National Academy of Sciences of the United States of America*, vol. 97, no. 13, pp. 7376–7381, 2000.
- [59] E. E. Grundy, N. Diab, and K. B. Chiappinelli, “Transposable element regulation and expression in cancer,” *FEBS Journal*, vol. 289, no. 5, pp. 1160–1179, 2022.
- [60] C. D. Todd, Ö. Deniz, D. Taylor, and M. R. Branco, “Functional evaluation of transposable elements as enhancers in mouse embryonic and trophoblast stem cells,” *Elife*, vol. 8, Article ID e44344, 2019.
- [61] S. Kobayashi, N. Goto-Yamamoto, and H. Hirochika, “Retrotransposon-induced mutations in grape skin color,” *Science*, vol. 304, no. 5673, p. 982, 2004.
- [62] Y. Yang, J. Ke, X. Han, W. A. Wuddineh, G. Song, and G.-Y. Zhong, “Removal of a 10-kb *Gret1* transposon from *VvMybA1* of *Vitis vinifera* cv,” *Horticulture Research*, vol. 9, Article ID uhac201, 2022.
- [63] D. Lijavetzky, L. Ruiz-García, J. A. Cabezas et al., “Molecular genetics of berry colour variation in table grape,” *Molecular Genetics and Genomics*, vol. 276, no. 5, pp. 427–435, 2006.
- [64] Q. Zhang, J. Arbuckle, and S. R. Wessler, “Recent, extensive, and preferential insertion of members of the miniature inverted-repeat transposable element family *Heartbreaker* into genic regions of maize,” *Proceedings of the National Academy of Sciences of the United States of America*, vol. 97, no. 3, pp. 1160–1165, 2000.
- [65] J. Lin, M. Massonnet, and D. Cantu, “The genetic basis of grape and wine aroma,” *Horticultural Research*, vol. 6, no. 1, p. 81, 2019.
- [66] D. M. Martin, S. Aubourg, M. B. Schouwey et al., “Functional annotation, genome organization and phylogeny of the grapevine (*Vitis vinifera*) terpene synthase gene family based on genome assembly, FLcDNA cloning, and enzyme assays,” *BMC Plant Biology*, vol. 10, no. 1, p. 226, 2010.
- [67] O. Kohany and J. Jurka, “LTR retrotransposons from grapevine,” *RepBase Reports*, vol. 7, p. 684, 2007.
- [68] H. Takase, K. Sasaki, G. Ikoma, H. Kobayashi, H. Matsuo, and S. Suzuki, “Farnesyl diphosphate synthase may determine the accumulation level of (–)-rotundone in ‘Syrah’ grapes,” *VITIS - Journal of Grapevine Research*, vol. 34, pp. 99–106, 2016.
- [69] L. Caputi, S. Carlin, I. Ghiglieno et al., “Relationship of changes in rotundone content during grape ripening and winemaking to manipulation of the ‘peppery’ character of wine,” *Journal of Agricultural and Food Chemistry*, vol. 59, no. 10, pp. 5565–5571, 2011.
- [70] R. G. V. Bramley, T. E. Siebert, M. J. Herderich, and M. P. Krstic, “Patterns of within-vineyard spatial variation in the ‘pepper’ compound rotundone are temporally stable from year to year: spatial variation of rotundone is temporally stable,” *Australian Journal of Grape and Wine Research*, vol. 23, no. 1, pp. 42–47, 2017.

- [71] V. V. S. R. Gupta, R. G. V. Bramley, P. Greenfield, J. Yu, and M. J. Herderich, "Vineyard soil microbiome composition related to rotundone concentration in Australian cool climate 'peppery' Shiraz grapes," *Frontiers in Microbiology*, vol. 10, p. 1607, 2019.
- [72] M. J. Herderich, T. E. Siebert, M. Parker, D. L. Capone, D. W. Jeffery, and P. Osidacz, "Spice up Your life: analysis of key aroma compounds in Shiraz," in *ACS Symposium Series*, M. C. Qian and T. H. Shellhammer, Eds., American Chemical Society, Washington, DC, USA, 2012.
- [73] C. A. Onetto, C. M. Ward, and A. R. Borneman, "The phased diploid genome assembly of *Vitis vinifera* cv," Cold Spring Harbor Laboratory, Laurel Hollow, New York, 2022.

Research Article

Performance of a Leaf-Galling Phylloxera (*Daktulosphaira vitifoliae*) on Roots of Diverse *Vitis* spp. Rootstocks in North East Victoria, Australia

C. W. Clarke ¹, K. S. Powell ¹, S. Norng², B. M. Carmody¹, M. Walpole³,
and J. P. Cunningham ²

¹Agriculture Victoria Research, 124 Chiltern Valley Road, Rutherglen, Victoria 3685, Australia

²Agriculture Victoria Research, Agribio 5 Ring Rd, La Trobe University Bundoora, Melbourne, Victoria 3083, Australia

³Consultant Independent Researcher, 203 Fighting Gully Road, Beechworth, Victoria 3747, Australia

Correspondence should be addressed to C. W. Clarke; catherine.clarke@agriculture.vic.gov.au

Received 30 October 2022; Revised 20 March 2023; Accepted 24 April 2023; Published 10 May 2023

Academic Editor: K. J. Evans

Copyright © 2023 C. W. Clarke et al. This is an open access article distributed under the Creative Commons Attribution License, which permits unrestricted use, distribution, and reproduction in any medium, provided the original work is properly cited.

Background and Aims. Grape phylloxera in Australia comprises diverse genetic strains that feed on roots and leaves of *Vitis* spp. The G38 phylloxera strain was detected on roots of *Vitis* spp., for the first time in North East Victoria in 2015. Prior to 2015, G38 phylloxera was only known to feed on leaves. The aim of this study was to evaluate the survival and development of G38 phylloxera on roots of diverse *Vitis* spp. under field, controlled laboratory, and greenhouse conditions. **Methods and Results.** In the field, emergence traps quantified first instars and alates emerging from roots of diverse rootstocks and *Vitis vinifera* L. High numbers of phylloxera were collected in traps placed at vines of rootstocks 101-14, 3309 Courderc and Schwarzmann. Nodosity were also observed on roots of 101-14, 3309 Courderc and Schwarzmann in the field and in-pot vines experiments. The better performance of G38 phylloxera on these three rootstocks compared to *V. vinifera* in the field and in potted vines paralleled the excised roots experiments. **Conclusions.** The relatively high performance of G38 phylloxera on the 101-14, 3309 Courderc and Schwarzmann rootstocks suggest a susceptible response and could be associated with rootstock parentage. Further investigation is warranted to determine implications for rootstocks development. **Significance of the Study.** These findings are fundamental for decision-making in phylloxera risk assessment and rootstock selection. The study reaffirms the need for triphasic (in vitro, in planta, and in-field) rootstock screening protocols for phylloxera.

1. Introduction

Grapevine phylloxera, *Daktulosphaira vitifoliae* (Fitch), is a pest of major economic significance to viticulture worldwide. Phylloxera feed on roots and leaves of *Vitis* spp. [1, 2]. The phylloxera root-feeding form, called the radicle, is typical on ungrafted cultivated varieties of *Vitis vinifera* (L.) ssp. *Sativa* throughout the world. On young nonlignified root tips, phylloxera root feeders induce hooked galls (called nodosities) and malformed swellings (called tuberosities) on older lignified roots. Nodosities and tuberosities are a source of nutrition and sites for oviposition and larval development [3–5]. Individual insects attach at feeding sites and develop

through four intermediate stages to adults that lay up to 400 eggs [6]. Nodosities impede root growth and tuberosities cause splits on the roots. The splits lead to decay because of secondary fungal infections eventually causing vine death [7, 8]. The leaf-feeding form, called the gallicole, not only feeds on leaves of North American *Vitis* species [2, 9] but can also attack leaves of *V. vinifera* [1, 10–12].

The phylloxera life cycle is complex and varies in different viticultural environments. High genotypic diversity and reproduction that is predominantly asexual have been revealed in *D. vitifoliae* populations in Europe [3] and Australia [13–15]. In Europe, separate introductions from the North East coast of North America can be traced back to

two genetic groups of the dominant American species *V. riparia* and *V. labrusca* [16]. A significant deviation from Hardy–Weinberg equilibrium suggests that parthenogenesis is the primary reproductive mode of reproduction for Californian *D. vitifoliae* populations [17]. The asexual females feed on either roots (radicole) or leaves (gallicole). During the growth season, gallicoles and radicoles undergo several asexual generations where the parthenogenetic females lay several hundred eggs [3, 18, 19]. The first instars are mobile and move to the leaves and/or roots where they establish new feeding sites on growing shoots or young root tips. Radicoles overwinter as first instar nymphs under the bark of roots [18, 20] and can give rise to winged adults (called alates) that emerge from the ground to disperse and find new feeding sites.

In Australia, management of phylloxera is achieved in part through quarantine [21]. For long term management, North American *Vitis* spp. that have coevolved with phylloxera are broadly used due to host responses that resist or tolerate infestations [2, 21]. Lack of complete resistance and, in some cases, potential breakdown in resistance limits the uptake and durability of rootstocks. Studies in Europe and the USA indicate that biotype-C phylloxera is adapted to feeding on rootstocks with the *riparia* parentage, including the Teleki rootstocks, 101-14 and Schwarzmann [22]. As a result, vineyard productivity in some regions may be lower where biotype-C populations predominate. To date, several phylloxera resistant loci have been identified in the Borner rootstock [23], *V. cinerea* C2-50 [24], *Muscadine rotundifolia*, and a complex hybrid [25]. DNA-markers linked to these phylloxera resistance loci can now be used to breed durable resistant rootstocks harbouring two or more resistant loci [26]. Aside from phylloxera resistance, rootstocks are also used to counteract other soilborne pests, such as nematodes, as well as maintain vine productivity in response to abiotic stress, soil pH, and porosity [27].

Phylloxera resistance or tolerance attributes of rootstocks is determined by insect genotype-plant interactions [28, 29]. On tolerant rootstocks, phylloxera can feed and then reproduce and maintain a population for several years without causing yield loss or vine death [30]. Previous rootstock screening studies in Australia have focused on six root-galling phylloxera strains using a triphasic screening approach [28, 31]. This encompasses a suite of protocols that integrate laboratory (excised roots) and greenhouse (potted vines) trials to screen new and existing rootstocks for phylloxera resistance [1, 21] and to analyse the ability of phylloxera to survive and develop on rootstocks [1, 32]. Small-scale field trials in commercial vineyards are conducted where possible [22, 33, 34]. Together, this information is incorporated into management decision-making tools, such as the Grapevine Rootstock Selector, to provide information that enables growers to select rootstocks that are resistant or tolerant to both phylloxera and root-knot nematodes [35].

In Australia, phylloxera has been established in the North East Victoria Phylloxera Infested Zone (PIZ) since the early 1900s [13, 14, 36]. Most vineyards are infested by parthenogenetic lineages that feed on roots, and there is

insufficient evidence to support the classical life cycle [37]. Gallicoles predominate on *Vitis* spp. in North America, Europe, and South America [3, 19, 38, 39]. In Australia, gallicoles have only been observed infrequently in the North East Victoria Phylloxera Infested Zone (PIZ) [37, 40]. The winter egg has been recorded only once in Australia [41], and it is not clear how the leaf-galling populations are sustained from year to year. Corrie and Hoffmann [37] found some genotypes of phylloxera on leaves and roots with evidence that those on roots arose from sexual reproduction in leaves. Eighty-three diverse phylloxera genetic strains were characterised in the early 2000s, of which 49 were identified as root feeders, 23 leaf feeders, and 11 that feed on both leaves and roots [14, 42]. Recent extensive surveys on vine roots conducted in the King Valley region of the North East Victoria PIZ, where only G4 phylloxera strain had been reported [13], identified 32 newly characterised genetic strains [15].

This publication reports on a case study conducted over three consecutive years (2015–2018) in a commercial vineyard named BGM located 274 km north-east of Melbourne, Australia in the North East Victoria Phylloxera Infested Zone (PIZ) [36]. This site was of interest because of the detection of G38 phylloxera strain previously reported only as leaf-galling under field conditions. The G38 phylloxera was first characterised from a leaf-galling sample that was collected near the Warby Ranges and Mount Glenrowan south east Australia on the AxR#1 rootstock [13, 37, 43]. The results of that study implied that G38 could be the outcome of sexual reproduction between individuals of G2 and G3 phylloxera that were sampled from both leaf and root [43].

The vines in this study site were planted in 1988 on uncultivated soil without a previous history of grapevine cultivation. The vines used in this study were in four rows, planted in a randomised complete block trial in which the plots were *V. vinifera* on own roots and grafted to different rootstocks. In the summer of 2015, the vines were observed to have yellowing leaf symptoms comparable to phylloxera infestations for the first time. Root inspection revealed nodosities and yellow clusters similar to phylloxera colonies on several rootstock cultivars and *V. vinifera*. The insects from the roots were collected for morphological and molecular identification. They were confirmed as phylloxera and characterised as the G38 genetic strain using six nuclear DNA microsatellite markers [14, 44]. No leaf galls were observed on the canopy of vines. The detection of the G38 phylloxera strain on roots at a site with existing replicates of *V. vinifera* vines on own roots or on different rootstocks offered a serendipitous opportunity to study the survival and development of the G38 phylloxera strain under field conditions and subsequently under controlled environments using insects collected from the BGM vineyard.

2. Methods

2.1. Insect Stock Cultures. In February 2016, adults, eggs, and first instars of the G38 phylloxera strain were randomly collected from roots of grafted rootstocks and *V. vinifera* vines in the BGM vineyard described in the introduction.

The insects were collected from four rows where the G38 phylloxera strain was first detected. Several single adult lineages of the G38 phylloxera were cultured and established in the laboratory under controlled conditions ($25 \pm 2^\circ\text{C}$; 12 h L:D). The genetic lineage of the insects was confirmed as the G38 phylloxera strain using six nuclear DNA microsatellite markers as per methods by Umina et al. [14] and Agarwal et al. [44] before the cultures were multiplied.

To produce a stock culture for laboratory and glasshouse experiments, insects were maintained under quarantine and mass reared on excised roots of *V. vinifera* cv. Chardonnay as per methods by Kingston [45].

2.2. Description of Vines in Four Rows at BGM Vineyard Used for In-Field Assessments. The four rows of vines used for in-field assessments (Table S1) were established in 1991 from callused rootstock cuttings of the varieties Schwarzmann, 101-14, 3309 Courderc, 125AA Kober, 1103 Paulsen, 5A Teleki, SO4, R99 and Sori and callused cuttings of own root Cabernet Sauvignon (clone LC10), were established through 600 mm wide polythene film in 1991. The rootstock cuttings were sourced from the Murray Valley Vine Improvement Association; and the Cabernet Sauvignon (clone LC10) were sourced from a local vineyard in North East Victoria. In the following season the rootstocks were subsequently field grafted to Cabernet Sauvignon (clone LC10) and trained up to form a bilateral cordon. The own rooted Cabernet Sauvignon vines were also trained up in the same season to the equivalent system. Both the Cabernet grafted rootstock vines and the own rooted Cabernet Sauvignon vines were reworked to Sangiovese (clone MAT 7) in the spring of 2005.

2.3. Plant Material Used for Laboratory and Glasshouse Experiments. Vines used for controlled glasshouse and laboratory experiments were sourced as dormant cuttings from the Yalumba Nursery, Nuriootpa, South Australia which is in a Phylloxera Exclusion Zone and free from phylloxera. The cuttings were planted in 4.5L plastic black pots using heat sterilised 80% general purpose potting mix (Spotswood Potting Mixes and Fertilisers, Yarra Glen, Victoria) and 20% perlite (Peards Nursery, Albury, NSW) and fertilised with 3.5 g Osmocote™ per pot. The vines comprised the following varieties; *V. vinifera* (own rooted Pinot Noir), Ramsey (Pinot Gris), Schwarzmann (Saperavi), 101-14 (Malbec 1056 FSAC), 3309 Courderc (Cabernet Sauvignon), 5BB Kober (Pinot noir), 110 Richter (Shiraz), 1103 Paulsen (Cabernet Sauvignon), 140 Ruggieri (Shiraz), Börner (Shiraz), and 420A (Shiraz) (Table 1). Once planted, vines were kept in a shade house and drip irrigated for two min daily over 12 months to allow optimal root development before inoculating with G38 phylloxera eggs from stock cultures.

2.4. In-Field Assessment of G38 Phylloxera

2.4.1. Emergence Trapping. The development of the G38 phylloxera on diverse *Vitis* spp. was assessed under field conditions on four rows of vines at the BGM vineyard

(Table 1). The assessment was conducted using cylindrical 4-litre durable clear plastic containers (Décor™) emergence traps that were installed at vines as per methods by [48]. To install the traps, a container was placed on levelled ground at approximately 10 cm from the base of trunk on each of the experimental vine and secured with metal tent pegs.

Trapping commenced over the vegetation period from mid-Spring until mid-Autumn (November–April) of 2015/2016 following the first detection of phylloxera on roots of vines in the vineyard and continued for three subsequent summer seasons (2015/2016, 2016/2017, and 2017/2018) during phylloxera peak activity [49]. Vines on which traps were placed were randomly selected from four rows of a block of mixed rootstock and own rooted vines (*V. vinifera*) (Figure 1). One trap was placed per vine. Eight to ten replicate vines were selected for each rootstock cultivar and *V. vinifera*. Ten *Vitis* varieties were selected for the study (Table S1).

Emergence trap samples were collected once every month over the three seasons. Sample collection involved rinsing the traps condensate with 80% ethanol and pouring contents into sampling containers. The traps were thereafter rinsed with tap water and replaced. Trap samples were transported to a quarantine laboratory at Agriculture Victoria, Rutherglen. The samples were observed under a low power dissecting microscope and first instars and alate adults found in each trap were quantified (Table S2). Total number of first instars and alates in traps over the three years were summed up for each *Vitis* spp. cultivar.

2.4.2. Root Inspection–Confirming Presence/Absence of Phylloxera on Vines Roots. Insects may have been caught in traps placed on resistant vines through the movement of first instars along the roots from nearby susceptible vines. Roots were, therefore, visually inspected to record the presence or absence of phylloxera life stages from a sample of vines where traps were placed for each *Vitis* spp. Visual detection of adults with eggs and 2nd–4th instars intermediate stages confirmed the successful development and completion of an asexual generation (Table S3). To conduct the visual assessment, a quantitative destructive technique was used. A dozen lignified and nonlignified root sections (5–30 cm in length) per vine were dug up to a depth of 5–20 cm and roots and soil samples were collected. Roots of eight replicate vines per rootstock type and *V. vinifera* on own roots were visually inspected. The samples were transported to a quarantine laboratory at Agriculture Victoria, Rutherglen where they were inspected for presence of phylloxera life stages with the aid of a low power dissecting microscope. Visual leaf symptoms noted as chlorosis on leaves were observed at veraison on experimental vines during the third year of study (Figure S1).

2.5. Performance of G38 Phylloxera in Potted Vines. The development of G38 phylloxera on diverse *Vitis* spp. was studied using potted vines. The experiment used a completely randomised block design with eight replicate vines

TABLE 1: Description of *Vitis* spp. used to study the survival and development of the G38 phylloxera.

Vine variety	Names of breeder (year*)	Country of origin	Vitis parentage		Method and resistance rating			
			Country of origin	Vitis parentage	In-field	Potted vine	Excised roots	
<i>Vitis vinifera</i>	Domesticated	Mediterranean		Own root	Susceptible	Tolerant	Tolerant	Tolerant
101-14	Millardet and de Grasset (1882)	France		<i>V. riparia</i> × <i>V. rupestris</i>	Susceptible	Susceptible	Susceptible	Susceptible
Schwarzmann	Schwarzmann (1891)	Czech republic		ND × <i>V. riparia</i> "Gloire de Montpellier"	Tolerant	Tolerant	Tolerant	Tolerant
3309 Couderc	Couderc (1881)	France		ND	Tolerant	Tolerant	Tolerant	Tolerant
1103 Paulsen	Paulsen (1895)	Italy		<i>V. berlandieri</i> 'Rességuier 2' × <i>V. rupestris</i> "du Lot"	Resistant	Tolerant	Resistant	Resistant
140 Ruggieri	Ruggieri (1896)	Italy		<i>V. berlandieri</i> "Boutin" × <i>V. rupestris</i> "du Lot"	NT	Resistant	Resistant	Resistant
110 Richter	Richter (1902)	France		<i>V. berlandieri</i> "Boutin" × <i>V. rupestris</i> "du Lot"	NT	Resistant	Resistant	Resistant
Richter 99	Richter (1902)	France		<i>V. berlandieri</i> "Rességuier 2" × <i>V. rupestris</i> "du Lot"	Resistant	Resistant	Resistant	Tolerant
5A Teleki	Teleki (1900)	Hungary		<i>V. berlandieri</i> "Rességuier 2" × <i>V. riparia</i> "Gloire de Montpellier"	Tolerant	NT	NT	NT
SO4	Teleki and Fuhr (1896)	Germany		<i>V. berlandieri</i> "Rességuier 2" × <i>V. riparia</i> "Gloire de Montpellier"	Tolerant	NT	NT	NT
125AA Kober	Teleki and Kober (1896)	Austria		<i>V. berlandieri</i> "Rességuier 2" × <i>V. riparia</i> "Gloire de Montpellier"	Tolerant	NT	NT	NT
420A	Millardet and de Grasset (1886)	France		<i>V. berlandieri</i> "Rességuier 2" × <i>V. riparia</i> "Gloire de Montpellier"	Tolerant	NT	NT	NT
5BB Kober	Teleki and Franz Kober (1896)	Austria		<i>V. berlandieri</i> "Rességuier 2" × <i>V. riparia</i> "Gloire de Montpellier"	Tolerant	Resistant	Resistant	Tolerant
Ramsey	Thomas Munson (1900)	USA		<i>V. berlandieri</i> "Rességuier 2" × <i>V. riparia</i> "Gloire de Montpellier"	NT	Resistant	Resistant	Tolerant
Börner	Börner (1936)	Germany		<i>V. candicans</i> × <i>V. rupestris</i>	NT	Resistant	Resistant	Tolerant
Sori	Seeliger (1925)	Germany		<i>V. riparia</i> "Gm183" × <i>V. cinerea</i> "Arnold"	NT	Tolerant	Tolerant	Tolerant
		Germany		<i>V. solonis</i> × <i>V. riparia</i>	Tolerant	NT	NT	NT

*Maul and Töpfer [46]; McGovern et al. [47]; ND = not determined. NT = not tested. Vines used for in-field assessments are presented in bold text. Vines were classified from evidence presented in the literature cited as resistant if nodosities, tuberosities and phylloxera adults were absent; tolerant if nodosities were present with phylloxera life stages except for adults with eggs; susceptible if nodosities and/or tuberosities were present and, phylloxera survived to reproductive adult.

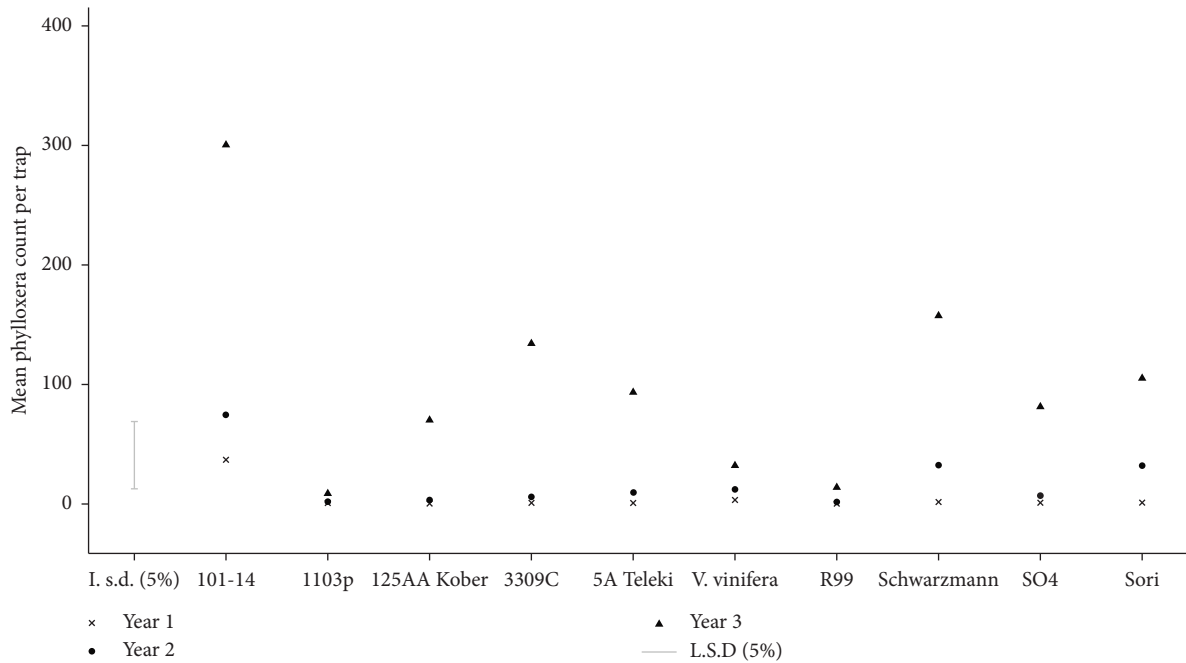


FIGURE 1: Mean numbers of G38 phylloxera (sum of first instars and alates) that were trapped from vines of nine rootstock cultivars and *V. vinifera* from 2015 to 2018. Least significant differences (L.S.D) between means ($p = 0.05$).

comprising of *V. vinifera* (susceptible control) and ten *Vitis* rootstock varieties. The rootstocks had various scion varieties and comprised of Ramsey (Pinor Gris), Schwarzmann (Saperavi), 101-14 (Malbec 1056 FSAC), 3309 Courderc (Cabernet Sauvignon), 5BB Kober (Pinor Gris), 110 Richter (Shiraz), 1103 Paulsen (Cabernet Sauvignon), 140 Ruggeri (Shiraz), Börner (Shiraz), and 420A (unknown) (Table 1). Sori and Richter 99 were not available for the potted trials. The vines were obtained from Yalumba nursery, Nuriootpa in South Australia.

Vines were infested with the G38 phylloxera as per methods by Forneck et al. [1] and Korosi et al. [31]. Briefly, the vines were removed from pots and a lignified root (5 mm in diameter) and surrounding fibrous roots enclosed in a muslin cloth. The roots were inoculated with 20 eggs of G38 phylloxera, and a small amount of potting mix immediately placed gently around the roots. The ends of the cloth were carefully tied with a cable tie to enclose the eggs, roots, and soil into a “root pocket.” A sticky gum-based insect barrier, Tanglefoot™, was applied along the edges of the cloth to stop phylloxera from escaping and the vine repotted by topping up with a potting mix and perlite mixture. The root pockets were repotted with the rest of the roots and the vines thereafter fertilised with 3.5 g Osmocote™ and 500 ml Thrive™ per potted vine. The vines were maintained in the glasshouses at $22 \pm 2^\circ\text{C}$ and a relative humidity of 60–70% and drip irrigated for 2 min daily.

The experiment ran for eight weeks. Vines were removed from pots and the root pocket snipped to assess phylloxera development and damage on roots. Assessments were done under a low power dissecting microscope. The following parameters were calculated: (i) total insects summed up as

the phylloxera developmental stages (eggs, first instars, intermediate instars, adults and alate); (ii) count of nodosities; and (iii) counts of tuberosities (Table S4).

2.6. Performance of G38 Phylloxera on Excised Roots. Roots of 10 *Vitis* varieties (*V. vinifera*, Ramsey, Schwarzmann, 101-14, 3309 Courderc, 5BB Kober, 110 Richter, 1103 Paulsen, and 140 Ruggeri and Börner) were cut into 4-5 cm lengths and placed in plastic Petri dishes (90 × 25 mm). Ten 1–4-day old eggs of G38 phylloxera were placed on a root piece using an artists’ paint brush. A Petri dish with one excised root and 10 eggs was considered a replicate. Each treatment (rootstocks and *V. vinifera*) consisted of five replicates. Petri dishes were sealed with cling film and then aluminium foil to restrict light filtering through and maintained in the growth room at $25^\circ\text{C} \pm 2^\circ\text{C}$. Over the entire experiment, cotton wool on the end of the roots was saturated with 2 mL ultrapure water once every week to keep the roots hydrated and viable.

The number of eggs that hatched was recorded at day 8. First, instars that established feeding sites and subsequently survived to adults were recorded at days 18, 25 and 32. Adults were distinguishable from intermediates if they had eggs in proximity. Eggs that were laid on days 18 and 25 were counted and removed from the roots to discount for overlapping generations. Parameters were calculated as follows: (i) survival was calculated as the number of adults that developed from the initial eggs inoculated on roots; (ii) average fecundity was calculated as the number of eggs produced per adult per day after the first adult detection; (iii) gross fecundity was calculated at day 32 as the total eggs laid over the lifetime of all adults per root. This was the sum of

the number of adults in each root for each of days 18, 25 and 32; (iv) proportion of inoculated eggs reaching the adult stage was calculated as adults at day 32 out of total eggs inoculated on roots ($n = 10$) (Table S5).

2.7. Statistical Analysis. Generalised Linear Models (GLMs) with Poisson distributions were used to compare the total number of insects caught in traps over the three years across the *Vitis* spp. A GLM with Poisson distribution was used to compare trap catches over three years with the trapping year and rootstock fitted in the model. A GLM was also used to compare the total number of nodosities, and total number of insects (eggs, intermediates, and adults) recorded among *Vitis* spp varieties in pots, net and gross fecundity among excised root varieties. The proportion of eggs that reached the adult stage among excised root varieties was analysed using a GLM and model was fitted with a binomial distribution. All models were built in R using the “MASS” package and evaluated using loglikelihood tests in the “epiDisplay” package.

Tukey’s *post hoc* tests with corrections were used to compare different treatments using the “lsmeans” package where our GLM model was significantly different to a null model as determined by the loglikelihood tests. All residual values were examined graphically to ensure normality and homogeneity of variances. Observations with standardised residuals greater than 3.0 were excluded from analyses.

For observations from roots, the number of phylloxera caught in traps over the three years was modelled using logistic regression, and the odds ratio was calculated. From the odds ratio, the probability of phylloxera reaching adulthood for each rootstock was calculated using the formula, $p = (e^z / 1 + e^z)$ where p = probability and z is the relevant odds ratio [50]. The analysis was performed in GenStat 18th Edition [51].

For each trial type, phylloxera survival from eggs to adults on the vines was used to define rootstock resistance and susceptibility ratings. Rootstocks were rated resistant if neither insect nor nodosities and tuberosities were present on roots, tolerant if nodosities, first instars at low numbers (<5) and intermediate stages without adults were present on roots and susceptible if nodosities and tuberosities and all phylloxera life stages were present on roots.

3. Results

3.1. In-Field Assessments of G38 Phylloxera

3.1.1. Emergence Traps. Phylloxera was captured in emergence traps across all rootstock treatments during the study (Table 2). The GLM revealed that the total number of insects caught in traps was significantly different across the vine cultivars ($\chi^2 = 44503$; d.f=9; $p < 0.0001$). Traps placed at the 101-14 vines consistently caught the highest numbers of phylloxera over the three years (Table 2). In comparison, less than 10 first instars were caught in traps collected from the 1103 Paulsen and Richter 99 rootstock vines (Table 2). There were no statistical differences between trap catches for Sori, Schwarzmamm, 5A Teleki, 3309 Couderc, SO4, 125AA Kober,

TABLE 2: Mean numbers (\pm standard error) of total G38 phylloxera (first instars and alates) caught in traps placed at vines of nine rootstock cultivars and *V. vinifera* over three consecutive years (2015, 2016 and 2017).

Rootstock	<i>n</i>	Mean total insects
101-14	9	137 \pm 22c
Sori	9	46 \pm 9ab
Schwarzmann	9	64 \pm 17b
5A Teleki	9	35 \pm 9ab
3309 Couderc	9	47 \pm 16ab
SO4	9	30 \pm 12ab
125AA Kober	9	25 \pm 7ab
<i>V. vinifera</i>	10	16 \pm 3ab
1103 Paulsen	9	4 \pm 1a
Richter 99	9	5 \pm 2a
d.f		44503
Chi square probability		<0.001

Means with different letters are significantly different (post hoc Tukey’s test $p < 0.05$).

and *V. vinifera* (Table 2). Alates were caught in trap samples from *V. vinifera* and all rootstock cultivars except for 1103 Paulsen and Richter 99 (data not shown).

The number of insects captured in traps increased significantly over the three seasons following the initial detection of the G38 phylloxera and differences were attributable to vine cultivar ($\chi^2 = 3973$; d.f=29; $p < 0.001$; Figure 1). Traps placed on vines with the 101-14 rootstock captured highest number of insects during the third year of the study, followed by Schwarzmamm, 3309 Courderc, Sori, Teleki 5A, SO4, and 125AA Kober (Figure 1). Collectively across all the rootstocks and *V. vinifera*, phylloxera catches in traps were highest in December and April (data not shown), indicative of multiple generations per season.

3.1.2. Root Inspection–Confirming Presence/Absence of G38 Phylloxera Stages. We confirmed successful development from the egg to the adult stage of G38 on each rootstock cultivar. The G38 phylloxera successfully developed and reproduced on all rootstock cultivars except for Richter 99 (Table 3). Scions of *V. vinifera*, Schwarzmamm, 101-14, Sori, 3309 Courderc, 125AA Kober, and SO4 showed yellowing symptoms consistent of those of phylloxera infestations by the third year of study (Table 3; Figure S1).

3.2. Performance of G38 Phylloxera in Potted Vines. There were no significant differences among rootstocks for the number of nodosities ($P > 0.05$; Table 4). Rootstocks typically had less than ten nodosities expect for 420A which developed no nodosities 8 weeks after inoculation with G38 phylloxera eggs (Table 4). Tuberosities on lignified roots were observed on Schwarzmamm, Börner, 1103 Paulsen, 101-14, Ramsey, and 110 Richter (Table 4), and no statistical differences were observed between the rootstocks ($P > 0.05$; Table 4).

There were significant differences among rootstocks for the number of insects recorded in root pockets (d.f=10; $p < 0.003$; Table 4). Successful development as determined

TABLE 3: Probability of G38 phylloxera survival (egg to adult with eggs) on roots of neighbouring rootstock cultivars and *V. vinifera*.

Rootstock type	Adults	Eggs	Intermediates
<i>V. vinifera</i> *	1.000	1.000	0.874
Schwarzmann*	1.000	1.000	0.799
101-14*	0.857	0.857	0.857
Sori*	0.799	0.799	0.599
3309 Courderc*	0.666	0.666	0.666
125AA Kober*	0.599	0.599	0.599
SO4	0.666	0.666	0.500
5A Teleki	0.334	0.334	0.334
1103 Paulsen	0.199	0.199	0.199
Richter 99	0.001	0.001	0.001

*Indicates scion-rootstock *Vitis* spp that showed yellowing due to phylloxera infestations by the third year of study. The odds ratio, estimated from regression analysis, was used to calculate each probability.

TABLE 4: Mean (\pm standard errors) of nodosities, tuberosities and total count of phylloxera (eggs, intermediates and adults) on roots of eleven *Vitis* spp ($n = 8$). The roots were contained in muslin cloth pockets and cocultivated with the G38 phylloxera for 8 weeks.

Rootstock	Nodosities	Tuberosities	Total count of insects
3309C	11 \pm 4	0	3 \pm 2ab
Schwartzmann	9 \pm 3	8 \pm 6	16 \pm 8a
<i>Vitis vinifera</i>	8 \pm 2	0	1 \pm 1b
Borner	7 \pm 6	4 \pm 0	0b
1103 Paulsen	5 \pm 2	6 \pm 4	1 \pm 1b
101-14	5 \pm 2	3 \pm 0	2 \pm 2b
140 Ruggeri	3 \pm 2	0	0b
Ramsey	2 \pm 1	2 \pm 0	0b
5BB Kober	2 \pm 1	0	0b
110 Richter	1 \pm 1	10 \pm 0	0b
420A	0 \pm 0	0	0b
df	10	5	10
Chi square probability	<0.057	0.06	<0.001

Means with different letters are significantly different (post hoc Tukey's test $p < 0.05$).

by an asexual generation (egg to adult) of the G38 phylloxera was recorded in root pockets of 3309 Courderc, Schwarzmann, and 101-14 (Table 4). Eggs were recorded on Schwarzmann ($n = 21$), 3309C ($n = 5$) and 101-14 ($n = 3$) while no eggs were found on all the other rootstocks. The high count of eggs on Schwarzmann indicated a potential peak in generation during the eight weeks incubation period.

3.3. Performance of G38 Phylloxera on Excised Roots. On excised roots, the G38 phylloxera showed significant differences in survival on diverse rootstock cultivars. The proportion of eggs that reached the adult stage was 0–0.4 and differed among the rootstock varieties (GLM: $\chi^2 = 22$; $d.f = 9$; $p = 0.008$; Table 5). Survival of inoculated eggs to the adult stage also differed among vine cultivars (GLM: $\chi^2 = 221$; $d.f = 9$; $p < 0.001$; Table 5). Eggs inoculated on rootstock 101-14 had the highest proportion of eggs surviving to the adult stage (40%). Although at least 60% of eggs inoculated on 110 Richter, 1103 Paulsen, and 140 Ruggeri hatched, first instars neither established feeding sites nor developed to adulthood

(data not shown). A single egg developed to the adult stage for the Börner, 5BB Kober, Ramsey and *V. vinifera*, and 3309 Courderc rootstocks (Table 5). The G38 phylloxera did not survive on rootstocks 110 Richter, 1103 Paulsen, and 140 Ruggeri (Table 5).

Average fecundity was affected by the *Vitis* varieties ($\chi^2 = 1278$; $d.f = 9$; $p < 0.001$; Table 5) and was highest on the 101-14 vines (Table 5). The average fecundity was below 10 egg/adult/day on Schwarzmann, *V. vinifera*, Ramsey, 5BB Kober, 3309 Courderc, and Börner vines (Table 5) and was associated with low numbers (<2) of insects developing to reproductive adults on these *Vitis* spp. Only one first instar insect developed to an adult that reproduced a single egg on 1103 Paulsen, Börner, 3309 Courderc, 110 Richter, and 1103 Paulsen. Gross fecundity was also affected by the rootstock varieties (GLM: $\chi^2 = 9$; $d.f = 5701$; $p < 0.0001$; Table 5), with the G38 phylloxera multiplying nine-fold on 101-14 by day 32 (Table 5).

3.4. Susceptibility Rating. G38 phylloxera reproduced freely on 101-14 under field conditions, consistent with these vines being classified as susceptible to this strain (Table 1). The rootstocks Sori, Schwarzmann, 5A Teleki, 3309 Courderc, SO4, and 125AA Kober appeared to tolerant the G38 phylloxera strain. Traps placed on vines with rootstocks 1103 Paulsen and Richter 99 caught the least number of insects and thus appear to be resistant to the G38 phylloxera strain (Table 1). Furthermore, the probability of G38 phylloxera completing an asexual generation on 1103 Paulsen and Richter 99 rootstocks was negligible.

Neither nodosities nor reproductive adults were observed on potted vines of rootstocks 110 Richter and 1103 which further supports classification of these rootstocks as being resistant to G38 phylloxera (Table 1). Survival and completion of an asexual generation by the G38 phylloxera accompanied by nodosities and/or tuberosities upon root inspection were recorded for 3309 Courderc, Schwarzmann, Sori, and 101-14, with means being higher than those recorded for *V. vinifera* on own roots. Potted vines of these rootstocks are, therefore, likely to tolerate G38 phylloxera. Survival and reproduction of the G38 phylloxera on excised roots was greatest for rootstock 101-14 compared to the other nine rootstocks tested, consistent with this rootstock being classified as susceptible to strain G38.

4. Discussion

This study reports that G38 phylloxera, which is known to be a leaf-galling strain also occurs as root galling on diverse rootstocks and *V. vinifera*. This finding presented an opportunity to examine the performance of a phylloxera strain that feeds on both roots and leaves on diverse rootstocks, employing the triphasic screening approach, which utilises field trials together with more controlled laboratory and greenhouse trials. No leaf galls were observed on vines in the block under study during the three years. An important outcome from the field trial was that the rootstock cultivars, 101-14, 3309 Courderc, Sori, 5A Teleki, and Schwarzmann,

TABLE 5: Proportion of inoculated eggs that reached the adult stage, survival, average, and gross fecundity of G38 phylloxera on excised roots of ten *Vitis* cultivars.

<i>Vitis</i> species	Proportion of eggs reaching adulthood	Survival to adult	Average fecundity	Gross fecundity
101-14	0.43 ± 0.05a	4.2 ± 0.5a	23.4 ± 4.0a	98.3 ± 39.2a
Schwarzmann	0.15 ± 0.03b	1.5 ± 0.3b	9.3 ± 3.9b	19.6 ± 10.1b
<i>V. vinifera</i>	0.08 ± 0.04bc	0.8 ± 0.4cb	2.6 ± 1.2cb	4.5 ± 3.1b
Ramsey	0.06 ± 0.02bc	0.6 ± 0.2cb	2.8 ± 1.5cb	2.5 ± 1.9b
5BB Kober	0.06 ± 0.02bc	0.6 ± 0.2cb	1.5 ± 0.7cb	3.0 ± 2.0b
3309 Courderc	0.01 ± 0.01c	0.1 ± 0.1c	0.7 ± 0.5cb	0.9 ± 0.9b
Börner	0.01 ± 0.01c	0.1 ± 0.1c	0.4 ± 0.4c	0.6 ± 0.5b
110 Richter	0c	0c	0c	0b
1103 Paulsen	0c	0c	0c	0b
140 Ruggeri	0c	0c	0c	0b
df	9	9	9	9
Chi square probability	0.008	<0.001	<0.001	<0.001

Data are means ± standard error of insects living on roots at days 18, 25, and 32. Means with different letters are significantly different (post hoc Tukey's test $p < 0.05$).

hosted relatively higher numbers of G38 phylloxera compared to *V. vinifera* on own roots, which is generally considered susceptible to phylloxera. This is the first record of G38 phylloxera on roots of these rootstocks.

Formation of galls and tuberosities was observed on some rootstocks under this study. Phylloxera survival is dependent on gall formation for nutrition and development of immature stages [49–56]. Rootstocks that showed a propensity to form galls, such as 101-14, Schwarzmann, Sori, and 3309 Courderc, could be a preferred food source favouring phylloxera reproduction. Subsequently, several generations may occur continuously with significant overlap in developmental stages, as evidenced by the trapping of alate stages. The production of alates suggests dispersive movement across rootstock vines that could be triggered by overcrowding or deteriorating root quality [2, 49, 57]. The dispersive movement of G38 phylloxera could explain why resistant rootstocks such R99 and 1103 Paulsen had positive trap samples yet neither nodosities nor reproductive adults were found when the roots were inspected. This observation suggests that some tolerant rootstocks, if planted near to those that are susceptible to strains such as the G38 phylloxera, could provide alternative food source, thus favouring the spread of phylloxera to neighbouring vines in blocks and vineyards.

Results from the three types of assays used in this study demonstrated that the rootstock 101-14 is susceptible to G38 phylloxera, and this phylloxera strain may be selected under diverse rootstock plantings [58–60]. Using excised root bioassays, the gross fecundity of G38 phylloxera was highest on 101-14 rootstock compared to the other nine *Vitis* varieties tested. Though excised root bioassays do not indicate a complete plant response, they are considered to be a suitable measure for phylloxera biotyping [55]. Results suggest that the G38 phylloxera possibly belongs to the biotype-C group, which is a classification that includes strains that show superior performance on nodosities on roots of rootstocks derived from American *Vitis* spp. such as 5C Teleki and 101-14 and 3309 Courderc and reduced ability to establish on *V. vinifera* roots [22, 61, 62]. Rootstocks that

had very low populations, such as was observed in 1103 Paulsen, 140 Ruggeri, Ramsey, 5BB Kober, and 110 Richter using potted vines assays, may use hypersensitivity as a resistance mechanism [63]. The root response to phylloxera expressed as tissue browning, indicative that the oxidation of phenolic compounds and nodosities are unsuitable as feeding sites for developing nymphs [64].

Rootstocks with parentages that are susceptible to certain phylloxera types have caused enormous economic losses. For instance, the rootstock AXR#1 (*V. vinifera* × *V. rupestris*) succumbed to infestations of virulent phylloxera biotypes in California, causing loss in production of between US\$1 billion and \$6 billion [65, 66]. The failure of AXR#1 led to caution concerning the use of rootstocks with insufficient tolerance to phylloxera, especially those with parentages that are highly susceptible. In this study, several rootstock cultivars had the riparia parentage, but it appears that only those with *V. riparia* × *V. rupestris* were susceptible or tolerant to the G38 phylloxera. The 1103 Paulsen and Richter 99 both with *V. berlandieri* × *V. rupestris* parentage had low insect populations consistently across the three experimental methods and are potentially tolerant to the G38 phylloxera. Our findings corroborate those in California that have shown phylloxera biotypes adapted to feeding on rootstocks with *V. riparia* parentage, such as 101-14 and Schwarzmann and some Teleki hybrids [22, 67, 68]. There is evidence to suggest that two genes are involved in nodosity formation based on findings from a study of traits related to phylloxera susceptibility from the *V. vinifera* and *V. rupestris* hybrid AXR1 [69]. There is also a report of a hybrid of *V. riparia* and *V. cinerea* Arnold that shows high resistance to phylloxera [23].

The emergence of biotype-C genetic strains that are adapted to feeding on *V. riparia* rootstocks has been highlighted as a concern when selecting rootstocks due to the potential for resistance breakdown [24]. The ability of phylloxera strains to utilise rootstocks as a food source and their interactions with hybrids such as *V. riparia* in conferring resistance needs to be studied further to enable access

to suitable traits for rootstock breeding programs. Our understanding of phylloxera genetic diversity in Australia is limited by lack of extensive surveys, especially in regions where phylloxera has existed since the early 1900s, which could explain why G38 phylloxera may not have been found on roots before. Recent surveys in the King Valley region, however, found a higher phylloxera genetic diversity than was previously thought [15].

In the current study, Börner rootstock, a hybrid from *V. riparia* and *V. cinerea* “Gm183,” was found to tolerate infestations by G38 phylloxera in potted vines and excised roots assays. Generally, Börner is considered to resist phylloxera infestations [23, 70, 71] and high level resistance has been demonstrated against some phylloxera genetic strains [21, 28, 72, 73]. This result is consistent with the findings of Powell [21] and Powell and Krstic [28] who found Börner to be tolerant to the root-galling G19 phylloxera strain under field assessments and tolerant to the G30 phylloxera strain *in vitro*. In the study of Powell and Krstic [28], Börner had higher numbers of G19 phylloxera in traps compared to other rootstocks and *V. vinifera* under field conditions. Since Börner is considered an attractive genetic resource for rootstock breeding due to its good grafting characteristics and adaptation to varied soil types [24, 72, 74], further studies are needed to confirm the contribution of *V. riparia* to incomplete resistance of plant accessions to some phylloxera strains such as the G38.

Screening for resistance of rootstocks to different phylloxera strains forms an essential component of rootstock selection and provides planting recommendations to the grape and wine industry. The three screening methods employed each have their disadvantages and advantages, such as ease of replication and/or applicability to the field, and differences in overall findings have been observed in the past when comparing the three screening methods [15, 28, 61]. In this study, rootstocks such as 1103 Paulsen and 110 Richter led to different findings when the results of the three trials were compared, implying that environmental conditions in the field could affect the response of these rootstocks to phylloxera. Potted vines always had optimal water content and relative humidity was high compared to likely conditions in the field. We did, however, observe necrotic nodosities on roots within the pockets, and this could contribute to restrict feeding due to deteriorating nutrition leading to insect mortality. We, therefore, recommend inoculating eggs on the roots of potted vines without the pocket enclosure. Furthermore, the G38 phylloxera was cultured on Chardonnay. The original feeding host could have influenced the ability of the G38 phylloxera to feed on different *Vitis* spp. varieties [75].

The reliance of the Australian grape and wine industry on a few popular rootstock varieties is of concern, as it is currently the only recommended management approach for phylloxera. For instance, growers favouring 101-14 risk having their rootstocks succumb to infestations by phylloxera genetic strains such as G38 phylloxera, which show relatively high virulence and preference for particular rootstocks. With the uptake of new rootstocks and growers preferring certain rootstocks over others, phylloxera tolerant

vines—if widely planted—may inadvertently promote the spread of phylloxera feeding forms such as G38, which could spread quickly across certain rootstocks. Phylloxera strains such as G38, which exist as both root and leaf galling forms and show high levels of galling and fecundity on rootstocks, ought to be included as test strains in screening trials that evaluate rootstock resistance. Future studies could explore whether situations exist in vineyards that might promote adaptive changes in feeding and phylloxera fitness. An improved understanding on these parameters would shape the grape rootstock breeding programs with the development of new rootstocks that are better adapted to situations in Australian vineyards. Selection of rootstocks with broad resistance to multiple phylloxera strains will also reduce the risk of phylloxera dispersal and hence strengthen quarantine.

5. Conclusion

The relatively high numbers of G38 phylloxera on rootstocks indicate that host preference is a survival mechanism with potential to increase the risk of phylloxera spreading to uninfested vineyards in Australia under poor containment practices. The introduction of unknown phylloxera lineages that feed on both leaves and roots thus presents a potential additional risk factor in the management of phylloxera. Management efforts in Australia should not only focus solely on the radicicole phylloxera forms but also the gallicole forms. The results from this study should initiate further investigations into the persistence of phylloxera strains that exist as both root and leaf because their impact on rootstocks is likely to be underestimated due to limited research. Human assisted and potentially natural dispersal of leaf-galling phylloxera forms between regions is a high risk for the industry and their management needs to be considered in existing quarantine protocols.

Data Availability

The data used to support the findings of this study are included within the supplementary information files.

Conflicts of Interest

The authors declare that there are no conflicts of interest regarding the publication of this paper.

Acknowledgments

The authors thank Dr. Harley Smith and Dr. Tony Dugdale for reviewing earlier versions of this manuscript. The authors would also like to thank Dr. Jessi Henneken for reviewing the statistical analysis and the second version of this manuscript. The authors acknowledge the assistance of grape growers in north-east Victoria for allowing access to their vineyards to collect insects and vine roots used for maintaining stock phylloxera populations. The Yalumba nursery, Nuriootpa, South Australia, is thanked for supplying vines for the potted vines experiments. This research was co-funded by Wine Australia and Agriculture Victoria.

Supplementary Materials

Supplementary 1. Table S1: Four rows of grafted rootstock and *V. vinifera* vines at the BGM vineyard located in the North East Victoria Phylloxera Infested Zone where field assessments were conducted. Emergence traps were placed at base of trunk of selected vines marked in bold font. Supplementary 2. Table S2: Counts of first instars and winged adults (alates) collected in emergence traps over three summer seasons (in 2015, 2016 and 2017). Supplementary 3. Table S3: Visual inspection of roots for phylloxera life stages on selected rootstocks and *V. vinifera*. Visual inspections were performed by digging and assessing roots for presence of eggs, first instars, and intermediate stages and adults (winged and wingless) in the 3rd year of study to confirm that the G38 phylloxera completed an asexual generation cycle on the vine at which traps were placed. Supplementary 4. Table S4: Counts of phylloxera eggs, first instars, intermediates and adults, nodosities and tuberosities eight weeks after infestation with the G38 phylloxera genetic strain using potted vine experiments. Supplementary 5. Table S5: G38 phylloxera living on excised roots of various rootstock varieties and *V. vinifera* on days 18, 25, and 32. Supplementary 6. Figure S1: Visual symptoms of rootstock vines that were monitored for G38 phylloxera infestations using bucket traps. Images were taken at veraison during the third year of study. (*Supplementary Materials*)

References

- [1] A. Forneck, K. S. Powell, and M. A. Walker, "Scientific opinion: improving the definition of grape phylloxera biotypes and standardizing biotype screening protocols," *American Journal of Enology and Viticulture*, vol. 67, no. 4, pp. 371–376, 2016.
- [2] J. Granett, M. A. Walker, L. Kocsis, and A. D. Omer, "Biology and management of grape phylloxera," *Annual Review of Entomology*, vol. 46, no. 1, pp. 387–412, 2001a.
- [3] A. Forneck and L. Huber, "(A)sexual reproduction - a review of life cycles of grape phylloxera, *Daktulosphaira vitifoliae*," *Entomologia Experimentalis et Applicata*, vol. 131, pp. 1–10, 2009.
- [4] J. Granett, "Comparison of swellings caused by indoleacetic acid and tuberosities induced by grape phylloxera (Homoptera: phylloxeridae)," *Journal of Economic Entomology*, vol. 83, no. 2, pp. 494–499, 1990.
- [5] A. D. Omer, J. A. Benedictis, and J. Granett, "Grape phylloxera, *Daktulosphaira vitifoliae* (Fitch) (Hom., Phylloxeridae), population response to preformed tuberosities," *Journal of Applied Entomology*, vol. 119, no. 1–5, pp. 653–657, 1995.
- [6] B. G. Coombe, "Phylloxera and its relation to south australian viticulture," *South Australian Department Technical Bulletin*, vol. 31, 1963.
- [7] J. P. Edwards, K. S. Powell, and J. Granett, "Tritrophic interactions between grapevines, phylloxera and pathogenic fungi - establishing the root cause of grapevine decline," *The Australian and New Zealand Grapegrower and Winemaker*, vol. 513, pp. 33–37, 2006.
- [8] A. D. Omer and J. Granett, "Relationship between grape phylloxera and fungal infections in grapevine roots. Zeitschrift für Pflanzenkrankheiten und Pflanzenschutz," *Journal of Plant Diseases and Protection*, vol. 107, pp. 285–294, 2000.
- [9] L. Yin, M. D. Clark, E. C. Burkness, and W. D. Hutchison, "Grape phylloxera (Hemiptera: phylloxeridae), on cold-hardy hybrid wine grapes (*Vitis* spp.): a review of pest biology, damage, and management practices," *Journal of Integrated Pest Management*, vol. 10, no. 1, 2019.
- [10] J. G. Molnár, C. S. Neméth, J. Máyer, and G. G. Jahnke, "Assessment of phylloxera leaf galling incidence on European grapevines in Badacsony, Hungary," *Acta Horticulturae*, vol. 816, pp. 97–104, 2009.
- [11] M. Botton and M. A. Walker, "Grape phylloxera in Brazil," *Acta Horticulturae*, vol. 816, pp. 39–40, 2009.
- [12] M. V. Vidart, M. V. Mujica, L. Bao et al., "Life history and assessment of grapevine phylloxera leaf galling incidence on *Vitis* species in Uruguay," *SpringerPlus*, vol. 2, no. 1, p. 181, 2013.
- [13] A. M. Corrie, R. van Heeswijck, and A. A. Hoffman, "Evidence for host-associated clones of grape phylloxera *daktulosphaira vitifoliae* (hemiptera: phylloxeridae) in australia," *Bulletin of Entomological Research*, vol. 93, pp. 193–201, 2003.
- [14] P. A. Umina, A. M. Corrie, K. S. Herbert, V. L. White, K. S. Powell, and A. A. Hoffmann, "The use of DNA markers for pest management - clonal lineages and population biology of grape phylloxera," *Acta Horticulturae*, vol. 733, pp. 183–195, 2007.
- [15] C. W. Clarke, P. J. Cunningham, B. Carmody, M. Blacket, and R. Kwong, *Integrated Management of Established grapevine Phylloxera*, Agriculture Victoria, Wine Australia and Department of Jobs Regions and Precincts, Melbourne, Australia, 2020.
- [16] J. Tello, C. Roux, H. Chouiki et al., "A novel high-density grapevine (*Vitis vinifera* L.) integrated linkage map using GBS in a half-diallel population," *Theoretical and Applied Genetics*, vol. 132, no. 8, pp. 2237–2252, 2019.
- [17] S. Riaz, K. T. Lund, J. Granett, and M. A. Walker, "Population diversity of grape phylloxera in California and evidence for sexual reproduction," *American Journal of Enology and Viticulture*, vol. 68, no. 2, pp. 218–227, 2017.
- [18] G. A. Buchanan, "The distribution, biology and control of grape phylloxera, *Daktulosphaira vitifoliae* (fitch)," Victoria. Ph. D. Thesis, p. 179, Department of Zoology, School of Biological Sciences, La Trobe University, Melbourne, Australia, 1990.
- [19] D. Downie and J. Granett, "A life cycle variation in grape phylloxera *Daktulosphaira vitifoliae* (Fitch)," *Southwestern Entomologist*, vol. 23, pp. 11–16, 1998.
- [20] J. Granett, L. Kocsis, L. Horvath, and E. B. Horvathne, "Grape phylloxera gallicole and radicolle activity on grape rootstock vines," *HortScience*, vol. 40, no. 1, pp. 150–153, 2005.
- [21] K. S. Powell, "A holistic approach to future management of grapevine phylloxera," in *Arthropod Management in Vineyards: Pests, Approaches and Future Directions*, N. Bostanian, C. Vincent, and R. Isaacs, Eds., pp. 239–251, Springer Science and Business Media B.V, London, UK, 2012.
- [22] L. Kocsis, J. Granett, and M. A. Walker, "Performance of Hungarian phylloxera strains on *Vitis riparia* rootstocks," *Journal of Applied Entomology*, vol. 126, no. 10, pp. 567–571, 2002.
- [23] J. Zhang, L. Hausmann, R. Eibach, L. J. Welter, R. Topfer, and E. M. Zyprian, "A framework map from grapevine V3125 (*Vitis vinifera* 'Schiava grossa' x 'Riesling') x rootstock cultivar 'Börner' (*Vitis riparia* x *Vitis cinerea*) to localize determinants

- of phylloxera root resistance,” *Theoretical and Applied Genetics*, vol. 119, no. 6, pp. 1039–1051, 2009.
- [24] H. M. Smith, C. W. Clarke, B. P. Smith et al., “Genetic identification of SNP markers linked to a new grape phylloxera resistant locus in *Vitis cinerea* for marker-assisted selection,” *BMC Plant Biology*, vol. 18, no. 1, p. 360, 2018.
- [25] M. D. Clark, S. L. Teh, E. Burkness et al., “Quantitative trait loci identified for foliar phylloxera resistance in a hybrid grape population: foliar phylloxera resistance,” *Australian Journal of Grape and Wine Research*, vol. 24, no. 3, pp. 292–300, 2018.
- [26] J. Dunlevy, P. Clingleffer, and H. Smith, “Breeding next generation rootstocks with durable pest resistance using DNA marker-assisted selection,” *Wine and Viticulture Journal*, vol. 34, pp. 40–44, 2019.
- [27] M. A. Walker, K. Lund, C. Agüero et al., “Breeding grape rootstocks for resistance to phylloxera and nematodes - it’s not always easy,” *Acta Horticulturae*, vol. 1045, pp. 89–97, 2014.
- [28] K. S. Powell and M. Krstic, “Phylloxera: rootstock tolerance and resistance to different genetic strains of phylloxera Wine and Viticulture,” *Journal*, vol. 30, pp. 48–51, 2015.
- [29] C. Arancibia, S. Riaz, C. Agüero et al., “Grape phylloxera (*Daktulosphaira vitifoliae* Fitch) in Argentina: ecological associations to diversity, population structure and reproductive mode,” *Australian Journal of Grape and Wine Research*, vol. 24, no. 3, pp. 284–291, 2018.
- [30] J. Granett, A. D. Omer, and A. Walker, “Seasonal capacity of attached and detached vineyard roots to support grape phylloxera (Homoptera: phylloxeridae),” *Journal of Economic Entomology*, vol. 94, no. 1, pp. 138–144, 2001b.
- [31] G. A. Korosi, C. J. Trethowan, and K. S. Powell, “Screening for rootstock resistance to grapevine phylloxera genotypes from Australian vineyards under controlled conditions,” *Acta Horticulturae*, vol. 733, pp. 159–166, 2007.
- [32] J. A. De Benedictis and J. Granett, “Laboratory evaluation of grape roots as hosts of California grape phylloxera biotypes,” *American Journal of Enology and Viticulture*, vol. 44, no. 3, pp. 285–291, 1993.
- [33] A. D. Omer, J. Granett, L. Kocsis, and D. A. Downie, “Preference and performance responses of California grape phylloxera to different *Vitis* rootstocks,” *Journal of Applied Entomology*, vol. 123, no. 6, pp. 341–346, 1999.
- [34] K. S. Powell, G. A. Korosi, and A. M. Mackie, “Monitoring grape phylloxera populations using simple non-destructive trapping systems,” *Acta Horticulturae*, vol. 816, pp. 29–34, 2009.
- [35] Wine Australia, “Grapevine rootstock selector tool,” 2019, <https://www.wineaustralia.com/news/media-releases/grapevine-rootstock-selector-tool-upgraded>.
- [36] Agriculture Victoria, “Phylloxera Management Zones,” 2022, <https://agriculture.vic.gov.au/biosecurity/protecting-victoria/victorian-viticulture-biosecurity/compliance-movement-conditions/phylloxera-management-zones>.
- [37] A. M. Corrie and A. A. Hoffmann, “Fine-scale genetic structure of grape phylloxera from the roots and leaves of *Vitis*,” *Heredity*, vol. 92, no. 2, pp. 118–127, 2004.
- [38] A. Forneck, M. A. Walker, and R. Blaich, “Ecological and genetic aspects of grape phylloxera *Daktulosphaira vitifoliae* (Hemiptera: phylloxeridae) performance on rootstock hosts,” *Bulletin of Entomological Research*, vol. 91, no. 6, pp. 445–451, 2001.
- [39] K. T. Lund, S. Riaz, and M. A. Walker, “Population structure, diversity and reproductive mode of the grape phylloxera (*Daktulosphaira vitifoliae*) across its native range,” *PLoS One*, vol. 12, p. e0170678, 2017.
- [40] K. S. Powell, “Risks and management of endemic and exotic phylloxera,” *DEP*, vol. 1301, 2017.
- [41] G. Ordish, *The Great Wine Blight*, Sidgwick and Jackson Limited, London, UK, 1972.
- [42] A. M. Corrie, *Genetic Structure of Grape Phylloxera Populations in Australia*, School of Molecular Sciences, La Trobe University, Bundoora, Australia, 2003.
- [43] A. M. Corrie, R. H. Crozier, R. Van Heeswijck, and A. A. Hoffmann, “Clonal reproduction and population genetic structure of grape phylloxera, *Daktulosphaira vitifoliae*, in Australia,” *Heredity*, vol. 88, no. 3, pp. 203–211, 2002.
- [44] A. Agarwal, J. P. Cunningham, I. Valenzuela, and M. J. Blacket, “A diagnostic LAMP assay for the destructive grapevine insect pest, phylloxera (*Daktulosphaira vitifoliae*),” *Scientific Reports*, vol. 10, no. 1, Article ID 21229, 2020.
- [45] K. B. Kingston, *Digestive and Feeding Physiology of Grape Phylloxera (*Daktulosphaira Vitifoliae* Fitch)*. PhD, Faculty of Science, Australian National University, Canberra, Australia, 2007.
- [46] E. Maul and R. Töpfer, “International Variety Catalogue (VIVC),” *Vitis*, Federal Research Centre for Cultivated Plants, Quedlinburg, Germany, 2022, <https://www.vivc.de>.
- [47] D. L. McGovern, L. J. Glusker, and E. M. M. Voigt, “Neolithic resinated wine,” *Nature*, vol. 381, pp. 480–481, 1996.
- [48] K. S. Powell, K. S. Korosi, and A. Mackie, “Monitoring grape phylloxera populations using simple non-destructive trapping systems,” *Acta Horticulturae*, vol. 816, pp. 29–34, 2009.
- [49] K. S. Herbert, A. A. Hoffmann, and K. S. Powell, “Changes in grape phylloxera abundance in ungrafted vineyards,” *Journal of Economic Entomology*, vol. 99, no. 5, pp. 1774–1783, 2006.
- [50] I. Valenzuela, M. Sandanayaka, K. S. Powell, S. Norng, and J. Vereijssen, “Feeding behaviour of *Bactericera cockerelli* (šulc) (Hemiptera: psyllodea: trioziidae) changes when infected with *Candidatus liberibacter solanacearum*,” *Arthropod-Plant Interactions*, vol. 14, no. 5, pp. 653–669, 2020.
- [51] Vsn International, *Genstat for Windows 22nd Edition*. VSN International, Web page: Genstat.co.uk, London, UK, 2022.
- [52] A. V. Kellow, M. Sedgley, and R. V. Heeswijck, “Interaction between *Vitis vinifera* and grape phylloxera: changes in root tissue during nodosity formation,” *Annals of Botany*, vol. 14, no. 5, pp. 581–590, 2004.
- [53] A. Forneck, S. Kleinmann, R. Blaich, and S. F. Anvari, “Histochemistry and anatomy of phylloxera (*Daktulosphaira vitifoliae*) nodosities in young roots of grapevine (*Vitis* spp.),” *Vitis*, vol. 41, pp. 93–97, 2002.
- [54] M. Griesser, N. C. Lawo, S. Crespo-Martinez et al., “Phylloxera (*Daktulosphaira vitifoliae* Fitch) alters the carbohydrate metabolism in root galls to allowing the compatible interaction with grapevine (*Vitis* spp.) roots,” *Plant Science*, vol. 234, pp. 38–49, 2015.
- [55] M. Eitle and A. Forneck, “Comparison of bioassays to biotype grape phylloxera (*Daktulosphaira vitifoliae* Fitch) on *Vitis* spp,” *Vitis*, vol. 56, pp. 141–146, 2017.
- [56] P. D. Nabity, M. J. Haus, M. R. Berenbaum, and E. H. DeLucia, “Leaf-galling phylloxera on grapes reprograms host metabolism and morphology,” *Proceedings of the National Academy of Sciences*, vol. 110, no. 41, pp. 16663–16668, 2013.
- [57] G. A. Buchanan, *Dispersal of Grape Phylloxera within Vineyards*, The Australian Grapegrower and Winemaker, Melbourne, Australia, 1986.
- [58] J. A. De Benedictis and J. Granett, “Variability of responses of grape phylloxera (Homoptera: phylloxeridae) to bioassays

- that discriminate between California biotypes,” *Journal of Economic Entomology*, vol. 85, no. 4, pp. 1527–1534, 1992.
- [59] D. J. Hawthorne and S. Via, “Variation in performance on two grape cultivars within and among populations of grape phylloxera from wild and cultivated habitats,” *Entomologia Experimentalis et Applicata*, vol. 70, no. 1, pp. 63–76, 1994.
- [60] G. C. Song and J. Granett, “Grape phylloxera (Homoptera: phylloxeridae) biotypes in France,” *Journal of Economic Entomology*, vol. 83, no. 2, pp. 489–493, 1990.
- [61] A. Forneck, M. A. Walker, and R. Blaich, “An *in vitro* assessment of phylloxera (*Daktulosphaira vitifoliae* Fitch) (Hom., Phylloxeridae) life cycle,” *Journal of Applied Entomology*, vol. 125, no. 8, pp. 443–447, 2001b.
- [62] P. D. King and G. Rilling, “Variations in the galling reaction of grapevines: evidence of different phylloxera biotypes and clonal reaction to phylloxera,” *Vitis*, vol. 24, pp. 32–42, 1985.
- [63] M. F. El-Nady and M.-B. Schroder, “Cytology of the hypersensitivity reaction in rootstocks - Improvement of rootstock breeding,” *Acta Horticulturae*, vol. 617, pp. 17–23, 2003.
- [64] A. V. Kellow, G. McDonald, A. Corrie, and R. Heeswijck, “*In vitro* assessment of grapevine resistance to two populations of phylloxera from Australian vineyards,” *Australian Journal of Grape and Wine Research*, vol. 8, no. 2, pp. 109–116, 2002.
- [65] P. Birebent, “Phylloxera in California or after AXR1,” *Progres agricole et viticole*, vol. 114, pp. 61–68, 1997.
- [66] G. Gale, “Saving the vine from Phylloxera: a never-ending battle,” in *Wine: A Scientific Exploration*, S. Sandler and R. Pindler, Eds., pp. 70–91, Taylor and Francis, London, UK, 2003.
- [67] L. Kocsis, J. Granett, A. Walker, H. Lin, and A. D. Omer, “Grape phylloxera populations adapted to *Vitis berlandieri* X *V. riparia* rootstocks,” *American Journal of Enology and Viticulture*, vol. 50, no. 1, pp. 101–106, 1999.
- [68] S. Riaz, D. Pap, J. Uretsky et al., “Genetic diversity and parentage analysis of grape rootstocks,” *Theoretical and Applied Genetics*, vol. 132, no. 6, pp. 1847–1860, 2019.
- [69] T. L. Roush, J. Granett, and M. A. Walker, “Inheritance of gall formation relative to phylloxera resistance levels in hybrid grapevines,” *American Journal of Enology and Viticulture*, vol. 58, no. 2, pp. 234–241, 2007.
- [70] P. Hafner, “Börner - a new grape rootstock,” *Obst und Weinbau*, vol. 35, p. 370, 1998.
- [71] L. Hausmann, R. Eibach, E. Zyprian, and R. Topfer, “Genetic analysis of phylloxera root resistance in cultivar Börner,” *Acta Horticulturae*, vol. 904, pp. 47–52, 2011.
- [72] J. Schmid, F. Manty, and E. H. Ruhl, “Utilizing the complete Phylloxera resistance of *Vitis cinerea* Arnold in rootstock breeding,” *Acta Horticulturae*, vol. 603, pp. 393–400, 2003.
- [73] J. Schmid, E. Sopp, and E. H. Ruhl, “Breeding rootstock varieties with complete phylloxera resistance,” *Acta Horticulturae*, vol. 473, pp. 131–138, 1998.
- [74] P. Pavloušek, “Screening of rootstock hybrids with *Vitis cinerea* Arnold for phylloxera resistance,” *Open Life Sciences*, vol. 7, no. 4, pp. 708–719, 2012.
- [75] J. Wilmink, M. Breuer, and A. Forneck, “Effects of grape phylloxera leaf infestation on grapevine growth and yield parameters in commercial vineyards: a pilot study,” *OENO One*, vol. 56, no. 1, pp. 197–208, 2022.

Research Article

Evaluating the Potential of High-Resolution Visible Remote Sensing to Detect Shiraz Disease in Grapevines

Yeniu Mickey Wang ^{1,2}, Bertram Ostendorf ³, and Vinay Pagay ¹

¹School of Agriculture, Food & Wine, Waite Research Institute, University of Adelaide, PMB 1, Glen Osmond, SA 5064, Australia

²CSIRO, Manufacturing, Autonomous Sensors Future Science Platform, 13 Kintore Ave, Adelaide, SA 5000, Australia

³School of Biological Sciences, The University of Adelaide, Molecular Life Sciences Building, North Terrace Campus, Adelaide, SA 5005, Australia

Correspondence should be addressed to Vinay Pagay; vinay.pagay@adelaide.edu.au

Received 11 November 2022; Revised 8 December 2022; Accepted 20 March 2023; Published 5 May 2023

Academic Editor: K. J. Evans

Copyright © 2023 Yeniu Mickey Wang et al. This is an open access article distributed under the Creative Commons Attribution License, which permits unrestricted use, distribution, and reproduction in any medium, provided the original work is properly cited.

Background and Aims. Shiraz disease (SD) is a viral disease associated with *Grapevine virus A* that causes significant yield loss in economically important grape cultivars in Australia such as Shiraz and Merlot. Current diagnostic methods are time-consuming and costly. This study evaluates an alternative methodology using visible remote sensing imagery to detect SD in Shiraz grapevines. **Methods and Results.** High-resolution visible remote sensing images were captured of Shiraz grapevines in two South Australian viticultural regions over two seasons. The projected leaf area (PLA) of individual grapevines was estimated from the images. Virus-infected vines had significantly lower PLA than healthy vines in the early season but fewer difference after veraison. The lower PLA was only observed in grapevines coinfecting with grapevine leafroll-associated viruses (GLRaVs) and Grapevine virus A (GVA). Shiraz vines infected with either GLRaVs or GVA had similar PLA to healthy vines. **Conclusions.** High-resolution RGB remote sensing technology has the potential to rapidly estimate SD infection in Shiraz grapevines. Our observations of shoot devigouration only in coinfecting vines calls into question the etiology of SD. Further validation of the PLA technique incorporating different regions, seasons, cultivars, and combinations of viruses is needed for improving the robustness of the method. **Significance of the Study.** This preliminary study presents a new rapid and low-cost surveillance method to estimate SD infections in Shiraz vineyards, which could significantly lower the cost for growers who conduct on-ground SD visual assessments or lab-based tissue testing at the vineyard scale.

1. Introduction

Shiraz disease (SD) is a devastating viral disease of grapevines that was first reported on Merlot from South Africa [1]. SD disrupts the physiological development of grapevines and causes significant yield loss in specific cultivars, including Shiraz, Merlot, Malbec, and Sumoll [2]. The symptoms of SD infection in Shiraz include delayed budburst with restricted spring growth, lack of lignification on some canes, and delayed leaf senescence well into the dormant season [3, 4]. SD symptoms are latent (no symptoms) in tolerant cultivars such as Chardonnay and Cabernet Sauvignon; however, the viruses can be transmitted to susceptible cultivars (Shiraz and Melot) by mealybugs and soft scales [5, 6]. *Grapevine virus A*

(GVA) group II variants were associated with SD [7, 8]. GVA also causes a rugose wood disease known as “Kober stem grooving” [9]. GVA often coexists with grapevine leafroll-associated viruses (GLRaVs) [6, 10–12], which is a group of viruses that causes Grapevine leaf disease (GLD) [13]. In Australia, GLRaV-1, GLRaV-3, and GLRaV-4 strain 9 (GLRaV-9) are commonly associated with GVA in SD-infected vines [14]. There are only a few effective methods to control grapevine viral diseases including roguing infected vines, replanting with certified, virus-free material, and controlling the vectors to stop the virus from spreading [15, 16]. It is therefore critical to accurately detect the patterns and extent of viral infections in vineyards to stop the virus from spreading further.

Standard detection methods for SD include serological methods, nucleic acid-based methods, and visual assessment [17, 18]. Lab-based methods are costly, thus limiting the number of grapevines tested and, consequently, an underestimation of the true incidence of virus infection in vineyards [17, 19]. Currently, the recommended minimum test rate by commercial diagnostic labs is five vines per thousand (0.5%) across the block [20]. Conducting on-ground visual assessments is labour-intensive, subjective, and sometimes unreliable. Low-altitude airborne remote sensing enables the capture of high detail with greater potential to rapidly survey the vineyards. Various optical sensors including red-green-blue (RGB), multispectral, hyperspectral, and thermal sensors have been used on the ground or platforms like unmanned aerial vehicles (UAVs) and manned fixed-wing aircraft for grapevine disease detection [21–26]. RGB imagery acquired through UAV-based remote sensing was used for the current study due to its relative simplicity compared to multi and hyperspectral images. A vertical projection of the canopy from the aerial image, the projected leaf area (PLA), for each vine was calculated from the image to compare the canopy size between healthy and SD-infected vines. PLA acquired from remote sensing imagery has a positive correlation to the canopy area. For example, Raj et al. [27] achieved an R^2 of 0.84 and RMSE of 0.36 by using PLA calculated from UAV RGB image and compared to leaf area index of maize.

In this study, we used high-resolution RGB remote sensing imagery to systematically assess PLA of individual healthy and diseased vines to predict SD infection in Shiraz grapevines in the field. The specific objectives of this study were: (1) to develop a simple remote sensing methodology that can consistently assess grapevine canopy size (using PLA as a surrogate) as a visual indicator of SD infection; (2) to confirm PLA-based disease status classification with lab-based tissue analysis; (3) to evaluate the time series of remote sensing imagery in order to conduct a spatial-within-season temporal analysis of canopy size differences between healthy and infected vines; and (4) to evaluate the temporal consistency of seasonal patterns of canopy development across multiple growing seasons. Our overarching goal was to develop a rapid and low-cost surveillance platform for SD detection at the vineyard scale.

2. Materials and Methods

2.1. Study Sites and Visual Estimation of Virus Infection. Two virus-infected Shiraz blocks (some vines previously tested positive with GVA and GLRaVs) were selected in different climatic wine regions in South Australia (SA) for this study. The first vineyard was in Monash, located in the warm inland region of Riverland ($34^{\circ}13'28''\text{S}$, $140^{\circ}33'01''\text{E}$). A block of 1.5 ha of Shiraz was selected for the study. The soil type of vineyard was sand over limestone. The block was drip-irrigated with $7.5\text{ ml}\cdot\text{ha}^{-1}$ of water per year. Approximate $50\text{ kg}\cdot\text{ha}^{-1}\text{N}$ and $50\text{ kg}\cdot\text{ha}^{-1}\text{P}$ fertiliser were applied through fertigation annually. The vines were consistently machine spur pruned with a same size box shape each winter. Vineyard management was consistent between seasons. Integrated pest management was as per

convention in this region, which generally has low disease pressure due to its warm-to-hot climate. The second vineyard was in the Barossa region, located in Lyndoch, SA ($34^{\circ}35'28''\text{S}$, $138^{\circ}53'01''\text{E}$). A 1.5 ha block was chosen for the study. The soil type of the block was Calcic on red Sodosol. It was drip-irrigated with approximate $1\text{ ml}\cdot\text{ha}^{-1}$ water per year. Both solid fertiliser and fertigation were applied at the rate of $130\text{ kg}\cdot\text{ha}^{-1}\text{N}$, $55\text{ kg}\cdot\text{ha}^{-1}\text{P}$, and $9\text{ kg}\cdot\text{ha}^{-1}\text{K}$ annually. Shiraz was consistently two-bud spur pruned to 20 buds per m each winter. Details of the study sites (vineyards) are provided in Table 1.

2.2. Virus Testing. Laboratory-based tissue testing was used for ground-truthing (Figure 1(b)). Tissue samples were collected based on visual symptoms for virus testing, of which half the vines were symptomatic and half were asymptomatic. Leaf petioles were sampled near harvest time [28]. The leaves were carefully selected from the base of the shoots to avoid errors associated with sampling from a potential long shoot coming through from a neighbour vine. Four petioles near the base of the shoots (two from each side of the canopy) were sampled and transported with chilled ice packs.

All samples were virus-tested in the lab using an enzyme-linked immunosorbent assay (ELISA) [29]. The ELISA test kits produced by Bioreba (Reinach, Switzerland) were used to test GVA, GLRaV-1, GLRaV-3, and GLRaV-4 strains. 20% of these leaves samples were tested with reverse-transcription polymerase chain reaction (RT-PCR) [17, 30] for confirmation of the ELISA results. The RT-PCR test was conducted by a commercial diagnostics lab that routinely tests for grapevine viruses. Six commonly occurring grapevine viruses in Australia [31] were tested: GVA, GLRaV-1, GLRaV-3, GLRaV-4, GLRaV-4 strain 6, and GLRaV-4 strain 9. The result showed a 100% match between PCR and ELISA, confirming the reliability of the ELISA test. The number of vines in each class is shown in Table 2. Because GLRaV-1, -3, and -4 complexes cause similar GLD symptoms in grapevines, vines infected with either a single or combination of any GLRaVs were treated as a GLRaV infection. In total, there were four classes: (i) healthy, (ii) GVA only, (iii) GLRaVs only, and (iv) GVA + GLRaVs.

2.3. High-Resolution Remote Sensing: Data Collection and Processing. DJI Mavic 2 Pro (SZ DJI Technology Co., Ltd, Shenzhen, China) was used for image collection in this study (Figure 1(a)). The UAV uses a Hasselblad RGB camera with a 28 mm focal length and $f/2.8$ – $f/11$ aperture. The field of view is approximate 77° and the image size is 5472×3648 . Flight planning was automated by the Pix4D app (Pix4D S.A., Prilly, Switzerland) with the setting of nadir view, side and forward overlapping at approximate 80%, altitude at 45 m above ground level, and forward flight direction. The calculated spatial resolution of the images was approximate 1 cm pixel^{-1} .

Aerial image data were collected between October to April in S1 and September to April in S2. Data were captured at approximate monthly intervals (one flight per month) based on weather conditions (low wind and sunny) which resulted in six flights in Riverland and ten flights in Barossa (Table 1).

TABLE 1: Vineyard study sites used in the trial.

Vineyard locations	Planting year	Rootstock	Spacing (row × vine)	Vine density (vines ha ⁻¹)	Occurrence of symptoms (%)	Flight per season		Images per block
						S1	S2	
Riverland	1998	K51-40	3.5 × 3.5 m	816	5	6	8	288
Barossa	Grafted in 2015	Cabernet sauvignon	3.2 × 1.5 m	2165	15	10	8	290

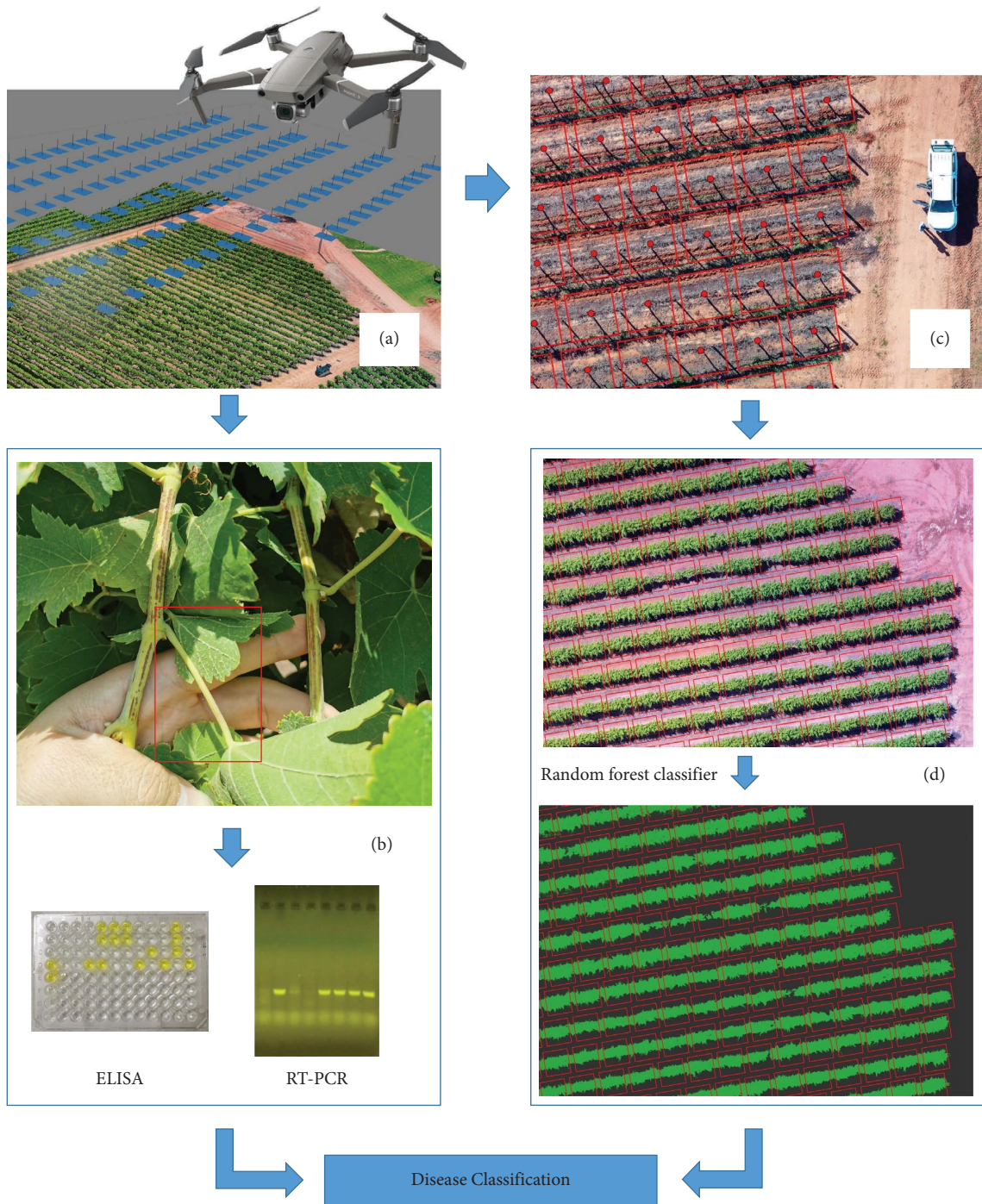


FIGURE 1: The workflow for disease classification with UAV images. (a) UAV data collection; (b) tissue sampling (petiole) and virus testing; (c) geo-locating and buffer creation for individual vines using the image at dormancy; and (d) grapevine canopy classification using random forest classifier.

All remote sensing imagery was captured under sunny and cloudless conditions between 11:00 to 15:00 h. In each flight, 288 images were taken for the Riverland block and 290 images for the Barossa block.

UAV Image mosaicking was conducted with Agisoft Metashape Professional, Version 1.6.2. (Agisoft LLC, St. Petersburg, Russia) to generate projected images with geo-information for each vineyard at each time point. Based on flight altitude and the resolution of the DJI Mavic 2 Pro

camera, the mosaicked images produced a 1 cm pixel^{-1} ground sampling distance. The image geo-processing was conducted with ArcGIS Pro V2.8 (Esri, Redlands, California, US). Individual vines were geolocated using the image at dormancy when the shadow of vine trunks was clearly visible. Grapevine locations were manually digitised, and square buffers were created along with the orientation of row lines (Figure 1(c)). The size of the buffer was adjusted to about 90% of vine spacing to avoid the overlapping area

TABLE 2: The ELISA test results. Samples classified as “healthy” tested negative for GVA, GLRaV-1, -3, and -4; GVA only is grapevine virus A positive (single infection) but GLRaVs negative; GLRaVs only is single or any combination of grapevine leafroll-associated virus-1, -3, or -4 positive but GVA negative; GVA + GLRaVs is coinfection of both GVA and one or more GLRaV-1, -3 or -4.

	Healthy	GVA only	GLRaVs only	GVA + GLRaVs	Total
Riverland	23	3	0	16	42
Barossa	19	7	6	14	46

between vines. The vine spacing was larger in the Riverland Shiraz block (3.5 × 3.5 m vine and row spacing) compared to Barossa and Adelaide Hills vineyards (spacing 1.5 × 3.0 m), which results in a larger canopy therefore a larger buffer area per vine. Orthomosaics from each date were georeferenced to the dormancy image in order to accurately coalign vines.

The grapevine canopy was mapped using a supervised random forest classifier [32] (also called the random tree method in ArcGIS Pro). We used the ArcGIS Pro V2.8 random trees method with a maximum number of trees of 30 and a maximum tree depth of 15. Pixels in the image were classified as “Grapevine,” “Soil,” “Shadow,” and “Weeds.” We manually labelled 5–7 training polygons in each training class and found the training data was sufficient to train Random Tree for classifying all pixels in the images. The “Soil,” “Shadow,” and “Weeds” classes were combined into a “non-grapevine” class to obtain a binary image for canopy area calculation (Figure 1(d)). To improve classification accuracy, different training data sets were created for early, middle, and later seasons as changing colour in the canopy over time. As undervine weeds were well controlled in all blocks, the grapevine was visually clearly distinguishable from the nongrapevine. The classification results were visually assessed by comparing the RGB and classified images, and results were consistent in all images, thus quantitative accuracy assessment of classification results was not required.

The projected leaf area (PLA) per individual vine was calculated as the sum of pixels that classified to “Grapevine” within square reference areas that were adapted to the vine and row spacing of the different vineyards. We used a square area of 3 × 3 m in Riverland, and 1.4 × 1.4 m in Barossa.

2.4. Statistical Analysis. Two-way ANOVA was used for statistical analysis using GraphPad Prism v9.0.0 (San Diego, CA, US). The PLA value of all virus-tested vines was used for analysis. Mean PLA values between each class (healthy, GVA only, GLRaVs only, and GVA + GLRaVs) at each time point were compared. Tukey’s multiple comparisons test was used as a post hoc test ($p < 0.05$).

3. Results and Discussion

3.1. Symptoms of Shiraz Disease. The ground visual observations showed that SD-infected Shiraz vines had delayed budburst by approximate 15–20 days and smaller canopies in spring as indicated visually (Figure 2(a)). However, by

midsummer (approximate fruitset stage), healthy and infected vines had indistinguishable canopies (Figure 2(b)). However, the canes of infected vines showed a lack of lignification, as shown in Figure 2(c). SD-infected vines were clearly identified in winter due to delayed leaf fall (delay approximate 15–20 days), which shows red leaves attached to the vine, while healthy vines had no leaves (Figure 2(d)). The SD symptoms consistently showed in two seasons and locations, this matched with observations in other studies [2, 4, 33].

3.2. PLA Difference between SD Symptomatic and Asymptomatic Canopy. The average PLA was calculated for each class (healthy, GVA only, GLRaVs only, and GVA + GLRaVs) in both blocks and seasons at each time point (Figure 3). In Riverland, the average size of coinfecting (GVA + GLRaVs) vines was consistently approximate 1 m² smaller than healthy vines at 25 days after budburst (2.24 m² for healthy and 1.32 m² for coinfecting vines) and flowering stage (4.42 m² for healthy and 3.62 m² for coinfecting vines) in S1 (Figure 3(a)). The statistical analysis showed the GVA + GLRaVs classes were significantly ($p < 0.0001$) different from healthy in the early season. However, the difference in PLA between the two classes decreased after flowering. Figure 3(b) shows PLA of coinfecting vines was approximate 1.3 m² smaller than healthy vines at 24 days after budburst (1.92 m² for healthy and 0.72 m² for coinfecting vines) and flowering stage (4.26 m² for healthy and 2.82 m² for coinfecting vines) in S2. Similar to S1, the difference in S2 between healthy and coinfecting vines decreased after flowering; however, it still has a significant difference before veraison (with $p < 0.0001$).

In the Barossa vineyard, the PLA of coinfecting Shiraz was also significantly smaller than that of healthy in the early season, especially at the flowering stage. In S1, the average PLA of the healthy and coinfecting vines at the flowering stage was approximate 1.5 m² and 1.0 m² ($p < 0.0001$), respectively, thus coinfection resulted in 33% smaller PLA (Figure 3(c)). However, the difference between the two classes started to decrease at veraison and no significant differences were observed in PLA in the latter part of the growing season. The PLA difference between diseased and healthy vines was reduced by veraison although still significant ($p = 0.0307$). The p -values for the difference between healthy and coinfecting vines were more significant around the flowering stage than at other times in both seasons.

The results indicated the symptomatic SD infection in Shiraz could be predicted using PLA calculated from RGB remote sensing images. The PLA of healthy and SD-infected vines had the highest difference between 20 and 70 days after bud burst, which unveils the optimum time window for SD detection as symptoms could be easily identified due to the significantly smaller PLA of the diseased vines. The PLA of SD-infected vines were 30%–70% smaller than the average healthy vines. We suggest setting a PLA threshold of 70% in healthy vines to classify as an SD infection in Shiraz. Therefore, PLA values at or less than 70% are classified as being SD infected. This threshold works between 15–45 days

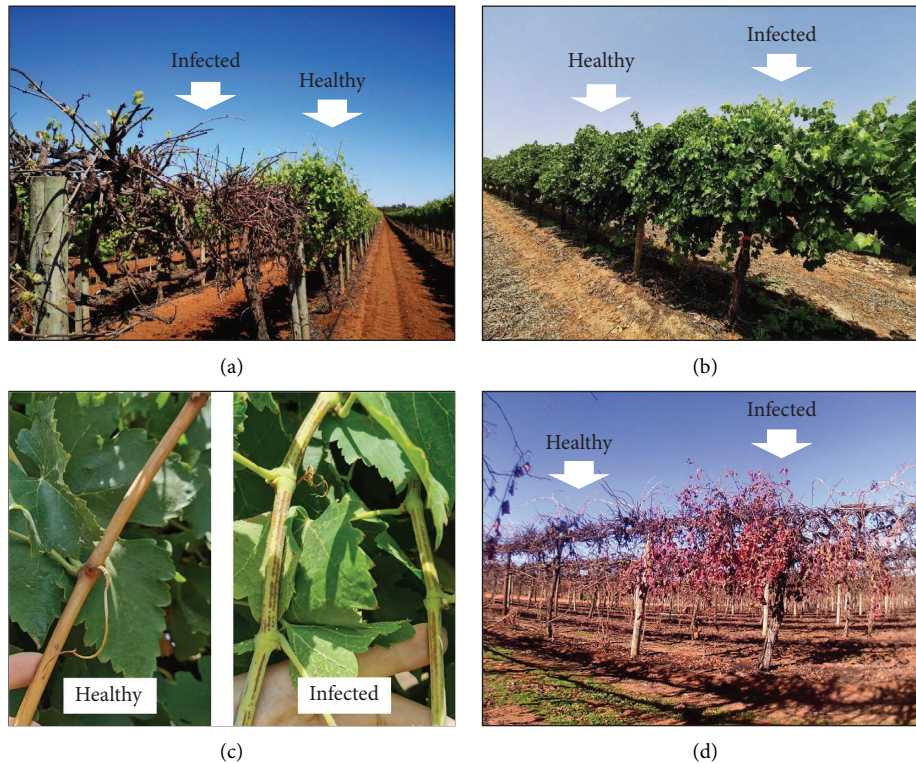


FIGURE 2: Symptoms of SD-infected Shiraz. (a) Restricted spring growth with delayed bud burst in Shiraz; (b) Shiraz canopies fully developed in midsummer at fruit set (EL-27); (c) canes of infected Shiraz show a lack of lignification at véraison (EL-35); and (d) red leaves remain on infected Shiraz vines while healthy vines drop all leaves during the dormant season.

after the budburst in the Riverland region and between 30–60 days after the budburst in the Barossa region. From veraison onwards, this method appeared to be less effective as canopy size differences between infected and healthy vines become smaller. However, our early PLA results could not distinguish SD from Grapevine trunk disease (GTD), a debilitating fungal disease that affects grapevines worldwide, causing devigourated shoots, and sometimes dead cordons [34]. The PLA of GTD-infected vines would likely remain low throughout the season since dieback results in very few growing shoots and death of the cordons [35, 36]. In contrast, SD-infected vines appear similar in growth to GTD-infected vines, but in contrast to GTD vines, have fully-developed canopies by the veraison stage; this key difference can be used to differentiate SD infection from GTD or dead vines. The PLA of SD-infected vines were 5%–15% smaller than the average healthy vines at this stage. Thus, we suggest that an 85% PLA threshold be used at the veraison stage to distinguish between SD- and GTD-infected or dead vines. Therefore, if the PLA is at or below 85% of the PLA of healthy vines between 90–120 days after budburst, the vine could possibly have GTD or be dead. Therefore, a minimum of two data collection timepoints are suggested per season, one in the early season and one in the mid-to-late season for determining SD using remote sensing. However, as the technique is an indirect detection method, which measures the canopy response to the virus, we cannot exclude the possibility that various other factors could be altering the phenotype. For example, other biotic stresses

(fungal diseases), abiotic stresses (drought, salinity, heat stress, and mechanical damage), and virus strains and coinfections could influence vegetative growth and alter PLA [37]. Therefore, this remote sensing technique is indicative but not a conclusive method for SD infection. The current results were based on two study sites and years, the further assessments and virus testing validations are needed for the different regions, years, the age of vines, and cultivars. As additional information is acquired, different recommendations of the PLA threshold can be used for vineyards that have similar conditions.

If validated, this method can potentially be scaled to larger regions using RGB imaging from manned aircraft, or even satellite imagery in the future as their camera resolutions continue to increase.

3.3. Difference between Coinfection and Single Infections. Canopy development of coinfecting vines (GVA + GLRaVs) lagged behind healthy vines due to delayed budburst in spring. This pattern was consistent in both vineyards and seasons (Figure 3). In comparison, the development of GVA and GLRaV (single infection) infected vines had no significant difference from healthy vines in both blocks or seasons. Despite previous studies showing that GVA and its variants are associated with SD [8], there is little systematic information between coinfection and SD symptoms. As the coinfection of GLRaVs and GVA is commonly found in vines, it is important to

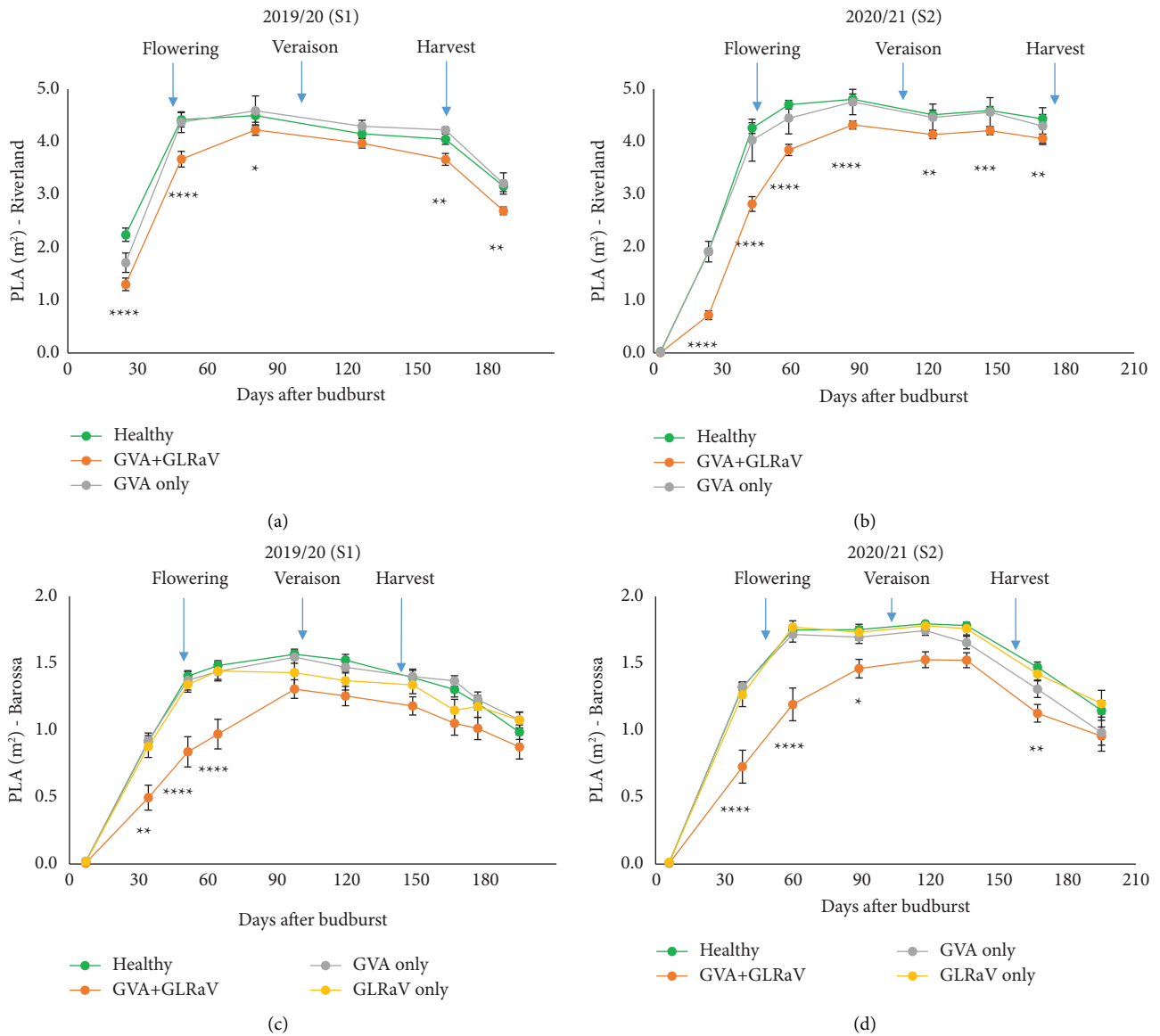


FIGURE 3: Average PLA for each lab-tested class at different times for both seasons in two vineyards. The p -value of healthy vs GVA + GLRaV shows in the graph, with * $p \leq 0.05$, ** $p \leq 0.01$, *** $p \leq 0.001$, **** $p \leq 0.0001$, and nonsignificant with a blank. (a, b) Riverland Shiraz in S1 and S2; (c, d) Barossa Shiraz in S1 and S2.

consider both coinfection as well as environmental factors when studying disease symptoms.

The study found that SD symptoms in both Shiraz blocks only occur in vines that are coinfecting with GVA and one or more GLRaVs, which in the vineyards we surveyed, were found to be mostly GLRaV-1 or GLRaV-4 strain 9 (GLRaV-9). We did not observe any typical SD symptoms when Shiraz vines were infected with GVA only (i.e., without GLRaVs). Similarly, Goszczynski and Habili [8] reported that SD symptoms in Shiraz were always associated with GVA group II and GLRaV-3 in South Africa. Consistent with the results of the present study, the same authors also observed that some vines did not exhibit any SD symptoms when infected with GVA group II alone; however, only visual evidence, but no quantitative evidence, was provided.

GVA variants of group II have been closely associated with SD, but not groups I and III [3]. As the ELISA serological method is unable to discriminate between virus variants, the asymptomatic GVA-infected vines in our study could belong to group I and/or III. A previous study also reported that the variant GTR1-2 in GVA group II did not produce SD symptoms in Shiraz; however, other group II variants (BMO32-1, KWVMo4-1, and P163M5) produced SD symptoms in both Shiraz and Merlot [33]. The GVA variants in our study were unknown because the GVA primers used for the RT-PCR test in our study were not variant-specific. However, if the GVA variants in the present study did not belong to either group I or III, or the GTR1-2 variant (in group II), we could then infer that coinfection of GVA and GLRaVs is a requisite for SD symptoms in Shiraz. We are

unaware of any systematic studies that have been done to understand the relationship between SD symptoms and the combination of various viruses and their variants. This hypothesis requires a comprehensive investigation, potentially by using next-generation sequencing techniques to screen all GVA and GLRaVs strains in the samples.

4. Conclusion

Reliable detection of grapevine viruses in the field remains challenging due to varying symptomatology. This study systematically compared the canopy growth response of SD-infected vines to healthy vines and proposed a rapid method to predict the SD infection in the Shiraz blocks using visible remote sensing technology. This technique has the potential to rapidly detect SD in the field, thereby providing prompt guidance for sampling locations for tissue testing of viruses as well as vineyard management. Further validation studies including various sites, seasons, cultivars, and virus strains are needed for this emerging technology. An additional, but important finding was that coinfection of GVA and GLRaVs results in significant vine devigoration in Shiraz, which does not occur with GVA or GLRaV alone. This observation was consistent across different soils and seasons under different weather conditions.

Data Availability

The raw and processed data used to support the study are available from the corresponding author upon request.

Conflicts of Interest

The authors declare that there are no conflicts of interest regarding publication of this work.

Acknowledgments

The authors gratefully acknowledged funding from South Australian Vine Improvement Association and Riverland Wine. We appreciate the top-up scholarship supported by Wine Australia. Special thanks to the industry collaborators: Kies Family Wines, and Mr Omer Najjar from CCW Co-operative Limited.

References

- [1] M. K. Corbett and J. Wiid, "Closterovirus-like particles in extracts from diseased grapevines," *Phytopathologia Mediterranea*, vol. 24, pp. 91–100, 1985.
- [2] Q. Wu, N. Habili, F. Constable et al., "Virus pathogens in Australian vineyards with an emphasis on Shiraz Disease," *Viruses*, vol. 12, no. 8, p. 818, 2020.
- [3] D. E. Goszczynski, "Single-strand conformation polymorphism (SSCP), cloning and sequencing reveal a close association between related molecular variants of Grapevine virus A (GVA) and Shiraz disease in South Africa," *Plant Pathology*, vol. 56, no. 5, pp. 755–762, 2007.
- [4] N. Habili, "Australian shiraz disease: an emerging virus disease of *Vitis vinifera* cv. Shiraz," *Wine and Viticulture Journal*, vol. 28, no. 1, pp. 59–61, 2013.
- [5] J. Charles, K. Froud, R. Van Den Brink, and D. Allan, "Mealybugs and the spread of grapevine leafroll-associated virus 3 (GLRaV-3) in a New Zealand vineyard," *Australasian Plant Pathology*, vol. 38, no. 6, pp. 576–583, 2009.
- [6] G. Hommay, V. Komar, O. Lemaire, and E. Herrbach, "Grapevine virus A transmission by larvae of *Parthenolecanium corni*," *European Journal of Plant Pathology*, vol. 121, no. 2, pp. 185–188, 2008.
- [7] D. E. Goszczynski and A. E. C. Jooste, "Identification of divergent variants of Grapevine virus A," *European Journal of Plant Pathology*, vol. 109, no. 4, pp. 397–403, 2003.
- [8] D. E. Goszczynski and N. Habili, "Grapevine virus A variants of group II associated with Shiraz disease in South Africa are present in plants affected by Australian Shiraz disease, and have also been detected in the USA," *Plant Pathology*, vol. 61, no. 1, pp. 205–214, 2012.
- [9] S. Chevalier, C. Greif, and P. Bass, B. Walter, Investigation on the aetiology of kober stem grooving disease," in *Proceedings of the 11th Meeting ICVG*, Montreux, Switzerland, September, 1993.
- [10] R. Credi, "Characterization of grapevine rugose wood disease sources from Italy," *Plant Disease*, vol. 81, no. 11, pp. 1288–1292, 1997.
- [11] M. Digiario, M. P. Bedzrob, A. M. D'Onghia, D. Boscia, and V. N. Savino, "On the correlation between grapevine virus A and rugose wood," *Phytopathologia Mediterranea*, vol. 33, pp. 187–193, 1994.
- [12] G. K. Blaisdell, S. Zhang, A. Rowhani et al., "Trends in vector-borne transmission efficiency from coinfecting hosts: grapevine leafroll-associated virus-3 and Grapevine virus A," *European Journal of Plant Pathology*, vol. 156, no. 4, pp. 1163–1167, 2020.
- [13] R. Naidu, A. Rowhani, M. Fuchs, D. Golino, and G. P. Martelli, "Grapevine leafroll: a complex viral disease affecting a high-value fruit crop," *Plant Disease*, vol. 98, no. 9, pp. 1172–1185, 2014.
- [14] N. Habili, Q. Wu, and V. Pagay, "Virus-associated Shiraz Disease may lead Shiraz to become an endangered variety in Australia," *Wine and Viticulture Journal*, vol. 31, pp. 47–50, 2016.
- [15] R. Almeida, K. Daane, V. Bell et al., "Ecology and management of grapevine leafroll disease," *Frontiers in Microbiology*, vol. 4, pp. 94–13, 2013.
- [16] K. D. Ricketts, M. I. Gomez, S. S. Atallah et al., "Reducing the economic impact of Grapevine leafroll disease in California: identifying optimal disease management strategies," *American Journal of Enology and Viticulture*, vol. 66, no. 2, pp. 138–147, 2015.
- [17] A. V. Zherdev, S. V. Vinogradova, N. A. Byzova, E. V. Porotikova, A. M. Kamionskaya, and B. B. Dzantiev, "Methods for the diagnosis of grapevine viral infections: a review," *Agriculture*, vol. 8, no. 12, p. 195, 2018.
- [18] E. Rubinson, N. Galiakparov, S. Radian, I. Sela, E. Tanne, and R. Gafny, "Serological detection of grapevine virus A using antiserum to a nonstructural protein, the putative movement protein," *Phytopathology*, vol. 87, no. 10, pp. 1041–1045, 1997.
- [19] R. R. Martin, K. C. Eastwell, A. Wagner, S. Lamprecht, and I. E. Tzanetakis, "Survey for viruses of grapevine in Oregon and Washington," *Plant Disease*, vol. 89, no. 7, pp. 763–766, 2005.
- [20] Affinitylabs, "Virus testing [Online]," 2022, <https://affinitylabs.com.au/virus-testing/>.
- [21] J. Albetis, S. Duthoit, F. Guttler et al., "Detection of Flavescence dorée Grapevine Disease using unmanned aerial

- vehicle (UAV) multispectral imagery,” *Remote Sensing*, vol. 9, no. 4, pp. 308–328, 2017.
- [22] F. Vanegas, D. Bratanov, K. Powell, J. Weiss, and F. Gonzalez, “A novel methodology for improving plant pest surveillance in vineyards and crops using UAV-based hyperspectral and spatial data,” *Sensors*, vol. 18, no. 1, p. 260, 2018.
- [23] J. Ouyang, R. De Bei, and C. Collins, “Assessment of canopy size using UAV-based point cloud analysis to detect the severity and spatial distribution of canopy decline,” *OENO One*, vol. 55, no. 1, 2021.
- [24] S. L. Macdonald, M. Staid, M. Staid, and M. L. Cooper, “Remote hyperspectral imaging of grapevine leafroll-associated virus 3 in Cabernet Sauvignon vineyards,” *Computers and Electronics in Agriculture*, vol. 130, pp. 109–117, 2016.
- [25] S. Zia-Khan, M. Kleb, N. Merkt, S. Schock, and J. Müller, “Application of infrared imaging for early detection of Downy Mildew (*Plasmopara viticola*) in grapevine,” *Agriculture*, vol. 12, no. 5, p. 617, Agriculture, 2022.
- [26] Y. M. Wang, B. Ostendorf, D. Gautam, N. Habili, and V. Pagay, “Plant viral disease detection: from molecular diagnosis to optical sensing technology—a multidisciplinary review,” *Remote Sensing*, vol. 14, no. 7, p. 1542, 2022.
- [27] R. Raj, J. P. Walker, R. Pingale, R. Nandan, B. Naik, and A. Jagarlapudi, “Leaf area index estimation using top-of-canopy airborne RGB images,” *International Journal of Applied Earth Observation and Geoinformation*, vol. 96, Article ID 102282, 2021.
- [28] J. Monis and R. K. Bestwick, “Detection and localization of Grapevine Leafroll Associated Closteroviruses in greenhouse and tissue culture grown plants,” *American Journal of Enology and Viticulture*, vol. 47, no. 2, pp. 199–205, 1996.
- [29] E. Engvall and P. Perlmann, “Enzyme-linked immunosorbent assay, elisa,” *The Journal of Immunology*, vol. 109, no. 1, pp. 129–135, 1972.
- [30] G. Gambino, “Multiplex RT-PCR method for the simultaneous detection of nine grapevine viruses,” *Methods in Molecular Biology*, vol. 1236, pp. 39–47, 2015.
- [31] F. E. Constable and B. C. Rodoni, *Grapevine Leafroll-Associated Viruses*, Wine Australia, Adelaide, Australia, 2014.
- [32] L. Breiman, “Random forests,” *Machine Learning*, vol. 45, no. 1, pp. 5–32, 2001.
- [33] D. E. Goszczynski, J. Du Preez, and J. T. Burger, “Molecular divergence of Grapevine virus A (GVA) variants associated with Shiraz disease in South Africa,” *Virus Research*, vol. 138, no. 1-2, pp. 105–110, 2008.
- [34] F. Fontaine, D. Gramaje, J. Armengol et al., *Grapevine Trunk Diseases. A Review*, OIV Publications, Paris, France, 2016.
- [35] C. Bertsch, M. Ramírez-Suero, M. Magnin-Robert et al., “Grapevine trunk diseases: complex and still poorly understood,” *Plant Pathology*, vol. 62, no. 2, pp. 243–265, 2013.
- [36] D. Gramaje, J. R. Urbez-Torres, and M. R. Sosnowski, “Managing grapevine trunk diseases with respect to etiology and epidemiology: current strategies and future prospects,” *Plant Disease*, vol. 102, no. 1, pp. 12–39, 2018.
- [37] G. P. Martelli, “Grapevine virology highlights 2006–2009,” in *Proceedings of the 16th Meeting of the International Council for the Study of Virus and Virus-like Diseases of the Grapevine*, Dijon, France, September, 2009.

Research Article

Climate Services for Agriculture: Tools for Informing Decisions Relating to Climate Change and Climate Variability in the Wine Industry

Leanne Webb ¹, Carly Tozer,² Lynette Bettio ³, Rebecca Darbyshire,⁴ Bella Robinson,⁵ Aysha Fleming,² Sigrid Tijs,³ Roger Bodman ¹ and Mahesh Prakash⁶

¹CSIRO, Environment, Private Bag 1, Aspendale 3195, Australia

²CSIRO, Environment, GPO Box 1538, Hobart, TAS 7001, Australia

³Bureau of Meteorology, GPO Box 1289, Melbourne, VIC 3001, Australia

⁴CSIRO, Agriculture and Food, GPO Box 1700, Canberra, ACT 2601, Australia

⁵CSIRO's Data61, GPO Box 1700, Canberra, ACT 2601, Australia

⁶CSIRO's Data61, Private Bag 10, Clayton South 3169, Australia

Correspondence should be addressed to Lynette Bettio; lynette.bettio@bom.gov.au

Received 20 October 2022; Revised 6 March 2023; Accepted 22 March 2023; Published 27 April 2023

Academic Editor: Paul Petrie

Copyright © 2023 Leanne Webb et al. This is an open access article distributed under the Creative Commons Attribution License, which permits unrestricted use, distribution, and reproduction in any medium, provided the original work is properly cited.

Background and Aims. Australia's changing climate is already impacting the agriculture sector and will continue to do so in the future. To help respond to these impacts, the Climate Services for Agriculture (CSA) platform presents readily accessible climate data, including future climate projections, relevant to specific agricultural commodities. This wine industry example aims to demonstrate the functionality and utility of the CSA for national use across a broad range of commodities. *Methods and Results.* The platform includes commodity-relevant climate indices designed in consultation with experts to ensure that they are as salient to producers as possible; the wine-grape specific indices include measures of growing season temperature, rainfall, extreme heat, and frost. Here, we describe the research behind the wine-grape specific indices and present sample outputs from the CSA platform for a site within a selected winegrowing region. We note the CSA platform has been developed through an extensive and continuing user engagement initiative, ensuring it meets the needs of the agriculture community as they grapple with how to make decisions based on longer term climate projections. *Conclusions.* Provision of past, seasonal outlook, and future climate information for Australia and for a range of important agricultural commodities can help improve on-farm planning and decision-making to respond to climate risks. The wine industry provides a leading example of how to use these data for decision-making, noting ongoing adjustments will be needed. *Significance of the Study.* The CSA platform brings together historical climate data, seasonal climate outlooks, and future climate projections to assist agricultural producers to better manage climate variability and climate change. It aims to nationalise this information for all major agricultural commodities in Australia. We use wine production as a demonstration case here.

1. Introduction

Human-induced climate change is already affecting weather and climate extremes in every region across the globe. Evidence of observed changes in climate extremes such as heatwaves, heavy precipitation, droughts, and tropical cyclones, has strengthened over recent years [1–3], as has attribution to human influence [4].

Sectors such as agriculture, which are exposed to climatic variability and change, will become increasingly more impacted as the climate continues to change [5]. The wine industry, like other agricultural industries, will need to continue to manage the effects of the changing climate. The industry will need to identify opportunities and respond to threats that these changes will bring, both now and in the coming decades, to continue to be successful [6]. Evidence of

wine-grape sensitivity to climate has already been observed in Australia with shifts toward earlier harvest dates [7, 8] attributed in part to increased growing season temperatures and changes to water availability [9]. This shift in harvest timing can impact profitability by affecting wine quality [10] and increasing complexity in wine-grape harvest logistics [11].

Climate data and information can assist wine-grape growers and the agriculture sector more broadly to adapt to climate change (e.g., [12, 13]) but information needs to be contextualised and tailored in order to facilitate decision-making [13], including for Australia's wine industry [14]. The Climate Services for Agriculture (CSA) platform, developed by the Bureau of Meteorology (BoM) and the Commonwealth Scientific and Industrial Research Organisation (CSIRO) with funding through the Australian Government's Future Drought Fund [15], aims to build the resilience of Australian agriculture to climate change and variability by providing access to tailored and targeted climate information. The CSA methodology features a co-design approach [16], which involves significant user engagement.

Innovation of the CSA platform lies in the nationally scoped historical, seasonal forecast, and future projection climate information provided in one place, with data available for "point-and-click" locations across Australia. A key feature of the tool is the agriculturally relevant climate indices, which have been tailored specifically for major Australian commodities, drawing on the scientific literature, with guidance from producers and other commodity experts. This combination of national scope and multi-industry application makes the CSA platform unique. The platform is designed to allow farmers to access climate risk knowledge across multiple commodities if required. Historically, research in this area has tended to be subnational in focus and for singular commodities [17].

For the wine industry, an improved understanding of historical, current, and future growing season temperatures at any given site can assist with targeting the most suitable selection of grape varieties and/or wine styles to best align with climate conditions [11]. Related to the warming climate are changes to rainfall which will also have implications for wine-grape production (e.g., quality), and as described by Essling [18], irrigation access and disease pressure. As projected changes to rainfall are not uniform across wine-growing regions, or across the seasons [19], the CSA platform can be employed to better understand how these future conditions may unfold in different regions, especially as climate change may alter the range of historic experience.

Here, we will describe the development of the CSA platform, including how a codesign process has directly influenced the features presented on the platform. We will also discuss the climate risk indices that have been included that specifically relate to wine production and provide an example of the use of the platform for a winegrowing region. This example aims to demonstrate the functionality and utility of the CSA platform for the wine industry.

2. Materials and Methods

2.1. Codesign (User-Centric) Approach. In order to develop a platform that is relevant and provides value to users, it is important to use codesign. In this context, we use the co-design term to describe the process of engaging with users to design and develop features of the CSA platform. This engagement is ongoing and ranges from individual face-to-face interviews to test and showcase the platform at industry gatherings. We provide examples of how user engagement has directly influenced the development of features of the platform below and has shaped what data are presented, and in what form. Engagement with the wine industry has been particularly informative, as wine producers are already thinking about a longer-term time horizon for climate change adaptation and mitigation.

Through employing a user-centric design approach, each successive release of the CSA platform is moving its focus from that of a climate data delivery tool to a focus on developing insights relating to adaptation outcomes. The goal is shifting from a focus on improving access to information, to improve how the information is used. This requires a novel approach to research that is flexible, transdisciplinary, and iterative (learning). The high-level roadmap (Figure 1) provides a timeline summary plan of how this will be progressed:

2.2. Wine Industry Climate Indices. The CSA team identified eight climate indices related to the wine industry (Table 1). The indices and their parameterisation are based on peer-reviewed literature, industry reports, domain expert interviews, and end-user feedback. The inclusion of indices was determined by the availability of climate data, limitations of the science relating to projections, project scope, and technical feasibility of data provision.

2.3. Growing Season Temperature Indices. Numerous temperature-based indices have been used to characterise suitable regions for different varieties and wine styles. These include mean growing season temperature (GST) [20–22], growing degree days (GDD) [22, 23], mean January temperature (MJT) [24–26], biologically effective growing degree days (BEDD) [27], and the Huglin heliothermal Index (HI) [28]. Of these, no single metric has been found to outperform all others across the range of decisions that these metrics are used to inform (e.g., matching variety to regions, predicting phenology). For CSA, in the interest of pragmatism, advice was sought during expert-interviews on narrowing the selection to the more commonly applied indices with mean growing season temperature, GDD, and mean January temperature being included. All growing season temperature metrics currently displayed on the platform were calculated for 1 October to 30 April, a common estimate of the growing season across all wine-grape regions in Australia [8, 10, 20–22, 29]. Future versions of the CSA platform will allow for some customisation of the

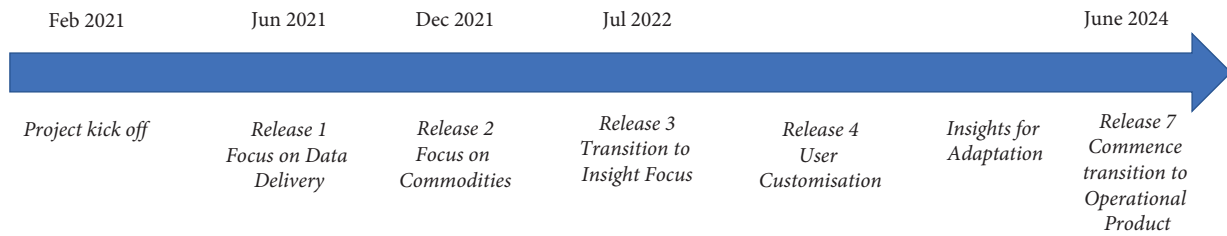


FIGURE 1: CSA focus transition from “data delivery” to “insights for adaptation.”

indices, e.g., changing of temperature thresholds or growing season window to suit growers’ specific requirements.

2.4. Extreme Heat Index. The impact of extreme temperatures on wine-grape production was demonstrated by the significant crop losses being recorded after the 2009 heat-wave in southern Australia [30], which coincided with the veraison stage of the south-eastern Australian wine-grape crop. This was likely caused by the combination of a heat-wave event in Australia’s southeast in early 2009 and, in some areas, a lack of access to irrigation water [30, 31]. Extreme heat events can affect vines’ production and quality across several different growth phases. Extreme temperatures reduce photosynthetic rates and increase transpiration, reducing productivity [32], affect fruit set, and cause berry shrivel [33] which reduces yield, and interfere with berry chemical composition [32].

The temperature thresholds for extreme heat in the context of viticulture have been defined differently in different studies with maximum temperature greater than 35°C, being common across these [21, 22, 30]. While extreme heat on a single day may cause damage, “heatwaves” defined as three or more consecutive days above 35°C, are more difficult to manage and tend to cause more damage than single day heat events. Using a heatwave definition also aligns with practical application, with Hayman et al. [33] noting that many viticulturists make vineyard management decisions based on heatwave definition of three or more consecutive days above 35°C or 40°C. As noted above, future versions of the CSA platform will allow for selectable options relating to thresholds to be adjusted to suit growers’ specific requirements, noting extreme heat definitions vary depending on the region [30].

2.5. Frost Index. Incidences of frost across the wine-grape growing season can cause minor damage through to total crop loss. An example of a costly frost event occurred in November 2018 in Western Australia, where wine-grape growers reported 70 to 80% crop loss from a single event [34]. More severe frost events may also affect the production potential of the following season due to more significant damage to the vines [35].

To estimate potential frost risk, counts of days below a 2°C minimum temperature threshold [22, 36] are presented on the CSA platform. Under many conditions, a temperature of 2°C measured at the height of the Stevenson

Screen thermometer (about 1.2 m above the ground) is approximately equivalent to a temperature of 0°C at ground level (e.g., [37]). The frost risk period defined by the CSA platform of 15 August to 30 November captures the likely frost risk period for sensitive growing tissues, is relevant across regions and varieties, and based on other definitions of frost sensitivity [21, 23, 36] and expert feedback.

2.6. Rainfall Indices. Total summer rainfall can be a guide for investigating potential changes to disease (bunch rot and Botrytis) and grape ripening conditions at harvest [18, 21, 38]. This index provides insights into potential trends in disease pressure and ripening conditions in the lead up to harvest. It does not predict actual disease incidence or severity which is dependent on the presence of the disease, other climate conditions (e.g., temperature and wind), and grower management prior to and during any outbreak. It does provide an indication of potential changes to risk in the future.

Rainfall received over the growing season can influence yield (particularly for nonirrigated vines) and minimise irrigation costs [38]. A study investigating inter- and intraregion *terrior* in Australia used growing season rainfall (1st October to 30th April), along with other indicators, to help differentiate regions [24]. Following these examples, we represent growing season rainfall as total rainfall received from 1st October to 30th April.

Nongrowing season rainfall (1st May to 30th September) [22], is important for two reasons. First, for vineyards with on-farm irrigation dams, nongrowing season rainfall contributes to replenishing dam levels. Second, low soil moisture levels at the beginning of the season can reduce shoot growth and, thus, canopy size, which reduces the ability of the vine to generate carbon resources to support berry growth [39, 40], potentially influencing yield.

2.7. Historical Climate Data. The daily historical rainfall and temperature data are from the Bureau of Meteorology’s Australian Gridded Climate Data (AGCD) dataset [41, 42]. This nationally consistent, gridded dataset from which the CSA data are sourced starts in 1900 for rainfall and 1910 for temperature. The AGCD gridded data are produced by interpolating data from Bureau weather stations around Australia and presenting it on a uniform national 5 km grid. This dataset meets the CSA goal of national accessibility of climate risk information.

TABLE 1: Wine-grape indices codeveloped for the CSA platform.

Index name	Index equation
Growing season temperature (°C) (April to October)	$\sum_{1 \text{ Oct}}^{30 \text{ Apr}} T_{\text{mean}}$
Growing degree days (°C) (April to October)	$\sum_{1 \text{ Oct}}^{30 \text{ Apr}} \text{if } (T_{\text{mean}} > 10^{\circ}\text{C}; (T_{\text{mean}} - 10))$ $\sum_{1 \text{ Oct}}^{30 \text{ Apr}} \text{if } (T_{\text{mean}} \leq 10^{\circ}\text{C}; 0)$
Mean January temperature (°C)	$\sum_{1 \text{ Jan}}^{31 \text{ Jan}} T_{\text{mean}}$
Extreme heat risk (heatwaves) (per year)	$\sum_{i=1}^{30 \text{ June}} \text{if } (T_{\text{max}_i} \text{ and } T_{\text{max}_{i+1}} \text{ and } T_{\text{max}_{i+2}} \geq 35^{\circ}\text{C}; 1)$ $\sum_{i=1}^{30 \text{ June}} \text{if } (T_{\text{max}_i} \text{ or } T_{\text{max}_{i+1}} \text{ or } T_{\text{max}_{i+2}} < 35^{\circ}\text{C}; 0)$
Frost risk (days) (August to November)	$\sum_{15 \text{ Aug}}^{30 \text{ Nov}} \text{if } (T_{\text{min}} \leq 2^{\circ}\text{C}; 1)$ $\sum_{15 \text{ Aug}}^{30 \text{ Nov}} \text{if } (T_{\text{min}} > 2^{\circ}\text{C}; 0)$
Summer rainfall (mm) (Dec to Feb)	$\sum_{1 \text{ Dec}}^{28 \text{ Feb}} \text{Rainfall}$
Growing season rainfall (mm) (April to October)	$\sum_{1 \text{ Oct}}^{30 \text{ Apr}} \text{Rainfall}$
Nongrowing season rainfall (mm) (May to September)	$\sum_{1 \text{ May}}^{30 \text{ Sept}} \text{Rainfall}$

i = day of year. NB: daily T_{mean} , daily T_{max} and daily T_{min} are used in above formula.

2.8. Seasonal Rainfall Outlooks. In addition to climate change risk, CSA draws upon the Bureau of Meteorology official seasonal outlooks [43] to help growers manage current seasonal rainfall variability for the upcoming season. This information is presented as a probability (or chance) of rainfall exceeding a specific threshold (e.g., the chance of rainfall being above the median, expressed as a percentage). These are available for both seasonal and monthly timeframes. The forecast is updated weekly in line with the Bureau of Meteorology updates.

Different users relate differently to outlook information, particularly in relation to rainfall. Some users are interested in specific rainfall amounts (e.g., 200 mm for the season), while others make decisions at specific probabilities (e.g., if there is a 75% chance it will be drier than average). To meet these diverse needs, the CSA platform presents the spread of plausible rainfall amounts into rainfall scenarios that can be viewed in the following ways:

- (i) Chance of at least: the chances that rainfall for the selected outlook period will exceed defined thresholds, e.g., chance of at least 200 mm over the coming three months, or 10 mm in a week.
- (ii) Outlook scenarios: rainfall amounts that are likely at a particular percentage chance, e.g., 25% chance of receiving the given rainfall amount for the period.
- (iii) Rainfall at your location for historical median, past year comparison, and recent period.

2.9. Climate Projections. The CSA platform has been built using both application-ready future climate data from the Climate Change in Australia (CCiA) set of national climate projections [19] and from the National Hydrological Projection dataset [44]. Here we specifically describe application-ready data from CCiA, from which we present rainfall and temperature variables. Data from this product is available at a daily time scale on a 5 km grid across Australia for three future timeframes centred around 2030 (2016–2045), 2050 (2036–2065), and 2070 (2056–2085). These data use information from the Coupled Model Intercomparison Project phase 5 (CMIP5) [45], which provide a repository of simulations from the international climate modelling groups. Specifically, the CCiA application-ready data incorporate projected climate changes simulated by a set of eight CMIP5 models selected to represent most of the range of projected change for Australia [19]. These data are well-established, well-documented, and have been thoroughly evaluated (e.g., see list of Technical Reports and peer-reviewed literature on <https://www.climatechangeinaustralia.gov.au>).

It is important to acknowledge that climate projections are derived from climate models that have limitations:

- (i) Global climate models (GCMs) can provide useful climate projections over the next two decades and beyond at global and continental scales. However, uncertainties at regional and local scales over the next decade are strongly influenced by natural variability, which is hard to predict.

- (ii) Global climate models (GCMs) have coarse resolution and cannot adequately represent weather-scale (1–10 km) phenomena, so downscaling methods have been used.

The “downscaling” method used to produce the application-ready data is a scaling method, whereby the changes projected by the global climate models (~200 km resolution) are applied to the historic observed gridded data (~5 km resolution). In this way, the climate and underlying weather conditions from the observational period are carried forward in a perturbed sense to represent plausible future conditions. The numerical precision of these data must not be confused with accuracy; the downscaled projections are plausible, rather than precise.

The CMIP5 repository includes model simulations of different “Representative Concentration Pathways” (RCPs) that describe how the energy imbalance of the climate system, or “radiative forcing” due to greenhouse gas emissions and other anthropogenic forcings may evolve [46]. It is desirable that a range of RCPs are used in climate risk assessments to assess different plausible future pathways for socio-economic change, technological change, energy generation, and land-use change and associated emissions and atmospheric concentrations of greenhouse gases and air pollutants. Two RCPs, RCP8.5 termed “high emissions” and RCP4.5 termed “medium emissions,” are represented on the CSA platform [19].

The high, RCP8.5, pathway reflects a future in which little additional action on reducing greenhouse gas emissions is taken. Under this scenario global greenhouse gas emissions continue to increase significantly until near the end of the 21st century, and global warming relative to preindustrial times is very likely in the range of 3.3 to 5.7°C at the end of the century. RCP4.5 corresponds to a greenhouse gas emissions pathway that peaks in 2040 and then declines to 1960s emission levels by 2090 [4]. Under this scenario, the very likely range for global warming at the end of the century is 2.1 to 3.5°C, and the Paris Agreement global warming limit of 2°C is extremely likely to be exceeded [47].

3. Using the CSA Platform: Rutherglen Example

To demonstrate the functionality of the CSA platform, we use a site in the Rutherglen wine-growing region (Figure 2) as an example.

The platform presents two historical 30-year periods (Figure 3, top left). A 30-year period is deemed long enough to capture the year-to-year variability of the climate in the selected region but short enough for long-term climate trends not to be a dominant influence [48]. By comparing the recent period (1991–2020) to the past period (1961–1990), a user can determine if there have been any recorded changes in climate in their region over time. This also provides context for any projected climate changes in their region. For example, in the climate metric MJT (°C), there has been an observed increase in the average temperatures of 1.1°C from 1961 to 1990 (23.2°C) to 1991–2020 (24.3°C) in Rutherglen.


Climate Services for Agriculture

Helping farmers and communities plan for the impacts of climate variability.


Select your location

See tailored climate information relevant to your local area by entering your location or clicking on the map below:


🔍 Rutherglen




Continue →




Australian Government
Department of Agriculture,
Fisheries and Forestry



Future
Drought
Fund



CSIRO



Australian Government
Bureau of Meteorology

© 2022

FIGURE 2: CSA interface indicating how a user selected their location (<https://climateservicesforag.indraweb.io/>).

Future projections are shown under two emission scenarios (RCP4.5 and RCP8.5), as well as the past observations split into two periods (Figure 3, bottom left). For the projections, the distribution of the data are based on data from 8 GCMs. For each of those models, we have 30 years of data, and we can calculate an average across those 30 years for each model. This means we have a set of 8 model averages. The range across these, represented by the 10th and 90th percentile values, is shown as the inner, lighter shaded box (Figure 3). It is useful to think of these as describing the range of the average state of the climate. The thin horizontal bar shows the average of this set of values.

If we combine all the data from each of the 8 models, we can calculate the projected range of values. This is calculated as the 10th and 90th percentile across the full dataset (8 models \times 30 years) and is presented as the outer, darker shaded box. It is useful to think of this as the range due to natural year-to-year variability. Incorporating year-to-year variability shows, for instance, that the coolest 10% of Januarys during 1991–2020 had MJT of 21.8°C or less, and the warmest 10% of Januarys had MJT of 26.5°C or greater (Figure 3, bottom left).

In the example shown, depending on the emission scenario, MJT might increase on average from 23.2°C

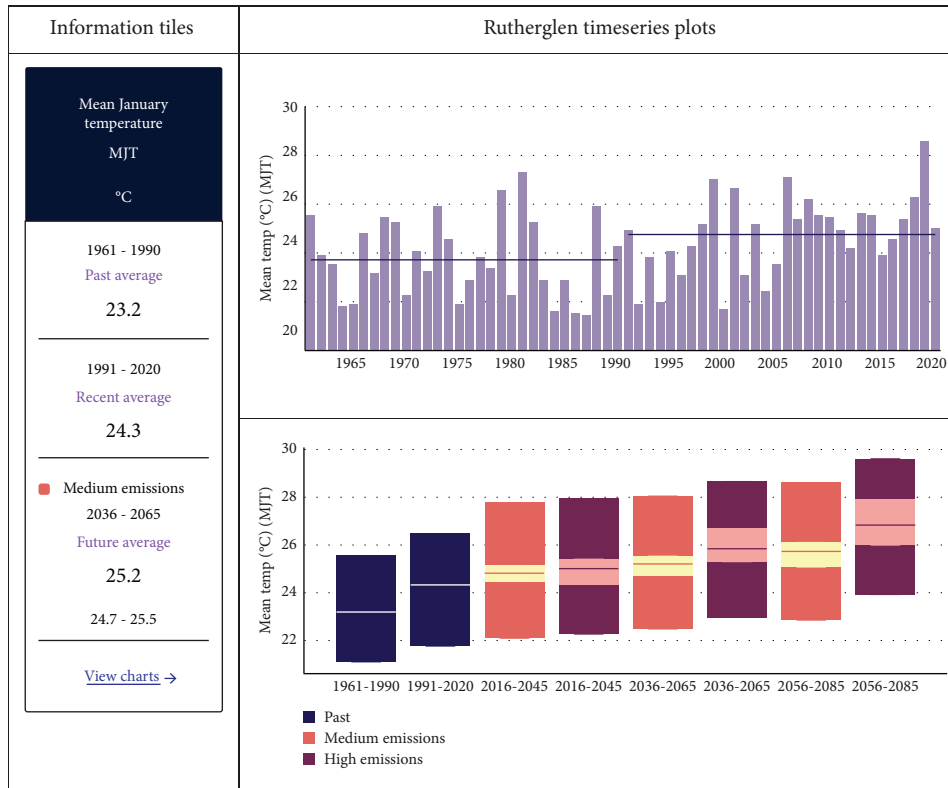


FIGURE 3: Mean January temperature (MJT) (°C) for Rutherglen for specified past and future periods summary (left). Past observations (1961–2020) split into two epochs (1961–1990) and (1991–2020) (epoch average denoted by the black horizontal line) (top right). Past (1961–1990; 1991–2020) (period average blue line, full dark blue bar including year to year variability) and projected 2030 (2016–2045), 2050 (2036–2065), and 2070 (2056–2085) period average and model average range (central lighter colour of the bar), and including variability (10th to 90th percentile indicated by the full extent of the bar) of MJT (°C) (medium emissions, RCP4.5; yellow/orange) and (high emissions, RCP 8.5; pink/purple) (bottom right). Data for past climate sourced from AGCD [41, 42] and future projections are from eight CMIP5 models.

(1961–1990) to 25.2°C (low emissions) or 25.8°C (high emissions) by 2050. Note that this is the average MJT; year-to-year natural variability is greater than these ranges. Incorporating year-to-year variability, the upper end of the model range (90th percentile) under high emissions (RCP8.5) by 2050 indicates an MJT of 28.7°C (Figure 3, bottom left). The information tiles (Figure 3, right) summarise the information in the plots.

We can further consider changes in extreme years using the platform. Figure 4 indicates how the frequency of this “extreme year” may change in the future. For example, by 2056–2085, under RCP4.5, the chance of experiencing an MJT of below 21.8°C (the lower threshold experienced in the 1991–2020 period) is likely to be close to zero (Figure 4, left), yet for this same timeframe an MJT of 26.5°C, the upper threshold from the 1991–2020 period, may be exceeded around 3.9 (2.3–5.7) years out of 10 (Figure 4, right). This type of information may inform management decisions around variety selection for a particular region (refer to the discussion part).

Seasonal rainfall outlooks provide insights into decisions made in the current season. For the wine industry, seasonal rainfall outlooks are useful to inform planning, in particular

irrigation scheduling and disease management. The outlooks are probabilistic, providing the chance of receiving a certain amount of rainfall for the next month or season (Figure 5).

An indication of the past accuracy of the outlooks is also provided. Past accuracy is a measure of how well the model has performed for the same selected time of year in the past. Accuracy is often tied to the evolution of large climate scale drivers such as the El Niño Southern Oscillation and Indian Ocean Dipole. These drivers have a strong impact on seasonal to annual Australian rainfall and temperature (e.g., [49]). In autumn, these drivers are still evolving and are often in their “neutral” phase and so there tends to be lower skill in predicting autumn climate. By winter and spring these drivers have matured and are more predictable, so accuracy of winter and spring outlooks tends to be higher especially over eastern parts of the country.

3.1. End-User and Stakeholder Engagement in Action. “Likely incidence in ten years” tool

As described above, the CSA platform has been developed using a user-centred design approach. Here, we present an example of how this approach has been implemented.

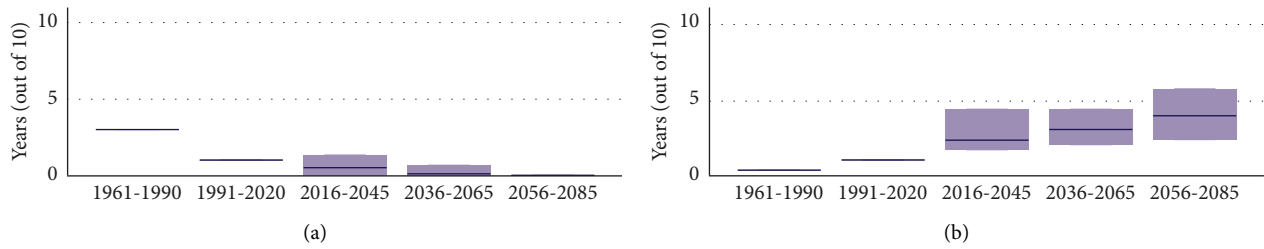


FIGURE 4: Number of years (out of 10) with mean January temperature (MJT) (°C) below 21.8°C (a) and above 26.5°C (b) under RCP4.5. The range on the boxplots indicates future projections across different climate models. Data for past climate sourced from AGCD [41, 42] and future projections are from eight CMIP5 models.

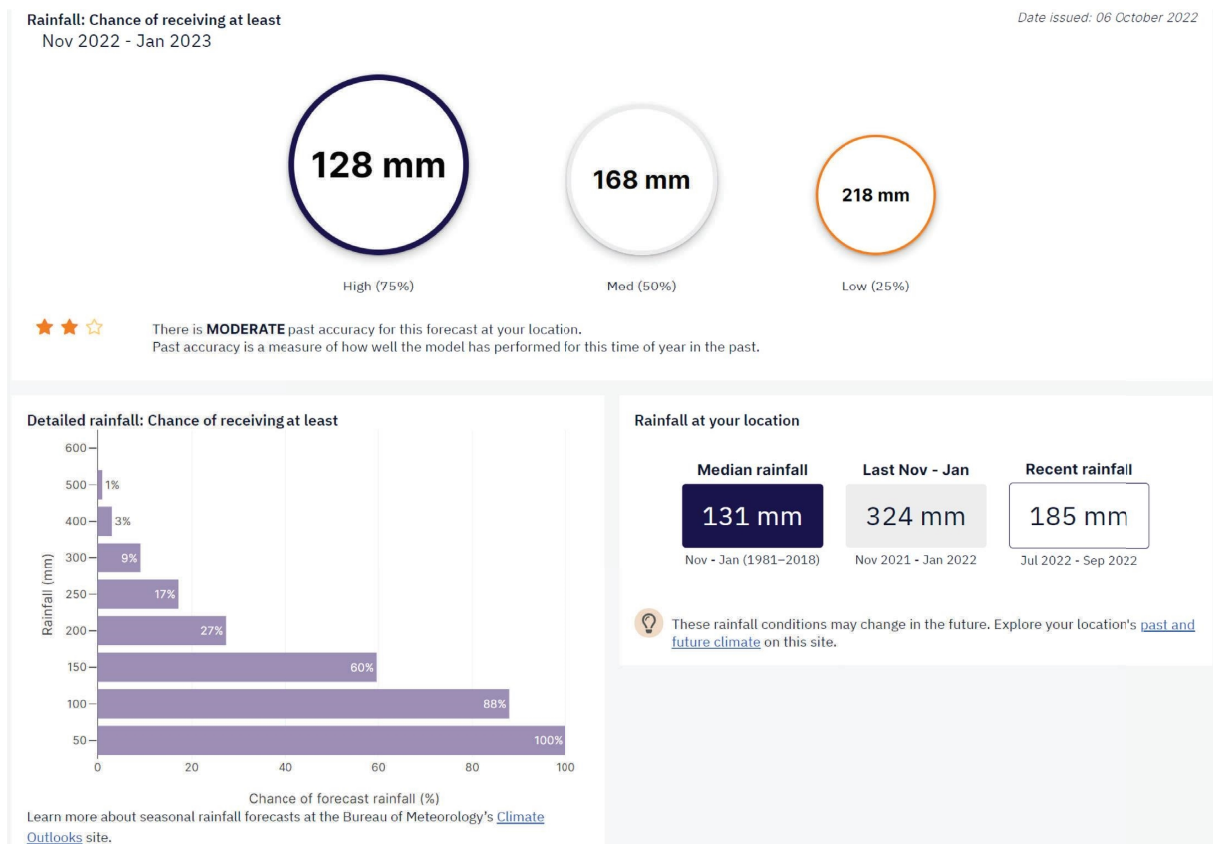


FIGURE 5: Seasonal expected rainfall for the season ahead (next 3 months) with a certain (75%, 50%, or 25%) “Chance of receiving at least” a given rainfall total is indicated by each of three circles (top), or a given rainfall amount (for the coming season (bottom left), or different periods’ rainfall totals (1981–2018 median), last year’s seasonal rainfall, and this year’s previous season.

User feedback was received, acknowledged, and used to drive the development of the new tool (Figure 6). This shows how users play a key role in building the CSA platform.

3.2. *Map View Tool.* Another example of how user engagement is driving the development of the CSA platform can be seen in the prototype “Map view tool.” This tool was developed based on user desire to see information at a broader spatial scale, rather than for an individual location. A visual example of the tool is given in Figure 7. The tool, which is currently being tested with users, serves up the data

in a map view and gives users the ability to select among the different commodities, related indices, and for current and future periods (under different scenarios). Single model or ensemble averages can also be selected (Figure 7). In this example, the ACCESS1.0 model forced under RCP4.5 is illustrated. The “pop-up” (Figure 8) appears when the user clicks on the “yellow pin” grid cell (refer to Figure 7), indicating the mean and 10th–90th percentiles of year-to-year variability in MJT (°C) across past periods and into the future, with results from all eight models included. The RCP scenarios can be toggled on/off, with RCP4.5 (Figure 8). This tool may be particularly relevant to users who desire to explore and compare climate changes across a broad region.

The new CSA prototype tool (released July 2022) includes a “Likely Incidence in Ten Years” tool. This customisable threshold tool was developed in response to user feedback asking for a more intuitive presentation of the climate data. The tool’s development was influenced by users asking questions around other CSA features such as “How often would we be on that average line?” as well as comments being made about “good-, bad-, very wet-, or very dry-years” users had experienced. Different ways of presenting these data were explored, with the table display (below) being well received, with articulation of likelihood and frequency of events, relating to hottest-, driest-, or the coldest- and wettest conditions. The example below shows the average frequency of exceeding MJT thresholds (years out of 10) for Rutherglen across past and future periods (the full range of these results is presented more clearly on the platform).

Year Range	Number of years with mean January temperature (MJT) below 21.5 (°C)	Number of years with mean January temperature (MJT) above 26.5 (°C)
1961-1990	3 in 10 years	0.3 in 10 years
1991-2020	1 in 10 years	1 in 10 years
2016-2045	0.5 in 10 years	2.3 in 10 years
2036-2065	0.1 in 10 years	3 in 10 years
2056-2085	0 in 10 years	3.9 in 10 years

The preferred definition of ‘thresholds’ varied amongst end-users, with some preferring to see changes in frequency of recorded historical extremes, while others wanted to use their own ‘good’ and ‘bad’ years’ experience. Both options have been made available on the platform.

As a result of the new “Likely Incidence” tool, discussions between users and the CSA team now focus on what the information means. For example: ‘What will farming be like in this type of environment?’, rather than about how to read and interpret the data.

Using this information about projected changes to the frequency of climate events enables farmers to better visualise farm management going forward. In discussions, they now consider actions that could alleviate some of the anticipated challenges, without needing to discuss the science of climate change. Through exploring the platform and related discussions, CSA therefore assists in increasing farmer understanding of their individual future climate challenges and the types of decisions they may need to make to adapt to future farming scenarios. The engagement component of the CSA Program remains ongoing, with user feedback continuing to be incorporated into the platform.

FIGURE 6: Linking stakeholder feedback to platform outcomes “likely incidence in ten years” or number of years (out of 10) tool (see Figure 4).

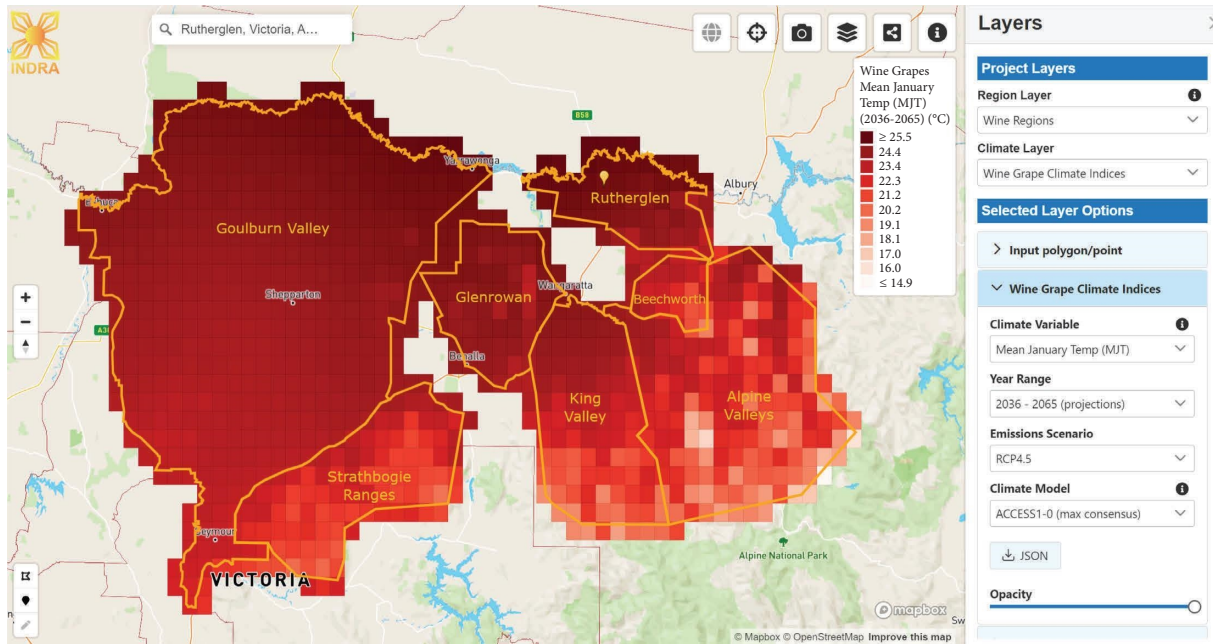


FIGURE 7: Mean January temperature (MJT) (°C) for northern Victorian wine regions (yellow boundaries) for 2050 (2036–2065) under RCP4.5 for the ACCESS1.0 GCM (global climate model).

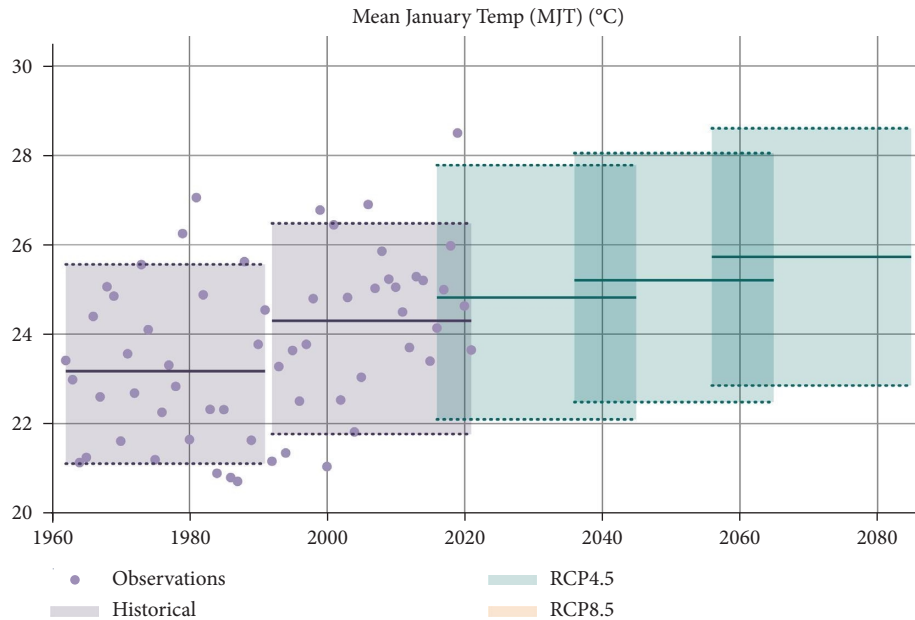


FIGURE 8: Range of MJT (°C) for past periods (1961–1990; 1991–2020) (purple with individual years indicated with dots) and projected 2030 (2016–2045), 2050 (2036–2065), and 2070 (2056–2085) average and range (10th to 90th percentile) of MJT (°C) (medium emissions, RCP4.5; green), an example Rutherglen grid cell pop-up window showing MJT observations and projections.

Further user testing will determine whether this tool is presented on the public facing CSA platform or whether further development is required to ensure its utility. This again highlights how users can have a direct influence on the development of a tool being presented on the CSA platform.

4. Discussion

The CSA platform provides wine-grape relevant climate indices that can be used for planning at a range of decision time scales (e.g., selecting wine-grape varieties that match the future climate of a region).

As described for Rutherglen, depending on the emission scenario, by 2050, MJT might increase from around 24°C currently, to 25.2°C (low emissions) or 25.8°C (high emissions) by 2050 (Figure 2), remembering also this is the average MJT and year-to-year natural variability is greater than these ranges. Noting these shifts, planting suitable varieties will help grapes ripen at a time when they have the best chance of retaining desired quality attributes. A compelling aspect of the CSA platform is that for any location, it is easy to see if there have been any notable changes through the past climate, and better understand what may evolve in future. Over the longer term, therefore, growers can change varieties to better fit with the warmer projected climate. While the CSA platform does not attempt to make varietal recommendations, much literature matching varieties to climatic characteristics of regions is available for Australia (e.g., [27]), and through using a global analogue approach [50].

The CSA platform presents different measures of growing season temperature: GDD (Oct to Apr) (°C); MJT (°C); average growing season temperature (Oct to April) (°C), as these relate to the variety suitability. Some indices

were not selected for the following reasons. For example, Hall and Jones [20] evaluated both GST and BEDD for Australia's wine-grape growing regions under future climate change. They note that BEDD is less useful for considering suitability for hotter regions as it includes an upper threshold of 19°C [27]. Jarvis et al. [8] evaluated several indices for Australia wine-grape growing areas to consider maturity timing. The Huglin heat sum index, similar to the BEDD though not capped and slightly modified according to latitude, was assessed. They found the HI was problematic for application in Australia due to the latitude adjustment feature being less appropriate in Australia than in the northern hemisphere. The versatility of the platform enables a range of different metrics to be re-assessed and or introduced later if deemed helpful by users. Capability is also being built so that users of the CSA platform can customize commodity indices based on their lived experience.

Users of the climate data should acknowledge the uncertainties and limitations associated with the information presented on the CSA platform and consider how these might affect their conclusions and the confidence that they express in them. For example, the detailed application-ready projection data are a useful guide to plausible future climate conditions. However, the full uncertainty in future climate conditions is not reflected as there may be local effects on climate changes that are not represented by global climate models. This is most likely to be the case in mountainous or coastal areas. The CSA platform is evolving, which also means that data sources may change (or new data added), in response to user requirements. This may include the addition of new climate projection sources.

Confidence in a climate projection is a measure of how plausible the projected range of change is for a given emission scenario. Confidence ratings are assigned to

projections based on multiple lines of evidence including how well our GCMs simulate key features of the climate system (e.g., do they simulate El Niño events well?), and how well we understand the drivers of change and how coherent the projections are with past observed climate trends. Across Australia there is high to very high confidence in temperature projections, including minimum and maximum temperature extremes such as heatwaves and frosts. The confidence in rainfall projections across Australia and for specific seasons is more variable. For example, in southwest Western Australia, there is high confidence that there will be a continuation of the trend of decreasing winter rainfall but on the eastern seaboard, decreases in winter rainfall are projected with medium confidence. Regional climate change information, including associated confidence levels are reported for Australia (see [19]).

Regarding the historical climate data, the Bureau of Meteorology has a large network of manually read and automated rain gauges across Australia, but it is not possible to place this equipment every few kilometres. While these stations provide rainfall data at point locations when available, gridded analysis utilises computer modelling to provide rainfall information in much wider areas. This is important as it means an estimate of rainfall conditions can be provided in data-sparse areas and provides a consistent coverage across Australia and over time. However, this means that the closest grid point to a particular location will represent both temperature and rainfall from several nearby stations. For this reason, the rainfall, and related frost risk, at any particular grid point might not be the same as the rainfall at any single gauge. Good understanding of a property's mesoclimate as it relates to the surrounding area is especially important in this regard.

The CSA platform is not designed to replace other forms of climate information used in specific industries. We encourage users to complement their exploration of the CSA platform with other relevant information which may influence production including soil type, landscape aspect, access to water, or logistical constraints. This assessment further does not account for a number of other factors that will influence the outcome from shifts in climate:

- (i) Other weather variables (e.g., wind (important in the calculation of evapotranspiration), cloud)
- (ii) Different adaptation practices which can be implemented. For example, the use of reflective sprays or trellis type, application of winter irrigation, or pruning strategies.
- (iii) Influence of stored soil moisture on plant water balance, being affected by soil type
- (iv) Timing and intensity of rainfall, which can influence yield and quality
- (v) Access to water from dams or irrigation schemes
- (vi) Varietal differences in the time of the growing season or potential phenological shifts to the growing season resulting from climate change

- (vii) All climate-related decisions are only part of the many other factors influencing on-farm operations

A case in point is that a minimum temperature threshold does not necessarily represent a frost event with other conditions also contributing (wind, soil moisture, proximity to water body, land cover, and vineyard orientation). Further, occurrence of frost is not the same as damage from frost noting frost mitigation strategies can modulate potential risk (e.g. [35]). Thus, this minimum temperature threshold approach represents risk potential, not a frost or frost damage prediction.

We note the extreme heat metric is useful for considering historical and future trends in the potential for damage however, the scaling method used to create the projections, delta scaling [19], does not account for any changes in the sequencing, duration and/or frequency of weather events (e.g., increased duration and/or frequency of hot days).

The CSA platform is receiving positive feedback from the agricultural community. With the introduction of the "Likely Incidence in Ten Years" feature, conversations with end-users are now not only about how to navigate the platform and understanding the data, but about how management practices may need to change in a future climate. This transition is key to successful industry (and more broadly, national) preparedness for climate change. These conversations are being further developed by the CSA team, ensuring this beneficial interaction continues.

Feedback from the wine industry already enacted:

"Would love to have the grapevine commodity on the platform as soon as possible, happy to advise on the indices."

While some are yet to be incorporated:

"I'd would like to see data that shows bushfire projections for the future 2040-2050 climate for our regions."

Regarding climate change adaptation methods, we were told:

"We can change the trimming of the vines, to protect from sun in years with very high heatwaves, canopy cooling with frost sprinklers pulsing at night. Under-vine sprinklers are also cooling techniques. Mulching, composting to conserve water and the keep the humidity lower in the vine canopy."

5. Conclusions

The CSA platform is a timely addition to the farmer and advisor information-toolbox to assist with planning in a changing climate. The information is targeted to agricultural production at a commodity level across Australia, with a spatial scale that aims to deliver nuanced climate-related information. This ground-breaking initiative provides national access to past and future climate information

on one platform and is targeted to different agricultural commodities including wine-grapes with users and experts responding very positively regarding its utility. Assistance with planning decisions and discussions around climate variability and climate change is available for many Australian farming districts and is a key focus for continued research in all agricultural industries. Further development of the platform, driven by user needs, endeavours to increasingly improve its' functionality. [51].

Data Availability

The platform utilises the following data for delivery at national scale: (i) Historical temperature and rainfall data from the Bureau of Meteorology. (ii) Rainfall and temperature projections for 2030, 2050, and 2070 from CSIRO and the Bureau of Meteorology (<https://www.climatechangeinaustralia.gov.au>) for medium (RCP 4.5) and high (RCP 8.5) scenarios. (iii) Historical and projected surface water data from the Bureau of Meteorology. (iv) Seasonal Forecast data from the Bureau of Meteorology.

Conflicts of Interest

The authors declare that they have no conflicts of interest.

Acknowledgments

The authors would like to thank AWITC for the invitation to publish the research in this special issue and for covering the article processing charge. The authors would like to thank the Australian Government Department of Agriculture, Fisheries and Forestry for funding the Climate Services for Agriculture Program under the Future Drought Fund. Drafts of this article were reviewed by Dave Henry (CSIRO), Ian Macadam (CSIRO), Alison Oke (BoM), and Ross Henry (BoM). For the projections data, the authors acknowledge the World Climate Research Programme's Working Group on Coupled Modelling, which is responsible for CMIP, and the authors thank the climate modelling groups for producing and making available their model output. For CMIP, the U.S. Department of Energy's Program for Climate Model Diagnosis and Intercomparison provides coordinating support and leads development of software infrastructure in partnership with the Global Organisation for Earth System Science Portals.

References

- [1] P. Arias, "Climate Change 2021: The Physical Science Basis," *Contribution of Working Group I to the Sixth Assessment Report of the Intergovernmental Panel on Climate Change; Technical Summary*, IPCC, Geneva, Switzerland, 2021.
- [2] L. V. Alexander, J. M. J. W. Arblaster, and C. Extremes, "Historical and projected trends in temperature and precipitation extremes in Australia in observations and CMIP5," *Weather and Climate Extremes*, vol. 15, pp. 34–56, 2017.
- [3] S. Perkins, L. Alexander, and J. Nairn, "Increasing frequency, intensity, and duration of observed global heatwaves and warm spells," *Geophysical Research Letters*, vol. 39, no. 20, 2012.
- [4] IPCC, "Summary for policymakers," in *Climate Change 2021: The Physical Science Basis. Contribution of Working Group I to the Sixth Assessment Report of the Intergovernmental Panel on Climate Change*, V. Masson Delmotte, P. Zhai, A. Pirani et al., Eds., Cambridge University Press, Cambridge, UK, 2021.
- [5] P. R. Shukla, *Climate Change and Land: An IPCC Special Report on Climate Change, Desertification, Land Degradation, Sustainable Land Management, Food Security, and Greenhouse Gas Fluxes in Terrestrial Ecosystems*, IPCC, Geneva, Switzerland, 2019.
- [6] T. Holland and B. Smit, "Climate change and the wine industry: current research themes and new directions," *Journal of Wine Research*, vol. 21, no. 2-3, pp. 125–136, 2010.
- [7] L. Webb, P. Whetton, and E. Barlow, "Observed trends in winegrape maturity in Australia," *Global Change Biology*, vol. 17, no. 8, pp. 2707–2719, 2011.
- [8] C. Jarvis, E. Barlow, R. Darbyshire, R. Eckard, and I. Goodwin, "Relationship between viticultural climatic indices and grape maturity in Australia," *International Journal of Biometeorology*, vol. 61, no. 10, pp. 1849–1862, 2017.
- [9] L. B. Webb, P. H. Whetton, J. Bhend, R. Darbyshire, P. R. Briggs, and E. W. R. Barlow, "Earlier wine-grape ripening driven by climatic warming and drying and management practices," *Nature Climate Change*, vol. 2, no. 4, pp. 259–264, 2012.
- [10] L. B. Webb, P. H. Whetton, and E. W. R. Barlow, "Modelling the relationship between climate, winegrape price and winegrape quality in Australia," *Climate Research*, vol. 36, no. 2, pp. 89–98, 2008.
- [11] L. Webb, P. Whetton, and E. Barlow, "Modelled impact of future climate change on the phenology of winegrapes in Australia," *Australian Journal of Grape and Wine Research*, vol. 13, no. 3, pp. 165–175, 2007.
- [12] A. Belay, J. W. Recha, T. Woldeamanuel, and J. F. Morton, "Smallholder farmers' adaptation to climate change and determinants of their adaptation decisions in the Central Rift Valley of Ethiopia," *Agriculture & Food Security*, vol. 6, no. 1, p. 24, 2017.
- [13] R. S. Friedman, E. MacKenzie, R. Baiga, K. Inape, S. J. Crimp, and M. Howden, "Designing climate information services to enhance resilient farming activities: lessons from Papua New Guinea," *Frontiers in Climate*, vol. 4, 2022.
- [14] M. R. Dunn, J. A. Lindesay, and M. Howden, "Spatial and temporal scales of future climate information for climate change adaptation in viticulture: a case study of User needs in the Australian winegrape sector: future climate information scales for viticulture," *Australian Journal of Grape and Wine Research*, vol. 21, no. 2, pp. 226–239, 2015.
- [15] DAFF, "Drought resilience self-assessment tool," 2022, <https://www.agriculture.gov.au/agriculture-land/farm-food-drought/drought/future-drought-fund/drought-resilience-self-assessment-tool>.
- [16] A. Fleming, E. Bohensky, L. Dutra et al., "Perceptions of co-design, co-development and co-delivery (Co-3D) as part of the co-production process – insights for climate services," *Climate Services*, vol. 30, Article ID 100364, 2023.
- [17] R. Darbyshire, S. B. Johnson, M. R. Anwar et al., "Climate change and Australia's primary industries: factors hampering an effective and coordinated response," *International Journal of Biometeorology*, vol. 66, no. 6, pp. 1045–1056, 2022.
- [18] M. Essling, *Rainfall Close to Harvest*, Winetitles Media, Broadview, Australia, 2015.
- [19] CSIRO and Bureau of Meteorology, *Climate Change in Australia Information for Australia's Natural Resource*

- Management Regions: Technical Report*, CSIRO and Bureau of Meteorology, Melbourne, Australia, 2015.
- [20] A. Hall and G. V. Jones, "Effect of potential atmospheric warming on temperature-based indices describing Australian winegrape growing conditions," *Australian Journal of Grape and Wine Research*, vol. 15, no. 2, pp. 97–119, 2009.
- [21] P. Hayman and D. Thomas, *Assessment of Vulnerability to Climate Change across Australia's Wine Regions*, SARDI South Australian Research and Development Institute, Urrbrae, Australia, 2013.
- [22] T. A. Remenyi, *Australia's Wine Future: A Climate Atlas*, University of Tasmania, Hobart, Tasmania, 2019.
- [23] R. Faggian, M. Johnson, V. Sposito, and H. Romeijn, *Climate Smart Agricultural Development in the Goulburn Broken Region. Technical Report: Fruit Production Part 3 (Pear and Grape)*, Deakin University Burwood, Victoria, Australia, 2016.
- [24] R. G. V. Bramley, J. Ouzman, and M. C. T. Trought, "Making sense of a sense of place: precision viticulture approaches to the analysis of terroir at different scales," *Oeno One*, vol. 54, no. 4, pp. 903–917, 2020.
- [25] Orange Region Vignerons Association, "Orange Region Terroir: A Review of the Unique Features of the Orange Wine Region NSW (New South Wales) Australia," 2010, https://www.orange360.com.au/Portals/0/pdf/Orange_Terroir.pdf?ver=2019-06-25-110834-483.
- [26] R. Smart and P. Dry, *A climatic classification for Australian viticultural regions*, *Australian Grapegrower Wine-maker*, Winetitles Media, Broadview, Australia, 1980.
- [27] J. Gladstones, *Viticulture and Environment*, Winetitles, Broadview, Australia, 1992.
- [28] M. Huglin, "Nouveau mode d'évaluation des possibilités héliothermiques d'un milieu viticole/A new method of evaluating the heliothermal possibilities in the environment of grape culture," *Comptes rendus des seances*, vol. 15, 1978.
- [29] R. Firth, J. Kala, T. J. Lyons, and J. Andrys, "An analysis of regional climate simulations for Western Australia's wine regions-model evaluation and future climate projections," *Journal of Applied Meteorology and Climatology*, vol. 56, no. 7, pp. 2113–2138, 2017.
- [30] L. Webb, J. Whiting, A. Watt et al., "Managing grapevines through severe heat: a survey of growers after the 2009 summer heatwave in south-eastern Australia," *Journal of Wine Research*, vol. 21, no. 2-3, pp. 147–165, 2010.
- [31] C. Gunning-Trant, "Australian wine grape production projections to 2011-12," *ABARE Research Report 10.4 for the Grape and Wine Research and Development Corporation*, Australian Bureau of Agriculture and Resource Economics, Canberra, Australia, 2010.
- [32] X. Venios, E. Korkas, A. Nisiotou, and G. Banilas, "Grapevine responses to heat stress and global warming," *Plants*, vol. 9, no. 12, pp. 1754–1769, 2020.
- [33] P. Hayman, M. Longbottom, M. McCarthy, and D. Thomas, *Managing Vines during Heatwaves*, *Wine Australia for Australian Wine*, Wine Australia, Adelaide, South Australia, 2012.
- [34] J. Daly, *Record-breaking Cold Snap Wipes Out Vineyards in WA's South*, Wine Australia, Adelaide, South Australia, 2018.
- [35] J. E. Jones, S. J. Wilson, G. Lee, and A. M. Smith, "Effect of frost damage and pruning on current crop and return crop of Pinot Noir," *New Zealand Journal of Crop and Horticultural Science*, vol. 38, no. 3, pp. 209–216, 2010.
- [36] D. L. Gobbett, U. Nidumolu, and S. Crimp, "Modelling frost generates insights for managing risk of minimum temperature extremes," *Weather and Climate Extremes*, vol. 27, Article ID 100176, 2020.
- [37] S. J. Crimp, B. Zheng, N. Khimashia et al., "Recent changes in southern Australian frost occurrence: implications for wheat production risk," *Crop and Pasture Science*, vol. 67, no. 8, pp. 801–811, 2016.
- [38] R. M. B. Harris et al., *Australia's Wine Future: Adapting to Short-Term Climate Variability and Long-Term Climate Change*, Final report to Wine Australia, Hobart, Tasmania, 2019.
- [39] M. Bonada, E. J. Edwards, M. G. McCarthy, G. C. Sepúlveda, and P. R. Petrie, "Impact of low rainfall during dormancy on vine productivity and development," *Australian Journal of Grape and Wine Research*, vol. 26, no. 4, pp. 325–342, 2020.
- [40] M. Keller, P. Romero, H. Gohil et al., "Deficit irrigation alters grapevine growth, physiology, and fruit microclimate," *American Journal of Enology and Viticulture*, vol. 67, no. 4, pp. 426–435, 2016.
- [41] A. Evans, D. Jones, R. Smalley, and S. Lelleyett, *An Enhanced Gridded Rainfall Analysis Scheme for Australia*, Bureau of Meteorology, Melbourne, Australia, 2020.
- [42] D. A. Jones, W. Wang, and R. Fawcett, "High-quality spatial climate data-sets for Australia," *Australian Meteorological and Oceanographic Journal*, vol. 58, no. 4, pp. 233–248, 2009.
- [43] R. Wedd, O. Alves, C. de Burgh-Day et al., "ACCESS-S2: the upgraded Bureau of Meteorology multi-week to seasonal prediction system," *Journal of Southern Hemisphere Earth Systems Science*, vol. 72, no. 3, pp. 218–242, 2022.
- [44] L. Wilson, U. Bende-Michl, W. Sharples et al., "A national hydrological projections service for Australia," *Climate Services*, vol. 28, Article ID 100331, 2022.
- [45] K. E. Taylor, R. J. Stouffer, and G. A. Meehl, "An overview of CMIP5 and the experiment design," *Bulletin of the American Meteorological Society*, vol. 93, no. 4, pp. 485–498, 2012.
- [46] D. P. Van Vuuren, J. Edmonds, M. Kainuma et al., "The representative concentration pathways: an overview," *Climate Change*, vol. 109, no. 1-2, pp. 5–31, 2011.
- [47] Z. Hausfather and G. P. Peters, "Emissions—the 'business as usual' story is misleading," *Nature*, vol. 577, no. 7792, pp. 618–620, 2020.
- [48] L. Webb, J. Clarke, K. Hennessy, C. Heady, and T. Erwin, *Climate Change in Australia Projections for Australia's Natural Resource Management Regions: Data Delivery*, CSIRO and Bureau of Meteorology, Melbourne, Australia, 2015.
- [49] J. S. Risbey, M. J. Pook, P. C. McIntosh, M. C. Wheeler, and H. H. Hendon, "On the remote drivers of rainfall variability in Australia," *Monthly Weather Review*, vol. 137, no. 10, pp. 3233–3253, 2009.
- [50] L. B. Webb, I. Watterson, J. Bhend, P. H. Whetton, and E. W. R. Barlow, "Global climate analogues for winegrowing regions in future periods: projections of temperature and precipitation," *Australian Journal of Grape and Wine Research*, vol. 19, no. 3, pp. 331–341, 2013.
- [51] G. Zhou and Q. Wang, "A new nonlinear method for calculating growing degree days," *Scientific Reports*, vol. 8, no. 1, p. 10149, 2018.

Research Article

Modelling Smoke Flavour in Wine from Chemical Composition of Smoke-Exposed Grapes and Wine

Mango Parker ¹, WenWen Maddy Jiang ¹, Eleanor Bilogrevic ¹, Desireé Likos ¹,
John Gledhill,² Adrian D. Coulter ¹, Geoff D. Cowey,¹ Con A. Simos,¹ I. Leigh Francis ¹
and Markus J. Herderich ¹

¹The Australian Wine Research Institute, Glen Osmond, Adelaide, SA 5064, Australia

²WIC Winemaking Services, Glen Osmond, Adelaide, SA 5064, Australia

Correspondence should be addressed to Mango Parker; mango.parker@awri.com.au

Received 10 November 2022; Revised 23 January 2023; Accepted 24 March 2023; Published 21 April 2023

Academic Editor: Liz Waters

Copyright © 2023 Mango Parker et al. This is an open access article distributed under the Creative Commons Attribution License, which permits unrestricted use, distribution, and reproduction in any medium, provided the original work is properly cited.

Wine grapes exposed to smoke and wine made from grapes exposed to smoke can robustly be identified through their elevated concentrations of volatile phenols and phenolic glycosides serving as smoke markers, compared to concentrations typically found in non-smoke-exposed samples. Smoke-affected wines with high concentrations of volatile phenols and glycosides can have smoky flavours, but the relationship between concentrations of specific smoke markers in grapes and the intensity of smoky sensory attributes in the resulting wine has not been established. This study sought to determine whether volatile phenols and glycoside concentration in grapes and wine are suited to predict smoke flavour, to identify the key drivers of smoke flavour in both matrices. The study aimed to determine what concentrations of volatiles and glycosides in grapes impart an unacceptable smoke flavour in the resulting wine, to provide a guide for producers assessing suitability of smoke-exposed grapes for wine production. During vintage 2020, a total of 65 grape samples were collected from vineyards exposed to bushfire smoke, as well as unaffected vineyards. Chardonnay, Pinot Noir, and Shiraz grapes were harvested from vineyards in New South Wales, South Australia, and Victoria. Unoaked wines (50 kg scale) were produced under controlled conditions. The wines had a wide range of smoke flavour intensities rated by a trained sensory panel. Statistical models based on guaiacol, *o*-cresol, *m*-cresol, *p*-cresol, and some glycosides gave good predictions of smoke flavour intensity, with a slightly different optimal model for each cultivar. Subsequently, critical concentrations for quality defects were estimated to provide a guide for producers. A subset of smoke exposure markers in wine grapes affected by smoke from bushfires can be used to predict the degree of smoke flavour in wine. This information provides a first guide for assessing the risk of producing smoke tainted wine from smoke-exposed grapes.

1. Introduction

Bushfire smoke has caused billions of dollars of losses to the global wine industry since it was first identified in 2003 as the source of unpleasant smoky flavours [1, 2]. Volatile phenols in smoke are taken up by berries and metabolized, forming phenolic glycosides which accumulate during the season, resulting in elevated concentrations of volatile phenols and/or phenolic glycosides at harvest [3–5]. Wines made from smoke-affected grapes can have elevated concentrations of volatile phenols and phenolic glycosides, particularly for wines made with skin contact [1, 6, 7]. These wines have

unpleasant smoky aromas, flavours, and aftertaste, which are considered undesirable quality defects by many in the wine industry [8].

“Smoky,” “medicinal,” and “cold ash” aromas, flavours and aftertaste have been attributed to volatile phenols and glycosides, particularly the potent odorants guaiacol, *o*-cresol, *m*-cresol, and *p*-cresol [9–11]. “Smoky” and “medicinal” flavours are due to combinations of volatile phenols and phenolic glycosides, that can contribute even when below their individual sensory thresholds, due to sub-threshold interactions and additive effects [9]. Phenolic glycosides contribute to smoke flavour and aftertaste by

hydrolysis in-mouth during tasting [9, 10]. Earlier studies have shown that consumers dislike smoky flavours in rosé style wines made from smoke-exposed grapes, and red wines with 50 µg/L of guaiacol added [12, 13]. While the volatile phenols and glycosides have been related to smoke flavour in highly smoke-affected wines of various cultivars [9, 14], there is little information about the minimum concentrations of volatile phenols and/or phenolic glycosides required to impart a perceptible smoke flavour when present below individual sensory threshold concentrations.

Notably, some smoke flavours or compounds can be desirable in certain wine styles. For example, oaked wines can have distinct toasty or smoky flavours due to guaiacol and other volatile phenols formed during toasting of oak [15, 16]. Also, in some white wines, a smoky/struck flint character can be found, attributed to phenylmethanethiol (syn. benzenemethanethiol), a potent odorant with an odour detection threshold of approximately 0.3 ng/L [17].

Analytical protocols for identifying smoke exposure are available to the wine sector [18]. A suite of seven volatile phenols and six phenolic glycosides are routinely analysed to identify smoke exposure of grapes; guaiacol, 4-methylguaiacol, *o*-cresol, *m*-cresol, *p*-cresol, syringol, 4-methylsyringol, syringol gentiobioside, methylsyringol gentiobioside, cresol rutinosides (including rutinosides of *o*-, *m*-, and *p*-cresol), guaiacol rutinoside, methylsyringol rutinoside, and phenol rutinoside [18, 19]. In addition to those routinely analysed, a large number of phenolic glycosides including pentose-glucosides and trisaccharides have been identified [19–21]. Smoke exposed grapes and wine can be identified by comparing concentrations of volatile phenol and glycoside smoke markers to typical background levels found in non-smoke-exposed samples [22]. If volatile phenols or phenolic glycosides are above concentrations typically found in non-smoke-exposed samples for that cultivar, the sample is considered to be smoke-affected. If analysis of grapes shows high levels of smoke markers, growers may choose not to harvest affected blocks or winemakers might choose to modify their winemaking protocols or not to proceed with winemaking.

There are a number of steps that can be taken in the vineyard and winery to minimise the sensory impacts of smoke exposure. These include hand harvesting instead of machine harvesting, excluding leaves and stems, keeping fruit cool prior to juice extraction, separating press fractions, reducing fermentation time on skins, and fining techniques and reverse osmosis treatment for removal of negative characters from juice or wine [7, 13, 23].

When wine is made from smoke-affected grapes, phenolic glycosides in grapes are readily transferred into wine and can release volatile phenols, in addition to volatile phenols transferred directly from grape to wine [8]. The sum of phenolic glycosides remaining in wine compared to the concentrations in smoke-exposed grapes has been reported to range between 17 to 78% in individual examples from seven cultivars [5, 14]. Monitoring individual glycosides during winemaking, most glycosides decrease but some increase (e.g. guaiacol rutinosides) [6, 21, 24]. Apart from a small number of heavily smoke-affected samples, there is

little published data comparing the concentrations of volatile phenols and phenolic glycosides in grapes, with their concentrations in the wines and the intensity of smoky sensory attributes in the resulting wine, and no data are available for mildly smoke-exposed grapes [8].

Given the increasing number of smoke events, wine producers seek to understand the likelihood of producing an unacceptable smoky flavoured wine from mildly smoke-affected grapes. This information is needed in order to make production decisions on whether to harvest fruit, based on evidence of smoke exposure, and whether it is possible to produce wine from fruit without product quality downgrade or if winemakers are best advised not to proceed with expensive winemaking processes. There is a significant gap in the knowledge about predicting smoke flavour from volatile phenols and phenolic glycoside concentrations in grapes. Currently, it is not known whether the volatile phenols and phenolic glycosides used to assess smoke exposure are suitable to predict smoke flavour with acceptable rigour or whether additional analytical targets are needed for modelling smoke taint in wine from grape composition. Critically, the concentrations required to render a wine unacceptably smoky have not been defined.

This study aimed to establish relationships between the concentration of smoke markers in grapes from wildfire affected vineyards and the corresponding wine made under controlled or standard winemaking conditions and the smoky sensory attributes in the resulting wine. We included three cultivars widely grown across Australia and other grape producing countries: Chardonnay, Pinot Noir, and Shiraz which together constitute almost half of Australia's winegrape production [25, 26]. The study sought to determine whether the concentration of volatile phenols and phenolic glycosides in grapes and wine can adequately predict smoke flavour, to identify the key drivers of smoke flavour in both sample types. The study also aimed to determine what concentrations of volatiles and glycosides in grapes would impart a discernible smoke flavour in the resulting wine, to provide a guide for producers assessing suitability of smoke-exposed grapes for wine production.

2. Materials and Methods

2.1. Chemicals

2.1.1. Winemaking Additives. Maurivin PDM yeast and Rohavin-L pectolytic enzyme were sourced from AB Biotek, North Ryde, NSW, Australia, GoFerm from Lallemand, Edwardstown, SA, Australia, tartaric acid, diammonium phosphate, bentonite and potassium metabisulfite from E. E Muirs, Australia, and hydrogen peroxide from Rowe Scientific.

2.2. Grapes

2.2.1. Study A: Grapes Exposed to Early Season Smoke. The Cudlee Creek fire of December 2019 produced a large amount of smoke which affected vineyards in the Adelaide Hills with small green berries at Eichhorn–Lorenz (E-L) stage 29, after which, negligible further smoke exposure

occurred [27]. *Vitis vinifera* L. cv. Chardonnay, Shiraz, and Pinot Noir grapes from Adelaide Hills wine region in South Australia were hand harvested during March 2020. Eight samples were collected for each cultivar including samples from vineyards that had no evidence of smoke exposure (control samples); that had mild smoke exposure based on grape maturity smoke compound analysis; and samples from vineyards with evidence of mild fire activity within the block, such as burnt grass undervine and in the midrow. All details of the grapes, wines, and sensory analysis are described elsewhere [28].

2.2.2. Study B: Grapes Exposed to Diverse Smoke Events. *Vitis vinifera* L. cv. Chardonnay, Shiraz, and Pinot Noir grapes from Victoria, New South Wales, Canberra District, and South Australia were hand harvested during February–March 2020. A total of 40 samples were collected, representing at least nine samples per cultivar that had been exposed to smoke from multiple bushfires that burnt across eastern Australia in the spring and summer of 2019–2020. In addition, control samples with no known smoke exposure were sourced from Langhorne Creek, McLaren Vale, and parts of the Adelaide Hills that were not affected by smoke, as shown in Table S1. The geographic indications included Alpine Valleys, Beechworth, and King Valley in Victoria; Adelaide Hills, Barossa Valley, Langhorne Creek, and McLaren Vale in South Australia; Cowra, Mudgee, Orange, and Riverina in New South Wales; and Canberra District. The grapes were hand harvested at commercial ripeness for table wine styles (approximately 20°Brix), approximately 50–80 kg each. The whole bunches were frozen due to logistical and biosecurity considerations and transported frozen to WIC Winemaking Services in Adelaide in April 2020 for winemaking commencing late April.

Frozen grapes were thawed at 4°C over the weekend prior to commencement of winemaking. Once thawed, prior to winemaking, a randomised subsample of 2 kg of bunches was taken for grape analysis. Approximately 50 kg of each sample was used for winemaking, with one 50 kg fermentation replicate per cultivar. The primary goal was to capture as much variation as possible in smoke exposure at vineyard level, with replicated winemaking for each sample not feasible with the limited resources available.

2.3. Winemaking. The thawed Chardonnay grapes were destemmed and pressed, pectolytic enzyme added at a rate equivalent to 40 mL/tonne, tartaric acid adjusted to target a pH of between 3.4–3.5 where practical, batches with soluble solids greater than 22°Brix for Chardonnay grapes, and 24°Brix for Pinot Noir and Shiraz grapes were adjusted using reverse osmosis purified water generated in the winery (see Table S2), settled, racked to a new fermenter vessel targeting turbidity of 200 NTU, and then inoculated with 250 mg/L PDM yeast and GoFerm. Shiraz and Pinot Noir grapes were thawed then destemmed prior to inoculation. Fermentation temperature was kept between 14.2°C and 18.3°C, and all fermentations were completed within 11–14 days. Additions of 100–250 mg/L diammonium phosphate were made to the

ferments targeting 250 mg/L yeast available nitrogen at $8 \pm 2^\circ$ Baumé. Once fermentation was complete, 80 mg/L total sulfur dioxide (SO₂) was added as a 10% SO₂ solution made by dissolving potassium metabisulfite, and the wines were racked into 18 L stainless steel kegs for cold stabilisation at 0°C for 4 weeks, then racked off gross lees. The wines were filtered with a crossflow filter of nominal pore size 0.2 μm and bottled into 375 mL OI 30157 AG Punted Claret BVS bottles with screwcap closures (Vinpac International, Angaston, SA, Australia). Wines were stored at 15°C until analysis.

2.4. Wine Composition. Chemical analysis was performed on the wines by AWRI Commercial Services (now Affinity Labs) three weeks after bottling. Analysis included alcohol, glucose and fructose, malic acid, pH, titratable acidity (TA), free and total SO₂, and volatile acidity [29]. Affinity Labs also analysed the grapes and wines for smoke exposure markers: volatile phenols including guaiacol, 4-methylguaiacol, syringol, 4-methylsyringol, *o*-cresol, *m*-cresol, and *p*-cresol, and six glycosides of volatile phenols: syringol gentiobioside, methylsyringol gentiobioside, phenol rutinoside, guaiacol rutinoside, methylguaiacol rutinoside, and cresol rutinosides [19]. Note that the calibration range for the phenolic glycosides was 1–200 μg/L or μg/kg for grape analysis, and values above 200 were estimated by extrapolating the calibration function. This was deemed an acceptable approach because the method was found to be linear up to 1,000 μg/L or μg/kg [19].

2.5. Sensory Smoke Rating. Formal sensory analysis was performed on the wines six weeks after bottling. The sensory assessment for Study A has been described previously [28] and a closely similar procedure was followed for Study B. A panel of screened, qualified, and experienced assessors was convened to evaluate each of the wine sets. The assessors were selected from a pool of AWRI staff members, all of whom were chosen for their ability to perceive smoke flavour from phenolic glycosides and have previous experience in smoke sensory analysis. The panel of assessors (10 for the Chardonnay, Pinot Noir, and Shiraz sets in Study A, and 9 for the Chardonnay, 12 for the Pinot Noir, and 10 for the Shiraz sets in Study B) rated smoke aroma (defined as any type of smoke aroma, including hickory or artificial smoke, phenolic, burnt aroma associated with ashes, ashtray, fire ash, including also medicinal and band aid), smoke flavour (defined as including bacon, smoked meat, and ashy aftertaste), overall fruit aroma (defined as including red fruit, red berry, strawberry, raspberry, and cherry for the Pinot Noir rosé and Shiraz and defined as any type of citrus fruit, stone fruit, and tropical fruits including pineapple for the Chardonnay), and overall fruit flavour for each of the wine sets. An “other” term was available for both aroma and flavour to capture any additional noteworthy characteristics in the wines. The intensity of each attribute was rated using an unstructured 15 cm line scale (0 to 10), with indented anchor points of “low” and “high” placed at 10% and 90%, respectively.

All wines were assessed in duplicate and separated by study and cultivar. Study A was assessed over 3 days (different cultivar per day), while Study B was assessed over 5 days (one day for Chardonnay assessment, and two days for each of the Pinot Noir and Shiraz sets) due to a larger number of wines in the set. All wines were presented to panellists in 30 mL aliquots in 3-digit-coded and covered, ISO standard wine glasses at 22–24°C, in isolated booths under colour-masking lighting, with randomised presentation order using a modified Williams Latin Square design generated by Compusense20 sensory evaluation software (Compusense, Guelph, ON, Canada). A minimum 30-second delay was enforced before assessors could finalise the palate ratings to account for any lingering attributes and aftertastes and then a 2-minute rest between each sample and a 10-minute rest between sets of two and three samples, to minimise carryover [23, 30]. Water was provided for palate cleansing. Data were acquired using Compusense Cloud sensory evaluation software.

2.6. Data Analysis. Panellist performance was assessed using Compusense software and R with the SensominerR (sensominer.free.fr/) and FactominerR (factominer.free.fr/) packages. The performance assessment included analysis of variance (ANOVA) for the effect of assessor, wine, and presentation replicate and their two-way interactions, degree of agreement with the panel mean, degree of discrimination across samples, and the residual standard deviation of each assessor by attribute. All assessors were found to be performing to an acceptable standard.

For the sensory data, ANOVA was conducted using XLSTAT (Addinsoft, 2020, Paris, France). For each cultivar in the separate studies, the fixed effects of wine, presentation replicate, the random effect of judge, and their two-way interactions were assessed, followed by a Dunnett's means comparison test to determine whether the wines were rated significantly higher than a control. It was decided that the control that received the higher smoke flavour score would be the wine used as the specified control for all Dunnett's calculations for that set to account for variation commonly observed in wines without smoke exposure.

Partial least squares (PLS) regression was carried out using The Unscrambler 11.0 (CAMO Technologies Inc., Woodbridge, NJ). All PLSR analyses were carried out using standardized data with full cross-validation, with the y data set being the sensory smoke flavour scores, and the x data set being the chemical compositional data. Where an analyte was reported as below the limit of quantification; the value of half of the limit of quantification was used for the PLS models. The correlation of predicted versus measured smoke flavour as indicated by R^2 of calibration, and standard error of cross-validation (SE) were used to compare the models.

3. Results and Discussion

3.1. Winemaking. Details for Study A have already been described [28]. Importantly, grapes in this study were exposed to smoke from a single wildfire, ca. 3 months prior to

harvest and winemaking, and sampled at the same day for each variety. This resulted in some variability in maturity across the samples but maintained the time between smoke exposure and sampling a constant. Smoke exposure did not affect the progress of the fermentations, with all musts completing primary fermentation at similar rates, and all within 11–14 days.

The basic wine compositional measures are provided in Table S1 and for Study A have been previously reported [28]. Chardonnay wines ranged in alcohol concentration from 12.0–15.8% (v/v). There was also variation in glucose and fructose, pH, and titratable acidity. The two Chardonnay control wines both had relatively high alcohol content (14.9 and 15.8% v/v), one contained some residual sugar (2.9 g/L glucose and fructose) and had relatively high pH values.

Pinot Noir wines also varied in their basic wine composition. Alcohol varied from 11.1–15.1% (v/v), all the Pinot Noir wines had a pH between 3.45 and 3.55, and titratable acidity ranged from 5.0 to 6.7 g/L tartaric acid equivalents, and malic acid was less than 0.2 g/L. All wines had residual sugar at or below 1 g/L glucose and fructose. Two wines were removed from the study due to a dominating 'nail polish remover' aroma, associated with a high ethyl acetate concentration (data not shown).

The Shiraz wines varied in alcohol from 12.8–14.8% v/v, pH from 3.40–3.69, and titratable acidity ranged from 5.9 to 6.8 g/L. All wines had less than 1 g/L of glucose and fructose, volatile acidity below 0.6 g/L, and malic acid less than 0.2 g/L.

3.2. Volatile Phenols and Glycosides in Grapes and Wines.

Compositional data for all control grape and control wine samples were consistent with data reported from non-smoke-exposed samples [22] for all phenolic smoke markers measured, with the exception of one Shiraz sample (SHI-03-Control) which had a slightly elevated concentration of guaiacol (Table S3 and [28]). These observations provide further confirmation of background levels of phenolic compounds typically found in grapes and wine without a history of known smoke exposure.

In Study A, vineyards had been exposed to a single smoke event pre-ripening when grapes were still, very small, hard, and unripe [28]. At harvest smoke-exposed grapes had elevated concentrations of many of the phenolic glycosides and volatile phenols compared to non-smoke-exposed samples in the study. Syringol gentiobioside was the most abundant phenolic glycoside, up to 150 $\mu\text{g}/\text{kg}$ in the grapes at harvest (Table 1). The concentrations of volatile phenols in grapes (up to 32 $\mu\text{g}/\text{kg}$ guaiacol and 16 $\mu\text{g}/\text{kg}$ *o*-cresol) was surprising and is in contrast to other reports. For example, grapes exposed to smoke in 2009 in Australia had concentrations of guaiacol below 5 $\mu\text{g}/\text{kg}$ and concentrations of syringol gentiobioside reaching 1623 $\mu\text{g}/\text{kg}$ [19], as well as samples affected by Californian fires in 2008 that had concentrations of guaiacol below 2 $\mu\text{g}/\text{kg}$ and high levels of guaiacol released by enzymes [31]. Syringol and 4-methylsyringol were not found above the limit of quantification in any of the grape samples.

TABLE 1: Summary of volatile phenol and phenolic glycoside abundance in smoke-exposed grapes.

Cultivar and study	4-Methyl-guaiacol ($\mu\text{g}/\text{kg}$)	Guaiacol ($\mu\text{g}/\text{kg}$)	<i>o</i> -Cresol ($\mu\text{g}/\text{kg}$)	<i>m</i> -Cresol ($\mu\text{g}/\text{kg}$)	<i>p</i> -Cresol ($\mu\text{g}/\text{kg}$)	GuRG ($\mu\text{g}/\text{kg}$)	MGuRG ($\mu\text{g}/\text{kg}$)	MSyGG ($\mu\text{g}/\text{kg}$)	PhRG ($\mu\text{g}/\text{kg}$)	CrRG ($\mu\text{g}/\text{kg}$)	SyGG ($\mu\text{g}/\text{kg}$)
Chardonnay Study A	Range	1-16	2.3-11	1.7-11	1.3-8.0	1-14	3-31	LoQ-25	1.5-7.0	2.8-11	2.3-136
	Median	8.7	6.7	6.9	4.5	6.6	15	9.4	5.0	7.7	55
Chardonnay Study B	Range	1-33	1-28	LoQ-9	LoQ-4	2-18	6-73	3-151	2-20	3-27	32-868
	Median	4.5	4.5	1.5	<LoQ	3.0	8.5	6.5	5.5	6.5	68
Pinot Noir Study A	Range	1.7-32	1.7-16	1.0-11	LoQ-4.7	2.9-11	3.0-49	1.0-16	2.2-27	2.9-54	2.8-146
	Median	16	7.2	5.0	2.2	5.4	15	7.8	9.7	15	59
Pinot Noir Study B	Range	2-20	3-15	LoQ-4	LoQ-2	2-19	4-48	2-35	5-47	4-49	21-456
	Median	6	5	1	<LoQ	5	11	5	10	12	56
Shiraz Study A	Range	5-16	1.0-4	LoQ-2.7	LoQ-1.7	4.3-22	6-44	LoQ-13	1.3-5.0	4-15	4.4-71
	Median	8.7	6.7	5.0	2.2	5.4	15	7.8	5.5	7.7	59
Shiraz Study B	Range	2-59	LoQ-17	LoQ-3	LoQ-1	6-74	5-93	3-189	2-25	3-27	24-977
	Median	5.0	2.0	0.5	<LoQ	18	21	17	14	12	164

LoQ, limit of quantitation = 1 $\mu\text{g}/\text{kg}$ for all analytes apart from 4-methylsyringol and syringol with LoQ = 2 $\mu\text{g}/\text{kg}$; 4-methylsyringol and syringol were at or below LoQ for all samples so have been excluded from this table; GuRG, guaiacol rutinoside; MGuRG, methylguaiacol rutinoside; MSyGG, methylsyringol gentiobioside; PhRG, phenol rutinoside; CrRG, cresol rutinoside; SyGG, syringol gentiobioside.

In the smoke-exposed grape samples of Study B, the concentrations of phenolic glycosides were much higher than those observed in Study A, with syringol gentiobioside reaching approximately 980 $\mu\text{g}/\text{kg}$ (Tables 1 and S3). The pattern of abundance was different to that observed in Study A, likely due to a number of factors such as smoke composition, the timing of smoke exposure and metabolism in the berries. In contrast, in Study B, the concentration of the volatile phenols relative to phenolic glycosides was generally lower (Table S3). Guaiacol again was the most abundant volatile phenol in the grapes, up to 59 $\mu\text{g}/\text{kg}$ in Shiraz grapes. In contrast to the phenolic glycosides, guaiacol was above typical concentrations found in non-smoke-exposed grapes in only 20 of the 40 samples. This is in line with recent observations of volatile phenols and phenolic glycosides in smoke-exposed grapes from the 2020 vintage [32]. *o*-Cresol was elevated in 17 of the 40 samples and was particularly abundant in the Chardonnay and Pinot Noir samples (up to 28 $\mu\text{g}/\text{kg}$). Syringol and 4-methylsyringol were below or near to the limit of quantitation in all of the grape samples. It is interesting to note in both studies that general patterns of abundance of volatile phenols and phenolic glycosides differed by cultivar, which could be due to possible differences in the chemical composition of the smoke in different vineyards, and differences in uptake and metabolism by the different cultivars [14].

In the wines of Study A, the guaiacol was the most abundant volatile phenol (up to 78 $\mu\text{g}/\text{L}$), followed by syringol (up to 65 $\mu\text{g}/\text{L}$) (Tables 2 and S4). Syringol and 4-methylsyringol were found in the wines despite being absent from the grape samples, presumably due to release from glycosidic precursors during winemaking. Syringol gentiobioside was the most abundant phenolic glycoside in wine, up to 71 $\mu\text{g}/\text{L}$. Each of the three cresol isomers was observed up to 17 $\mu\text{g}/\text{L}$ in the wines and were particularly abundant in the Pinot Noir wines.

In the wine samples of Study B, the most abundant smoke exposure marker was syringol gentiobioside (up to 690 $\mu\text{g}/\text{L}$) (Tables 2 and S4), and guaiacol was the most abundant volatile phenol in the wines (up to 125 $\mu\text{g}/\text{L}$), followed by syringol (61 $\mu\text{g}/\text{L}$) as was seen in Study A. Like Study A, cresols were particularly abundant in the Pinot Noir wines of Study B.

3.3. Comparing Volatile Phenols and Phenolic Glycosides in Grapes and Wine. As is common practice, the Chardonnay wines were made with minimal skin contact, and the red wines were fermented on skins. This resulted in different relationships between grape and wine composition between the red and white cultivars. The red wines, which were made with skin contact, had higher concentrations of volatile phenols. The concentrations of guaiacol and cresols were higher in the red wines compared to grapes (example Study B 59 $\mu\text{g}/\text{kg}$ guaiacol in grapes and 125 $\mu\text{g}/\text{L}$ in wine), which is likely due to both the extraction of guaiacol and cresols from the grape skins and release of guaiacol and cresols from glycosides during the winemaking process. Syringol and 4-methylsyringol were rarely detected in the grapes yet were

commonly found in both red and white wines (up to concentrations of 61 and 25 $\mu\text{g}/\text{L}$ respectively), due to release from glycosides during wine production. Refer to Tables 1, 2, S3–S5 for details of volatile phenols and phenolic glycoside concentrations in grapes and wines. On the other hand, lower concentrations of volatile phenols were found in the Chardonnay wines (example Study B max 14 $\mu\text{g}/\text{L}$ guaiacol in wine compared to max 33 $\mu\text{g}/\text{kg}$ guaiacol in grapes), in line with previous studies on the effect of skin removal [1, 6, 7, 33].

In contrast, the summed concentrations of the glycosides in the red wines were similar to those found in the grapes. Close examination of individual glycosides shows a complex pattern, and a variable proportion of individual glycosides persisted in the wine compared to the concentration in the grapes: some glycosides were lower in concentration in the wines than in the grapes, and some were higher in the wine. Shiraz and Pinot Noir wines generally had lower concentrations of syringol gentiobioside and methylsyringol gentiobioside in the wines compared to grapes, and higher concentrations of rutosides, with some individual samples showing other patterns. Guaiacol, cresols, guaiacol rutinoside, and cresol rutosides in grapes were strongly related to the concentrations found in Chardonnay and Pinot Noir wine, and the associations were weaker in Shiraz but unrelated to water additions to the musts to reduce excessive sugar concentrations.

3.4. Predicting Smoke Flavour Intensity from Volatile Phenols and Phenolic Glycosides in Wine. In both studies, smoke-affected red wines had a wide range of smoke aroma and flavour sensory rating values, whereas the smoke-affected Chardonnay wines had lower scores for smoke aroma and flavour (Table S6) [28]. Control wines for each cultivar generally had low scores for smoke aroma and flavour, showing the sensory panel was well trained and was able to differentiate non-smoke-exposed samples and smoke-affected samples. Not all wines made from smoke-exposed grapes had smoke ratings significantly higher than the control wines, and some smoke-exposed wines had lower ratings of smoke flavour than the controls. In addition, some wines exhibited strong “green,” “eucalyptus,” “reduced,” and “tropical” notes which could have masked smoke flavour, and others were “reduced” with burnt rubber characters that could be confused with smoke. Some assessors noted “smoky/struck flint” characters in some Chardonnay wines that are easily confused with smoke-related characteristics. Across all the wines, three were removed from the smoke flavour models due to comments indicating competing strong characteristics: one Shiraz with strong green/eucalyptus characters (SHZ-I Study A) and two Shiraz with reduced rubber and cooked vegetable notes (Study B SHZ-13-Smoke and SHZ-15-Smoke). A total of 20 samples for Chardonnay, 19 for Pinot Noir, and 21 for Shiraz wines were used for further data analysis. Notably, the smoke flavour was apparently unaffected by the water additions made to the musts with excessively high soluble solids.

TABLE 2: Summary of volatile phenol and phenolic glycoside abundance in smoke-exposed wines.

Cultivar and study	4-Methyl-guaiacol ($\mu\text{g/L}$)	Guaiacol ($\mu\text{g/L}$)	<i>o</i> -Cresol ($\mu\text{g/L}$)	<i>m</i> -Cresol ($\mu\text{g/L}$)	<i>p</i> -Cresol ($\mu\text{g/L}$)	4-Methyl-syringol ($\mu\text{g/L}$)	Syringol ($\mu\text{g/L}$)	GuRG ($\mu\text{g/L}$)	MGuRG ($\mu\text{g/L}$)	MSyGG ($\mu\text{g/L}$)	PhRG ($\mu\text{g/L}$)	CrRG ($\mu\text{g/L}$)	SyGG ($\mu\text{g/L}$)
Chardonnay Study A	Range Median	LoQ-2 1.0	LoQ LoQ	LoQ-1 LoQ	LoQ-2 1.0	LoQ LoQ	LoQ LoQ	1.5-7.8 4.9	LoQ-12 4.5	LoQ-2 <LoQ	1.1-3.9 2.3	LoQ-5.4 2.0	2.8-41 18
Chardonnay Study B	Range Median	LoQ-5 <LoQ	1-14 2.5	LoQ-10 2	LoQ-12 1.5	LoQ-2 <LoQ	LoQ-9 <LoQ	3-35 6.5	8-87 12	LoQ-44 3	2-28 6	4-45 10	17-525 53
Pinot Noir Study A	Range Median	2-15 7.0	5-52 26.0	2-11 4.0	3-17 8.0	3-15 6.0	LoQ-19 7.0	1.7-30 4.6	2.4-29 5.5	LoQ-3.1 LoQ	LoQ-6.8 1.6	3.3-19 4.4	2.1-63 13
Pinot Noir Study B	Range Median	1-13 3	5-53 16	5-29 11	3-22 9	1-15 4	LoQ-4 <LoQ	5-40 12	7-83 23	1-28 3	7-50 12	8-68 18	18-411 57
Shiraz Study A	Range Median	2-13 6.5	21-78 54.5	2-8 5.5	2-7 4.5	2-6 4.0	LoQ-2 2.0	11-53 28	8.4-55 41	LoQ-5.3 3.1	1.1-6.6 2.7	4.2-15 7.5	9.6-71 42
Shiraz Study B	Range Median	LoQ-25 1.0	11-125 23.0	2-24 3.0	LoQ-18 2.0	LoQ-8 2.0	LoQ-25 3.0	5-61 14.0	6-109 28	1-72 9.0	2-22 16	4-27 16	21-689 123

LoQ, limit of quantitation = 1 $\mu\text{g/L}$ for all analytes apart from 4-methylsyringol and syringol with LoQ = 2 $\mu\text{g/L}$; GuRG, guaiacol rutinoside; MGuRG, methylguaiacol rutinoside; MSyGG, methylsyringol gentiobioside; PhRG, phenol rutinoside; CrRG, cresol rutinosides; SyGG, syringol gentiobioside.

Smoke aroma was highly correlated with smoke flavour in the red wines ($r > 0.978$) and slightly less correlated in the Chardonnay wines ($r > 0.948$) (Table S6). Given the close correlation, with smoke flavour being more discriminating, it was considered the most reliable indicator of smoke taint.

The first step to modelling smoke flavour in wine from its chemical composition investigated whether volatile phenols and phenolic glycosides in wine could be used to predict smoke flavour intensity in wine. PLS models for smoke flavour were explored for each cultivar in each of the two studies (Table 3). Good models for predicting wine smoke flavour were generated from wine compositional data for each of the three cultivars, using all 13 smoke markers ($R^2 > 0.86$, $SE < 1.3$). The exception was Chardonnay wine set from Study A ($R^2 = 0.63$, $SE = 0.62$) where the model was not as predictive, likely as this set had overall low smoke flavour ratings (Table 3). Overall, the volatile phenols and phenolic glycosides could be used to predict smoke flavour in wine.

As a second step to identify the most important volatile phenols and phenolic glycosides for modelling smoke flavour, the PLS model coefficients were examined. Table 3 lists the PLS model coefficients of the independent variables (volatile phenols and phenolic glycosides) modelling smoke flavour. The jack-knife cross-validation method [34] was applied to identify significant variables which are highlighted in bold in the table, although variables can still be considered important to the model if they are nonsignificant in this particular statistical test. Generally, variables that have the largest regression coefficient values, greater than 0.1 are the most important to the model, and coefficients of less than 0.05 can be considered not important [34].

Guaiacol, which by itself is not necessarily a taint compound, was one of the most important predictors of smoke flavour for all the sample sets. The three cresol isomers were important to most of the sample sets, which is in line with previous observations that the volatile compounds guaiacol and the three cresols, in combination, are likely to drive the perception of smoke flavour in smoke-affected wines, due to their low sensory thresholds relative to the other volatile phenols (measured in red wine: guaiacol 23 $\mu\text{g/L}$, *o*-cresol 62 $\mu\text{g/L}$, *m*-cresol 20 $\mu\text{g/L}$, *p*-cresol 64 $\mu\text{g/L}$, and in water: 4-methylguaiacol 21 $\mu\text{g/L}$, syringol 570 $\mu\text{g/L}$, and 4-methylsyringol 10,000 $\mu\text{g/L}$) [9–11, 35, 36]. Syringol and 4-methylsyringol were found at concentrations much lower than the reported thresholds even in the most severely smoke-affected wines and were considered unlikely to contribute to the smoke flavour directly [9, 11]. 4-Methylguaiacol was generally found at much lower concentrations than guaiacol in smoke-affected wines and has a much higher threshold than guaiacol in water (21 $\mu\text{g/L}$ compared to 0.84 $\mu\text{g/L}$, respectively), so is less likely to contribute to smoke flavour directly [37]. Phenolic glycosides were strongly associated with the smoke flavour in both Pinot Noir wine sets, but the pattern differed across studies for the Shiraz, with only some glycosides strongly contributing to the models, and these compounds were generally less important to the Chardonnay models.

For the Chardonnay wines of Study B, the *p*-cresol, *m*-cresol, and guaiacol volatiles were strong predictors of

smoke flavour, and the glycosides were less important. The data from the Chardonnay wines of Study A generated a less strong model with lower regression coefficient values, with several glycosides contributing.

For the Pinot Noir wines, there was a particularly high degree of co-correlation among the smoke marker compounds. Almost all of the variables had similar strong regression coefficients for both Pinot Noir sets (one factor model) although syringol and 4-methylsyringol were indicated to have less importance in Study A.

For the Study B Shiraz wines (3 factor model), the compounds most associated with smoke flavour were guaiacol, *o*-cresol, and phenol rutinoside, whereas methylsyringol gentiobioside was strongly negatively associated. For the Study A Shiraz wine set 4-methylguaiacol, guaiacol and *o*-cresol were most important to the model and in contrast in Study B methylsyringol gentiobioside was positively associated as was syringol gentiobioside. 4-Methylguaiacol was a good predictor of smoke flavour for the red wines, but as the concentrations were below 30 $\mu\text{g/L}$ in all wine samples, and the threshold in water is reportedly 25 times higher than guaiacol, it was considered unlikely to be directly contributing to the smoke flavour in most samples [37]. Overall, the volatile phenols and phenolic glycosides in wine were able to predict the smoke flavour.

Guaiacol and the cresols have been previously indicated to be important compounds contributing to the perception of smoky and medicinal characters in smoke-affected wines [10]. In addition, glucosides of guaiacol and *m*-cresol have been shown to impart smoke flavour and aftertaste [9, 10]. It is plausible that the guaiacol, cresols, guaiacol glycosides, and cresol glycosides together contribute to the smoke flavour. To test this hypothesis, PLS models for smoke flavour were explored using a subset of the smoke marker compounds deemed most likely to be sensory drivers; guaiacol, *o*-cresol, *m*-cresol, *p*-cresol, guaiacol rutinoside, and cresol rutinosides.

Smoke flavour was predicted well by PLS regression analysis based on a subset of smoke compounds in wine (guaiacol, *o*-, *m*-, *p*-cresol, guaiacol rutinoside, and cresol rutinoside) for all sample sets ($R^2 > 0.90$) apart from Study A Chardonnay which was less well modelled ($R^2 = 0.59$). Guaiacol and *m*-cresol had the highest loadings in most models. *o*-Cresol was important to the model for the Pinot Noir wines in Study B and the Shiraz in Study A to a lesser extent. *p*-Cresol, guaiacol rutinoside, and cresol rutinoside were important for some sets. The best models were obtained for Pinot Noir. The low sensory scores for Chardonnay wines again limited the model development for this white varietal.

For most sample sets, the smoke flavour models could not be not significantly improved by adding basic wine parameters such as alcohol, pH, TA, residual sugar, other volatile phenol, and phenolic glycoside smoke markers. The exceptions to this were the Study B Pinot Noir and Shiraz models which were improved by adding basic wine composition, indicating that the sensory results were influenced by basic wine composition, particularly volatile acidity in the Pinot Noir wines and pH, TA, and alcohol in the Shiraz

TABLE 3: Partial least squares regression coefficients of the predictive models for smoke flavour from volatile phenols and phenolic glycosides in wine for two studies, each comprising three cultivars. Variables identified as significant by the martens and martens jack-knife cross-validation method are highlighted in bold.

	Chardonnay Study A	Chardonnay Study B	Pinot Noir Study A	Pinot Noir Study B	Shiraz Study A	Shiraz Study B
Number of factors	1	4	1	1	2	3
SE	0.62	0.67	1.21	0.78	1.1	0.52
R^2	0.63	0.93	0.87	0.86	0.93	0.96
4-Methylguaiacol	NA	0.18	0.20	0.12	0.33	0.24
Guaiacol	0.08	0.26	0.20	0.12	0.23	0.75
<i>o</i> -Cresol	0.06	0.27	0.20	0.12	0.19	0.30
<i>m</i> -Cresol	NA	-0.22	0.15	0.09	0.21	0.26
<i>p</i> -Cresol	NA	0.07	0.19	0.12	0.21	0.40
4-Methylsyringol	0.08	0.62	0.20	0.10	0.17	0.26
Syringol	0.07	-0.13	0.15	0.10	-0.27	0.18
Sum of volatile phenols	0.07	0.11	0.19	0.12	0.22	0.50
GuRG	0.05	0.09	0.18	0.12	-0.01	-0.12
MGuRG	0.05	0.03	0.18	0.12	0.19	-0.13
MSyGG	0.00	0.02	0.15	0.11	0.31	-0.42
PhRG	0.06	0.00	0.19	0.11	-0.17	0.35
CrRG	0.04	0.06	0.18	0.11	-0.11	0.10
SyGG	0.07	0.04	0.16	0.11	0.33	-0.35
Sum of phenolic glycosides	0.07	0.04	0.19	0.11	0.20	-0.29

SE = standard error of cross-validation, GuRG, guaiacol rutinoside; MGuRG, methylguaiacol rutinoside; MSyGG, methylsyringol gentiobioside; PhRG, phenol rutinoside; CrRG, cresol rutinosides; SyGG, syringol gentiobioside. Where analytes were not detected in the sample set, they are absent from the PLS model, and denoted NA. Note, the sum of volatile phenols includes the seven volatile phenols listed in the table, and sum of phenolic glycosides includes the six phenolic glycosides listed in the table.

wines. The effect of the basic wine composition was of most concern with the Study B Chardonnay wines, because the two unsmoked control wines were both high in alcohol, and one also contained residual sugar; however, the PLS models for smoke flavour did not improve when these parameters were added to the model. When 4-methylguaiacol was added to the model, the models did not improve. Overall, the results were in line with previous observations on smoke-affected wines from various regions, vintages, and cultivars which indicated that a range of volatile phenols and phenolic glycosides are important to model smoke flavour [9]. In summary, a subset of the smoke markers, namely guaiacol, *o*-, *m*-, *p*-cresol, guaiacol rutinoside, and cresol rutinosides, could predict wine flavour, using PLS regression models.

Many wine producers may not have access to specialised statistical software packages that would allow use of a multifactor model, and a simple, practical way to interpret the analysis results is preferred. In an attempt to streamline data analysis, we noted that the simple sum of [guaiacol + *o*-cresol + *m*-cresol + *p*-cresol concentrations] in wine enabled very good prediction of smoke flavour intensity in these sample sets (Figure 1). Also, it was evident that the models for the different cultivars had different slopes, likely reflecting variety-specific matrix effects as well as differences in chemical composition between the cultivars. For example, the Pinot Noir wines had particularly high concentrations of cresols, whereas Shiraz wines had high concentration of guaiacol, and Chardonnay had much lower volatile phenols. This simplified sum of concentrations parameter should be used with caution, bearing in mind that it does not take into account the contribution of the glycosides. There was a high degree of correlation observed among the volatile phenols

and phenolic glycosides in the samples, but this may not always be the case if treatments have been applied to selectively remove volatile phenols or phenolic glycosides, and the model may not be applicable to those wines.

Overall, smoke flavour in wine made from grapes with a varying degree of smoke exposure could be predicted by quantifying volatile phenols and phenolic glycosides in wine. The compounds key to predict smoke flavour were guaiacol, *o*-, *m*-, *p*-cresol, guaiacol rutinoside, and cresol rutinoside, although additional phenols and other compounds not measured in this study may be important too.

3.5. Predicting Smoke Flavour from Volatile Phenols and Phenolic Glycosides in Grapes. Preharvest chemical analysis data from grape samples are critical for making appropriate harvest or processing decisions for vineyards suspected of smoke exposure. The key question is if smoke exposure markers in *grape berries* can be reliably used to identify whether smoke flavour will be evident in *wine produced from smoke-affected grapes*? Encouraged by our ability to predict smoke flavour in wine from wine compositional data, PLS models to predict smoke flavour in wine from volatile phenols and phenolic glycosides in grapes were explored for each cultivar for both studies. The volatile phenols and phenolic glycosides in grapes predicted smoke flavour well in each cultivar and in each study ($R^2 > 0.86$, $SE < 1.2$ for Pinot Noir and Shiraz), although like the wine models, the models were not as strong for Chardonnay ($R^2 > 0.71$, $SE 0.68$) (Table 4). Table 4 lists the PLS model coefficients of the independent variables in grapes (volatile phenols and phenolic glycosides) predicting smoke flavour.

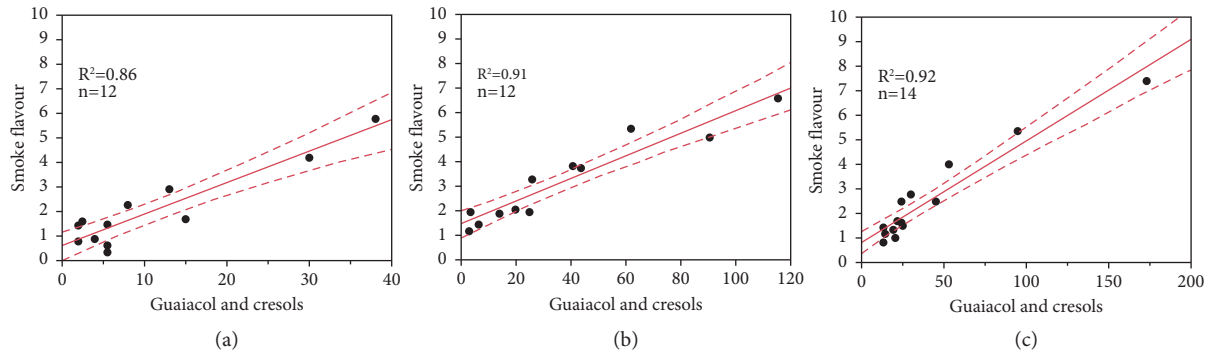


FIGURE 1: Correlation between the sum of guaiacol and cresols (*m*-cresol, *o*-cresol, and *p*-cresol) in wine and smoke flavour in each of the three cultivars: (a) Chardonnay (b) Pinot Noir, and (c) Shiraz shown here for Study B. Linear fit is shown by the solid line and confidence of the fit is shown by dotted lines.

TABLE 4: Partial least squares regression coefficients of the predictive model for smoke flavour in wine from volatile phenols and phenolic glycosides in grapes for two studies, each comprising three cultivars. Variables identified as significant by the Martens and Martens jack-knife cross-validation method are highlighted in bold.

	Chardonnay Study A	Chardonnay Study B	Pinot Noir Study A	Pinot Noir Study B	Shiraz Study A	Shiraz Study B
Number of factors	2	2	3	7	1	1
SE	0.68	0.87	0.83	0.58	1.1	0.75
R^2	0.71	0.86	0.99	0.99	0.88	0.88
4-Methylguaiacol	0.07	0.26	0.08	0.18	0.09	0.08
Guaiacol	0.22	0.25	0.33	1.48	0.09	0.08
<i>o</i> -Cresol	0.37	0.19	0.09	-0.60	0.10	0.08
<i>m</i> -Cresol	0.39	0.28	0.58	-0.25	0.10	0.08
<i>p</i> -Cresol	0.39	0.19	0.46	-0.54	0.08	0.06
Syringol	NA	NA	NA	NA	NA	0.04
Sum of volatile phenols	0.29	0.23	0.29	0.47	0.09	0.08
GuRG	-0.26	0.05	-0.39	0.41	0.07	0.08
MGuRG	-0.06	0.02	-0.19	0.44	0.08	0.08
MSyGG	-0.32	-0.04	0.03	-0.21	0.09	0.08
PhRG	-0.04	0.02	-0.16	0.01	0.04	0.07
CrRG	-0.04	0.04	-0.03	-0.11	0.05	0.06
SyGG	-0.17	0.01	-0.05	-0.28	0.09	0.08
Sum of phenolic glycosides	-0.17	0.01	-0.08	-0.13	0.09	0.08

SE = standard error of cross-validation, GuRG, guaiacol rutinoside; MGuRG, methylguaiacol rutinoside; MSyGG, methylsyringol gentiobioside; PhRG, phenol rutinoside; CrRG, cresol rutinosides; SyGG, syringol gentiobioside. Where analytes were not detected in the sample set, they are absent from the PLS model, and denoted NA. 4-methylsyringol was not listed in the table due to no detection. Note, the sum of volatile phenols includes the seven volatile phenols listed in the table and sum of phenolic glycosides includes the six phenolic glycosides listed in the table.

As found for the wine composition models, grape guaiacol concentration was one of the most important predictors across all sample sets. 4-Methylguaiacol and *m*-cresol were also strong predictors of smoke flavour in the Chardonnay wines of Study B, and surprisingly the glycosides were less important than the volatile phenols in the model prediction from both studies for this cultivar.

Guaiacol rutinoside and methylguaiacol rutinoside were strongly positively associated with wine smoky flavour in the Pinot Noir Study B set, and the cresols were negatively related. In contrast, *m*-cresol and *p*-cresol had high positive regression coefficients in the Study A set. The cresols were much higher in concentration in the grapes of Study A compared to Study B, possibly reflecting differences in the smoke composition and timing of exposure.

Almost all variables had equal high regression coefficients for the Shiraz grapes in both studies, with indications that cresol rutinoside, phenol rutinoside, *p*-cresol, and syringol were slightly less important. Overall, the volatile phenols and phenolic glycosides in grapes were able to predict the smoke flavour well in the corresponding wines for this cultivar.

In the models for smoke flavour from wine composition discussed above, the key drivers of predicting smoke flavour in wine from grape phenol analysis were identified as guaiacol, cresols, guaiacol rutinoside, and cresol rutinoside. Guaiacol and cresols in grapes can be transferred directly into the juice or must. Guaiacol glycosides and cresol glycosides in grapes can also hydrolyse to release guaiacol and cresols during wine production and ageing. Logically, guaiacol, cresols, and glycosides of guaiacol and cresols in

TABLE 5: Concentrations of volatile phenols and phenolic glycosides ($\mu\text{g}/\text{kg}$) in grapes that resulted in wines with significant smoke flavour (high risk) compared to controls, and concentrations above which only some wines were significantly smoky and some wines were not (moderate risk).

Analyte in grapes	Chardonnay		Pinot Noir		Shiraz	
	Moderate risk	High risk	Moderate risk	High risk	Moderate risk	High risk
4-Methylguaiaicol	4.0	5.7	n.d.	n.d.	1.0	n.d.
Guaiaicol	14.3	16.0	4.0	4.0	7.0	12.0
<i>o</i> -Cresol	10.3	10.3	3.0	5.0	2.0	3.0
<i>m</i> -Cresol	6.0	10.0	n.d.	n.d.	n.d.	n.d.
<i>p</i> -Cresol	2.0	7.3	n.d.	n.d.	n.d.	n.d.
4-Methylsyringol	n.d.	n.d.	n.d.	n.d.	n.d.	n.d.
Syringol	n.d.	n.d.	n.d.	n.d.	n.d.	n.d.
GuRG	9.2	13.7	3.5	3.8	9.2	23.0
MGuRG	25.0	30.6	6.1	10.0	22.3	23.0
MSyGG	15.9	25.4	2.0	5.0	5.3	18.0
PhRG	5.0	7.0	4.4	10.0	1.8	16.0
CrRG	11.1	11.0	5.9	13.0	5.4	14.0
SyGG	101.2	135.7	22.2	53.0	28.6	176.0

GuRG, guaiaicol rutinoside; MGuRG, methylguaiaicol rutinoside; MSyGG, methylsyringol gentiobioside; PhRG, phenol rutinoside; CrRG, cresol rutinosides; SyGG, syringol gentiobioside; n.d. not determined as concentrations were below LoQ.

grapes could contribute to smoke flavour in wine. A diverse range of glycoconjugates of guaiaicol and cresol have been identified in smoke-exposed grapes and wine, including monoglucosides, rutinosides, gentiobiosides, pentosylglucosides, trisaccharides, and more. While there is a lack of quantitative data about many of these compounds, the limited quantitative data available suggest they are highly correlated [19, 21]. The routinely analysed glycosides, guaiaicol rutinoside, and cresol rutinoside can be considered representatives of the broader diversity of glycoconjugates present [19]. Therefore, the subset of markers *in grapes* most likely to cause smoke flavour in wine was identified as guaiaicol, *o*-cresol, *m*-cresol, *p*-cresol, guaiaicol rutinoside, and cresol rutinoside.

Smoke flavour in wine was modelled surprisingly well by PLS regression analysis based on a subset of grape compounds (guaiaicol, *o*-, *m*-, *p*-cresol, guaiaicol rutinoside, and cresol rutinoside), for all sample sets ($R^2 > 0.86$) apart from Study A Chardonnay which was less well modelled ($R^2 = 0.77$). In fact, the models using a subset of the markers were as good or better than the models using all 13 volatile phenols and phenolic glycosides. Guaiaicol and *m*-cresol had the highest loadings in most models. *o*-Cresol and *p*-cresol were most important to the model for the Shiraz wines, especially in Study A and in Study B to a lesser extent. *p*-Cresol and guaiaicol rutinoside were notably important for some sets. The best models were obtained for Pinot Noir ($R^2 > 0.99$). The narrow range of smoke flavour intensity ratings for Chardonnay wines from Study B limited the model development, and the Chardonnay wines in Study A were considered not suitable for developing variable subset models (Table S6).

The PLS regression approaches discussed above suggest that volatile phenols in the grapes are the most important determinants of smoke flavour intensity in the resulting wine. It is worth reiterating that in this sample set, volatile phenols and glycosides were highly correlated in the grapes and wines. In other words, the most severely smoke-affected

grape samples had high concentrations of both volatile phenols and glycosides. Grape samples from different smoke events in different vintages have shown other patterns, such as high concentration of glycosides and low levels of volatile phenols [19, 31, 32], and anecdotal reports suggest that grapes with this pattern can also produce smoky wines. Further research is required to establish whether the relationships and observations from this study can be applied more broadly to other smoke events and cultivars. On the other hand, smoke flavour in wine can be minimised by tailoring wine production, for example minimising skin contact, and carbon fining juice prior to fermentation [7, 33]. If these treatments are applied, the relationships described above would not be expected to apply, and phenolic glycosides may play a more important role to drive and predict smoke flavour.

3.6. Critical Concentrations of Volatile Phenols and Phenolic Glycosides in Grapes Likely to Produce Smoky Wines. One of the aims of the study was to assess the concentrations of grape compounds that resulted in wines with perceptible smoke flavour and to provide practical guidance for producers assessing grape samples from smoke-exposed vineyards. Importantly, only some of the wines made from smoke-exposed grapes were rated as significantly more smoky by sensory analysis than the wines made from control grapes. In other words, a significant proportion of grape samples may have elevated concentrations of smoke exposure markers demonstrating smoke exposure of vineyards, yet not give rise to obviously smoke tainted wine after fermentation.

As a new approach in this study, wines were categorised as “smoky” if smoke flavour was significantly higher than the controls, using Dunnett’s means comparison test. Table 5 summarises the critical concentration of volatile phenols and phenolic glycosides and the risk, as defined here as moderate or high, of producing smoky

wines. All grape samples with a concentration at or above the high-risk value produced wines that were significantly smoky. For grapes with concentrations between the moderate risk and high-risk concentrations, some wines were significantly smoky and some wines were not. No significantly smoky wines were observed in this study below the moderate risk concentrations described in Table 5.

In summary, this study is the most comprehensive to date on the relationships between volatile phenols and phenolic glycosides in smoke-exposed grapes and smoke flavour in wine, using two separate sets of diverse grapes and wines sourced after various wildfire events, with both studies giving similar results. Still, it is limited to the one vintage in Australia (2019-2020), and we cannot fully rule out that different smoke-exposure events or cultivars may lead to different patterns of abundance in grapes and wines, such as low concentrations of volatile phenols concomitant with elevated concentrations of glycosides [31, 32]. The most important volatile phenols and phenolic glycosides to assess risk have been identified in this study, yet it would be prudent to consider assessing the profiles of additional compounds in future events. Finally, our data are based on sensory assessment of young wines at 6 weeks after bottling. While there is evidence that volatile phenols increase and glycosides are quite stable over 5-6 years ageing in bottle [38], there is a need to include more samples and monitor wines over time.

Notwithstanding the limitations of the current study, the results enable better decisions to be made when assessing smoke-exposed grapes and wines, a decision with major financial and business implications that has been lacking data until now. Winemakers will be less likely to produce undesirably smoky wines, by identifying the risk early and applying suitable production techniques. Grape growers may be able to seek alternative uses for smoke-affected grapes. Producers will be able to compare results from their grape and wine analysis to the data presented herein and better understand the risk of producing unacceptably smoky wine. This will enable the wine sector to be better prepared to manage smoke events of the future.

Abbreviations

GC-MS: Gas chromatography-mass spectrometry

LC-MS: Liquid chromatography-mass spectrometry.

Data Availability

All the data from the study are available in the supplementary information attached.

Conflicts of Interest

The authors' employer, The Australian Wine Research Institute, is a not-for-profit organisation and provides smoke marker analysis as a commercial service where clients cover the cost to third parties through Affinity Labs. The analytical method has been published, relevant standards are

commercially available, and other commercial laboratories within Australia and internationally also offer this service.

Acknowledgments

The authors thanked the members of The Australian Wine Research Institute for technical assistance, particularly Matt Holdstock, Dr. Patricia Williamson, Damian Espinase Nandorfy, Sheridan Barter, Dr. Lieke van der Hulst, Dr. Mark Krstic, Dr. Julie Culbert, Virginia Phillips, Flavour team, Sensory panellists, WIC Winemaking, and Metabolomics Australia. The authors thanked Affinity Labs (previously The Australian Wine Research Institute Commercial Services) for assistance with chemical analysis. Peter Leske, Ricky James, and Wine Industry partners across South Australia, Victoria, and New South Wales provided essential support for sampling, and Dr. John Blackman and Professor Leigh Schmidtke of Charles Sturt University assisted with grape sourcing. The support of Bioplatfroms Australia through the Metabolomics node is gratefully acknowledged. This work was supported by Australian grapegrowers and winemakers through their investment body Wine Australia, with matching funds from the Australian Government. Additional funding and in-kind contributions from PIRSA, AWRI, the South Australian, Victorian and NSW State Governments, Wine Victoria and NSW Wine are gratefully acknowledged. The Australian Wine Research Institute is a member of the Wine Innovation Cluster in Adelaide.

Supplementary Materials

The following data are provided in the supplementary materials: Table S1: Study B Region and basic wine composition. Table S2: Water additions made to musts of Study B to reduce high total soluble solids. Table S3: Study B Concentration of volatile phenols and phenolic glycosides in grapes. Table S4: Study B Concentration of volatile phenols and phenolic glycosides in wines. Table S5: Correlation coefficients for volatile phenols and phenolic glycosides comparing the concentrations in grapes to the concentrations in wine, for each cultivar and both studies. Table S6: Mean values of the smoke aroma and flavour ratings (0–10) for the wines from Study B. (*Supplementary Materials*)

References

- [1] P. Høj, I. Pretorius, and R. J. Blair, *The Australian Wine Research Institute Annual Report*, Urrbrae, South Australia, Australia, 2003.
- [2] M. Krstic, J. Culbert, M. Parker, and M. Herderich, "Managing wine quality," *Smoke Taint and Climate Change*, pp. 763–778, Elsevier, Amsterdam, Netherlands, 2021.
- [3] Y. Hayasaka, K. A. Dungey, G. A. Baldock, K. R. Kennison, and K. L. Wilkinson, "Identification of a beta-D-glucopyranoside precursor to guaiacol in grape juice following grapevine exposure to smoke," *Analytica Chimica Acta*, vol. 660, no. 1-2, pp. 143–148, 2010.
- [4] K. R. Kennison, K. L. Wilkinson, A. P. Pollnitz, H. G. Williams, and M. R. Gibberd, "Effect of timing and duration of grapevine exposure to smoke on the composition

- and sensory properties of wine,” *Australian Journal of Grape and Wine Research*, vol. 15, no. 3, pp. 228–237, 2009.
- [5] Y. Hayasaka, G. A. Baldock, M. Parker et al., “Glycosylation of smoke-derived volatile phenols in grapes as a consequence of grapevine exposure to bushfire smoke,” *Journal of Agricultural and Food Chemistry*, vol. 58, no. 20, pp. 10989–10998, 2010.
 - [6] R. Ristic, P. Osidacz, K. A. Pinchbeck, Y. Hayasaka, A. L. Fudge, and K. L. Wilkinson, “The effect of winemaking techniques on the intensity of smoke taint in wine,” *Australian Journal of Grape and Wine Research*, vol. 17, no. 2, pp. S29–S40, 2011.
 - [7] Y. A. Mirabelli-Montan, M. Marangon, A. Graça, C. M. Mayr Marangon, and K. L. Wilkinson, “Techniques for mitigating the effects of smoke taint while maintaining quality in wine production: a review,” *Molecules*, vol. 26, no. 6, p. 1672, 2021.
 - [8] M. P. Krstic, D. L. Johnson, and M. J. Herderich, “Review of smoke taint in wine: smoke-derived volatile phenols and their glycosidic metabolites in grapes and vines as biomarkers for smoke exposure and their role in the sensory perception of smoke taint,” *Australian Journal of Grape and Wine Research*, vol. 21, pp. 537–553, 2015.
 - [9] C. M. Mayr, M. Parker, G. A. Baldock et al., “Determination of the importance of in-mouth release of volatile phenol glycoconjugates to the flavor of smoke-tainted wines,” *Journal of Agricultural and Food Chemistry*, vol. 62, no. 11, pp. 2327–2336, 2014.
 - [10] M. Parker, P. Osidacz, G. A. Baldock et al., “Contribution of several volatile phenols and their glycoconjugates to smoke-related sensory properties of red wine,” *Journal of Agricultural and Food Chemistry*, vol. 60, no. 10, pp. 2629–2637, 2012.
 - [11] D. Kelly and A. Zerihun, “The effect of phenol composition on the sensory profile of smoke affected wines,” *Molecules*, vol. 20, no. 6, pp. 9536–9549, 2015.
 - [12] M. J. Herderich, T. E. Siebert, M. Parker et al., “Spice up your life: analysis of key aroma compounds in Shiraz,” in *Flavor Chemistry of Wine and Other Alcoholic Beverages*, M. Qian, Ed., pp. 3–13, ACS, Washington, DC, United States, 2012.
 - [13] M. Herderich and M. Krstic, *Mitigation Of Climate Change Impacts on the National Wine Industry by Reduction in Losses from Controlled burns and Wildfires and Improvement in Public Land Management*, The Australian Wine Research Institute, Urrbrae, South Australia, 2020.
 - [14] R. Ristic, A. L. Fudge, K. A. Pinchbeck et al., “Impact of grapevine exposure to smoke on vine physiology and the composition and sensory properties of wine,” *Theoretical and Experimental Plant Physiology*, vol. 28, no. 1, pp. 67–83, 2016.
 - [15] R. Wittkowski, J. Ruther, H. Drinda, and F. Rafiei-Taghanaki, “Formation of smoke flavor compounds by thermal lignin degradation,” in *Flavour precursors American Chemical Society*, vol. 490, pp. 232–243, 1992.
 - [16] P. J. Spillman, M. A. Sefton, and R. Gawel, “The effect of oak wood source, location of seasoning and coopering on the composition of volatile compounds in oak-matured wines,” *Australian Journal of Grape and Wine Research*, vol. 10, no. 3, pp. 216–226, 2004.
 - [17] T. Tominaga, G. Guimbertau, and D. Dubourdieu, “Contribution of benzenemethanethiol to smoky aroma of certain *Vitis vinifera* L. Wines,” *Journal of Agricultural and Food Chemistry*, vol. 51, no. 5, pp. 1373–1376, 2003.
 - [18] E. Wilkes, “Smoke analysis at the AWRI: a testing year,” *Australia and New Zealand Grapegrower and Winemaker*, vol. 684, pp. 58–61, 2021.
 - [19] Y. Hayasaka, M. Parker, G. A. Baldock et al., “Assessing the impact of smoke exposure in grapes: development and validation of a HPLC-MS/MS method for the quantitative analysis of smoke-derived phenolic glycosides in grapes and wine,” *Journal of Agricultural and Food Chemistry*, vol. 61, no. 1, pp. 25–33, 2013.
 - [20] M. Noestheden, E. G. Dennis, E. Romero-Montalvo, G. A. DiLabio, and W. F. Zandberg, “Detailed characterization of glycosylated sensory-active volatile phenols in smoke-exposed grapes and wine,” *Food Chemistry*, vol. 259, pp. 147–156, 2018.
 - [21] A. Caffrey, L. Lerno, A. Rumbaugh et al., “Changes in smoke-taintvolatile-phenol glycosides in wildfire smoke-exposed Cabernet Sauvignon grapes throughout winemaking,” *American Journal of Enology and Viticulture*, vol. 70, no. 4, pp. 373–381, 2019.
 - [22] A. Coulter, G. A. Baldock, M. Parker, Y. Hayasaka, I. L. Francis, and M. Herderich, “Concentration of smoke marker compounds in non-smoke-exposed grapes and wine in Australia,” *Australian Journal of Grape and Wine Research*, vol. 28, no. 3, pp. 459–474, 2022.
 - [23] A. Oberholster, Y. Wen, S. Dominguez Suarez et al., “Investigation of different winemaking protocols to mitigate smoke taint character in wine,” *Molecules*, vol. 27, no. 5, p. 1732, 2022.
 - [24] C. Szeto, R. Ristic, D. Capone et al., “Uptake and glycosylation of smoke-derived volatile phenols by Cabernet Sauvignon grapes and their subsequent fate during winemaking,” *Molecules*, vol. 25, no. 16, p. 3720, 2020.
 - [25] Wine Australia, “Vintage 2020: Quantity constrained but value continues to grow,” in *Market Bulletin* Wine Australia Vintage, Adelaide, South Australia, 2020.
 - [26] Wine Australia, “Vintage Survey Dashboard,” 2022, <https://marketexplorer.wineaustralia.com/vintage-survey>.
 - [27] B. G. Coombe, “Growth stages of the grapevine: adoption of a system for identifying grapevine growth stages,” *Australian Journal of Grape and Wine Research*, vol. 1, no. 2, pp. 100–110, 1995.
 - [28] W. Jiang, E. Bilogrevic, M. Parker et al., “The effect of pre-fermentation smoke exposure of grapes on phenolic compounds and smoky flavour in wine,” *Australian Journal of Grape and Wine Research*, vol. 2022, Article ID 9820204, 15 pages, 2022.
 - [29] P. Iland, N. Bruer, G. Edwards, S. Caloghris, and E. Wilkes, *Chemical Analysis of Grapes and Wine: Techniques and Concepts*, Patrick Iland Wine Promotions Pty Ltd, , Patrick Iland Wine Promotions Pty Ltd, Athelstone SA 5076, Australia, 2 edition.
 - [30] J. A. Fryer and E. Tomasino, “Analysis of retronasal flavor alterations in smoke-affected wines and the efficacy of various inter-stimulus rinse protocols in clearing smoke-related attributes,” *Beverages*, vol. 8, no. 2, p. 23, 2022.
 - [31] H. H. Chong and M. T. Cleary, “Smoke taint aroma assessment in 2008 California grape harvest,” *Flavor chemistry of wine and other alcoholic beverages*, American Chemical Society, vol. 1104 , pp. 67–79, 2012.
 - [32] K. Wilkinson and R. Ristic, *Comparing the Chemical and Sensory Consequences of grapevine Smoke Exposure in Grapes and Wine from Different Cultivars and Different Wine Regions in Australia* 13th International Terroir Congress, Adelaide, Australia, 2020.
 - [33] J. A. Culbert, W. Jiang, E. Bilogrevic et al., “Compositional changes in smoke-affected grape juice as a consequence of activated carbon treatment and the impact on phenolic

- compounds and smoke flavor in wine,” *Journal of Agricultural and Food Chemistry*, vol. 69, no. 35, pp. 10246–10259, 2021.
- [34] H. Martens and M. Martens, “Modified jack-knife estimation of parameter uncertainty in bilinear modelling by partial least squares regression (pls-r),” *Food Quality and Preference*, vol. 11, no. 1-2, pp. 5–16, 2000.
- [35] G. A. Burdock, *Fenaroli’s Handbook of Flavor Ingredients*, CRC Press, Boca Raton, FL, USA, 4 edition, 2002.
- [36] R. Lopez, M. Aznar, J. Cacho, and V. Ferreira, “Determination of minor and trace volatile compounds in wine by solid-phase extraction and gas chromatography with mass spectrometric detection,” *Journal of Chromatography A*, vol. 966, no. 1-2, pp. 167–177, 2002.
- [37] M. Czerny, M. Christbauer, M. Christbauer et al., “Re-investigation on odour thresholds of key food aroma compounds and development of an aroma language based on odour qualities of defined aqueous odorant solutions,” *European Food Research and Technology*, vol. 228, no. 2, pp. 265–273, 2008.
- [38] R. Ristic, L. van der Hulst, D. L. Capone, and K. L. Wilkinson, “Impact of bottle aging on smoke-tainted wines from different grape cultivars,” *Journal of Agricultural and Food Chemistry*, vol. 65, no. 20, pp. 4146–4152, 2017.

Erratum

Erratum to “Assessing the Short-Term Effects of No-Till on Crop Yield, Greenhouse Gas Emissions, and Soil C and N Pools in a Cover-Cropped, Biodynamic Mediterranean Vineyard”

Cristina Lazcano ¹, **Noelymar Gonzalez-Maldonado** ¹, **Erika H. Yao** ¹,
Connie T. F. Wong ^{1,2}, **Mia Falcone** ², **Jean Dodson Peterson** ³, **L. Federico Casassa** ⁴,
Bwalya Malama ² and **Charlotte Decock** ²

¹Department of Land, Air and Water Resources, University of California Davis, Davis, CA 95616, USA

²Natural Resources Management and Environmental Sciences Department, California Polytechnic State University, San Luis Obispo, CA 93407, USA

³Department of Viticulture and Enology, Washington State University, 2710 Crimson Way, Richland, WA 99354, USA

⁴Wine and Viticulture Department, California Polytechnic State University, San Luis Obispo, CA 93407, USA

Correspondence should be addressed to Cristina Lazcano; clazcano@ucdavis.edu

Received 2 April 2023; Accepted 2 April 2023; Published 20 April 2023

Copyright © 2023 Cristina Lazcano et al. This is an open access article distributed under the Creative Commons Attribution License, which permits unrestricted use, distribution, and reproduction in any medium, provided the original work is properly cited.

In the article titled “Assessing the Short-Term Effects of No-Till on Crop Yield, Greenhouse Gas Emissions, and Soil C and N Pools in a Cover-Cropped, Biodynamic Mediterranean Vineyard” [1], a reference was cited in the text but not included in the reference list; this is included in the text below as reference 73 [2]; this reference should supplement the following sentence found in the first paragraph of the Introduction:

“The production of root exudates can also contribute to substantial amounts of C sequestration [73].”

References

- [1] C. Lazcano, N. Gonzalez-Maldonado, E. H. Yao et al., “Erratum to “Assessing the Short-Term Effects of No-Till on Crop Yield, Greenhouse Gas Emissions, and Soil C and N Pools in a Cover-Cropped, Biodynamic Mediterranean Vineyard”,” *Australian Journal of Grape and Wine Research*, vol. 2022, Article ID 8100818, 12 pages, 2022.
- [2] N. W. Sokol, S. E. Kuebbing, E. Karlsen-Ayala, and M. A. Bradford, “Evidence for the primacy of living root inputs, not root or shoot litter, in forming soil organic carbon,” *New Phytologist*, vol. 221, no. 1, pp. 233–246, 2019.

Research Article

Distribution of 3-Isobutyl-2-methoxypyrazine across Rachis Components of *Vitis vinifera* Shiraz and Cabernet Sauvignon

Ross D. Sanders ^{1,2,3}, Paul K. Boss ^{2,3}, Dimitra L. Capone ^{1,3}, Catherine M. Kidman ⁴, Emily L. Nicholson ² and David W. Jeffery ^{1,3}

¹School of Agriculture, Food and Wine, and Waite Research Institute, The University of Adelaide, Waite Campus PMB 1, Glen Osmond, South Australia 5064, Australia

²CSIRO Agriculture and Food, Waite Campus, Locked Bag No. 2, Glen Osmond, South Australia 5064, Australia

³Australian Research Council Training Centre for Innovative Wine Production, The University of Adelaide, Waite Campus PMB 1, Glen Osmond, South Australia 5064, Australia

⁴Wynns Coonawarra Estate, Memorial Drive, Coonawarra, South Australia 5263, Australia

Correspondence should be addressed to David W. Jeffery; david.jeffery@adelaide.edu.au

Received 14 September 2022; Revised 15 December 2022; Accepted 24 March 2023; Published 18 April 2023

Academic Editor: Leigh Schmidtke

Copyright © 2023 Ross D. Sanders et al. This is an open access article distributed under the Creative Commons Attribution License, which permits unrestricted use, distribution, and reproduction in any medium, provided the original work is properly cited.

Rootstock can significantly alter the concentration of methoxypyrazines (MPs) in the bunch stem (rachis) of *Vitis vinifera* L. cv. Cabernet Sauvignon and Shiraz, which has implications for winemaking and wine style. The distribution of MPs across the rachis is an important consideration, but such information was not available. This study aimed to address this research question by comparing MP concentrations in different rachis components throughout grape maturation and in the absence of ambient light. Shiraz and Cabernet Sauvignon bunches were sampled throughout development, segmented into four components (peduncle, top rachis, bottom rachis, and pedicel), and 3-isobutyl-2-methoxypyrazine (IBMP) was quantified in each. For both cultivars, IBMP showed a negative correlation with grape maturity, with concentrations in pedicel at harvest being significantly higher than other rachis components. Additionally, light exclusion significantly increased IBMP concentrations in all rachis segments. The concentration of IBMP varied significantly between different rachis components. The greatest concentrations were measured in the pedicel, which also contributed the largest proportion among the components to total rachis by weight. Due to elevated IBMP concentrations in rachis and the difficulties in excluding matter other than grape from a fermentor, the presence of pedicel during fermentation could produce Shiraz and Cabernet Sauvignon wines with higher concentrations of MPs, thereby potentially increasing vegetal sensory characteristics.

1. Introduction

The chemical composition of berries is heterogeneous within a vineyard, vine and bunch, and this variability could alter the sensory properties of a wine if heterogeneous grape parcels are harvested [1]. Asynchronous berry development contributing to heterogeneity can be attributed to aspects of *terroir*, which encompass geographical and climatic differences between grape growing regions, and the spatial variation of soil, sunlight, slope, and water availability within a vineyard [2].

Within bunch, berry developmental heterogeneity is dependent on seed content, which alters hormonal dynamics and sugar accumulation [3]. Furthermore, factors such as the location of a berry within a bunch [4], berry surface temperature, or berry proximity to leaves or stems are hypothesised to impact berry composition and maturity [5]. However, within vine and bunch level heterogeneity is not exclusive to berries; concentrations obtained from rachis for rotundone [6], amino acids [7], and methoxypyrazines (MPs) (e.g., 3-isobutyl-2-methoxypyrazine (IBMP), 3-isopropyl-2-methoxypyrazine (IPMP), and 3-*sec*-butyl-2-

methoxy-pyrazine (SBMP)) [8] also vary throughout the growing season. Despite this, the potential contribution of rachis to wine aroma might often be overlooked.

Winemakers may opt to include rachis during whole- or partial-bunch fermentation to produce desirable tannin [9, 10], colour [10, 11], pH, or ethanol changes to the wine [9, 12]. However, these techniques are avoided for varieties that are known to produce IBMP (an impact odorant with green capsicum character) in rachis and berry, such as Cabernet Sauvignon, because they can cause the perception of “stemmy” flavours in wine [13]. Even for varieties where a portion of whole bunches is favourable in producing quality wines, such as Pinot noir, stem addition exceeding 60% can produce wines with sensory characteristics associated with MPs [9]. Rachis can also be unintentionally present during fermentation as a by-product of harvesting and destemming practices, as a component of matter other than grape (MOG). Historically, MOG levels of approximately 5% w/w have been found in machine harvested fruit [14]; however, recent technological advancements can decrease these levels to around 1% [15]. Even so, there should still be concern, given the potential for MOG in the form of rachis to impart undesirable and nonvarietal “green” sensory characteristics to a variety like Shiraz [16], which otherwise lacks the genetic ability to produce IBMP in the berry [17].

Being characteristic of certain grape varieties, IBMP is a “varietal” aroma compound that can contribute notes of “green capsicum” and “grassy” to red wine at concentrations of 10–15 ng/L [18]. Such sensory characteristics are desirable when in balance with an overall wine bouquet, but at elevated concentrations, IBMP can contribute “herbaceous” and “vegetative” aromas that can dominate the sensory experience, decreasing both consumer liking and positive emotions associated with the wine [19]. Furthermore, even at concentrations below its sensory threshold, IBMP can alter wine aroma through synergistic interactions increasing perception of “smoky” and “tar” notes or antagonistic interactions that decrease desirable “red berries” and “floral violet” aromas [20]. As such, understanding how to control the concentration of IBMP (and other MPs) in wine is essential.

Recent research has shown Shiraz [8, 21] and Cabernet Sauvignon [22] vines grafted to rootstock can have significantly higher IBMP concentrations in rachis than those on own roots. This was attributed in part to rootstock-mediated vine vigour altering ambient light exposure of bunches [21, 22]. Furthermore, in Shiraz rachis the concentrations of IBMP, IPMP, and SBMP increased throughout berry maturity [8], contrasting the negative relationship between these variables observed in the berry [23].

With respect to the contribution of rachis to MOG and likelihood of contributing unwanted sensory characters, it can be expected that the pedicel component of rachis could most easily enter a fermentor, due to its small size or attachment to the berry. Although studies have addressed MP concentrations in rachis overall, the MP concentration of different parts of the rachis remained to be investigated. This study aimed to fill that knowledge gap by determining the concentration of IBMP, IPMP, and SBMP in different rachis components throughout

grape maturation for *Vitis vinifera* L. cv Shiraz on Ramsey rootstock and own roots grown in the Barossa Valley, and Cabernet Sauvignon on 110 Richter rootstock grown in the Coonawarra. Trials exploring the exclusion of ambient light on MP distribution in Shiraz bunches were also undertaken. MPs were quantified by GC-MS/MS using an established stable isotope dilution assay and experimental data were analysed with linear mixed models (LMMs). Results from the study were intended to provide producers with an understanding of how the concentration of MPs across rachis components is influenced by grape maturity and light exposure, thereby giving information that helps to estimate their potential influence on wine sensory profiles.

2. Materials and Methods

2.1. Chemicals. Solvents and reagents were of analytical reagent (AR) grade or higher and were purchased from Sigma–Aldrich (Castle Hill, NSW, Australia). Labelled and unlabelled MPs used as analytical standards were previously synthesised [22].

2.2. Climate Data. Monthly average, minimum, and maximum temperatures and winter rainfall values were sourced from the Bureau of Meteorology’s automatic weather stations for Barossa Valley (Australian BOM Station 023373 at 34.47°S, 139.00°E) and Coonawarra (Australian BOM Station 026091 at 37.29°S, 140.83°E). The Huglin index was calculated according to [24] with the value of 1.00 used for the length of day coefficient. Rainfall and Huglin index data are summarised in Table S1 of the Supplementary Material.

2.3. Vineyard Sites. Samples from the Barossa Valley region were collected from the Department of Primary Industries and Regions site in Nuriootpa, South Australia (34°28′34.4″S, 139°00′26.8″E). The vineyard was established in 2001 and consists of *Vitis vinifera* L. cv. Shiraz clone 1654 on own roots and Ramsey rootstocks. Further details have been reported previously [25].

Samples from the Coonawarra region were collected from a premium commercial vineyard (37°15′47.4″S, 140°49′58.7″E). The vineyard was established in 2012 and consists of *Vitis vinifera* L. cv. Cabernet Sauvignon Reynella and SA125 clones on 110 Richter rootstock.

The parentage of rootstocks present in the trials is summarised in a recent publication [21]. No significant pest or disease pressures were observed during the experimental seasons.

2.4. Maturity Variation Experiment. In 2019/20, Shiraz samples were taken at flowering (80% cap fall) on the 26th of November, 50% veraison on the 8th of January, and harvest on the 9th of March. Sampling locations at each time point were chosen to provide a representative sample from the southern, centre, and northern regions of the vineyard. At flowering, twenty-four bunches were collected from each sampling location and used to create six biological replicates for each rachis

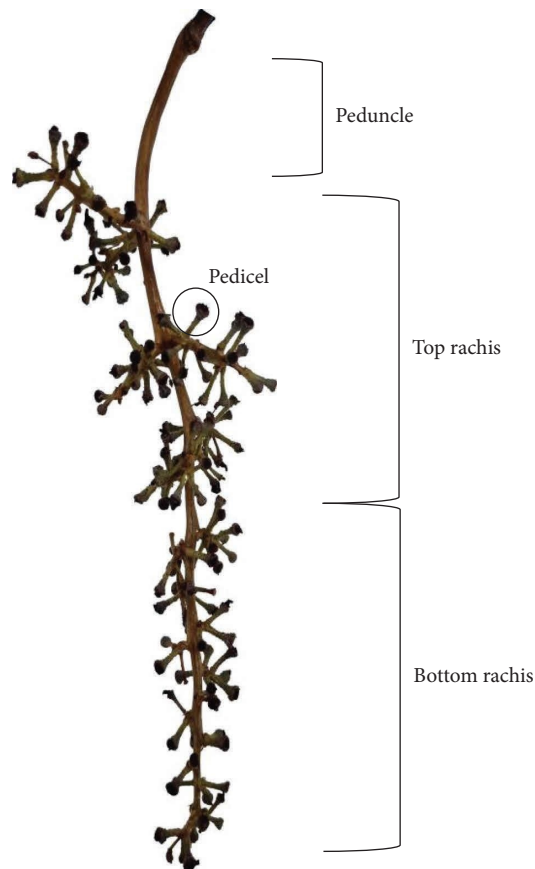


FIGURE 1: Schematic outlining the components that the rachis material was segmented into prior to extraction and analysis of methoxypprazines.

component (peduncle, top rachis, and bottom rachis). No pedicel material was retained at flowering due to its small size at this phenological stage and sampling limitations. At veraison and maturity, twelve bunches were collected from each sampling location and used to create six biological replicates of each rachis component (pedicel, peduncle, top rachis, and bottom rachis) (Figure 1). Shiraz sampled in 2021/22 was taken from the same locations within the vineyard as for 2019/20 at flowering (80% cap fall) on the 25th of November, 50% veraison on the 27th of January, and harvest on the 15th of March. In 2021/22, each sampling location was further divided into two six-vine subregions designated east and west. At all time points, twenty-four bunches (twelve from each east and west subregion) were collected from each vineyard location and used to create eight biological replicates (four from each east and west subregion) of each rachis component (peduncle, top rachis, bottom rachis, and pedicel) (Figure 1). As for 2019/20, pedicel material was only collected at veraison and maturity. All rachis material was transported to the laboratory on ice where berry material was removed, and rachis was segmented into components, cut into approximately 1 cm pieces, frozen in liquid nitrogen, and stored at -80°C until analysis. An overview of the sampling methodology for Shiraz from Barossa Valley can be found in Figure S1 of the Supplementary Information.

Cabernet Sauvignon was sampled in the 2019/20 season at 80% veraison on 13th February and at harvest on the 20th

of March. Sampling occurred prior to commercial harvest (15th of April) due to complications arising from the COVID-19 pandemic. Sampling locations were the same for each time point and were chosen to provide a representative sample from the southern, centre, and northern regions of the vineyard. From each sampling location, six bunches were chosen at random and used to create two biological replicates of each rachis component (peduncle, top rachis, bottom rachis, and pedicel) (Figure 1) per vineyard location. All rachis material was transported to the laboratory on ice where berry material was removed, and rachis was segmented into components, cut into approximately 1 cm pieces, frozen in liquid nitrogen, and stored at -80°C until analysis.

Shiraz and Cabernet Sauvignon grape bunches were collected at harvest from each sampling location and total soluble solids (TSS) ($^{\circ}\text{Brix}$) were measured from two biological replicates of homogenate prepared by manually crushing 50 fresh berries randomly selected from bunches.

2.5. Exclusion of Sunlight on the Distribution of Methoxypprazines in Grape Rachis. Experiments were performed over the 2021/22 growing season in the Barossa Valley and utilised opaque boxes designed to eliminate ambient light from the grape bunches while preventing temperature and humidity changes [26]. The experiment comprised boxed (box) and nonboxed (control) vines, with the treatment vines in each vineyard plot chosen to be representative samples of the southern, centre, and northern regions of the vineyard. Control bunches were those used in the maturity variation experiment and were sourced from vines located next to experimental vines. The box treatment was applied at 1 week postflowering (wpf) on the 23rd of November to whole bunches on own roots ($n = 24$) and Ramsey ($n = 20$). Samples were harvested at 14 wpf on the 15th of March and processed as described previously [22]. For box and control samples, TSS ($^{\circ}\text{Brix}$) were measured from a homogenate prepared by manually crushing 15 fresh berries randomly selected from each box. TSS values for control were taken as outlined above.

2.6. Weight of Individual Rachis Components in Shiraz. Shiraz material ($n = 26$) from Wrattenbully, South Australia was sampled at commercial harvest in 2022, frozen at -20°C , transported in Styrofoam boxes on ice, and stored at -30°C for 4 months until processing. Rachis material from each bunch was segmented into peduncle, top rachis, bottom rachis, and pedicel, and individual weights of each component were determined.

2.7. Measures of Canopy Architecture. A surrogate measure of vine vigour was obtained in the Barossa Valley on the 17th of January 2022 using a LICOR LAI-2200C Plant Canopy Analyser. For every six-vine subregion (east and west) at each sampling location, one above-canopy reading (ambient light), and four below-canopy readings were taken to provide an estimate of leaf area index (LAI).

2.8. Quantitation of Methoxy-pyrazines. MPs were quantified in grape and rachis tissue using a stable isotope dilution assay with headspace SPME-GC-MS/MS [22] with modifications to sample preparation. Briefly, the modifications involved frozen rachis tissue (0.5–2 g, dependent on component) being ground to a fine powder with a cryomill (Retsch, Germany) in liquid nitrogen. Approximately 200 mg of rachis from the sunlight exclusion experiment and 500 mg of rachis from the maturation trials was accurately weighed for extraction and analysis as per the previous report [22]. The respective limit of detection (LOD) and limit of quantitation (LOQ) values (ng/kg) were 0.13 and 0.44 for IBMP, 0.11 and 0.37 for IPMP, and 0.15 and 0.48 for SBMP [22].

2.9. Statistical Analysis. Data were analysed using R (version 4.1.2, R Foundation for Statistical Computing, Vienna, Austria) in RStudio (version 2022.07.1, RStudio Inc., Boston, MA). Mixed-effect linear regression models (linear mixed model, LMM) were used to determine treatment effects on log-transformed MP concentrations with the “lmerTest” package. For the Shiraz maturity variation experiment, rootstock, vintage, berry maturity, and rachis component were set as fixed effects, and vineyard block was set as a random factor. For the light exclusion trials, rachis component, light, and rootstock were set as fixed effects, and vineyard row and °Brix were included as random factors. For the Cabernet Sauvignon maturity variation experiment, rootstock, berry maturity, and component were set as fixed effects and vineyard row was set as a random factor. Estimated marginal means (statistically modelled variable mean response for each level of a predictor variable) and standard error (SE) values of the models were calculated on back-transformed values using the “emmeans” package and compared using Bonferroni-adjusted pairwise comparisons. Summary statistics for variables with measurements below the LOD and/or LOQ were calculated using the Kaplan–Meier technique with Efron’s bias correction using the “NADA” package. Summary plots were produced using “ggplot2”.

3. Results and Discussion

3.1. Concentration and Distribution of 3-Isobutyl-2-Methoxy-pyrazine in Shiraz Rachis Components throughout Berry Maturation. Shiraz bunches were collected at harvest in 2022 from the Wrattonbully wine region to determine the proportion (% w/w) of individual rachis components (peduncle, top rachis, bottom rachis, pedicel) of the total rachis fresh weight. Timing of sampling was an important consideration; rachis reaches its definite size by veraison [27] but dehydration of the peduncle continues until harvest [28], which would decrease its fresh weight and cause a concentration effect of IBMP within this component. In addition, Shiraz rachis grown on Ramsey rootstock and own roots has been shown to increase in IBMP concentration through berry maturation, reaching its maximum at harvest [8].

Shiraz rachis fresh weight at harvest was calculated as 6.5% of the total bunch weight, which falls within the range of 3–7% for *Vitis vinifera* rachis [27]. The proportion (% w/w) of individual rachis components of the total fresh rachis weight was calculated for peduncle (10%), top rachis (18%), bottom rachis (9%), and pedicel (63%) (Figure S2 of the Supplementary Material). These values were used throughout this publication to estimate the contribution from each rachis component to the total IBMP concentration present within an average Shiraz rachis. To the best of our knowledge, this is the first published segmentation data for rachis material, with a single previous study showing that peduncle was approximately 20% of Shiraz rachis fresh weight [28].

3.1.1. Rootstock and Stage of Grape Development. The concentration of IBMP in different rachis components from Shiraz grown on Ramsey and own roots in the Barossa Valley (Table S3 of the Supplementary Material) was dependent on rootstock and berry maturity ($P < 0.001$, Figure 2).

According to the LMM, concentrations of IBMP ranged at veraison from 2.51 ng/kg rachis for peduncle from own roots at harvest to 142 ng/kg rachis for Ramsey pedicel. At veraison, IBMP concentrations were significantly higher in Ramsey than own roots for pedicel (142 and 54.3 ng/kg rachis, respectively), top rachis (18.8 and 7.74 ng/kg rachis), and bottom rachis (12.9 and 3.58 ng/kg rachis), although this difference was no longer significant for any rachis component at harvest. This was somewhat surprising considering that own roots had a higher measure of vine vigour than Ramsey ($P < 0.001$, Table S2), and vigour has previously been positively correlated with rachis IBMP concentrations at harvest [21]. However, that prior research also showed no significant difference between IBMP concentrations in own roots and Ramsey Shiraz rachis at harvest for three vintages [21] that were sampled from the same vineyard used in the current work.

For both Ramsey and own roots, the concentration of IBMP in top rachis, bottom rachis, and peduncle significantly decreased between flowering and harvest ($P \leq 0.05$) with a downward trend evident as grape maturity increased (Figure 2). For pedicel, Ramsey was significantly lower at harvest (63.9 ng/kg rachis) than veraison (142 ng/kg rachis), and while own roots appeared to trend upwards from veraison (54.3 ng/kg rachis) to harvest (81.4 ng/kg rachis), there was no significant difference.

In contrast, previous research reported Shiraz rachis from the Murray Darling region of Victoria increased in MP concentration throughout the 2017/18 growing season, with IBMP, IPMP, SBMP being above the LOD by 8 wpf [8]. In the current study, however, SBMP remained below the LOD throughout both studied vintages, and IPMP was detected only sporadically and at low concentrations (data not shown). As rachis is composed of approximately 55 to 80% water [29], increased dehydration of rachis due to climate differences between the regions may have elevated the concentrations of MPs in Murray Darling rachis relative to

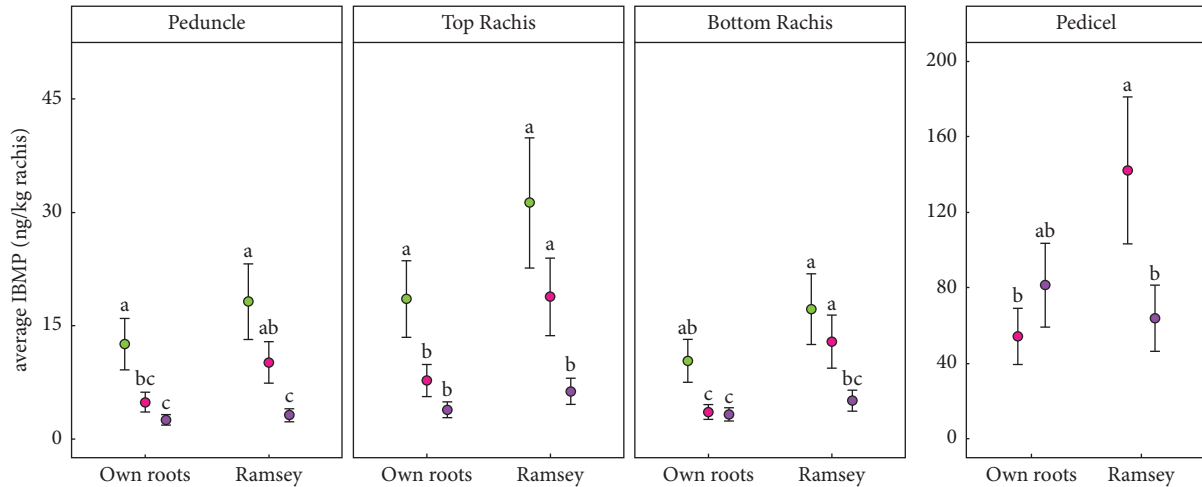


FIGURE 2: Estimated marginal means of IBMP (ng/kg of rachis ± SE) in the peduncle, top rachis, bottom rachis, and pedicel from Shiraz rachis sampled during the 2019/20 and 2021/22 vintages from the Barossa Valley, considering the interaction effect between rootstock (own roots and Ramsey) and berry maturity (flowering (● green), veraison (● red), and harvest (● purple)). Bars sharing the same letter within a component are not significantly different (linear mixed model, $\alpha = 0.05$, Bonferroni-adjusted). *Note.* Pedicel material was not sampled at flowering. Concentrations (ng/kg rachis) were calculated from ng/kg of component values (Figure S3 of the Supplementary Material) by considering component contribution (% w/w) to total rachis weight (Figure S2 of the Supplementary Material). Note the different y-axis scale for pedicel.

that from the Barossa Valley. As calculated by the Huglin index, the Murray Darling region was classified as very warm (3181) for the 2017/18 season, whereas Barossa Valley was classified as temperate warm for both 2019/20 (2379) and 2021/22 (2252).

Overall, the close agreement in trends and concentrations for Ramsey and own root rachis seen herein suggest that rootstock may have no bearing on the way that IBMP is distributed within rachis. Alternative explanations for the distribution of IBMP in different rachis components could relate to differences in light environment due to berry or vine shading.

3.1.2. Vintage and Stage of Grape Development. The concentration of IBMP in Shiraz rachis components from the Barossa Valley was shown to be dependent on the simple main effect of vintage ($P < 0.001$) according to the LMM, with an average IBMP concentration of 103 ng/kg and 57.6 ng/kg in the 2019/20 and 2021/22 growing seasons, respectively. Grape maturity at harvest (as a surrogate measure of rachis maturity) varied significantly ($P < 0.001$) between vintages, with 2019/20 (27.4° Brix) being significantly lower than 2021/22 (28.9° Brix). Broadly these results suggest a negative relationship between IBMP concentration in rachis and grape maturity, similar to that observed for Cabernet Sauvignon berries [23].

In addition, the concentration of IBMP in rachis was dependent upon a three-way interaction between component, vintage, and berry maturity ($P = 0.03$) according to the LMM (Figure 3). IBMP concentrations ranged from a high of 110 ng/kg rachis for pedicel at veraison in 2019/20 down to 0.87 ng/kg rachis for peduncle at harvest in the same season. IBMP concentrations in pedicel were higher than all other rachis components at veraison and harvest, but pedicel

did not significantly differ at either maturity time point in 2019/20 or 2021/22 (Figure 3). In 2021/22, top rachis (18.4 ng/kg rachis) and bottom rachis (9.59 ng/kg rachis) were different ($P < 0.05$) at veraison, which may suggest that the regulation of IBMP distribution in these organs is somewhat variable. Light exposure can significantly alter MP accumulation in Shiraz rachis material [21], so it was theorised that top rachis could experience higher levels of ambient light than bottom rachis throughout the growing season, due to its more exposed position in the bunch. As pedicel was not separated by bunch position, it is feasible that pedicel material could also differ in IBMP content based on its location within a bunch. However, due to shading from the berry, the variability in pedicel light exposure across the bunch should be lower than for top versus bottom rachis, although this aspect could be evaluated in future.

While the average IBMP concentration was significantly higher in 2019/20 (103 ng/kg) than 2021/22 (57.6 ng/kg), all components at harvest except for pedicel were significantly higher in IBMP concentration in 2021/22 than 2019/20. Vintage effects in rachis IBMP are attributed to differences in growing season temperature, with a negative correlation between temperature and IBMP in rachis proposed for Shiraz [21] and Cabernet Sauvignon [22]. However, the vintage effects seen within the current results were not readily explained due to climatic variables. The Huglin index values of 2379 and 2252 the 2019/20 and 2021/22 growing seasons, respectively, were similar and both were classified as “temperate warm,” suggesting minimal temperature variation overall.

Notably, the IBMP concentration in pedicel material at harvest from either vintage was significantly higher than all other rachis components on a ng/kg of rachis basis (Figure 3), which suggests that pedicel is the most substantial source of rachis IBMP. As concentrations of IBMP in pedicel

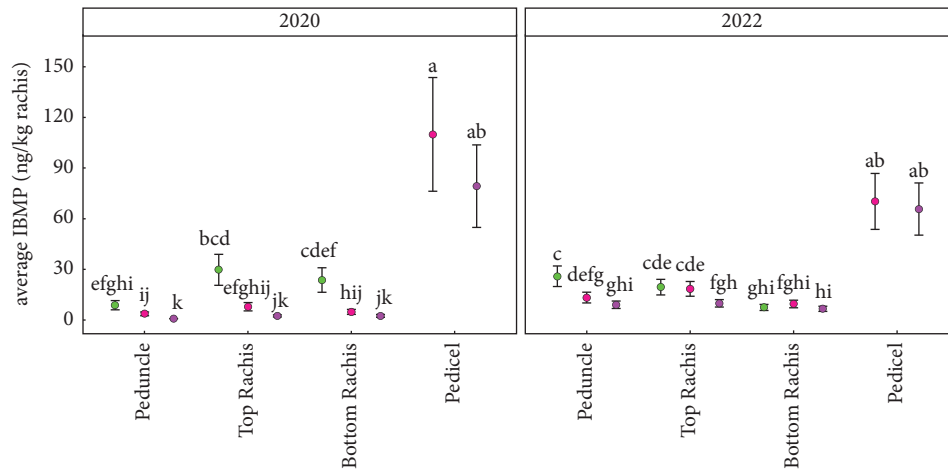


FIGURE 3: Estimated marginal means of IBMP (ng/kg rachis \pm SE) in the peduncle, top rachis, bottom rachis, and pedicel of Shiraz rachis sampled during the 2019/20 and 2021/22 vintages from the Barossa Valley at (flowering (● green), veraison (● red), and harvest (● purple)) considering the three-way interaction effect between component, vintage, and berry maturity. Bars sharing the same letter between the plots are not significantly different (linear mixed model, $\alpha = 0.05$, Bonferroni-adjusted). *Note.* Pedicel material was not sampled at flowering. Concentrations (ng/kg rachis) were calculated from ng/kg of component values (Figure S4 of the Supplementary Material) by considering component contribution (% w/w) to total rachis weight (Figure S2 of the Supplementary Material).

are not significantly different between veraison and harvest, testing the pedicel at veraison could provide valuable information about potential wine sensory outcomes for winemakers who are considering partial- or whole-bunch fermentation or mechanically harvesting fruit without any sorting.

3.1.3. Ambient Light Exclusion throughout Maturation.

As with berry, light exclusion is known to yield significantly higher concentrations of IBMP, IPMP, and SBMP in Shiraz [21] and Cabernet Sauvignon [22] rachis, but the effect of light on MP distribution across the rachis was unknown. Addressing the hypothesis that differences in natural light exposure could be responsible for the observed differences in IBMP concentration between rachis components (peduncle, top and bottom rachis, and pedicel), light exclusion boxes were applied to Shiraz grape bunches at 1 wpf on Ramsey rootstock and own roots (box) with nonboxed bunches (control) taken from nearby vines at harvest. There was no significant difference in maturity ($^{\circ}$ Brix) for Shiraz berries obtained from Ramsey (28.2 ± 1.53) and own roots (29.7 ± 1.41) box samples at harvest.

The concentration of IBMP in Shiraz rachis at harvest (Table S4 of the Supplementary Material) for box and control samples was significantly dependent upon the simple main effect of rootstock ($P < 0.001$) (Figure 4) according to the LMM. The estimated marginal means were 72.2 ng/kg rachis (own roots) and 143 ng/kg rachis (Ramsey) for control bunches, and 780 ng/kg rachis (own roots) and 1219 ng/kg rachis (Ramsey) for box bunches. Although slightly lower, these values were reflective of previous research involving light exclusion trials on Shiraz, with box bunches being substantially higher than controls [21]. IPMP and SBMP were not detected in any control samples but were above the LOD for 100% and 96% of Ramsey box

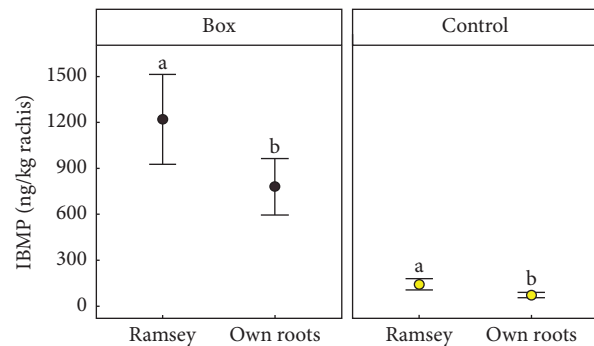


FIGURE 4: Estimated marginal means for IBMP concentration (ng/kg rachis \pm SE) in Shiraz rachis for control (● yellow) and box (● charcoal) treatments at harvest (2022) considering the simple main effect of rootstock (Ramsey and own roots). Bars sharing the same letter within the same plot are not significantly different (linear mixed model, $\alpha = 0.05$, Bonferroni-adjusted). *Note.* IBMP concentrations (ng/kg rachis) were calculated by adding the IBMP concentration of the respective components together for every biological replicate while considering component proportion (% w/w) (Figure S2 of the Supplementary Material).

samples (Table S4 of the Supplementary Material). However, due to their low concentrations, the data were not analysed further.

An interaction between rachis component and light ($P < 0.001$) significantly affected the concentration of IBMP according to the LMM. The impact of light exclusion on IBMP is visualised on a ng/kg rachis (Figure 5(a)) and a ng/kg component (Figure 5(b)) basis.

On a per kilogram of rachis basis (Figure 5(a)), the marginal means for IBMP concentration ranged from 6.58 ng/kg rachis (bottom rachis, control) to 597 ng/kg rachis (pedicel, box). Pedicel box was significantly higher in IBMP concentration than all other components,

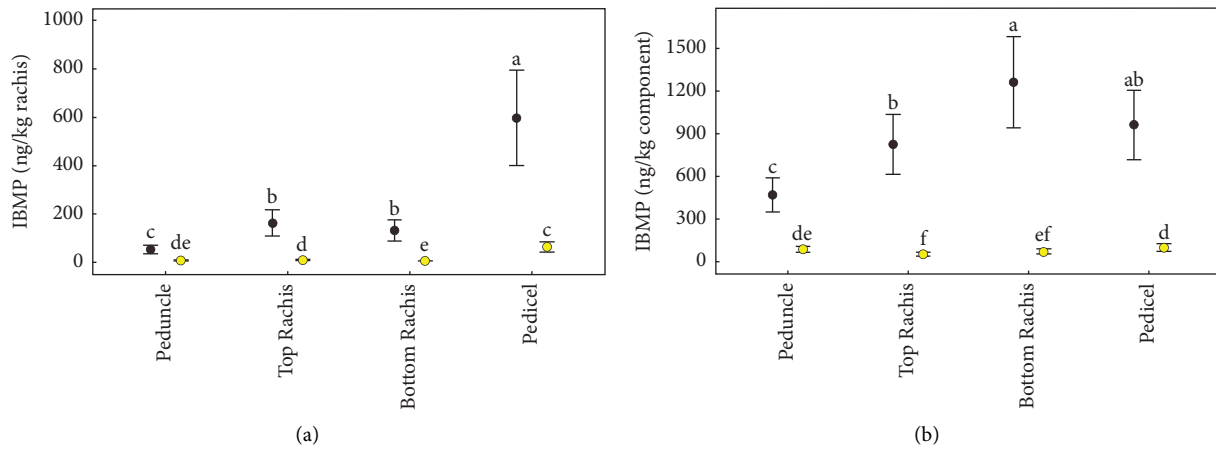


FIGURE 5: Estimated marginal means of IBMP concentration (a) (ng/kg rachis \pm SE) and (b) (ng/kg component \pm SE) in different Shiraz rachis components at harvest from control (● yellow) and box (● charcoal) grape bunches grown in the Barossa Valley (2022) considering the interaction between rachis component and light. Bars sharing the same letter within the same plot are not significantly different (linear mixed model, $\alpha = 0.05$, Bonferroni-adjusted). Values for Figure 5(a) were calculated from Figure 5(b) by considering the proportion (% w/w) of individual rachis components to total rachis fresh weight (Figure S2 of the Supplementary Material).

independent of light conditions. IBMP concentrations in pedicel control (64.5 ng/kg rachis) were equivalent to peduncle box (53.98 ng/kg rachis), and higher ($P \leq 0.05$) than top rachis control (9.85 ng/kg rachis), peduncle control (8.95 ng/kg rachis), and bottom rachis control (6.58 ng/kg rachis). Box and control samples trend in a similar manner, suggesting that bunch light exposure is an important consideration for controlling IBMP within a vineyard.

On a per kilogram of component basis (Figure 5(b)), the marginal means of IBMP varied from 53.8 ng/kg component (top rachis, control) to 1260 ng/kg component (bottom rachis, box). Concerning light excluded components, bottom rachis was significantly higher than top rachis (827 ng/kg component) and peduncle (469 ng/kg component), but not significantly different to pedicel (961 ng/kg component). Pedicel was equivalent to bottom and top rachis but higher than peduncle. Notably, the pattern of distribution across the rachis was dissimilar to the control samples, although there were still significant differences between rachis components (Figure 5(b)), suggesting that bunch light exposure might contribute to the regulation of IBMP movement, biosynthesis, and/or storage in various components of rachis, perhaps in unison with other regulatory processes.

IBMP biosynthesis from the precursor hydroxypyrazine (IBHP) is regulated in berry by the *VvOMT* gene family, primarily through the activity of the methyltransferase enzyme *VvOMT3* [30, 31]. Expression of *VvOMT3* is upregulated in the berry when ambient light is excluded, significantly increasing concentrations of IBMP [23]. The exclusion of light also increases the concentration of IBMP in rachis [21, 22], but the molecular basis remains unknown. A study of Shiraz rachis found that IBMP biosynthesis throughout the growing seasons was not correlated with the levels of *VvOMT3* expression [8]. Instead, those researchers proposed that translocation from other vines organs, particularly the roots where there are elevated concentrations of IBMP, could explain IBMP concentrations in the rachis.

However, while the expression of genes in the *VvOMT* family has been shown to vary between vine organs [32], the differential expression of *VvOMT3* across and within vine components remains unexplored. The significantly elevated concentrations of IBMP in the bottom rachis under light exclusion conditions (Figure 5(b)) may suggest that a targeted approach measuring gene expression in the different rachis components should be a consideration for future work that aims to elucidate IBMP biosynthesis in rachis.

Although light does not affect IBMP distribution in rachis in a uniform manner, the clear relationship between light and absolute IBMP concentration, established herein and elsewhere [21, 22], highlights that bunch light exposure might remain an important tool for grapegrowers to regulate IBMP not only in berry but also in rachis.

3.2. Methoxy pyrazine Distribution in Cabernet Sauvignon Rachis. Preliminary experiments were conducted over the 2019/20 growing season to quantify IBMP distribution in the rachis of Cabernet Sauvignon clones (Reynella and SA125) grown on 110 Richter rootstock in Coonawarra (Table S5 of the Supplementary Material). The concentration of IBMP in Cabernet Sauvignon rachis was significantly different between rachis components ($P < 0.001$) according to the LMM. The estimated marginal means ranged from 52.4 ng/kg component for peduncle to 229 ng/kg component for pedicel (Figure 6(a)). Pedicel had significantly higher concentrations than bottom rachis (140 ng/kg component) and top rachis (124 ng/kg component), which themselves were equivalent, and significantly higher than peduncle (52.4 ng/kg component). Additionally, IBMP concentrations in Cabernet Sauvignon rachis varied significantly with berry maturity ($P < 0.001$) (Figure 6(b)), from 148 ng/kg at veraison to 98 ng/kg at harvest. This suggests that IBMP concentrations in rachis are negatively correlated with berry maturity in a similar manner to IBMP in not only Cabernet Sauvignon

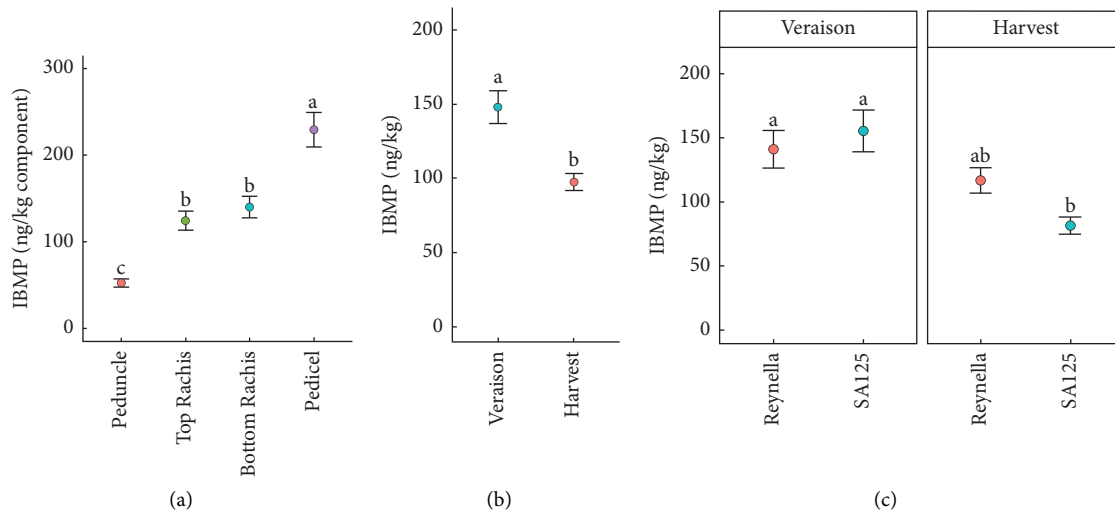


FIGURE 6: Estimated marginal means of IBMP concentration in rachis components (\pm SE) of Cabernet Sauvignon grown in Coonawarra over the 2019/20 season, considering the simple main effects of (a) component, (b) berry maturity, and (c) the interaction effect between berry maturity and clone. Bars sharing the same letter within the same plot are not significantly different (linear mixed model, $\alpha = 0.05$, Bonferroni-adjusted).

berries [31] but also Shiraz rachis, as described in an earlier section.

Although higher, the concentration of IBMP in Cabernet Sauvignon rachis trended similarly to Shiraz pedicel (126 ng/kg component), bottom rachis (27.2 ng/kg component), top rachis (13.5 ng/kg component), and peduncle (8.73 ng/kg component) sampled from the Barossa Valley at harvest in 2019/20 (Figure S4 of the Supplementary Material). As the Cabernet Sauvignon and Shiraz samples were sourced from different regions, the difference in IBMP concentration in rachis seen herein was difficult to attribute solely to varietal differences. Previous work has shown large variations in IBMP concentration for Shiraz rachis across multiple regions in a single vintage [21] and a regional influence could not be discounted in the present study.

IBMP concentration in Cabernet Sauvignon rachis components was dependent on an interaction effect between clone and berry maturity ($P = 0.006$) with values for SA125 varying significantly ($P \leq 0.05$) from veraison (155 ng/kg) to harvest (81.5 ng/kg) (Figure 6(c)). In comparison, Reynella did not vary significantly ($P > 0.05$) in IBMP concentration from veraison to harvest (141 ng/kg and 117 ng/kg, respectively). There was no statistical difference in IBMP between SA125 and Reynella rachis at harvest. This contrasted with previous findings, in which IBMP concentrations in the berry of Carm nere [33] and Sauvignon blanc [34] clones, and in the rachis of Shiraz clones 1654 and BVRC [21], varied significantly at harvest. Such variability is proposed to arise due to genetic variation between clones [34], but further research is required to understand the biological mechanism that leads to clonal variation in IBMP concentration in berry or rachis.

As vintage and rootstock have been shown to regulate MP accumulation in Cabernet Sauvignon rachis [22], further research encompassing these variables is necessary to support the preliminary trends in MP distribution observed in

the present study with Cabernet Sauvignon rachis grown on 110 Richter over a single vintage. Furthermore, the elevated IBMP concentration in pedicel at harvest implies that the presence of Cabernet Sauvignon pedicels in a fermentor has the potential to increase the concentration of IBMP and alter wine sensory characteristics. Pedicel is the most likely MOG to enter a fermentor, so it would be interesting to determine the proportion of MOG attributable to pedicel as a result of different crushing and sorting techniques, to ascertain the likely impact on wine style.

4. Conclusion

This research significantly expands upon existing knowledge by showing that IBMP distribution throughout Shiraz rachis is not equivalent and can be significantly impacted by rootstock, stage of grape development, and vintage. As the concentration of IBMP was not significantly different between veraison and harvest in pedicel, the main contributor of overall rachis IBMP, quantification of IBMP in pedicel at veraison could inform winemakers about potential sensory outcomes related to rachis presence during fermentation. This trial also reinforced the importance of bunch light exposure throughout the growing season in mediating IBMP concentrations in rachis at harvest, providing knowledge that will be useful for managing IBMP in the vineyard or winery. It remains to be determined how the variation in IBMP across Shiraz rachis components occurs. Additional research considering the impact of berry shape and cluster compactness on pedicel light exposure throughout the growing season may help to further explain the elevated concentrations of IBMP in pedicel observed in the present study.

In addition, the impact of viticultural region remained unexplored and, in conjunction with assessing other rootstock and scion combinations, would be an opportunity for

future research. Furthermore, a preliminary trial suggested that IBMP concentrations in Cabernet Sauvignon rachis may be affected by grape maturity and clone, which has implications for wine quality and style. Additional work could be useful to confirm these results and determine the impact of vintage and rootstock on the distribution of MPs across the bunch stem.

Putting the work into a practical context, in a best-case scenario, if only 1% w/w of MOG is permitted in top grade fruit with a maximum of 50% being rachis, such unintentional inclusion of rachis during fermentation would be insufficient to exceed the detection threshold of IBMP in red wine based on the results of this study. A direct effect on the sensory profile of wine would therefore be unlikely, even in the worst-case scenario of complete bunch light exclusion throughout the growing season. However, subthreshold concentrations of IBMP can alter the sensory profile of wine, so the presence of rachis components during fermentation should remain a primary consideration for winemakers.

Data Availability

The data used to support the findings of this study are included within the article and the supplementary information file.

Conflicts of Interest

The authors declare that they have no known conflicts of interest or personal relationships that could have appeared to influence the work reported in this paper. R.D.S is a recipient of an Australian Government Research Training Program Scholarship and a CSIRO iPhD scholarship, funded by the Australian Government with additional support from Wine Australia (WA Ph1901) and Treasury Wine Estates.

Acknowledgments

The authors thank Sue Maffei (CSIRO) for helping with sample preparation and analysis, and appreciate the contributions from Pietro Previtali and Claire Armstrong (The University of Adelaide) to field and laboratory work. The authors acknowledge Roger Maywald (Nuriootpa Research Centre) and Wynns Coonawarra Estate (Coonawarra) for providing access to vineyards and fruit. The authors thank AWITC for the invitation to publish our research in this Special Issue and for covering the article processing charge. The Australian Research Council Training Centre for Innovative Wine Production (<https://www.arcwinecentre.org.au/>; project number IC170100008) is funded by the Australian Government with additional support from Wine Australia, Waite Research Institute and industry partners. The University of Adelaide and CSIRO are members of the Wine Innovation Cluster.

Supplementary Materials

Supplementary data include figures showing average weight of rachis components and estimated marginal means for IBMP in rachis components based on interactions; tables

showing rootstock and climate information for the regions, leaf area index for Shiraz vines, average concentration of IBMP for rachis components of Shiraz sampled at different times, average concentrations of IBMP, IPMP, and SBMP in different rachis components of Shiraz in control and box experiments, and average concentration of IBMP for rachis components of Cabernet Sauvignon sampled at different times. (*Supplementary Materials*)

References

- [1] C. E. J. Armstrong, R. Ristic, P. K. Boss, V. Pagay, and D. W. Jeffery, "Effect of grape heterogeneity on wine chemical composition and sensory attributes for *Vitis vinifera* cv. Cabernet Sauvignon," *Australian Journal of Grape and Wine Research*, vol. 27, no. 2, pp. 206–218, 2021.
- [2] A. Deloire, E. Vaudour, V. Carey, V. Bonnardot, and C. van Leeuwen, "Grapevine responses to terroir: a global approach," *Journal International des Sciences de la Vigne et du Vin*, vol. 39, no. 4, pp. 149–162, 2005.
- [3] A. M. Vondras, S. Gouthu, J. A. Schmidt, A.-R. Petersen, and L. G. Deluc, "The contribution of flowering time and seed content to uneven ripening initiation among fruits within *Vitis vinifera* L. cv. Pinot noir clusters," *Planta*, vol. 243, no. 5, pp. 1191–1202, 2016.
- [4] S. Doumouya, M. Lahaye, C. Maury, and R. Siret, "Physical and physiological heterogeneity within the grape bunch: impact on mechanical properties during maturation," *American Journal of Enology and Viticulture*, vol. 65, no. 2, pp. 170–178, 2014.
- [5] P. Zhang, S. Barlow, M. Krstic, M. Herderich, S. Fuentes, and K. Howell, "Within-vineyard, within-vine, and within-bunch variability of the rotundone concentration in berries of *Vitis vinifera* L. cv. Shiraz," *Journal of Agricultural and Food Chemistry*, vol. 63, no. 17, pp. 4276–4283, 2015.
- [6] P. Zhang, S. Fuentes, Y. Wang et al., "Distribution of rotundone and possible translocation of related compounds amongst grapevine tissues in *Vitis vinifera* L. cv. Shiraz," *Frontiers of Plant Science*, vol. 7, Article ID 859, 2016.
- [7] A. M. Gourieroux, B. P. Holzapfel, G. R. Scollary, M. E. McCully, M. J. Canny, and S. Y. Rogiers, "The amino acid distribution in rachis xylem sap and phloem exudate of *Vitis vinifera* "Cabernet Sauvignon" bunches," *Plant Physiology and Biochemistry*, vol. 105, pp. 45–54, 2016.
- [8] D. L. Capone, I. L. Francis, P. R. Clingeleffer, S. M. Maffei, and P. K. Boss, "Evidence that methoxypyrazine accumulation is elevated in Shiraz rachis grown on Ramsey rootstock, increasing "green" flavour in wine," *Australian Journal of Grape and Wine Research*, vol. 28, no. 2, pp. 304–315, 2022.
- [9] P. M. Wimalasiri, K. J. Olejar, R. Harrison, R. Hider, and B. Tian, "Whole bunch fermentation and the use of grape stems: effect on phenolic and volatile aroma composition of *Vitis vinifera* cv. Pinot Noir wine," *Australian Journal of Grape and Wine Research*, vol. 28, no. 3, pp. 395–406, 2022.
- [10] S. Suriano, V. Alba, D. Di Gennaro, T. Basile, M. Tamborra, and L. Tarricone, "Major phenolic and volatile compounds and their influence on sensorial aspects in stem-contact fermentation winemaking of Primitivo red wines," *Journal of Food Science and Technology*, vol. 53, no. 8, pp. 3329–3339, 2016.
- [11] S. Suriano, V. Alba, L. Tarricone, and D. Di Gennaro, "Maceration with stems contact fermentation: effect on

- proanthocyanidins compounds and color in Primitivo red wines,” *Food Chemistry*, vol. 177, pp. 382–389, 2015.
- [12] L. Guerrini, P. Masella, G. Angeloni et al., “Harvest of Sangiovese grapes: the influence of material other than grape and unripe berries on wine quality,” *European Food Research and Technology*, vol. 244, no. 8, pp. 1487–1496, 2018.
- [13] K. Hashizume and T. Samuta, “Green odorants of grape cluster stem and their ability to cause a wine stemmy flavor,” *Journal of Agricultural and Food Chemistry*, vol. 45, no. 4, pp. 1333–1337, 1997.
- [14] P.-J. D. Huang, J. N. Cash, and C. R. Santerre, “Influence of stems, petioles and leaves on the phenolic content of Concord and Aurora Blanc juice and wine,” *Journal of Food Science*, vol. 53, no. 1, pp. 173–175, 1988.
- [15] A. Parenti, P. Spugnoli, P. Masella, L. Guerrini, S. Benedettelli, and S. Di Blasi, “Comparison of grape harvesting and sorting methods on factors affecting the must quality,” *Journal of Agricultural Engineering*, vol. 46, no. 1, pp. 19–22, 2015.
- [16] D. L. Capone, A. Barker, W. Pearson, and I. L. Francis, “Influence of inclusion of grapevine leaves, rachis and peduncles during fermentation on the flavour and volatile composition of *Vitis vinifera* cv. Shiraz wine,” *Australian Journal of Grape and Wine Research*, vol. 27, no. 3, pp. 348–359, 2021.
- [17] A. Koch, C. L. Doyle, M. A. Matthews, L. E. Williams, and S. E. Ebeler, “2-Methoxy-3-isobutylpyrazine in grape berries and its dependence on genotype,” *Phytochemistry*, vol. 71, no. 17–18, pp. 2190–2198, 2010.
- [18] D. Roujou de Boubée, C. Van Leeuwen, and D. Dubourdieu, “Organoleptic impact of 2-methoxy-3-isobutylpyrazine on red Bordeaux and Loire wines. Effect of environmental conditions on concentrations in grapes during ripening,” *Journal of Agricultural and Food Chemistry*, vol. 48, no. 10, pp. 4830–4834, 2000.
- [19] W. Jiang, J. Niimi, R. Ristic, and S. E. P. Bastian, “Effects of immersive context and wine flavor on consumer wine flavor perception and elicited emotions,” *American Journal of Enology and Viticulture*, vol. 68, pp. 1–10, 2017.
- [20] M. McKay, F. F. Bauer, V. Panzeri, and A. Buica, “Investigation of olfactory interactions of low levels of five off-flavour causing compounds in a red wine matrix,” *Food Research International*, vol. 128, Article ID 108878, 2020.
- [21] R. D. Sanders, P. K. Boss, D. L. Capone, C. M. Kidman, S. Maffei, and D. W. Jeffery, “Methoxy-pyrazine concentrations in the grape bunch rachis of *Vitis vinifera* L. cv Shiraz: influence of rootstock, region and light,” *Food Chemistry*, vol. 408, Article ID 135234, 2023.
- [22] R. D. Sanders, P. K. Boss, D. L. Capone et al., “Rootstock, vine vigour, and light mediate methoxy-pyrazines in the grape bunch rachis of *Vitis vinifera* L. cv. Cabernet Sauvignon,” *Journal of Agricultural and Food Chemistry*, vol. 70, no. 17, pp. 5417–5426, 2022.
- [23] J. D. Dunlevy, K. L. Soole, M. V. Perkins, E. L. Nicholson, S. M. Maffei, and P. K. Boss, “Determining the methoxy-pyrazine biosynthesis variables affected by light exposure and crop level in Cabernet Sauvignon,” *American Journal of Enology and Viticulture*, vol. 64, no. 4, pp. 450–458, 2013.
- [24] J. Tonietto and A. Carbonneau, “A multicriteria climatic classification system for grape-growing regions worldwide,” *Agricultural and Forest Meteorology*, vol. 124, no. 1–2, pp. 81–97, 2004.
- [25] C. M. Kidman, S. Olarte Mantilla, P. R. Dry, M. G. McCarthy, and C. Collins, “Effect of water stress on the reproductive performance of Shiraz (*Vitis vinifera* L.) grafted to rootstocks,” *American Journal of Enology and Viticulture*, vol. 65, no. 1, pp. 96–108, 2014.
- [26] L. Haselgrove, D. Botting, R. van Heeswijck et al., “Canopy microclimate and berry composition: the effect of bunch exposure on the phenolic composition of *Vitis vinifera* L. cv. Shiraz grape berries,” *Australian Journal of Grape and Wine Research*, vol. 6, no. 2, pp. 141–149, 2000.
- [27] P. Ribéreau-Gayon, D. Dubourdieu, B. Donèche, and A. Lonvaud, “The grape and its maturation,” in *Handbook of Enology: The Microbiology of Wine and Vinifications*, J. Towey, Ed., Vol. 1, John Wiley and Sons Ltd, pp. 241–294, Hoboken, NJ, USA, 2006.
- [28] Y. Fang, O. Kravchuk, and D. K. Taylor, “Chemical changes in grape stem and their relationship to stem color throughout berry ripening in *Vitis vinifera* L. cv Shiraz,” *Journal of Agricultural and Food Chemistry*, vol. 63, no. 4, pp. 1242–1250, 2015.
- [29] M. R. González-Centeno, C. Rosselló, S. Simal, M. C. Garau, F. López, and A. Femenia, “Physico-chemical properties of cell wall materials obtained from ten grape varieties and their byproducts: grape pomaces and stems,” *LWT - Food Science and Technology*, vol. 43, no. 10, pp. 1580–1586, 2010.
- [30] S. Guillaumie, A. Ilg, S. Réty et al., “Genetic analysis of the biosynthesis of 2-methoxy-3-isobutylpyrazine, a major grape-derived aroma compound impacting wine quality,” *Plant Physiology*, vol. 162, no. 2, pp. 604–615, 2013.
- [31] J. D. Dunlevy, E. G. Dennis, K. L. Soole, M. V. Perkins, C. Davies, and P. K. Boss, “A methyltransferase essential for the methoxy-pyrazine-derived flavour of wine,” *The Plant Journal*, vol. 75, no. 4, pp. 606–617, 2013.
- [32] J. D. Dunlevy, K. L. Soole, M. V. Perkins et al., “Two O-methyltransferases involved in the biosynthesis of methoxy-pyrazines: grape-derived aroma compounds important to wine flavour,” *Plant Molecular Biology*, vol. 74, no. 1–2, pp. 77–89, 2010.
- [33] A. Belancic and E. Agosin, “Methoxy-pyrazines in grapes and wines of *Vitis vinifera* cv. Carmenere,” *American Journal of Enology and Viticulture*, vol. 58, no. 4, pp. 462–469, 2007.
- [34] K. Šuklje, G. Antalick, A. Buica et al., “Clonal differences and impact of defoliation on Sauvignon blanc (*Vitis vinifera* L.) wines: a chemical and sensory investigation,” *Journal of the Science of Food and Agriculture*, vol. 96, no. 3, pp. 915–926, 2016.

Research Article

Using Zeolites to Cold Stabilize White Wines

**Tim Reilly,¹ Pawel Mierczynski,² Andri Suwanto,³ Satriyo Krido Wahono,³
Waldemar Maniukiewicz,² Krasimir Vasilev,⁴ Keren Bindon ,¹
and Agnieszka Mierczynska-Vasilev ¹**

¹The Australian Wine Research Institute, Waite Precinct, Hartley Grove Cnr Paratoo Road, Glen Osmond, SA 5064, Australia

²Institute of General and Ecological Chemistry, Lodz University of Technology, Zeromskiego 116, 90-924 Lodz, Poland

³Research Center for Food Technology and Processing, Research Organization for Agriculture and Food, National Research and Innovation Agency Republic of Indonesia (PRTTP—OR PP BRIN), Playen, Gunungkidul, Yogyakarta 55861, Indonesia

⁴College of Medicine and Public Health, Flinders University, Sturt Road, Bedford Park, SA 5042, Australia

Correspondence should be addressed to Agnieszka Mierczynska-Vasilev; agnieszka.mierczynska-vasilev@awri.com.au

Received 5 November 2022; Revised 30 January 2023; Accepted 23 March 2023; Published 7 April 2023

Academic Editor: Paul Kilmartin

Copyright © 2023 Tim Reilly et al. This is an open access article distributed under the Creative Commons Attribution License, which permits unrestricted use, distribution, and reproduction in any medium, provided the original work is properly cited.

Background and Aims. Tartrate stabilisation is a necessary step in commercial wine production. The traditional method to prevent crystallisation and precipitation of potassium bitartrate (KHT) after a wine is bottled is by adding seed KHT crystals to wine stored in a tank and holding temperatures below 0°C for a set period of time before bottling. This process requires time and energy and a filtration step to remove sediment. However, compared to other technical solutions such as reverse osmosis, electro dialysis, or ion exchange, it is still the most economical stabilisation option. This work aims to evaluate the ability of zeolites to cold stabilize white wines. Since zeolites can also remove proteins and thus heat-stabilize white wines, the new process can potentially combine heat and cold stability in a single treatment. **Methods and Results.** Effective tartrate stabilisation was achieved by mixing a natural zeolite sample with white wine for three hours. Although the quantum of required zeolite was larger than bentonite, zeolite did not exhibit shrink-swell behaviour, thus enabling greater wine recovery and capacity to be regenerated. Effective heat and cold stability could be achieved using a low-calcium zeolite as a processing aid in a single treatment. To avoid aluminium leaching and elevated aluminium concentrations in the treated wine, the zeolite was calcinated before being added to the wine. The calcination process also reduced calcium content in the wine after treatment with zeolite, thus eliminating the risk of calcium instability. **Conclusions.** The application of zeolite as a processing aid can potentially be effective in cold-stabilizing white wines and removing proteins responsible for haze formation. **Significance of the study.** Zeolites may constitute an alternative technology in white wine production facilitating heat and cold stabilisation in a single treatment.

1. Introduction

Cold stabilisation is a process of removing excessive L-tartaric acid natural ionic salts (potassium bitartrate: KHT, and to a lesser extent, calcium tartrate: CaT) from the wine. After fermentation but before bottling, cold stabilisation is routinely carried out to prevent the wine salt KHT from precipitating out of the wine during storage or cooling in bottle.

Traditional cold stabilisation methods involve cooling the wine to a temperature just above freezing and keeping it

at this temperature for weeks or even months. Chilling the wine reduces the solubility of KHT and facilitates its crystallisation and removal through precipitation. During cold storage, precipitation of KHT occurs rapidly in the initial phase and slows down over time as the saturation level of KHT decreases. The temperature and storage time required to stabilize a wine depends on wine composition [1]. Wines with higher sugar and alcohol content require a lower storage temperature than dry wines with 11-12% alcohol [2]. The stability and precipitation of KHT are also influenced by other factors such as the concentration of acids, anions,

cations, the pH of the wine, and various complexing agents [2]. To achieve reproducible KHT precipitation, the wine must be clarified and filtered before refrigeration and cold storage. As mentioned previously, storing a wine at near-freezing temperatures is sufficient to remove excess KHT. To prevent the redissolution of the KHT, the wine must also be cold filtered after cold storage to remove the crystalline KHT precipitate. Wine stabilisation by cooling is widely used in the wine industry. The process is time-consuming and energy-intensive [1] and involves a filtration step to remove the sediment. According to the South Australian Wine Industry Association, refrigeration consumes between 50 and 70% of the electricity used in a typical winery. Other technical solutions to prevent precipitation of KHT after bottling are reverse osmosis [3], ion exchange [4], electro-dialysis [5], and inhibition methods involving additives such as carboxymethyl cellulose (CMC) [1, 6], meta tartaric acid [1, 7], mannoproteins [1, 8], or potassium polyaspartate [9]. Processes such as ion exchange and electro-dialysis require significant capital investment and considerable expertise to be used effectively. In addition, the cost of water and maintenance can also be high. Tartrate stabilisation has recently focused on the development of compounds capable of inhibiting tartrate crystallisation. However, the possibilities of achieving long-term stability in wines without compromising colour and favourable organoleptic properties are limited. Moreover, the addition of additives in winemaking contradicts the modern trend towards organic and additive-free winemaking envisaged by consumers.

Given these shortcomings of current practices, we tried to find a new solution to cold stabilisation, which could be performed at higher temperatures.

Zeolites [10, 11] are hydrated aluminosilicates of sodium, potassium, calcium, or other heteroatoms [12]. These materials are formed naturally by volcanic activity (natural zeolites) but can also be synthesized in the laboratory (synthetic zeolites) [12]. Zeolites are extensively used in various technological applications, e.g., as catalysts [13, 14] and molecular sieves [10], to separate and sort molecules [15], to dehydrate [16, 17], to purify water [18] and air [19–21], and to remove radioactive contaminants [22]. In this work, we explored the potential of zeolites for the cold stabilisation of white wines.

The rationale for applying natural zeolites in cold stabilisation of white wines was based on our previous research [23] and the knowledge that the selective removal of potassium ions from wine down to, i.e., 10–30% of the initial potassium amount, likely inhibits the precipitation of potassium bitartrate salts [24]. We therefore hypothesised that natural zeolites could be a material with a promise to be successfully used in cold stabilisation of white wines.

2. Materials and Methods

2.1. Natural Zeolites. Samples used for the present studies came from Australian zeolite distributors such as ZeoNatural (Z1), Orku (Z2), and Nikita Naturals (Z3) and an Indonesian mining company (CV Mountain Stones) in micronised powder form (Z4).

The fifth zeolite sample came from Enfield Produce in a granular form and was micronized by Bureau Veritas Minerals for our purposes, referred to in the text as grind zeolite (Z5). Natural zeolite samples were used after three hours of rehydrating in Milli-Q water at a zeolite : water ratio of 1 : 10. The wines were transferred to 50 ml centrifuge tubes and treated with the zeolite suspension by stirring on a rotary mixer for three hours. The zeolite was then separated from the wine by centrifugation (3,750 rpm, 10 min) as previously specified in the optimisation procedure [23]. The zeolite treatment for Z1, Z2, Z3, and Z5 included a preliminary test with a range of zeolite doses (from 4 g/L to 10 g/L, increasing by 0.5 g/L) to determine the optimum dose to achieve protein stability. The same optimum zeolite dose was also used in the cold stability testing. A higher zeolite dose range was investigated for Z4 (from 8 g/L to 18 g/L with an increase of 1 g/L). As it was not possible to achieve protein stability of the wines with Z4, the 10 g/L dose was used for SAB and CHA wines and the 16 g/L dose was used for Muscat Gordo wine in the cold stability test.

To reduce aluminium leaching into wine after treatment with the zeolites, they were also subjected to a calcination process. In the text, these zeolites are referred to as calcinated zeolites. During calcination, zeolites were placed in an oven at 400°C for two hours.

In addition, two other zeolite samples, Z6 and Z7, were dealuminated using 3N HCl by soaking for 24 hours, followed by neutralization by washing them several times in water and finally drying at 100°C. The dealuminated zeolites are referred to in the text as Z6 dealuminated and Z7 dealuminated. Like Z4, samples Z6 and Z7 were also supplied in the form of micronised powder by CV Mountain Stones, an Indonesian mining company.

2.2. White Wines. Unstable Muscat Gordo, Sauvignon Blanc, Chardonnay, and Pinot Grigio wines expected to give tartrate and protein precipitates when bottled without further treatment were used in this study. All wines were donated by commercial producers, produced according to standard and commercial-scale winemaking processes, filtered (0.45 μm filters), and stored at cellar conditions (15°C) before conducting the experiments. The basic chemistry of wines was studied, and the results are presented in S1 (Supplementary Materials). The wines, which were fined with zeolites to test cold stability, were stored at 15°C in the cellar for nine months.

2.3. X-Ray Diffraction (XRD). Powder X-ray diffraction patterns were recorded at room temperature using a PANalytical X'Pert Pro MPD diffractometer in the Bragg–Brentano reflection configuration. Copper Cu K α radiation from a sealed tube was used. Data were collected in the 2θ range of 5–90° with a step of 0.0167° and exposure per step of 27 s. Since the raw diffraction data contained some noise, the background during the analysis was subtracted using the algorithm of Sonneveld and Visser [25]. The data were then smoothed with a cubic polynomial function.

2.4. Fourier Transform Infrared Spectroscopy (FTIR). An IRTracer-100 FTIR spectrometer (Shimadzu), equipped with a liquid nitrogen-cooled MCT detector, was used for all measurements. Measurements were performed using the Quest Single Reflection ATR Accessory (Specac), equipped with a diamond ATR crystal. In all cases, 128 scans were performed with a resolution of 4 cm^{-1} to achieve a satisfactory signal-to-noise ratio. The ATR effect and atmospheric contributions from carbon dioxide and water vapor were corrected by the background performed on an empty ATR device.

2.5. X-Ray Photoelectron Spectroscopy (XPS). To determine the surface composition of the five zeolites used, XPS analysis was performed. The XPS spectra were obtained with a Specs SAGE XPS spectrometer using an Al K α radiation source ($h\nu = 1253.6\text{ eV}$) at 10 kV and 20 mA. Elements present on the sample surface were identified from the survey spectrum recorded in the energy range 0–1,000 eV with a pass energy of 100 eV and a resolution of 0.5 eV. The areas under the selected photoelectronic peaks in a broad scan spectrum were used to calculate the percentage of atomic concentrations. High-energy-resolution spectra (0.1 eV) were then recorded for the relevant photoelectronic peaks at passing energy of 20 eV to identify the possible chemical bonding environments for each element. All binding energies were referred to the neutral carbon C1s peak at 285 eV to compensate for the effect of surface charge. Data processing and curve fitting were performed with the Casa XPS software.

2.6. Scanning Electron Microscopy/Energy Dispersive X-Ray (SEM/EDX). SEM was used to determine the morphology of the natural zeolite samples, while the elemental composition of the zeolites was determined with EDX. An FEI Quanta 450 FEG-ESEM with an EDAX Apollo X Energy Dispersive X-ray (EDX) spectrometer was used for the analysis.

2.7. Specific Surface Area and Porosity. The specific surface area of the natural zeolite samples was determined using the Brunauer, Emmett, and Teller adsorption technique (BET). Pore size distribution was determined using the BJH method of Barrett et al. [26]. Measurements were performed on the Micrometrics ASAP 2020 adsorption instrument (Surface Area and Porosity Analyzer, Micromeritics Instrument Corporation, Norcross, GA, USA).

2.8. Quantification of Tartaric Acid in Wine by HPLC. Wine samples were diluted with water and injected onto an Agilent Technologies Hi-Plex H column ($300\text{ mm} \times 7.7\text{ mm}$). Separation was performed with an isocratic 10 mM sulfuric acid/water solvent at a flow rate of 0.6 mL/min. Tartaric acid was detected at 210 nm and quantified against a standard curve of known tartaric acid concentration.

2.9. Crystal Quantification by HPLC. For the crystal quantification method, 10 mL of filtered wine was cooled to -4°C and kept at this temperature for 72 hours. After returning to the room temperature, the sample was centrifuged to ensure that all loose crystals were collected at the bottom of the tube. The supernatant was decanted, and the remaining sample was washed with 1 mL of absolute ethanol. After another centrifugation, the supernatant was decanted again, and the sample was dried. Dilute hydrochloric acid was then added to dissolve any tartrate crystals before the solution was analyzed for tartaric acid by HPLC. Quantification was performed using a tartaric acid standard curve.

2.10. Protein Quantification in Wine by HPLC. The concentration of wine proteins was measured by HPLC (Agilent Technologies) according to the previously published method [27]. Briefly, filtered wine samples were injected onto an Agilent 1.260 UHPLC with a Prozap C18 column. Separation was performed using 0.1% trifluoroacetic acid (TFA)/H₂O and 0.1%TFA/ACN at 0.75 mL/min. Protein detection was achieved by diode array monitoring at 210 nm. Protein identification was obtained by comparing the retention times of the peaks of the samples with those of the isolated standards, and quantification was performed by comparing the areas of the peaks with those of a thaumatin standard curve.

2.11. Metal Analysis. Metals content in wine was determined by inductively coupled plasma-optical emission spectrometry (ICP-OES) performed by Affinity Labs.

2.12. Analysis of the Si/Al and Ca Content of Indonesian Natural Zeolite. XRF was applied to determine the bulk composition of Indonesian natural zeolite. The micronized natural zeolite was prepared as a pellet by high-pressure technique. The XRF analysis was conducted using PAN-analytical Epsilon4 at BRIN Laboratory, Yogyakarta.

2.13. Statistical Analysis. Data significance was assessed by Student's *t*-test. The mean values with a different letter were significantly different ($p < 0.05$). Figures were prepared using Origin 6.0 and CorelDRAW 11 software.

3. Results and Discussion

3.1. Characterization of Natural Zeolites. The surface properties and structure of the natural zeolites used in this work are listed in Table 1. In addition, S2 (Supplementary Materials) shows the X-ray diffraction patterns of the five zeolites studied. According to the X-ray diffraction studies, the five zeolites (Z1 to Z5) have a distinct crystalline structure with the characteristic peaks of clinoptilolite [28] ((Na₄K₄)(Al₈Si₄₀O₉₆)·24 H₂O) and mordenite [29] (Na₈(Al₈Si₄₀O₉₆). Interestingly, besides clinoptilolite and mordenite, Z4 is the only one with calcite Ca (CO₃) structure, which confirms previous studies [30–32].

TABLE 1: Characterisation of natural zeolites.

Nos.	Zeolites	BET surface areas (m ² /g)	Pore volumes (cm ³ /g)	Pore diameters (nm)	Structure by XRD
Z1	ZeoNatural	17.4	0.05	11	Mordenite and clinoptilolite
Z2	Orku zeolite	18.2	0.06	14	Mordenite and clinoptilolite
Z3	Nikita zeolite	26.0	0.04	7	Mordenite and clinoptilolite
Z4	Indonesian zeolite	60.0	0.07	5	Calcite, mordenite, and clinoptilolite
Z5	Grind zeolite	17.2	0.06	14	Mordenite and clinoptilolite

The average pore diameter, surface area, and pore volume are important physical properties that influence the quality and utility of zeolites and are determined using the BET adsorption technique. The average pore size of the Z4 and Z3 was smaller (5 and 7 nm, respectively) than that of Z5, Z2, and Z1 (14, 14, and 11 nm, respectively). The BET surface area of the Z4 was the highest at 60 m²/g, resulting in a pore volume of 0.07 cm³/g. In contrast, the lowest surface area was measured for Z2, Z5, and Z1, with BET surface areas of 18.2, 17.2, and 17.4 m²/g, and pore volumes of 0.06, 0.06, and 0.05 cm³/g, respectively. The Z3 had a surface area of 26 m²/g and the lowest pore volume of 0.04 m²/g.

Figure 1 presents the SEM images of the natural zeolites. The SEM images indicate that the zeolites are crystalline, which is also confirmed by XRD. Overall, the images depicted zeolite crystals with smooth surfaces and a flake-like crystal configuration. The chemical composition of the zeolites in bulk and at the surface was determined by EDX and XPS measurements, respectively (see Table 2). All zeolites had a Si:Al ratio of nearly 4:1, which classifies these zeolites as intermediate Si/Al zeolites. However, it is noteworthy that the Z4 had the highest sodium and calcium contents as measured by EDX. The XPS analysis showed that the Z4 did not contain sodium ions on the surface.

FTIR was performed to determine the chemical functional groups of the zeolites Z1–Z5 (Figure 2). The bands in the range 650–745 cm⁻¹ were assigned to the symmetrical T-O-T vibrations in the framework of the zeolites. A dip also appeared at 1,000 cm⁻¹, which is a characteristic band for asymmetric Si-O-Si and Si-O-Al stretching vibrations in most zeolitic materials. Another small shoulder peak at 1,075 cm⁻¹ is due to symmetric Si-O-Al stretching. As can be seen from the figure, Z1, Z2, Z3, and Z5 have similar fingerprints, while the Z4 zeolite shows differences in peaks and transmission intensities. Furthermore, the spectrum of the Z4 shows a hydrogen bonding peak of water at the 2,490 cm⁻¹, which is absent in the other zeolites.

3.2. Exchange of Zeolite Sodium and Calcium Ions with Wine Potassium Ions. Zeolites are widely used in various fields of science and industrial applications mainly because of their ion-exchange properties, which are amongst the most important parameters characterising their sorption and technological properties. The ion exchange property of natural zeolites depends on several factors, including ion shape, size, charge density of the mineral network, framework structure, ion charge, and concentration of ions in the external solution [33].

Metal analysis was carried out to investigate the effects of zeolite treatment on the metal content of the treated wines and to understand which metals are involved in the ion-exchange process. Figure 3 shows the changes in potassium, sodium, and calcium concentrations after treatment of wine with natural zeolites. The changes in metal concentrations indicate that an ion exchange mechanism is taking place. It is known that potassium ions have the highest ion exchange potential compared to other metal cations (Ca²⁺, Mn²⁺, Fe²⁺, or Mg²⁺). Therefore, potassium ions in wine can be exchanged with Na⁺ and Ca²⁺ ions in zeolites [34, 35]. This explains the decrease in the concentration of potassium ions and the increase in the concentration of sodium (Figures 3(a) and 3(b) and in Supplementary Materials S3A–S3D) and calcium ions in the wine after treatment with zeolites Z1–Z5. In Z1, Z2, Z3, and Z4, the reduction of potassium ions in the treated wines was predominantly due to the cation exchange of potassium ions with sodium ions, hence the increase of sodium ions in the wine after treatment with these zeolites. As they are located at the surface, sodium ions can be exchanged with potassium [36]. In the case of the Z4, mainly an exchange of Ca²⁺ with K⁺ occurs as this zeolite does not have sodium ions on the surface, but has 4.8% calcium, which was determined by XPS.

The calcium content in Muscat Gordo wine after treatment with Z4 increased considerably as compared to Z1, Z2, Z3, and Z4 (Figure 3(c)). It is important to note that a high Ca²⁺ content in wine is highly undesirable, as calcium-induced instabilities are a major cause of problems in bottled wines.

A possible ion exchange mechanism is depicted in Figure 4.

As shown in Figure 3(a), for all zeolites tested, the potassium content in Muscat Gordo wine was reduced by 47–60% after treatment, resulting in reduced crystallisation and precipitation of KHT. At the same time, the sodium concentration in wine increased to an average of 130 mg/L.

In Sauvignon Blanc, the initial potassium concentration in the wine was approximately 750 mg/L and decreased to 650 and 515 mg/L, representing a 13 to 30% decrease in potassium concentration after treatment (Supplementary Materials S3A). The Chardonnay control wine had a higher potassium concentration of 920 mg/L. When treated with Z1–Z5, this concentration decreased by 18 to 28% (Supplementary Materials S3B). The sodium concentration in these wines increased to similar levels after treatment, with a maximum sodium concentration of 70 mg/L, as shown in Supplementary Materials S3C and S3D.

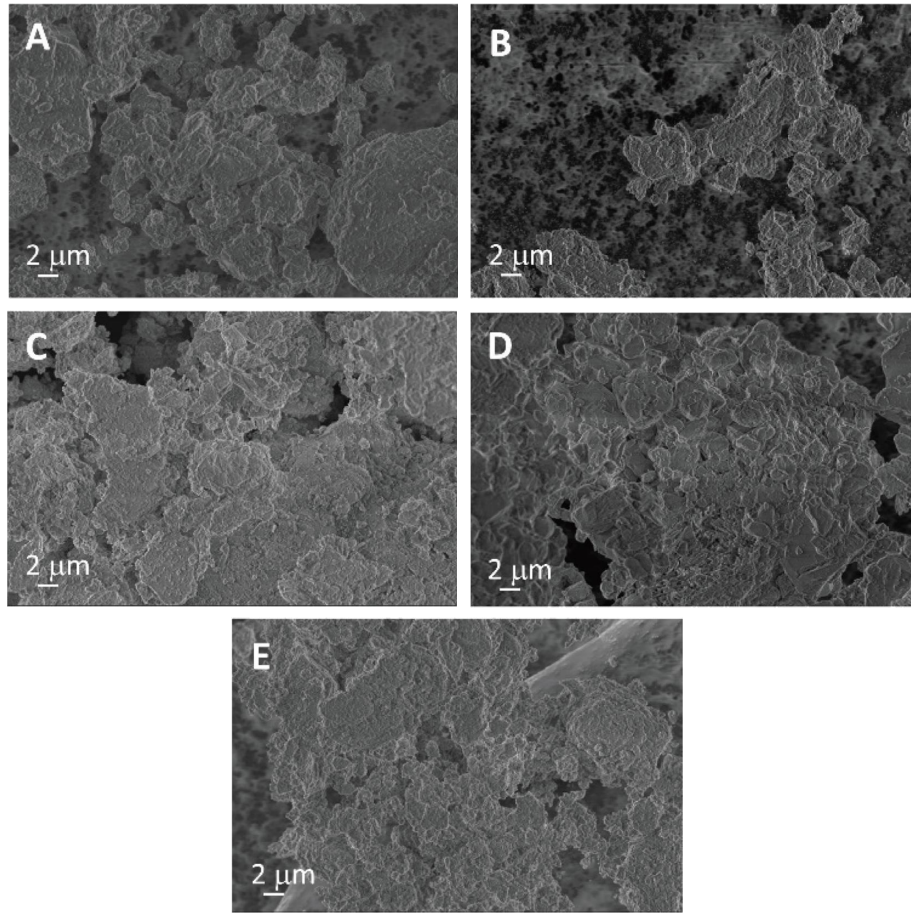


FIGURE 1: SEM images of (a) Z1, (b) Z2, (c) Z3, (d) Z4, and (e) Z5 zeolite.

TABLE 2: The bulk and surface elemental composition of natural zeolite samples.

Zeolites	Analysis	C	O	Si	Al	Ca	Mg	Fe	K	Na	SiO ₂ /Al ₂ O ₃
Z1	XPS	16.3	54.7	17.2	4.9	1.1	0.6	0.2	4.1	0.9	4.01
	EDX	2.9	52.4	30.4	8.5	2.5	1.0	0.6	0.6	1.1	4.08
Z2	XPS	21.0	51.6	15.7	4.0	1.1	0.3	0.2	5.3	0.7	4.43
	EDX	11.7	62.7	18.1	5.7	0.5	0.3	—	0.5	0.5	3.68
Z3	XPS	16.6	54.7	17.1	4.6	1.1	0.7	0.2	4.2	0.9	4.22
	EDX	3.1	64.8	23.5	6.1	1.1	0.5	0.3	0.3	0.3	4.35
Z4	XPS	21.0	57.1	12.9	3.6	4.8	—	0.5	—	—	4.08
	EDX	23.8	59.7	1.7	0.5	11.2	0.1	0.1	1.1	1.8	3.9
Z5	XPS	15.5	55.3	17.1	5.1	1.3	0.6	0.3	3.9	0.9	3.85
	EDX	5.9	66.2	20.2	5.8	0.4	0.2	0.2	0.7	0.4	3.98

Although with decrease in the potassium content of tested Muscat Gordo, SAB and CHA, the sodium content has increased, the concentrations of these metals were within the range common for wines. Few wines generally contain more than 200 mg/L of sodium, and most have less than 100 mg/L. Most wines contain between 500 mg/L and 1,300 mg/L potassium. Foods with less than 140 milligrams of sodium per serving are considered low in sodium.

The calcium concentration in wine after treatment with zeolites Z1, Z2, Z3, and Z5 increased on average from approximately 40 mg/L to approximately 110 mg/L in Muscat Gordo (Figure 3(c)) and from approximately

60 mg/L to approximately 85 mg/L in SAB and CHA wines (Supplementary Materials S3E and S3F), which is still within the typical range for wines averaging 90 mg/L. However, the increase in calcium content in these wines after treatment with Z4 is four to five times the average concentration of white wines. This indicates that zeolites with lower calcium content or low calcium leaching properties should be selected for wine treatment, as presence of calcium may cause instability problems (as calcium tartrate deposits) [37]. Therefore, chemical analysis of calcium is critical to avoid the precipitation of calcium DL tartrate in the bottle.

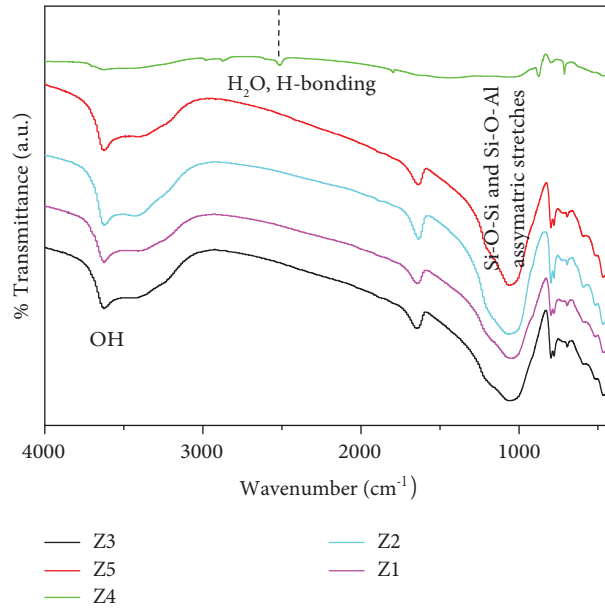


FIGURE 2: FTIR spectra of five natural zeolites used in this work.

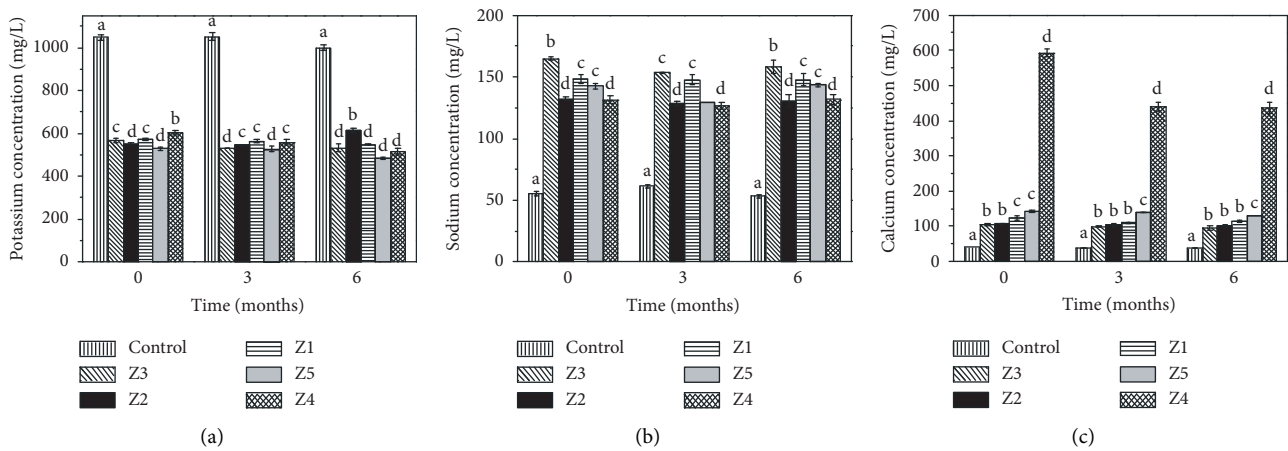


FIGURE 3: Concentration of (a) potassium, (b) sodium, and (c) calcium in control and zeolite-treated muscat gordo wines as a function of time.

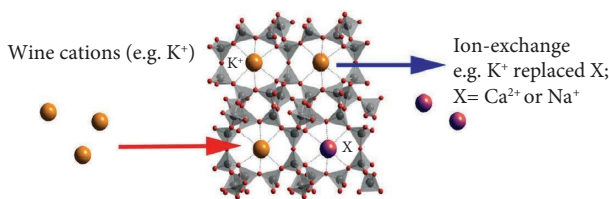


FIGURE 4: Schematic representation of the cation exchange mechanism between potassium ions in the wine and sodium/calcium ions in the zeolite.

3.3. Testing Cold Stability of Wine. A refrigeration/brine test was conducted to determine the cold stability of wines after treatment with zeolites, which is commonly referred to as “crystal quantification.” The weight of precipitated tartaric acid crystals from wine without and with zeolite addition

was measured immediately after zeolite treatment and after three and six months of wine storage in the cellar at 15°C. Figure 5 shows the results for highly cold-unstable Muscat Gordo wine. As it can be seen from Figure 5(a), Z4 was found to be the most effective in removing tartaric acid crystals from the wine. Z4 reduced the concentration of tartaric acid crystals in the wine by 99.4, 99.8, and 100% after treatment and after three and six months of wine storage. Z1, Z2, Z3, and Z5 zeolites were also highly effective. These zeolites reduced the concentration of tartaric acid crystals by an average of 95.5, 98, and 99% after treatment and after three and six months of wine storage. Simultaneously, tartaric acid concentrations in Muscat Gordo wine decreased after treatment with Z1, Z2, Z3, and Z5 zeolites due to reduced KHT crystallisation and precipitation (Figure 5(b)). At the same time, the pH value of the wine changed only minimally. The situation was different when

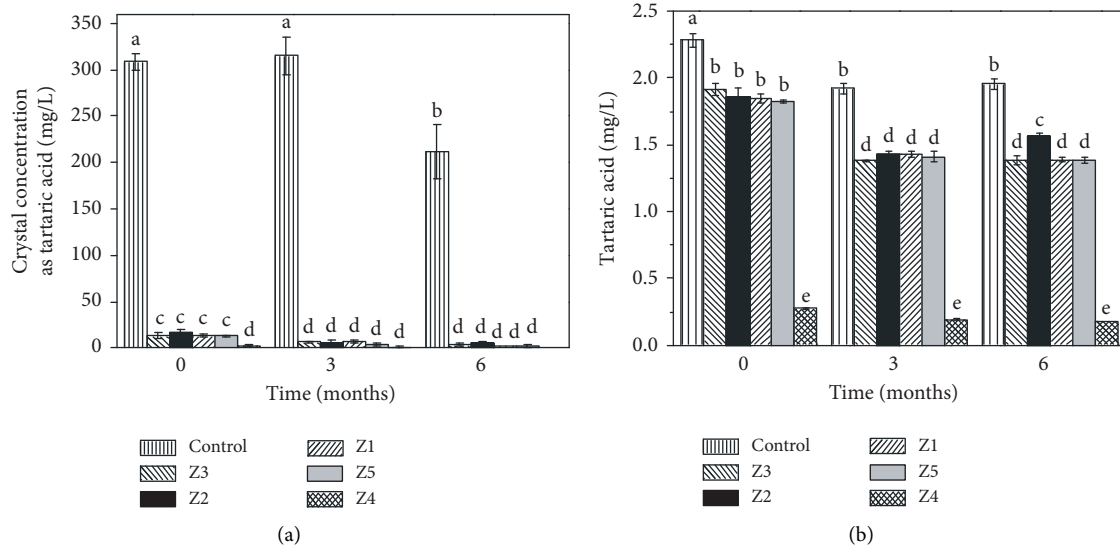


FIGURE 5: Concentration of tartaric acid crystals (a) and tartaric acid (b) in control Muscat Gordo wine and wine treated with natural zeolites.

Muscat Gordo wine was treated with Z4 zeolite. In this case, the tartaric acid concentration decreased so drastically after treatment that the pH of the wine increased from pH 3.6 to pH 5.2. The same high pH was measured for SAB and CHA wines treated with Z4 zeolite. No pH change was observed in these wines after treatment with Z1, Z2, Z3, and Z5 zeolites. An 8% reduction in tartaric acid was observed for SAB and CHA wines when Z1, Z2, Z3, and Z5 zeolites were used for treatment (Supplementary Materials S4C and S4D). However, when SAB and CHA wine were treated with Z4 zeolite, the tartaric acid was almost completely removed (only 2% left), which explains why the pH of these wines increased after treatment.

Sauvignon Blanc was initially cold unstable and remained unstable until three months of storage in the cellar (Supplementary Materials S4A). After treatment with natural zeolite, the concentration of tartaric acid crystals in this wine initially decreased by an average of 92% and by 98% after three months of storage in the cellar. After six months of storage, the wine was almost cold stable even without zeolite addition. Chardonnay was cold stable almost from the beginning, indicating that no treatment was required to cold stabilize the wine (Supplementary Materials S4B).

3.4. Effect of Zeolites on Aluminium Content in Treated Wines. Metal analysis of the treated wines revealed that the aluminium concentration was drastically increased, particularly, after treatment with Z1, Z2, Z3, and Z5 zeolites. As presented in Figure 6(a), the concentration of aluminium in control Muscat Gordo wine was 0.2 mg/L. After treatment, the aluminium concentration increased to 9 mg/L for Z3, Z2, and Z1, to 11 mg/L for Z5 zeolite, and to 2 mg/L for Z4 zeolite. After six months of wine storage in the cellar, these aluminium concentrations dropped to around 7 mg/L for all Australian zeolites. However, the levels were still high.

A high aluminium concentration was also found in SAB and CHA wines after treatment with Z1, Z2, Z3, and Z5 (Supplementary Materials S3G and S3H). At the beginning, the aluminium content was 16 mg/L for Z5. After three and six months of storage, the aluminium content decreased significantly but remained high, between 10 and 5 mg/L after treatment with Z1, Z2, Z3, and Z5 zeolites. A moderate increase was observed for all treated wines after treatment with Z4 zeolite (approximately 1.5-1.6 mg/L). The increase in aluminium content was no surprise, since it is well-documented that, for example, the addition of aluminosilicate minerals such as bentonite contributes to the aluminium content in wines [38]. What was surprising was the magnitude of this increase, which was between twenty-five and thirty-five-fold. After the addition of bentonite, the aluminium content can increase about two-fold [38].

Two processes were used to reduce aluminium release/leaching from zeolites, namely, zeolite dealumination and calcination. Although dealumination is known to reduce aluminium content in zeolites [30, 32, 39, 40], the process was not entirely successful in reducing the aluminium concentration in Muscat Gordo wine after treatment with Z6 dealuminated and Z7 dealuminated (Supplementary Materials S5). Nevertheless, dealuminated zeolites significantly decreased the leaching behaviour of calcium, as shown in Supplementary Materials S5. Contrary to the dealumination process, calcination of zeolite resulted in a substantial decrease in aluminium, as shown in Figures 6(b) and 6(c) for Muscat Gordo and Pinot Grigio wines, respectively. It is known that the calcination process of zeolites stabilises the structure and functional surface when carried out at an appropriate temperature [31, 32, 41]. The calcination treatment significantly reduced aluminium content, bringing it to the acceptable level for wine with lower dose of zeolite required.

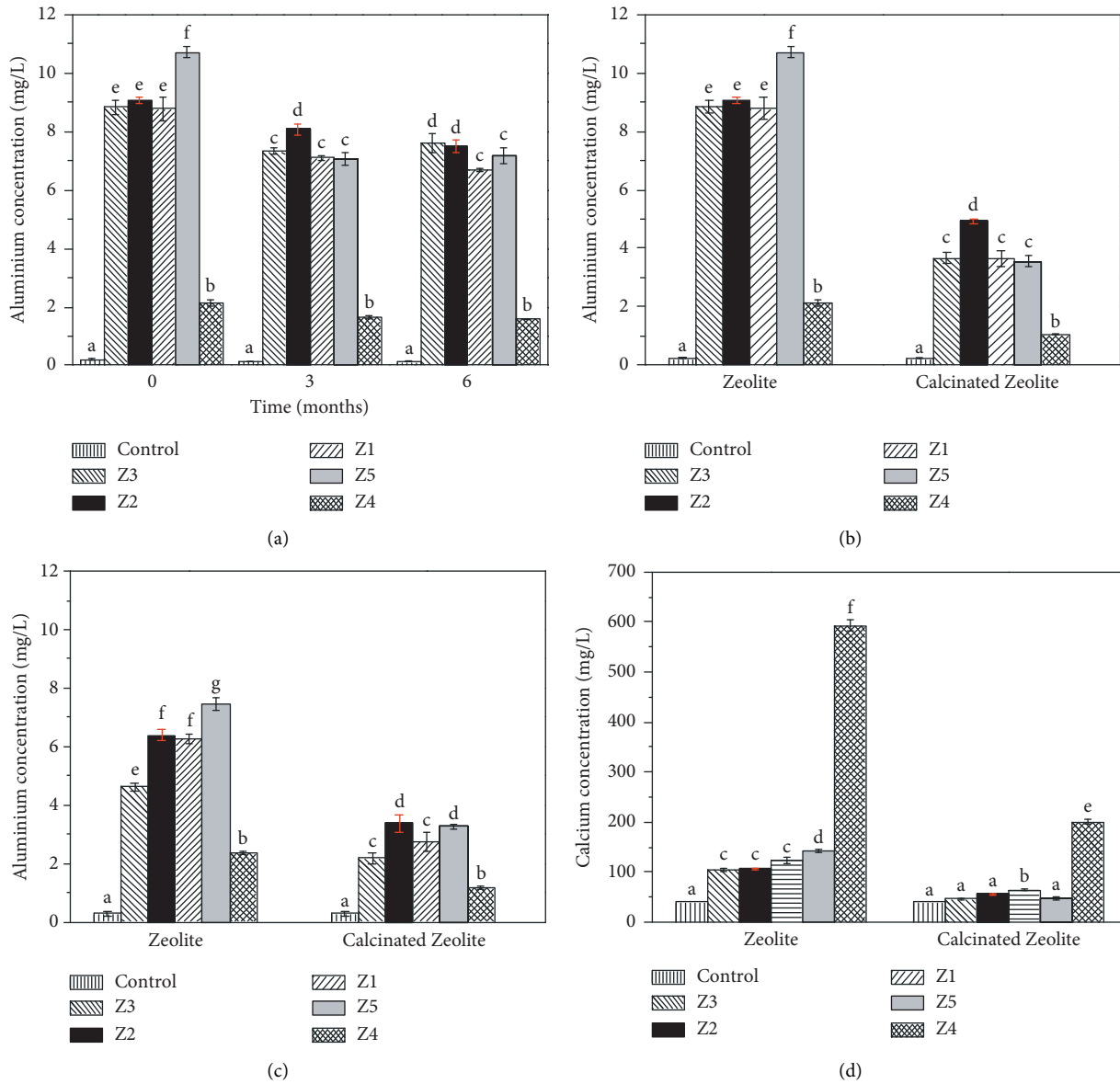


FIGURE 6: (a) Aluminum concentration in Muscat Gordo wine measured initially after zeolite treatment and after three and six months of wine storage in the cellar. Comparison of aluminum content in wines after treatment with zeolites and zeolites calcinated for two hours at 400°C for (b) Muscat Gordo (16 g/L zeolite dose) and (c) pinot grigio (5 g/L zeolite dose). (d) Comparison of calcium content in Muscat Gordo wine after treatment with zeolites and calcinated zeolites.

Aluminium is the most abundant metal and the third most common element in the Earth’s crust. It is found in relatively high concentrations in drinking water, pharmaceutical products, and processed foods. However, only traces of aluminium are found in the human body, as the body does not appear to use aluminium for any biological purpose. The small amount of aluminium that is absorbed by the body is normally excreted by the kidneys in the urine.

The total body burden of aluminium in healthy individuals is 30–50 mg because the skin, lungs, and gastrointestinal tract greatly limit the absorption of aluminium from environmental sources. Concern about the toxicology of aluminium has led to many studies on the analysis of aluminium in foods and beverages and on the relationship

between aluminium intake and the onset of body disorders or malfunctions [42]. Research has shown that there is a huge difference between oral exposure to aluminium, and injected aluminium. For example, less than 1% of ingested aluminium is absorbed through the gastrointestinal tract (between 0.1% and 0.3% according to most studies), whereas 100% of injected aluminium is absorbed over a period of time that can vary depending on the individual’s state of health.

In addition to the toxicity of aluminium, the contamination of wine with this metal (>10 mg/L) can lead to spoilage through haze formation and the generation of undesirable flavours [43]. Several elements, including aluminium (Al), copper (Cu), iron (Fe), manganese (Mn),

TABLE 3: Survey of aluminium in 267 wines *. ©1992 American Society for Enology and Viticulture AJEV 43:166–170.

Al ranges (mg/L)	White	Red	Sparkling	Fortified
Low ≤0.2	0	3	0	0
Intermediate 0.21–2.99	63	148	30	16
High ≥3	4	2	1	0

*Modified with permission from reference [38].

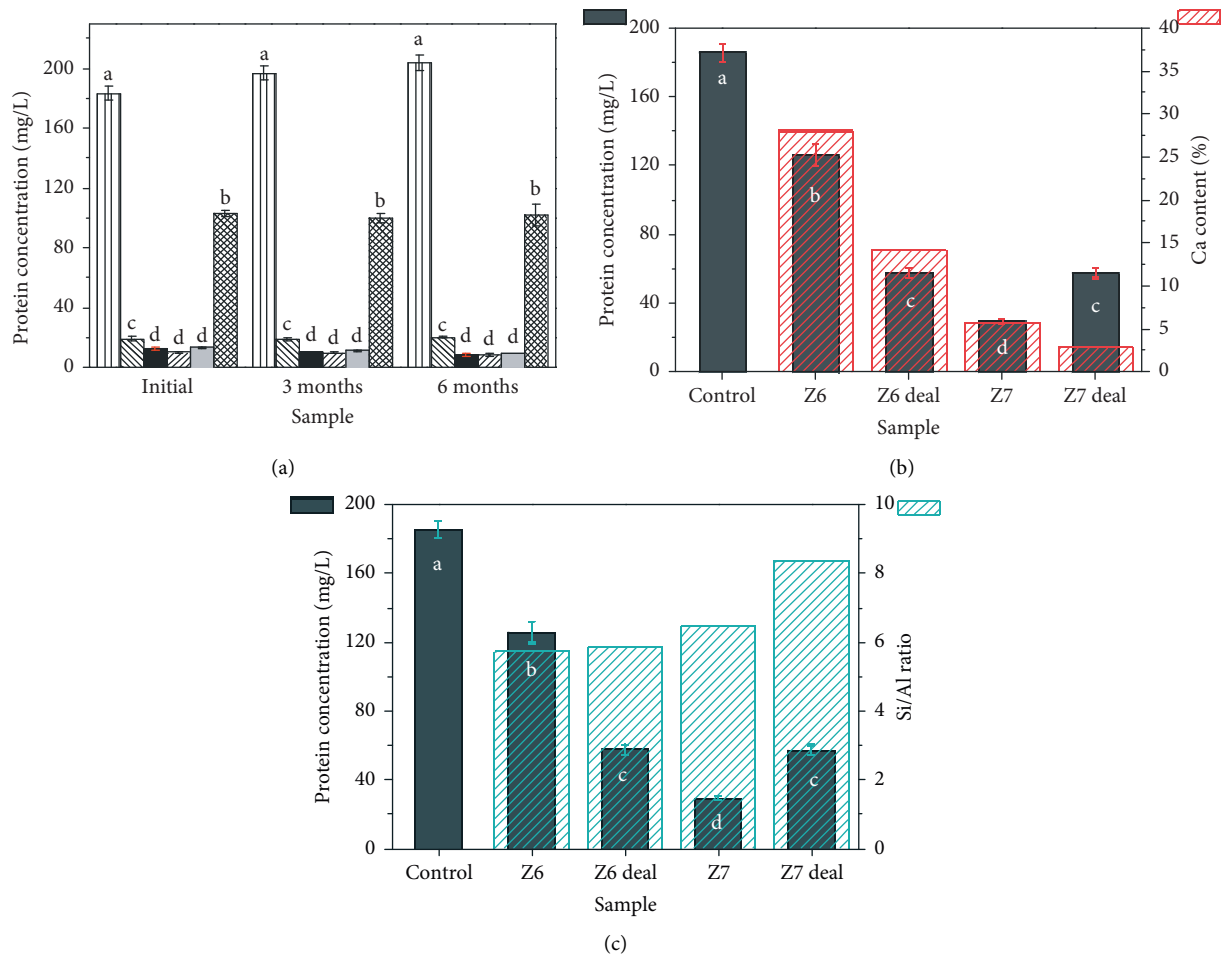


FIGURE 7: (a) Protein concentration in control Muscat Gordo wine and wine after treatment with five different natural zeolites. (b) Protein concentration in control and treated Muscat Gordo wines for Indonesian zeolites with different Ca content (shown in red bars) in the sample. (c) Protein concentration in control and treated Muscat Gordo wines for Indonesian zeolites with different Si/Al ratios (shown in cyan bars).

nickel (Ni), and zinc (Zn), contribute to the haze formation and the change of colour as they tend to form complexes with anthocyanins and tannins [44]. The average aluminium level in wine, based on a simple classification as red, white, sparkling, or fortified is given in Table 3. The suggested maximum aluminium concentration for wine stability is 3 mg/L [43]. In addition, the calcination process also reduced calcium content in the wine after treatment, as presented in Figure 6(d). The decrease in calcium content in Muscat Gordo wine from an average of 120 mg/L for wine treated with zeolite to an average of 54 mg/L for wine treated with calcinated zeolite is a significant improvement. This is

because wines with calcium levels above 70–80 mg/L are considered to be at risk of instability [37]. Lowering the Ca²⁺ content in wine has eliminated the risk of calcium instability in these wines.

3.5. Protein Concentration in Zeolite Treated Wines. As demonstrated in our previous work [23], Indonesian zeolite can protein-stabilize white wines. In this work, we were also able to protein-stabilize Muscat Gordo wine using Z1, Z2, Z3, and Z5 zeolites. Different zeolite doses were required to achieve protein stabilisation. Protein stabilisation was

performed with 8 g/L of Z2 and Z5 zeolite and 10 g/L of Z3 and Z1 zeolite. As shown in Figure 7(a), the protein concentration in the zeolite-treated Muscat Gordo wine was reduced by 90, 94, 94, and 95% after treatment with Z3, Z1, Z5, and Z2 zeolite, respectively, and these wines became heat stable after treatment. SAB and CHA wines could also be made protein stable with Z1, Z2, Z3, and Z5 zeolites. Protein stabilisation of SAB required 6 g/L of Z3 zeolite, 7 g/L of Z5 zeolite, 5 g/L of Z1, and 5 g/L of Z2 zeolites. For protein stabilisation of CHA, the same dose of Z3 and Z5 zeolites was used as for SAB. For Z1 4.5 g/L and for Z2 5.5 g/L to accomplish this task (Supplementary Materials S4E and S4F).

Interestingly, we could not protein-stabilize Muscat Gordo wine with Z4 zeolite, even when 16 g/L zeolite was added to the wine. As can be seen in Figure 7(a), 16 g/L of Z4 zeolite removed only 53% of the proteins. This result was unexpected, as in our previous work, Z4 zeolite protein-stabilized wines with similar protein content to Muscat Gordo (183 mg/L). For example, 6 g/L of Z4 zeolite protein-stabilized Sauvignon Blanc wine with an initial protein content of 182 mg/L or 4 g/L of Z4 zeolite stabilized Semillon wine with 165 g/L initial protein content [23]. A similar, unexpected result was obtained for SAB and CHA. After treatment with 10 g/L Z4 zeolite, the protein concentration in the wines was reduced by 34 and 16% for SAB and CHA wines, respectively, and the wines remained heat unstable (Supplementary Materials S4C and S4D). Interestingly, in our earlier work, we succeeded in making SAB and CHA heat stable after adding 6 g/L of Z4 zeolite [23]. This led us to conclude that even though the two Z4 zeolites used were from the same Indonesian mining company, they must have some significant differences. The differences between the two Z4 zeolite samples were the Ca content and the Si/Al ratio. It is worth noticing that the two samples came from the same Indonesian mining site but from two different batches. In our previously published study, the Ca concentration of the Z4 zeolite measured by EDX was 3.5%. In the current work, the concentration of Ca ions was 11.2%, also measured by EDX.

To examine the role of Ca ions on the protein removal capacity of zeolites, we have used four Indonesian zeolites (Z6, Z6 dealuminated, Z7, and Z7 dealuminated) with different Ca content. The lowest Ca content was 3%, and the highest was 28%. The Si/Al ratio was also different in these samples as presented in Supplementary Material S6. Based on structure-activity studies, as presented in Figures 7(b) and 7(c), we found that zeolites with a lower calcium content (6%) had a better capacity to remove haze-forming proteins from wines than zeolites with higher (14 and 28%) or very low (3%) Ca content. Furthermore, the zeolite with a very high Si/Al ratio (8.4) was less effective in removing haze-forming proteins from wines than the zeolite with a lower Si/Al ratio (6.5). The most effective in removing haze-forming proteins from Muscat Gordo wine was zeolite Z7. This zeolite had a Ca content of 5.8%, and the ratio of Si to Al for this zeolite was 6.5.

The alumina-silicate lattice in the zeolite has an overall negative charge with either sodium (Australian zeolites) or calcium (Indonesian zeolites) ions occupying the interlattice

space. Protein removal takes place by ion exchange. Haze-forming proteins have a net positive charge at wine pH [45–47]. Thus, positively charged proteins can replace sodium or calcium ions and once mixed and settled, the zeolite-protein solids can be removed. Since zeolites can also remove potassium ions through the ion exchange, competition occurs between proteins and potassium ions. Due to its high calcium content, it appears that the Indonesian zeolite removes potassium cations first. Once calcium ions are realised into the treated wine, complexes between protein and calcium might be formed. Proteins bind calcium via the carboxyl groups of glutamic and aspartic acid residues. These complexes present a steric hindrance. As a result, only some proteins and a quarter to half of the protein in these experiments could be removed through zeolite addition. Australian zeolites have sodium ions instead of calcium ions on their surface. It seems that the removal of potassium ions and proteins occurs simultaneously for Australian zeolites.

4. Conclusions

This work demonstrates that zeolites can remove excessive haze proteins and tartaric acid in a single treatment to achieve heat and cold stability, which is a considerable advantage over conventional bentonite fining and refrigeration. One of the main disadvantages of zeolite treatment appears to be relatively high dosage levels, aluminum leaching into a wine after treatment, and that some zeolites are less effective than others at protein removal. However, this work identifies means to address these shortcomings. Unlike bentonites, zeolites can be regenerated for example by treatment with (10%) NaCl solution, which results in a much more sustainable process. Furthermore, calcinating the zeolite before adding it to the wine is an effective method to reduce undesired aluminium leaching. The calcination process also reduces calcium content in the wine after treatment with zeolite, thus eliminating the risk of calcium instability. Based on structure-activity studies, we found that natural zeolites with low calcite content had a better ability to remove haze-forming proteins in wines, making these zeolites more attractive for use as they might induce both heat and cold stability in a single treatment. In addition, zeolites with low calcium content are a lower risk to produce calcium instability in the bottle. Preliminary results presented in this work indicate that zeolites can/may be an effective way to achieve wine cold and heat stability. Further testing and sensory evaluation will be required in the near future to fully validate the usefulness of these products in winemaking.

Data Availability

The data supporting the findings of this study are available within the paper and Supplementary Materials. The data can also be available upon request from the corresponding author.

Conflicts of Interest

The authors declare that they have no conflicts of interest.

Acknowledgments

The authors would like to thank AWITC for sponsoring the special issue of the Australian Journal of Grape and Wine Research and for covering the article processing charges. The authors would also like to thank Affinity Labs staff, Mr. Matthew Wheal, for analysing the metals in wines and Accolade Wines, Australia, for donating unfinned wines for this research. The Australian Wine Research Institute, a member of the Wine Innovation Cluster in Adelaide, is supported by Australian grape growers and winemakers through their investment body, Wine Australia, with matching funds from the Australian Government.

Supplementary Materials

Supplementary 1: The following are available online at the publisher's website: <https://wiley.com/doi>. Supplementary 2: S1: Basic chemical analysis of the wines used in this study. Supplementary 3: S2: XRD of natural zeolite samples. Supplementary 4: S3: Potassium concentration in control and zeolite treated A SAB and B CHA wines as a function of time. Sodium concentration in control and zeolite-treated C SAB and D CHA wines as a function of time. Calcium concentration in control and zeolite-treated E SAB and F CHA wines as a function of time. Aluminum concentration in G SAB and H CHA wine measured initially after zeolite treatment and after three and six months of wine storage in the cellar. Supplementary 5: S4: Concentration of tartaric acid crystals in control wine and wine treated with natural zeolites, A SAB, and B CHA. Tartaric acid content in C SAB and D CHA measured directly after treatment and three and six months later after storage in the cellar. Protein concentration in control wine and wine after treatment with five different natural zeolites, E SAB, and F CHA. Supplementary 6: S5: Aluminium and calcium concentration in control and zeolite-treated wines including dealuminated zeolites. Supplementary 7: S6: Si/Al ratio and Ca content in Indonesian zeolites. (*Supplementary Materials*)

References

- [1] C. Lasanta and J. Gomez, "Tartrate stabilization of wines," *Trends in Food Science & Technology*, vol. 28, no. 1, pp. 52–59, 2012.
- [2] M. Dharmadhikari, "Methods for tartrate stabilization of wine," 2016, <https://www.extension.iastate.edu/wine/wp-content/uploads/2021/09/Methods-for-Tartrate-Stabilization-of-Wine-PDF.pdf>.
- [3] A. Massot, M. Mietton-Peuchot, C. Peuchot, and V. Milisic, "Nanofiltration and reverse osmosis in winemaking," *Desalination*, vol. 231, no. 1-3, pp. 283–289, 2008.
- [4] H. Mira, P. Leite, J. M. Ricardo-da-Silva, and A. S. Curvelo-Garcia, "Use of ion exchange resins for tartrate wine stabilization," *OENO One*, vol. 40, no. 4, pp. 223–246, 2006.
- [5] S. Fok, "PG&E studies electro dialysis for cold stability," *Practical Winery & Vineyard Journal*, vol. 29, no. 9, pp. 51–55, 2008.
- [6] R. Guise, L. Filipe-Ribeiro, D. Nascimento, O. Bessa, F. Nunes, and F. Cosme, "Comparison between different types of carboxymethylcellulose and other oenological additives used for white wine tartaric stabilization," *Food Chemistry*, vol. 156, pp. 250–257, 2014.
- [7] B. W. Zoecklein, *Wine Analysis and Production*, Chapman & Hall, New York, NY, USA, 1995.
- [8] C. Theron, *The Use of Mannoproteins for the Tartrate Stabilisation of Wine*, Wynboer. WineLand, Paarl, South Africa, 2007.
- [9] N. Scrimgeour, T. Almond, and E. Wilkes, "Is KPA the magic bullet for tartrate instability in wines?" in *Australian & New Zealand Grapegrower & Winemaker*, pp. 68–70, Grapegrower & Winemaker, Auckland, New Zealand, 2020.
- [10] D. W. Breck, *Zeolite Molecular Sieves*, Wiley, New York, NY, USA, 1974.
- [11] R. Szostak, *Molecular Sieves: Principles of Synthesis and Identification*, Blackie A & P, London, UK, 2 edition, 1998.
- [12] L. H. Chen, M. H. Sun, Z. Wang, W. Yang, Z. Xie, and B. L. Su, "Hierarchically structured zeolites: from design to application," *Chemistry Review*, vol. 120, no. 20, pp. 11194–11294, 2020.
- [13] P. Mierczynski, M. Mosinska, L. Szkudlarek et al., "Biodiesel production on monometallic Pt, Pd, Ru, and Ag catalysts supported on natural zeolite," *Materials*, vol. 14, no. 1, p. 48, 2020.
- [14] P. Mierczynski, L. Szkudlarek, K. Chalupka et al., "The effect of the activation process and metal oxide addition (CaO, MgO, SrO) on the catalytic and physicochemical properties of natural zeolite in transesterification reaction," *Materials*, vol. 14, no. 9, p. 2415, 2021.
- [15] V. L. B. Fuss, G. Bruj, L. Dordai, M. Roman, O. Cadar, and A. Becze, "Evaluation of the impact of different natural zeolite treatments on the capacity of eliminating/reducing odors and toxic compounds," *Materials*, vol. 14, no. 13, p. 3724, 2021.
- [16] S. K. Wahono, Hernawan, A. Kristiani, S. Tursiloadi, and H. Abimanyu, "Characterization and utilization of gunungkidul natural zeolite for bioethanol dehydration," *Energy Procedia*, vol. 47, pp. 263–267, 2014.
- [17] E. P. Favvas, C. G. Tsanaktisidis, A. A. Sapalidis, G. T. Tzilantonis, S. K. Papageorgiou, and A. C. Mitropoulos, "Clinoptilolite, a natural zeolite material: structural characterization and performance evaluation on its dehydration properties of hydrocarbon-based fuels," *Microporous and Mesoporous Materials*, vol. 225, pp. 385–391, 2016.
- [18] E. Chmielewska, "Natural zeolite: alternative adsorbent in purification or post-treatment of waters," *Modified Clay and Zeolite Nanocomposite Materials: Environmental and Pharmaceutical Applications*, vol. 10, pp. 87–112, 2019.
- [19] A. Sadchikov, S. Mitrofanov, V. Sokolov, and S. Naumov, "Use of natural zeolite in systems for separation and purification of gas mixtures containing methane," *Key Engineering Materials*, vol. 736, pp. 179–182, 2017.
- [20] S. K. Wahono, A. A. Dwiatmoko, A. Cavallaro et al., "Amine-functionalized natural zeolites prepared through plasma polymerization for enhanced carbon dioxide adsorption," *Plasma Processes and Polymers*, vol. 18, no. 8, Article ID 2100028, 2021.
- [21] S. K. Wahono and W. A. Rizal, "Biogas filter based on local natural zeolite materials," *International Journal of Renewable Energy Development*, vol. 3, no. 1, pp. 1–5, 2014.
- [22] P. Misaelides, "Application of natural zeolites in environmental remediation: a short review," *Microporous and Mesoporous Materials*, vol. 144, no. 1-3, pp. 15–18, 2011.
- [23] A. Mierczynska-Vasilev, S. K. Wahono, P. A. Smith, K. Bindon, and K. Vasilev, "Using zeolites to protein stabilize

- white wines," *ACS Sustainable Chemistry & Engineering*, vol. 7, no. 14, pp. 1583–12247, 2019.
- [24] C. Wyss and P. Cuénat, "Stabilisation tartrique des vins par traitement aux zéolithes," *Revue Suisse. Revue Suisse Vitic., Arboric., Hortic.*, vol. 37, no. 6, pp. 341–347, 2005.
- [25] E. J. Sonneveld and J. W. Visser, "Automatic collection of powder data from photographs," *Journal of Applied Crystallography*, vol. 8, no. 1, pp. 1–7, 1975.
- [26] E. P. Barrett, L. G. Joyner, and P. P. Halenda, "The determination of pore volume and area distributions in porous substances I Computations from nitrogen isotherms," *Journal of the American Chemical Society*, vol. 73, no. 1, pp. 373–380, 1951.
- [27] A. Mierczynska-Vasilev, P. Boyer, K. Vasilev, and P. A. Smith, "A novel technology for the rapid, selective, magnetic removal of pathogenesis-related proteins from wines," *Food Chemistry*, vol. 232, pp. 508–514, 2017.
- [28] E. Kouvelos, K. Kesore, T. Steriotis et al., "High pressure N₂/CH₄ adsorption measurements in clinoptilolites," *Microporous and Mesoporous Materials*, vol. 99, no. 1-2, pp. 106–111, 2007.
- [29] M. Sakizci and L. Ozgul Tanriverdi, "Influence of acid and heavy metal cation exchange treatments on methane adsorption properties of mordenite," *Turkish Journal of Chemistry*, vol. 39, no. 5, pp. 970–983, 2015.
- [30] S. K. Wahono, P. Dwi Joko, J. Tri Hadi et al., "Multi-stage dealumination for characteristic engineering of mordenite-clinoptilolite natural zeolite," in *Proceedings of the 11th Regional Conference on Chemical Engineering (Rcche 2018)*, vol. 2085, Article ID 20044, Tangerang, Indonesia, November 2019.
- [31] S. K. Wahono, P. Dwi Joko, J. Tri Hadi et al., "Transformation of mordenite-clinoptilolite natural zeolite at different calcination temperatures," in *Proceedings of the 2nd International Conference on Natural Products and Bioresource Sciences - 2018*, vol. 251, Article ID 12009, Tangerang, Indonesia, November 2019.
- [32] S. K. Wahono, J. Stalin, J. Addai-Mensah, W. Skinner, A. Vinu, and K. Vasilev, "Physico-chemical modification of natural mordenite-clinoptilolite zeolites and their enhanced CO₂ adsorption capacity," *Microporous and Mesoporous Materials*, vol. 294, Article ID 109871, 2020.
- [33] D. Kallo, "Applications of natural zeolites in water and wastewater treatment," *Reviews in Mineralogy and Geochemistry*, vol. 45, no. 1, pp. 519–550, 2001.
- [34] D. Bonenfant, M. Kharoune, P. Niquette, M. Mimeault, and R. Hausler, "Advances in principal factors influencing carbon dioxide adsorption on zeolites," *Science and Technology of Advanced Materials*, vol. 9, no. 1, pp. 13007–13014, 2008.
- [35] H. Lin and L. Wang, "Physicochemical properties and mechanism study of clinoptilolite modified by NaOH," *Microporous and Mesoporous Materials*, vol. 218, pp. 174–179, 2015.
- [36] R. P. Townsend and E. N. Coker, "Ion exchange in zeolites," *Studies in Surface Science and Catalysis*, vol. 137, pp. 467–524, 2001.
- [37] B. C. Rankine, *Making Good Wine: A Manual of Winemaking Practice for Australia and New Zealand*, Sun Books, Melbourne, Australia, 1989.
- [38] A. J. Mckinnon, R. W. Cattrall, and G. R. Scollary, "Aluminum in wine - its measurement and identification of major sources," *American Journal of Enology and Viticulture*, vol. 43, no. 2, pp. 166–170, 1992.
- [39] C. Wang, S. Leng, H. Guo et al., "Quantitative arrangement of Si/Al ratio of natural zeolite using acid treatment," *Applied Surface Science*, vol. 498, Article ID 143874, 2019.
- [40] A. Dziedzicka, B. Sulikowski, and M. Ruggiero-Mikolajczyk, "Catalytic and physicochemical properties of modified natural clinoptilolite," *Catalysis Today*, vol. 259, pp. 50–58, 2016.
- [41] J. Lu, Z. Zhao, C. Xu, A. Duan, and P. Zhang, "Effects of calcination temperature on the acidity and catalytic performances of HZSM-5 zeolite catalysts for the catalytic cracking of n-butane," *Journal of Natural Gas Chemistry*, vol. 14, pp. 213–220, 2005.
- [42] C. Exley, "The toxicity of aluminium in humans," *Morphologie*, vol. 100, no. 329, pp. 51–55, 2016.
- [43] B. Rankine, "Aluminum haze in wine," *The Australian wine brewing and spirit review*, vol. 80, pp. 14–15, 1962.
- [44] I. Esparza, I. Salinas, C. Santamaria, J. Garcia-Mina, and J. Fernandez, "Electrochemical and theoretical complexation studies for Zn and Cu with individual polyphenols," *Analytica Chimica Acta*, vol. 543, no. 1-2, pp. 267–274, 2005.
- [45] F. Brissonnet and A. Maujean, "Characterization of foaming proteins in a champagne base wine," *American Journal of Enology and Viticulture*, vol. 44, no. 3, pp. 297–301, 1993.
- [46] R. B. Ferreira, S. Monteiro, M. A. Picarra-Pereira, M. C. Tanganho, V. B. Loureiro, and A. R. Teixeira, "Characterization of the proteins from grapes and wines by immunological methods," *American Journal of Enology and Viticulture*, vol. 51, no. 1, pp. 22–28, 2000.
- [47] J. C. Hsu and D. A. Heatherbell, "Isolation and characterization of soluble-proteins in grapes, grape juice, and wine," *American Journal of Enology and Viticulture*, vol. 38, no. 1, pp. 6–10, 1987.

Research Article

Assessing the Short-Term Effects of No-Till on Crop Yield, Greenhouse Gas Emissions, and Soil C and N Pools in a Cover-Cropped, Biodynamic Mediterranean Vineyard

Cristina Lazcano ¹, Noelymar Gonzalez-Maldonado ¹, Erika H. Yao ¹,
Connie T. F. Wong ^{1,2}, Mia Falcone ², Jean Dodson Peterson ³, L. Federico Casassa ⁴,
Bwalya Malama ² and Charlotte Decock ²

¹Department of Land, Air and Water Resources, University of California Davis, Davis, CA 95616, USA

²Natural Resources Management and Environmental Sciences Department, California Polytechnic State University, San Luis Obispo, CA 93407, USA

³Department of Viticulture and Enology, Washington State University, 2710 Crimson Way, Richland, WA 99354, USA

⁴Wine and Viticulture Department, California Polytechnic State University, San Luis Obispo, CA 93407, USA

Correspondence should be addressed to Cristina Lazcano; clazcano@ucdavis.edu

Received 26 August 2022; Revised 30 September 2022; Accepted 5 October 2022; Published 1 December 2022

Academic Editor: Paul Petrie

Copyright © 2022 Cristina Lazcano et al. This is an open access article distributed under the Creative Commons Attribution License, which permits unrestricted use, distribution, and reproduction in any medium, provided the original work is properly cited.

Background and Aims. No-till is considered a core practice of conservation and climate-smart agriculture. Nevertheless, recent evidence suggests that the benefits of this practice for climate change mitigation might be overestimated, particularly in the short term. **Methods and Results.** In a three-year field experiment, we investigated the environmental and agronomic performance of this practice by looking at changes in soil physical properties, C and N pools, as well as vine yield and grape quality. No-till increased stratification in the distribution of active soil C (POXC), further accentuating the already existing difference between top and subsoil. No-till also slightly reduced the daily efflux of CO₂ from the soil during the rainy season, showing that these plots were less prone to lose C than tilled plots. Nonetheless, no-till did not increase total soil C stocks. This, together with the lack of differences in cumulative N₂O emissions, resulted in similar global warming potential in till and no-till plots. Vine yield and grape quality remained unchanged in the no-till compared to the tilled plots. **Conclusions.** Even though no-till did not result in short-term climate change mitigation, results of this study suggest changes in the ecological processes leading to C accumulation and mineralization and that may result in future C sequestration. There were no deleterious effects of no-till on grape yield and quality. **Significance of the Study.** This study shows that reducing tillage intensity in vineyards is a feasible strategy from an agronomic standpoint.

1. Introduction

Soil organic matter (SOM) provides a basal resource for the soil food web and is therefore considered to be the foundation of a healthy soil ecosystem. SOM dynamics including processes of mineralization, and stabilization, strongly regulate the release of greenhouse gases such as CO₂ and N₂O, and the sequestration of carbon (C) with consequences for climate change mitigation [1, 2]. The use of cover crops is

a well-recognized strategy to diversify cropping systems while increasing SOM and sequestering C [3–5]. Both above and belowground biomass of cover crops contributes to litter production and to the increase in soil C stocks in Mediterranean vineyards [3, 6]. The production of root exudates can also contribute to substantial amounts of C sequestration (Sokol et al., 2019). Nonetheless, cover crop management has large implications for the climate change mitigation potential of this practice.

Tillage is commonly used to incorporate cover crop residues into the soil and it is estimated that more than 90% of cultivated land worldwide is subjected to some degree of tillage [7]. In winegrape production, tillage is also commonly used to increase soil porosity and to manage weeds under the vines during the growing season. This practice is particularly critical for biodynamic vineyards where the use of synthetic herbicides is precluded [8]. There is a large amount of conflicting evidence on the effects of tillage and tillage intensity on SOM and C sequestration, and therefore, its potential to mitigate climate change [9–11]. Tillage promotes the rapid incorporation of plant residues and oxygenation of the soil, increasing microbial biomass and activity and therefore accelerating nutrient cycling. A large body of scientific evidence shows that this boost in decomposition rates triggers large emissions of CO₂ and therefore reduces the net amount of plant C sequestered in soils [12–14]. The disruption of soil aggregates leads to the exposure of previously protected C to microbial attack, further increasing soil C losses [15–17]. Destruction of soil structure has other associated negative effects on soil health, such as soil compaction and consequently reducing water infiltration and plant-available water [15].

In light of all the concurrent evidence described above, no-till is considered a core practice of conservation and climate-smart agriculture [18]. Nevertheless, the benefits of this practice for climate change mitigation are not yet clear. It has been suggested that no-till causes the redistribution and stratification of C within the soil profile, rather than a net increase, leading to the overestimation of C increases when only the topsoil (<10 cm depth) is analyzed [15, 19, 20]. While CO₂ emissions typically decrease under no-till [21], several studies suggest potential tradeoffs through the short-term increase in denitrification rates and release of N₂O, a greenhouse gas with a global warming potential 298 times higher than CO₂ [22–24]. This increase in N₂O emissions is associated with higher bulk density and anaerobic microsites under no-till [25], which have been suggested to be particularly relevant shortly after the transition to no-till but disappear in the long term as soil C accumulation leads to decreases in bulk density [26]. This means that the capacity of no-till to mitigate climate change may be overstated, at least in the short-term [27]. Some studies show high rates of SOM accumulation, higher C stabilization, and lower GHG emissions in highly disturbed tilled soils, due to a more efficient transformation of plant residues into microbial biomass and mineral-associated organic matter [28, 29].

Under certain crops and conditions, transition to no-till could decrease yields [30]. Data regarding the potential effects of no-till for winegrape production is still scarce but some studies have shown changes in fruit quality related to increases in grape anthocyanin contents [31], decrease in phenolic content [32] or no changes in fruit yield and quality [33]. This uncertainty regarding the benefits of no-till for climate change mitigation, crop yield, and quality increases farmer reluctance to incorporate this conservation practice. The lack of data is particularly critical in arid and semi-arid regions where issues of soil degradation and climate change

are most acute and where soil organic matter accumulates more slowly [34, 35]. As a perennial crop of large relevance in many semiarid regions, wine grapes could be critical in the conservation of soil resources when managed properly [36].

In this study, we evaluated the short-term effects of transitioning to no-till on the yield and quality of Syrah grapes, soil C and N pools, soil biophysical properties, and greenhouse gas emissions in a biodynamically-managed vineyard. This study builds on the study by Lazcano et al. [37]; which evaluated the combined effects of sheep grazing and tillage on soil C and GHG emissions during a 2-year period. We hypothesized that, after three years, no-tilled soils would show higher soil organic matter, active C aggregate stability, and infiltration rates. We also expected that no-tilled soils would also show a strong stratification in soil C, with shallow soil depth (0–15 cm) having significantly more C than the soil at 15–30 cm, whereas tilled soils would show a homogeneous distribution of soil C throughout the 30 cm depth.

2. Material and Methods

2.1. Experimental Design. A three-year field trial was conducted between April 2018 and February 2021 in a *Vitis vinifera* L. cv. Syrah (Dureza × Mondeuse Blanche) biodynamic commercial vineyard located in the Paso Robles American Viticulture Area (AVA), San Luis Obispo County (California, USA). The study was conducted in parallel to a two-year grazing and tillage trial as described in Lazcano et al. [37]. The climate in the area is Mediterranean with an annual average temperature of 15.3°C, average annual rainfall of 364 mm, and two well-differentiated seasons, the dry (April–October) and the wet season (November–March) (Figure 1). The soil at the experimental site is a linne-calodo complex classified as 12% Linne (Fine-loamy, mixed, thermic Calcic Pachic Haploxerolls) and 10–11% Calodo (Loamy, mixed, thermic, shallow Calcic Haploxerolls), with 30% clay. This soil is characterized by 6% CaCO₃ in the <2 mm fraction and a pH of 8.2.

The rootstock (140 RU, *Vitis* parentage *berlandieri* × *rupestris*) was planted in 1992 and grafted to Syrah in 2004 (Beaucastel clone “C”). Since vine establishment, soil management included annual seeding of a cover crop mix in the fall (15% *Avena sativa*, 30% *Vicia faba*, 20% *Vicia americana*, 10% *Vicia sativa*, and 25% *Pisum sativum* subsp. *Dundale*). Fertilizer management consists of broadcasting grape pomace compost (C:N ratio of 16.5) at a rate of 11 t·ha⁻¹ once a year in the fall. The vineyard has been tilled and subjected to compost application and sheep grazing during the dormant season (November–March) for around 6 to 8 years. Vines are watered using drip irrigation once after harvest to replenish the soil profile and, when necessary, through the growing season using visual cues of plant water stress.

We assessed the short-term effects of transitioning to no-till on soil C, N, and greenhouse gas emissions. The experimental design consisted of alternating till and no-till blocks, each block with four rows of vines and three tractor rows. Till and no-till blocks were not randomized but

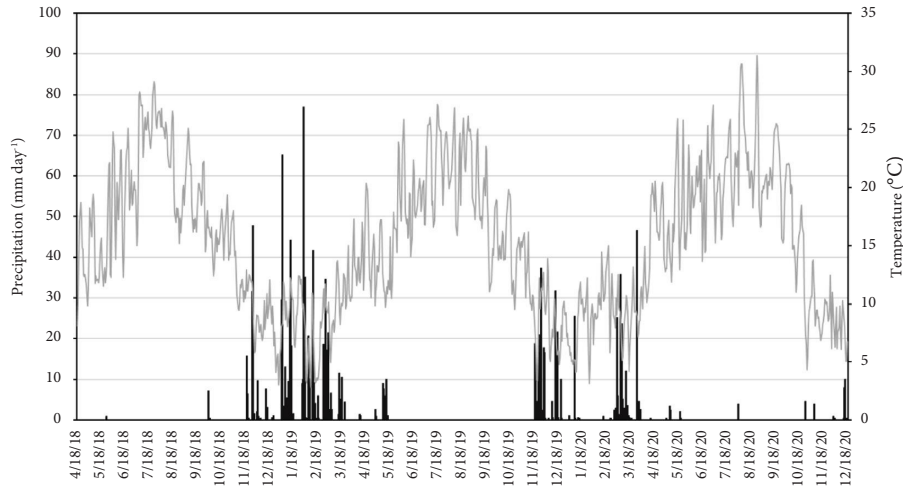


FIGURE 1: Precipitation and temperature were registered at the experimental site over the course of the study.

alternated side by side. Each treatment (till or no-till) was replicated four times, resulting in a total of 8 experimental plots. Within each plot, two functional locations, receiving different soil management, were considered: (1) the soil under the vine canopy (vine row), which receives water and is not tilled, and (2) the soil in the alleys (tractor row), which does not receive water through irrigation and may be tilled, depending on the treatment.

Management of the experimental plots included compost and cover crop seed broadcasting in Autumn each year during the wet seasons; mowing of the cover crop in the Autumn and Spring during the wet season when the cover crop reached sufficient height (30 cm approx.) (as described in [37]). Till plots were tilled a total of four times (November 2018, May 2019, November 2019, and May 2020) using a three-point offset disk to 10–25 cm depth, with two tractor passes in each event. No-till plots were left undisturbed and only mowed for the duration of the experiment (3 years).

2.2. Soil and Plant Sampling and Analysis. Aboveground cover crop biomass was measured three times during the study (April 2018, April 2019, and February 2020) by using a 1 m² quadrant as described in Lazcano et al. [37]. Total C and N were determined in dried and ground cover crop samples via dry combustion using a Vario Max CNS elemental analyzer (Elementar, Langensfeld, Hesse, Germany).

In March 2021 after three years of treatment implementation, we collected soil samples at the two functional locations within the central vine and tractor rows of each plot. Soil samples were collected to 30 cm depth using a Giddings manual bulk soil core sampler with a diameter of 5 cm (Windsor, CO, USA) and immediately split into two depths (0–15 and 15–30 cm). Additional soil samples were collected to a depth of 15 cm at the time of gas sample collection, directly after the tillage treatments and after harvest. Soils were stored in plastic bags at 4°C and transported to the lab prior to analysis. Grape yields were determined in mid-September in 2018, 2019, and 2020, when

berries reached approximately 23°C Brix. To determine yields we randomly selected 10 vines from the two central rows of each plot and measured the total number and fresh weight of all grape bunches on each vine [37]. A subsample of 200 berries was collected in each plot for further chemical analysis. Berries were homogenized to measure berry anthocyanins and total phenolics following a previously published protocol [37, 38].

Infiltration rates were determined in March 2021 at the time of soil sampling using mini-disk infiltrometers (METER Group Inc., USA). Soil moisture was determined gravimetrically by oven drying at 105°C for 24 hours. Soil bulk density (g cm⁻³) was determined based on the known volume of the soil core, the fresh weight of the soil core, and the gravimetric moisture content of the fresh soil sample. No significant amount of gravel was detected in the samples. Soil moisture was determined gravimetrically by oven drying at 105°C for 24 hours. Soil water-filled pore space (%WFPS) was calculated using the soil gravimetric water content (*w*) as follows:

$$\%WFPS = \frac{(w * \text{bulk density})}{[1 - (\text{bulk density}/2.65)]} * 100\%. \quad (1)$$

The water holding capacity of the soil samples was determined gravimetrically by determining the difference between the soil weight at field capacity and permanent wilting point. Aggregate stability was determined as the percentage of soil remaining on a 250 μm sieve after wet sieving. Ten grams of air-dried soil was placed on a 250 μm sieve and submerged in deionized water for 5 minutes to allow for rewetting. Subsequently, wet sieving took place by oscillating the sieve at a constant speed for 2 minutes. The soil remaining on the sieve was recovered and oven dried for the determination of the percent aggregate stability.

Total C and N were determined in dried and ground soil samples via dry combustion using a Vario Max CNS elemental analyzer. Combustion at 650°C was used to account for the maximum recovery of organic C and minimal inorganic C recovery [37, 39, 40]. Nitrate (NO₃⁻-N) and

ammonium ($\text{NH}_4^+\text{-N}$) in soil samples were determined colorimetrically in 2 M potassium chloride (KCl) soil extracts [41] using a Thermo Scientific Evolution 201 UV-visible spectrophotometer (Madison, Wisconsin, USA). Active C, also known as permanganate oxidizable carbon (POXC), was determined in 2.5 g air-dried soil samples based on a reaction with 2 M potassium permanganate (KMnO_4), after which the color change was determined on a spectrophotometer (Milton Roy, Houston, TX) at 550 nm [42].

Microbial biomass C (MBC) was determined through the fumigation-extraction method. Briefly, a soil subsample (6 g fresh weight) was subjected to fumigation with chloroform for 24 h prior to extraction with 0.5 M K_2SO_4 . In parallel, a second subsample was directly extracted with 0.5 M K_2SO_4 without fumigation. The concentration of dissolved organic C (DOC) was analyzed in fumigated and nonfumigated samples on a Dohrmann Phoenix 8000 UV-persulfate oxidation analyzer (Tekmar-Dohrmann, Cincinnati, OH). Microbial biomass C was calculated as the DOC in the fumigated minus the nonfumigated soil samples with a K_e factor of 0.35 (Horwath and Paul, 1994; Vance et al., 1987).

2.3. Analysis of Soil N_2O and CO_2 Emissions. Gas samples from the experimental plots were collected one day before and for 4-5 days after each of the main management events including mowing, tillage, irrigation, and harvest as well as after the first precipitation event in fall, to measure baseline and event-related fluxes. Sampling was done once a month between these management events as described in Lazcano et al. [37]. Fluxes of N_2O and CO_2 were measured using static flux chambers [43] made of two PVC rings (20 cm diameter and 12 cm height): a bottom ring or collar and a cap covered with insulating reflective material to reduce heating within the chamber. The chambers were vented and equipped with a thermocouple to track changes in chamber temperature during chamber closure. The collars were inserted into the soil to a depth of approximately 10 cm in the central tractor and vine row in each plot [37]. During flux measurements, the collars were capped, and gas samples were taken with an air-tight polypropylene syringe by slowly withdrawing 20 mL of gas through sampling ports capped with rubber septa. Gas samples were immediately transferred from the syringe into pre-evacuated 12-mL Exetainer glass vials (Labco Ltd., Buckinghamshire, UK). Gas samples were collected at regular time intervals of 0, 15, 30, and 45 min after chamber closure [37].

Gas samples were transported to the laboratory and analyzed on a Shimadzu GC-2014 gas chromatograph (Shimadzu Scientific, Kyoto, Japan). N_2O and CO_2 concentrations in the samples were calculated using a calibration curve based on a set of analytical grade standards. Chamber gas concentrations were converted to mass per volume units assuming ideal gas relations using chamber air temperature values [44]. Fluxes were calculated from the rate of change in chamber N_2O and CO_2 concentration over the sampling intervals, taking into account chamber

volume and soil surface area [37, 43, 45]. When the data had a nonlinear trend, the slope to the first derivative of the second-order polynomial was used as the flux, rather than the linear model, using the Microsoft Excel LINEST function [46]. Fluxes were not considered when the fit to the linear or LINEST function was poor ($R^2 < 0.80$). Cumulative emissions were determined by trapezoidal integration of daily fluxes measured in each chamber over a specific period (management events or baseline measurements between events). Cumulative emissions from each chamber location were calculated under the assumption that the measured fluxes represent mean daily fluxes, and that means daily fluxes change linearly between measurements [37]. Global warming potential (GWP) was calculated as follows:

$$\text{GWP} = \Delta\text{SOC}(\text{kg CO}_2\text{eq ha}^{-1}) + \text{N}_2\text{O}(\text{kg CO}_2\text{eq ha}^{-1}), \quad (2)$$

where ΔSOC is the difference between soil C stocks, in $\text{kg}\cdot\text{ha}^{-1}$, between 2018 and 2021. The change in soil C stock was then transformed to CO_2 equivalents by multiplying by 44/12. N_2O ($\text{kg CO}_2\text{eq}\cdot\text{ha}^{-1}$) is the cumulative emissions over the period of the study multiplied by 273.

2.4. Data Analysis. General linear models were used to evaluate the effects of tillage and functional location on the average daily emissions, cumulative emissions of N_2O and CO_2 , and ancillary soil variables measured at the time of gas sampling (%WFPS, NH_4^+ , and NO_3^-). Differences in average daily emissions at the different locations due to the tillage treatments were assessed throughout April 2018 through December 2020, including four tillage events. Daily emissions, cumulative emissions of N_2O , CO_2 , and ancillary soil variables, were also clustered into seasons (wet and dry) for further data analysis. Wet seasons (November through March) included the months with precipitation and coincided with vine dormancy whereas dry seasons included months without precipitation and with active grape vines (April through October) (Figure 2). A total of five seasons' worth of data were collected, including three dry seasons (2018, 2019, and 2020) and two wet seasons (2018-2019 and 2019-2020). The effect of tillage was assessed within the two functional locations (tractor and vine row) and within seasons (wet or dry). Tukey HSD tests were used for pairwise comparisons among the different treatment levels. When residuals were not normally distributed, response variables were transformed prior to the analysis by using $\log_{10} + 10$ (N_2O , CO_2) or square root (NO_3^-). Correlations between daily fluxes and ancillary variables measured at gas sampling were run using nonparametric Spearman's ρ .

General linear models were used to evaluate the effects of tillage treatments on soil N and C, at the two functional locations (vine, tractor row) and soil depths (0-15 cm, 15-30 cm), in 2021, three years after practice implementation. We also used general linear models to evaluate differences in crop yield with tillage, and year as fixed factors. All statistical analyses were conducted with JMP Pro v.15.1.0. (2019, SAS Institute Inc.).

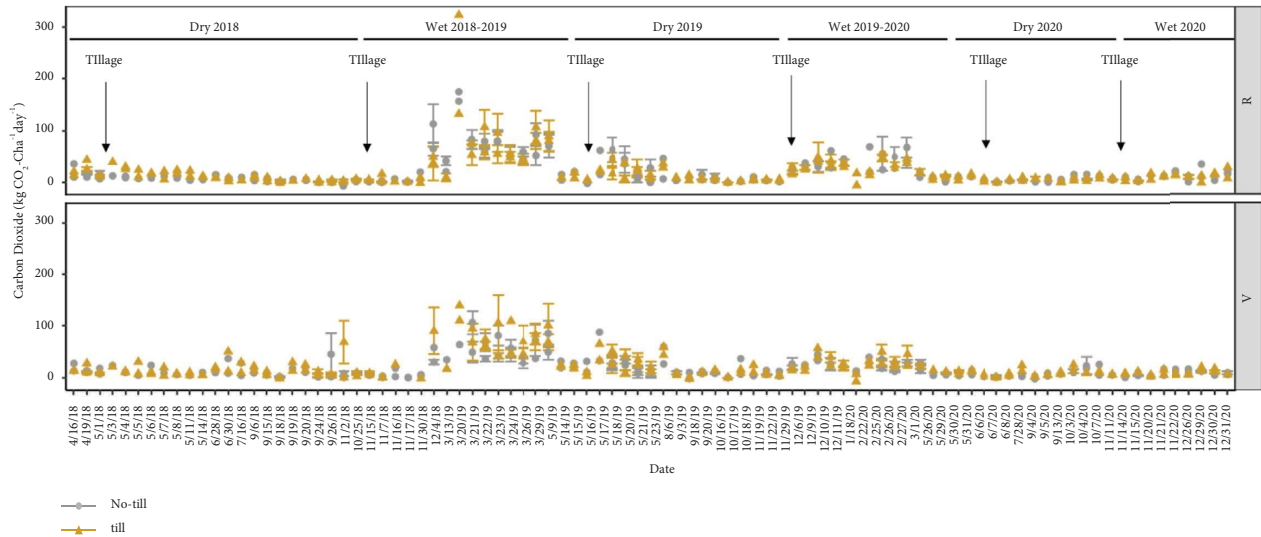


FIGURE 2: CO₂ daily fluxes were measured during the study in the soil in the tractor row (R) and under the vines (V) in either till (orange) or no-till (gray) plots. Values are means ± standard error of 4 replicates.

3. Results

3.1. Effects of the Tillage Treatments on Soil C and N Pools. Soil organic C was significantly higher in the topsoil (0–15 cm depth) as compared to the subsoil (15–30 cm depth) (depth: $F = 52.9$; $p < 0.001$) (Table 1). No statistically significant differences in soil organic C were observed between tilled and nontilled plots after three years of practice implementation. Similar trends were observed for total soil N, which was significantly higher in the topsoil (0–15 cm) as compared to the subsoil (depth: $F = 68.9$; $p < 0.001$), without significant differences between tilled and nontilled plots at either depth (Table 1).

The concentration of active C or POXC was also significantly higher in the topsoil as compared to the subsoil (depth: $F = 32.8$; $p < 0.001$) (Table 1). We observed a significant effect of tillage three years after the start of practice implementation, which depended on the soil depth interval. No-till plots showed statistically significant differences between the two soil depths, with topsoil having more POXC than subsoil, whereas tilled plots had similar POXC concentration at the two depths (depth \times tillage: $F = 4.20$; $p = 0.05$). Microbial biomass C (MBC) was similar between tractor and vine rows but higher in the 0–15 cm than in the 15–30 cm soil layer (depth: $F = 16.9$; $p < 0.001$) of both tractor and vine rows. Nonetheless, MBC remained unaffected by the tillage treatments. The concentration of plant-available N (NO_3^- -N) in soil samples was similar across depths locations and tillage treatments (Table 1). No significant differences were found in ammonium concentrations in soil samples collected at the different locations, depths, and tillage treatments (Table 1).

3.2. Effects of the Tillage Treatments on Soil Physical Properties. Analysis of soil physical properties in 2021, three years after the start of the experiment revealed that bulk density was

similar across locations and depths and remained unaffected by the tillage treatments (Table 2). Aggregate stability was significantly higher in the topsoil (0–15 cm) than in the subsoil (15–30 cm) (Table 2) (depth: $F = 4.34$; $p = 0.049$), although no differences were found between tillage treatments at either location or depth. No significant differences were found in water infiltration rates in the tractor row of tilled versus nontilled plots (Table 2). Soil water holding capacity (WHC) was unaffected by tillage, although we observed a trend for slightly higher WHC in the topsoil of no-till plots ($F = 3.54$; $p = 0.073$) (Table 2) that would be worth investigating in long-term experiments.

3.3. Effects of the Tillage Treatments on GHG Emissions and GWP. Daily fluxes of CO₂ and N₂O measured from April 2018 to December 2020 were analyzed by season for a total of five seasons including 3 dry seasons and 2 wet seasons. The daily fluxes of CO₂ ranged from 0 to 399 kg CO₂-C ha⁻¹·day⁻¹ being generally higher in wet as compared to dry seasons throughout the study (Figure 1). Emissions of CO₂ were significantly higher in tilled vs. nontilled plots during the 2018 dry season (tillage: $F = 6.92$; $p = 0.009$) and 2018–2019 wet season (tillage: $F = 5.71$; $p = 0.017$), irrespective of the location (vine or tractor row) (Figure 1). This trend was reversed in the 2019–2020 wet season where no-till plots had significantly higher emissions as compared to tilled plots (tillage: $F = 4.19$; $p = 0.0423$). No significant differences in CO₂ emissions were found between the tractor and the vine row. Despite the differences observed in daily fluxes, cumulative emissions of CO₂ were not different between treatments or locations at any of the seasons included in this study (Table 3).

Daily fluxes of N₂O ranged between –13 and 70 g N₂O-N ha⁻¹·day⁻¹ throughout the study (Figure 3). Fluxes of N₂O were not significantly different between tilled and nontilled plots at either of the locations studied (vine or tractor row) in

TABLE 1: Different C and N pools were analyzed in the soil samples collected at two depths (0–15 and 15–30 cm) from the tractor and vine rows of the experimental plots in 2021, three years after practice implementation. Values are means \pm standard errors. Letters within the same column indicate significant differences between treatments, locations, and depths at $p < 0.05$.

		Total C (%)	Total N (%)	SOM (%)	POXC ($\text{mg}\cdot\text{kg}^{-1}$)	MBC ($\text{mg}\cdot\text{kg}\text{ soil}^{-1}$)	$\text{NH}_4^+\text{-N}$ ($\mu\text{g}\text{g soil}^{-1}$)	$\text{NO}_3^-\text{-N}$ ($\mu\text{g}\text{g soil}^{-1}$)	
Tractor <i>r</i>	0–15	No-till	3.0 ± 0.2^a	0.3 ± 0.02^a	5.17 ± 0.31^a	827.3 ± 32^a	453.24 ± 113^a	1.28 ± 0.07	11.9 ± 0.9
		Till	3.0 ± 0.1^a	0.3 ± 0.0^a	5.14 ± 0.16^a	774.7 ± 15^{ab}	378.46 ± 62^a	1.41 ± 0.09	9.0 ± 0.6
	15–30	No-till	2.1 ± 0.0^b	0.2 ± 0.0^b	3.69 ± 0.06^b	631.6 ± 38^c	221.58 ± 25^b	1.37 ± 0.23	12.9 ± 2.3
		Till	2.5 ± 0.1^b	0.3 ± 0.01^b	4.25 ± 0.14^b	652.8 ± 52^{bc}	162.42 ± 19^b	1.33 ± 0.16	10.8 ± 2.1
Vine <i>r</i>	0–15	No-till	3.0 ± 0.2^a	0.3 ± 0.02^a	5.22 ± 0.30^a	846.8 ± 62^a	369.24 ± 40^a	1.15 ± 0.15	9.9 ± 0.7
		Till	2.8 ± 0.1^a	0.3 ± 0.01^a	4.77 ± 0.21^a	783.7 ± 25^{ab}	381.27 ± 51^a	1.28 ± 0.11	8.5 ± 1.2
	15–30	No-till	2.2 ± 0.1^b	0.2 ± 0.01^b	3.80 ± 0.25^b	639.1 ± 21^c	186.37 ± 46^b	1.29 ± 0.08	10.8 ± 1.4
		Till	2.2 ± 0.2^b	0.2 ± 0.02^b	3.79 ± 0.30^b	714.7 ± 17^{bc}	270.46 ± 83^b	1.66 ± 0.22	11.4 ± 2.1

TABLE 2: Physical properties of the soil samples collected from the tractor and vine rows of the experimental plots in 2021, three years after practice implementation. Values are means ± standard errors. Letters within the same column indicate significant differences between treatments, locations, and depths at $p < 0.05$.

			Bulk density ($\text{g}\cdot\text{cm}^{-3}$)	Stable aggregates (%)	WHC ($\text{g}\cdot\text{g soil}^{-1}$)
Tractor <i>r</i>	0–15 cm	No-till	0.844 ± 0.05	66.5 ± 4.57 ^a	1.11 ± 0.03
		Till	0.897 ± 0.05	69.2 ± 1.83 ^a	1.03 ± 0.06
	15–30 cm	No-till	0.791 ± 0.09	64.9 ± 5.04 ^b	1.12 ± 0.03
		Till	0.862 ± 0.06	60.6 ± 2.53 ^b	1.11 ± 0.02
Vine <i>r</i>	0–15 cm	No-till	0.805 ± 0.06	65.7 ± 4.48 ^a	1.10 ± 0.02
		Till	0.859 ± 0.04	69.7 ± 1.90 ^a	1.04 ± 0.01
	15–30 cm	No-till	0.769 ± 0.04	60.7 ± 2.57 ^b	1.09 ± 0.02
		Till	0.798 ± 0.12	65.1 ± 1.74 ^b	1.05 ± 0.02

TABLE 3: Cumulative CO₂ and N₂O emissions by season were measured at the tractor row and soil under the vines in tilled and nontilled plots. Letters within the same row (season) indicate significant differences between tillage treatments at $p < 0.05$.

	Tractor row		Vine row	
	No-till	Till	No-till	Till
kg CO₂-C ha⁻¹ season⁻¹				
Dry 2018	428 ± 170	1029 ± 467	656 ± 266	125 ± 934
Dry 2019	1610 ± 810	4305 ± 1787	1839 ± 1109	3514 ± 989
Dry 2020	789 ± 129	970 ± 245	1183 ± 568	1556 ± 564
Wet 2018-2019	28853 ± 19789	80296 ± 45596	9893 ± 3730	44724 ± 24205
Wet 2019-2020	10320 ± 5376	6612 ± 3199	12071 ± 3991	9143 ± 9562
Wet 2020	221 ± 95	366 ± 113	376 ± 136	162 ± 46
g N₂O-N ha⁻¹ season⁻¹				
Dry 2018	48.2 ± 31	114.3 ± 104	89.1 ± 82	48.7 ± 30
Dry 2019	363 ± 303	177 ± 103	383 ± 186	194 ± 113
Dry 2020	119.3 ± 148	145.5 ± 55	62.9 ± 26	141.9 ± 52
Wet 2018-2019	441 ± 385	790 ± 750	78.6 ± 34	3102 ± 2031
Wet 2019-2020	1246 ± 412	1598 ± 556	260 ± 106	1521 ± 1303
Wet 2020	-13.3 ± 15	1.6 ± 3	-48.7 ± 49	2.9 ± 2

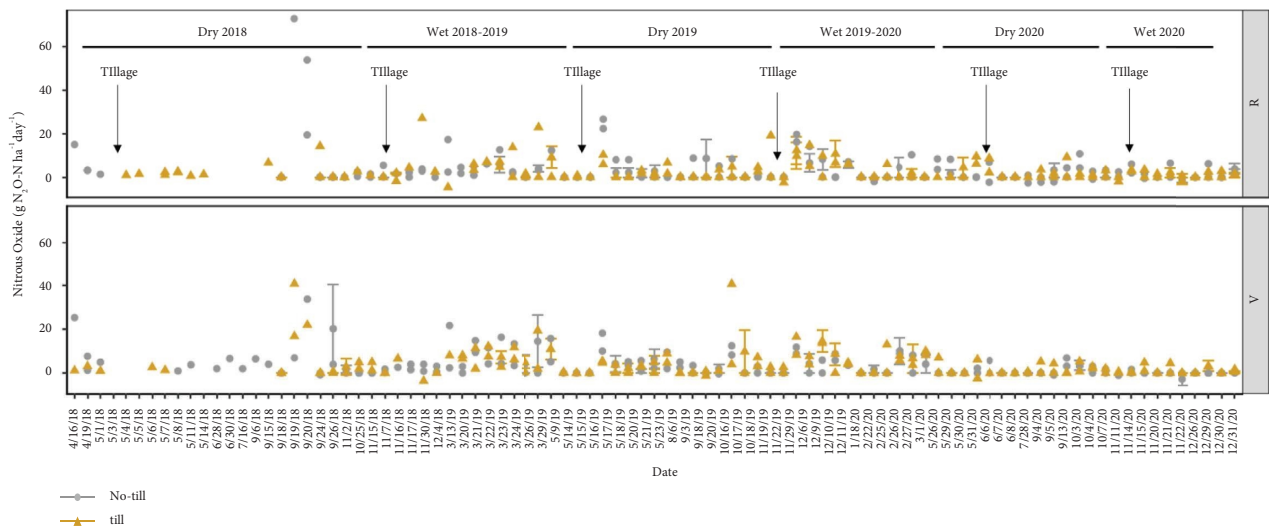


FIGURE 3: N₂O daily fluxes were measured during the study in the soil in the tractor row (R) and under the vines (V) in either till (orange) or no-till (gray) plots. Values are means ± standard error of 4 replicates.

the 2018 dry season (tillage: $F = 0.79$; $p = 0.391$), 2018-2019 wet season (tillage: $F = 2.09$; $p = 0.153$), 2019 dry season (tillage: $F = 3.74$; $p = 0.061$), 2019-2020 wet season (tillage:

$F = 0.17$; $p = 0.678$), and 2020 dry season (tillage: $F = 1.02$; $p = 0.323$) (Figure 3). We did not have sufficient data and degrees of freedom to perform statistical analysis for the

TABLE 4: Change in soil C stocks, CO₂ equivalents and global warming potential of the till and no-till plots during the three years of this study. Values are averages of 4 replicates ± standard errors. Negative values indicate C drawdowns or inputs into the system while positive C indicates C outputs or losses. Letters within the same column indicate significant differences between treatments and years at $p < 0.05$.

		Δ soil C (kg CO ₂ eq·ha ⁻¹)	GWP N ₂ O (kg CO ₂ eq·ha ⁻¹)	GWP (kg CO ₂ eq·ha ⁻¹)
Tractor <i>r</i>	No-till	39.17 ± 82	315.3 ± 78	354.5 ± 56
	Till	-248.1 ± 221	404.2 ± 175	156.1 ± 356
Vine <i>r</i>	No-till	187.4 ± 67	117.9 ± 35	305.29 ± 68
	Till	23.1 ± 128	718.4 ± 476	741.6 ± 525

2020 wet season. During the 2019-2020 wet season, the tractor rows had slightly higher N₂O emissions than the vine rows (location: $F = 5.03$; $p = 0.032$), but no other differences between the locations were found throughout the study. Despite the differences observed in daily fluxes, cumulative emissions of N₂O were not different between treatments or locations at any of the seasons included in this study (Table 3).

The CO₂ and N₂O daily fluxes throughout the study were significantly and positively correlated ($p < 0.0001$). N₂O fluxes were positively correlated to soil water-filled pore space ($p = 0.031$) and negatively correlated to the soil content of ammonium (NH₄⁺-N) ($p < 0.001$). The CO₂ fluxes were negatively correlated to the soil content of ammonium (NH₄⁺-N) ($p < 0.001$).

We used the cumulative N₂O emissions of the till and no-till treatments as well as the change in C stocks to calculate the global warming potential (GWP) of the practices over the three years of the study (Table 4). No significant differences were found among tillage treatments in the change of C stocks ($F = 2.64$; $p = 0.13$), or GWP ($F = 0.21$; $p = 0.65$) at either of the locations sampled in this study (tractor and vine row).

3.4. Effects of the Tillage Treatments on Cover Crop and Vine Yield. Large interannual variability was observed in cover crop growth and therefore potential C and N inputs to the soil. Cover crop biomass was significantly higher in 2019 compared to 2018 and 2020 (Table 5) ($F = 18.76$; $p < 0.001$). The N input from the cover crop was higher in 2019 ($F = 19.48$; $p < 0.001$) although C inputs were higher in 2018 compared to 2020 ($F = 8.31$; $p = 0.0028$). No differences were observed in cover crop biomass C and N inputs between till or no-till plots.

No significant differences were observed either in crop yield between tilled or no-tilled plots, irrespectively of the year (Table 5) (tillage: $F = 0.05$; $p = 0.815$), although we did observe strong interannual variability in this parameter (year: $F = 7.05$; $p = 0.005$). We did not detect any significant differences between tillage treatments in crop quality as assessed through the content of anthocyanins (tillage: $F = 0.008$; $p = 0.929$) and phenolics (tillage: $F = 0.30$; $p = 0.588$), although both quality parameters showed strong interannual variability (anthocyanin: $F = 121.6$; $p < 0.001$; phenolics $F = 48.74$; $p < 0.001$) as it would be expected.

4. Discussion

Soils under no-till are subjected to a lower degree of disturbance than tilled soils, having generally higher structural stability and C sequestration [47, 48]. These changes have

been shown to have direct impacts on C and N cycling, potentially reducing C turnover and CO₂ emission but triggering the release of N₂O through denitrification in anaerobic microsites [23, 49].

In this study, three years after the transition to no-till in this biodynamically-managed vineyard, we observed little change in soil physical properties, C and N pools. No-till increased stratification in the distribution of active soil C (POXC), further accentuating the already existing difference between top and subsoil. Similar increases in topsoil POXC with no-till were observed by Bongiorno et al., [50] in 10 long-term experiments evaluating the effects of tillage across an edaphoclimatic gradient in Europe. It is well known that the transition to no-till systems causes a redistribution of C within the soil profile rather than a net increase [51]. Thus, no-till soils accumulate more C and have a higher bulk density on the surface than tilled soils where soil C is incorporated at depth [47, 52–54]. Our results suggest a trend for higher C accumulation in the topsoil of no-till plot and potential for future C sequestration [55], although no significant differences were observed between till and no-till plots in SOM, total C and N at either depth.

Transition to no-till slightly reduced the daily efflux of CO₂ from the soil during the rainy season, showing that these plots were less prone to lose C than tilled plots. Nonetheless, these differences in daily fluxes were not translated to cumulative seasonal emissions. Similar increases in CO₂ efflux from tilled vineyard soils during precipitation events were reported by Steenwerth et al., [56]; who suggested that these fluxes were driven by changes in soil C content, WFPS, and temperature.

Emissions of N₂O from vineyard soils are generally lower than other crops grown in Mediterranean regions [6]; yet, the lack of tillage disturbance can trigger emissions of this greenhouse gas, especially in fine-textured soils, as the one in this study [23]. In our study, daily fluxes of N₂O were positively correlated to soil WFPS and negatively to ammonium concentration suggesting higher emissions from nitrification and denitrification processes. However, opposite to what we had expected, no significant increases in N₂O daily fluxes and cumulative emissions were observed in the no-till plots through the course of this study, which suggests that seasonal changes in soil moisture and available N were stronger drivers than soil management. These results are in line with Garland et al. [57]; who reported no significant differences in N₂O emissions between tilled and no-till plots in a Mediterranean vineyard one year after the start of the treatments, and show that there are no associated environmental tradeoffs to conversion to no-till.

TABLE 5: Effects of tillage on cover crop (CC) biomass and associated C and N inputs, vine yield, and grape chemistry in 2018, 2019, and 2020. Letters within the same column indicate significant differences between treatments and years at $p < 0.05$.

		CC biomass (g·m ⁻²)	CC C input (g·m ⁻²)	CC N input (g·m ⁻²)	Yield (kg·vine ⁻¹)	Anthocyanins (mg·g ⁻¹)	Phenolics (mg·g ⁻¹)
2018	No-till	123 ± 25 ^b	52.3 ± 10.6 ^a	1.6 ± 0.3 ^b	2.63 ± 0.4 ^b	0.26 ± 0.02 ^b	0.09 ± 0.04 ^b
	Till	158 ± 25 ^b	67.4 ± 11.3 ^a	2.4 ± 0.3 ^b	2.72 ± 0.5 ^b	0.30 ± 0.02 ^b	0.05 ± 0.03 ^b
2019	No-till	222 ± 27 ^a	38.2 ± 4.9 ^{ab}	4.8 ± 0.9 ^a	3.86 ± 0.3 ^a	0.23 ± 0.03 ^b	0.03 ± 0.02 ^b
	Till	154 ± 18 ^a	49.1 ± 11.2 ^{ab}	3.4 ± 0.4 ^a	3.94 ± 0.5 ^a	0.20 ± 0.03 ^b	0.04 ± 0.02 ^b
2020	No-till	59 ± 17 ^c	24.4 ± 7 ^b	1.3 ± 0.3 ^b	2.99 ± 0.1 ^b	0.89 ± 0.07 ^a	0.14 ± 0.07 ^a
	Till	62 ± 5 ^c	25.4 ± 2 ^b	1.5 ± 0.1 ^b	2.60 ± 0.2 ^b	0.88 ± 0.08 ^a	0.16 ± 0.08 ^a

Altogether, the lack of differences in soil C stocks and cumulative GHG emissions led to similar GWP between till and no-till plots. This lack of effects could be due to the short duration of the study relative to the SOM buildup in semiarid, Mediterranean regions. The slower buildup of SOM is expected given that the rate of carbon accumulation for a given practice is strongly dependent on environmental conditions (i.e., temperature and precipitation) that regulate microbial activity [58, 59]. This suggests that the building of organic matter and soil C stocks in no-till vineyards may take more than 5 years [51, 60–62]. For instance, Wolff et al., [63] reported significant increases in SOC seven years after the transition to no-till in a California vineyard, which caused significant decreases in the GWP of the practice as compared to conventional tillage with a disk to 10 cm depth.

It is also possible that the lack of significant differences between tilled and nontilled plots SOM, C, and N is due to the tillage implement used in this vineyard (disk) compared to other systems, such as moldboard plow or chisel plow, which are known to produce a higher disturbance intensity [21]. In this region of California, growers employ different implements and apply different tillage intensities and frequencies depending on the type of soil and production goals. Laudicina et al. [48] reported a significant short-term (5 years) reduction in bulk density together with increases in aggregate stability, and total soil C of a Mediterranean vineyard soil but only when no-till was compared to rotary tiller (higher intensity), whereas there were almost no differences with a spading machine (lower intensity). A moderate degree of tillage intensity may not have negative effects on soil health and C sequestration, particularly when stacked with other conservation practices (cover crops, compost). In a long-term field experiment comparing different agricultural systems Autret et al., [64] estimated that, under conservation practices (i.e., no-till), the lack of tillage explained only 20% of the C accumulation while the majority of the C inputs were attributed to crop residues and cover crops.

The vineyard studied here has consistently received large inputs of cover crops and, despite being tilled for the last 6–8 years, it also shows some of the highest levels of SOM as compared to the typical values reported for vineyards in California [65]. These high levels of SOM could not only be partially explained by the fine texture of the soil which allows for the formation of stable, mineral-associated organic matter (MAOM) [66, 67] but also by long-term management as it has been observed previously for biodynamic systems

[68–71]. High levels of SOM in organically managed cropping systems have also been associated with tightly coupled N mineralization and immobilization [72] which explains the lack of differences between till and no-till plots in inorganic N observed in our study. Most likely, this is also associated with the lack of significant differences in crop yield and grape quality.

In summary, even though implementation of no-till for three years did not lead to increases in soil organic matter and soil C stocks, we observed a trend towards higher C stratification and reduced CO₂ emissions in no-till plots that suggest changes in the ecological processes leading to C accumulation and mineralization. Adopting no till-practices has associated environmental benefits through the reduction of the use of machinery and fuel consumption. This suggests the environmental benefits of this practice, although longer studies and life cycle analysis would be needed to verify this trend. There were no deleterious effects of no-till on grape yield and quality, proving that reducing tillage intensity is a feasible strategy from an agronomic standpoint.

5. Conclusions

Even though no-till did not result in short-term climate change mitigation, results of this study suggest changes in the ecological processes leading to C accumulation and mineralization and that may result in future C sequestration. There were no deleterious effects of no-till on grape yield and quality.

Data Availability

Data will be made available upon request.

Conflicts of Interest

The authors declare that they have no conflicts of interest.

Acknowledgments

This research was funded by the California Department of Food and Agriculture (CDFA) Healthy Soils Initiative (Grant 17-0624-000-HS). The authors are grateful to Jordan Lonborg (viticulturist) and the field personnel of Tablas Creek Vineyard for their help in establishing and maintaining this field trial. The authors thank AWITC for the invitation to publish our research in this Special Issue and for covering the article processing charge.

References

- [1] P. Smith, "Soils and climate change," *Current Opinion in Environmental Sustainability*, vol. 4, pp. 539–544, 2012.
- [2] R. Lal, "Soil health and carbon management," *Food Energy Secur.*, vol. 5, pp. 212–222, 2016.
- [3] K. Steenwerth and K. M. Belina, "Cover crops enhance soil organic matter, carbon dynamics and microbiological function in a vineyard agroecosystem," *Applied Soil Ecology*, vol. 40, pp. 359–369, 2008a.
- [4] F. Peregrina, C. Larrieta, M. Colina et al., "Spent mushroom substrates influence soil quality and nitrogen availability in a semiarid vineyard soil," *Soil Science Society of America Journal*, vol. 76, pp. 1655–1666, 2012.
- [5] C. Poeplau and A. Don, "Carbon sequestration in agricultural soils via cultivation of cover crops – a meta-analysis," *Agriculture, Ecosystems & Environment*, vol. 200, pp. 33–41, 2015.
- [6] K. Steenwerth and K. M. Belina, "Cover crops and cultivation: impacts on soil N dynamics and microbiological function in a Mediterranean vineyard agroecosystem," *Applied Soil Ecology*, vol. 40, pp. 370–380, 2008b.
- [7] H. Blanco-Canqui and S. J. Ruis, "No-tillage and soil physical environment," *Geoderma*, vol. 326, pp. 164–200, 2018.
- [8] A. Maykish, R. Rex, and A. K. Sikalidis, "Organic winemaking and its subsets; biodynamic, natural, and clean wine in California," *Foods*, vol. 10, p. 127, 2021.
- [9] A. J. VandenBygaert, "The myth that no-till can mitigate global climate change," *Agriculture, Ecosystems & Environment*, vol. 216, pp. 98–99, 2016.
- [10] Q. Feng, C. An, Z. Chen, and Z. Wang, "Can deep tillage enhance carbon sequestration in soils? A meta-analysis towards GHG mitigation and sustainable agricultural management," *Renewable and Sustainable Energy Reviews*, vol. 133, Article ID 110293, 2020.
- [11] H. V. Cooper, S. Sjögersten, R. M. Lark, and S. J. Mooney, "To till or not to till in a temperate ecosystem? Implications for climate change mitigation," *Environmental Research Letters*, vol. 16, Article ID 054022, 2021.
- [12] D. C. Reicosky, "Tillage-induced CO₂ emission from soil," *Nutrient Cycling in Agroecosystems*, vol. 49, pp. 273–285, 1997.
- [13] B. Rutkowska, W. Szulc, T. Sosulski, M. Skowrońska, and J. Szczepaniak, "Impact of reduced tillage on CO₂ emission from soil under maize cultivation," *Soil and Tillage Research*, vol. 180, pp. 21–28, 2018.
- [14] S. Franco-Luesma, J. Caverro, D. Plaza-Bonilla, C. Cantero-Martínez, J. L. Arrúe, and J. Álvaro-Fuentes, "Tillage and irrigation system effects on soil carbon dioxide (CO₂) and methane (CH₄) emissions in a maize monoculture under Mediterranean conditions," *Soil and Tillage Research*, vol. 196, Article ID 104488, 2020.
- [15] J. Balesdent, C. Chenu, and M. Balabane, "Relationship of soil organic matter dynamics to physical protection and tillage," *Soil and Tillage Research*, vol. 53, pp. 215–230, 2000.
- [16] J. Six, E. T. Elliott, and K. Paustian, "Soil macroaggregate turnover and microaggregate formation: a mechanism for C sequestration under no-tillage agriculture," *Soil Biology and Biochemistry*, vol. 32, pp. 2099–2103, 2000.
- [17] N. J. Sithole, L. S. Magwaza, and G. R. Thibaud, "Long-term impact of no-till conservation agriculture and N-fertilizer on soil aggregate stability, infiltration and distribution of C in different size fractions," *Soil and Tillage Research*, vol. 190, pp. 147–156, 2019.
- [18] L. Lipper, P. Thornton, B. M. Campbell et al., "Climate-smart agriculture for food security," *Nature Climate Change*, vol. 4, pp. 1068–1072, 2014.
- [19] G. Luo, V.-P. Friman, H. Chen et al., "Long-term fertilization regimes drive the abundance and composition of N-cycling-related prokaryotic groups via soil particle-size differentiation," *Soil Biology and Biochemistry*, vol. 116, pp. 213–223, 2018.
- [20] E. Slessarev, J. Zelikova, J. Hamman, D. Cullenward, and J. Freeman, *Depth Matters for Soil Carbon Accounting*, Cabonplan, United Kingdom, 2021.
- [21] S. J. Ruis, H. Blanco-Canqui, P. J. Jasa, and V. L. Jin, "No-till farming and greenhouse gas fluxes: insights from literature and experimental data," *Soil and Tillage Research*, vol. 220, Article ID 105359, 2022.
- [22] J. Six, H. Bossuyt, S. Degryze, and K. Denef, "A history of research on the link between (micro)aggregates, soil biota, and soil organic matter dynamics," *Soil and Tillage Research*, vol. 79, pp. 7–31, 2004.
- [23] P. Rochette, "No-till only increases N₂O emissions in poorly-aerated soils," *Soil and Tillage Research*, vol. 101, pp. 97–100, 2008.
- [24] J. Wang and J. Zou, "No-till increases soil denitrification via its positive effects on the activity and abundance of the denitrifying community," *Soil Biology and Biochemistry*, vol. 142, Article ID 107706, 2020.
- [25] J. Lipiec, J. Kuś, A. Słowińska-Jurkiewicz, and A. Nosalewicz, "Soil porosity and water infiltration as influenced by tillage methods," *Soil and Tillage Research*, vol. 89, pp. 210–220, 2006.
- [26] H. Blanco-Canqui, L. R. Stone, A. J. Schlegel et al., "No-Till induced increase in organic carbon reduces maximum bulk density of soils," *Soil Science Society of America Journal*, vol. 73, pp. 1871–1879, 2009.
- [27] D. S. Powlson, C. M. Stirling, M. L. Jat et al., "Limited potential of no-till agriculture for climate change mitigation," *Nature Climate Change*, vol. 4, pp. 678–683, 2014.
- [28] C. M. Kallenbach, A. S. Grandy, S. D. Frey, and A. F. Diefendorf, "Microbial physiology and necromass regulate agricultural soil carbon accumulation," *Soil Biology and Biochemistry*, vol. 91, pp. 279–290, 2015.
- [29] A. Shakoor, M. Shahbaz, T. H. Farooq et al., "A global meta-analysis of greenhouse gases emission and crop yield under no-tillage as compared to conventional tillage," *Science of the Total Environment*, vol. 750, Article ID 142299, 2021.
- [30] C. M. Pittelkow, B. A. Linquist, M. E. Lundy et al., "When does no-till yield more? A global meta-analysis," *Field Crops Research*, vol. 183, pp. 156–168, 2015.
- [31] J. Lee and K. L. Steenwerth, "Cabernet Sauvignon" grape anthocyanin increased by soil conservation practices," *Scientia Horticulturae*, vol. 159, pp. 128–133, 2013.
- [32] I. Buesa, J. M. Mirás-Avalos, J. M. De Paz et al., "Soil management in semi-arid vineyards: combined effects of organic mulching and no-tillage under different water regimes," *European Journal of Agronomy*, vol. 123, Article ID 126198, 2021.
- [33] K. L. Steenwerth, A. J. McElrone, A. Calderon-Orellana et al., "Cover crops and tillage in a mature merlot vineyard show few effects on grapevines," *American Journal of Enology and Viticulture*, vol. 64, pp. 515–521, 2013.
- [34] E. C. Suddick, K. M. Scow, W. R. Horwath et al., "The potential for California agricultural crop soils to reduce greenhouse gas emissions," in *Advances in Agronomy*, pp. 123–162, Elsevier, Amsterdam, Netherlands, 2010.

- [35] V. A. Laudicina, A. Novara, L. Gristina, and L. Badalucco, "Soil carbon dynamics as affected by long-term contrasting cropping systems and tillages under semiarid Mediterranean climate," *Applied Soil Ecology*, vol. 73, pp. 140–147, 2014.
- [36] C. Lazcano, C. Decock, and S. Willson, "Defining and managing for healthy vineyard soils, intersections with the concept of terroir," *Frontiers in Environmental Science*, vol. 8, 2020.
- [37] C. Lazcano, N. Gonzalez-Maldonado, E. H. Yao et al., "Sheep grazing as a strategy to manage cover crops in Mediterranean vineyards: short-term effects on soil C, N and greenhouse gas (N₂O, CH₄, CO₂) emissions," *Agriculture, Ecosystems & Environment*, vol. 327, Article ID 107825, 2022.
- [38] P. Iland, *Chemical Analysis of Grapes and Wine: Techniques and Concepts*, Patrick Iland Wine Promotions, Adelaide, 2013.
- [39] I. Bisutti, I. Hilke, J. Schumacher, and M. Raessler, "A novel single-run dual temperature combustion (SRDTC) method for the determination of organic, in-organic and total carbon in soil samples," *Talanta*, vol. 71, pp. 521–528, 2007.
- [40] X. Wang, J. Wang, and J. Zhang, "Comparisons of three methods for organic and inorganic carbon in calcareous soils of northwestern China," *PLoS One*, vol. 7, Article ID e44334, 2012.
- [41] T. A. Doane and W. R. Horwath, "Spectrophotometric determination of nitrate with a single reagent," *Analytical Letters*, vol. 36, pp. 2713–2722, 2003.
- [42] R. R. Weil, K. R. Islam, M. A. Stine, J. B. Gruver, and S. E. Samson-Liebig, "Estimating active carbon for soil quality assessment: a simplified method for laboratory and field use," *American Journal of Alternative Agriculture*, vol. 18, pp. 3–17, 2003.
- [43] G. L. Hutchinson and G. P. Livingston, "Use of chamber systems to measure trace gas fluxes," in *ASA Special Publications*, L. A. Harper, A. R. Mosier, J. M. Duxbury, and D. E. Rolston, Eds., pp. 63–78, American Society of Agronomy, Crop Science Society of America, and Soil Science Society of America, Madison, WI, USA, 1993.
- [44] T. B. Parkin and R. T. Venterea, "Sampling protocols. Chapter 3. Chamber-based trace gas flux measurements," in *Sampling Protocols*, pp. 1–39, R.F. Follett, USA, 2010.
- [45] G. L. Hutchinson and A. R. Mosier, "Improved soil cover method for field measurement of nitrous oxide fluxes," *Soil Science Society of America Journal*, vol. 45, pp. 311–316, 1981.
- [46] C. Decock, G. Garland, E. C. Suddick, and J. Six, "Season and location-specific nitrous oxide emissions in an almond orchard in California," *Nutrient Cycling in Agroecosystems*, vol. 107, pp. 139–155, 2017.
- [47] J. L. Hernanz, R. López, L. Navarrete, and V. Sánchez-Girón, "Long-term effects of tillage systems and rotations on soil structural stability and organic carbon stratification in semiarid central Spain," *Soil and Tillage Research*, vol. 66, pp. 129–141, 2002.
- [48] V. A. Laudicina, E. Palazzolo, P. Catania, M. Vallone, A. D. García, and L. Badalucco, "Soil quality indicators as affected by shallow tillage in a vineyard grown in a semiarid mediterranean environment," *Land Degradation & Development*, vol. 28, pp. 1038–1046, 2017.
- [49] C. van Kessel, R. Venterea, J. Six, M. A. Adviento-Borbe, B. Linquist, and K. J. van Groenigen, "Climate, duration, and N placement determine N₂O emissions in reduced tillage systems: a meta-analysis," *Global Change Biology*, vol. 19, pp. 33–44, 2013.
- [50] G. Bongiorno, E. K. Bünemann, C. U. Ogueji et al., "Sensitivity of labile carbon fractions to tillage and organic matter management and their potential as comprehensive soil quality indicators across pedoclimatic conditions in Europe," *Ecological Indicators*, vol. 99, pp. 38–50, 2019.
- [51] S. A. Belmonte, L. Celi, R. J. Stahel et al., "Effect of long-term soil management on the mutual interaction among soil organic matter, microbial activity and aggregate stability in a vineyard," *Pedosphere*, vol. 28, pp. 288–298, 2018.
- [52] Z. Luo, E. Wang, and O. J. Sun, "Can no-tillage stimulate carbon sequestration in agricultural soils? A meta-analysis of paired experiments," *Agriculture, Ecosystems & Environment*, vol. 139, pp. 224–231, 2010.
- [53] C. López-Fando and M. T. Pardo, "Soil carbon storage and stratification under different tillage systems in a semi-arid region," *Soil and Tillage Research*, vol. 111, pp. 224–230, 2011.
- [54] M. R. Nunes, D. L. Karlen, K. S. Veum, T. B. Moorman, and C. A. Cambardella, "Biological soil health indicators respond to tillage intensity: a US meta-analysis," *Geoderma*, vol. 369, Article ID 114335, 2020.
- [55] T. T. Hurisso, S. W. Culman, W. R. Horwath et al., "Comparison of permanganate-oxidizable carbon and mineralizable carbon for assessment of organic matter stabilization and mineralization," *Soil Science Society of America Journal*, vol. 80, pp. 1352–1364, 2016.
- [56] K. L. Steenwerth, D. L. Pierce, E. A. Carlisle, R. G. M. Spencer, and D. R. Smart, "A vineyard agroecosystem: disturbance and precipitation affect soil respiration under mediterranean conditions," *Soil Science Society of America Journal*, vol. 74, pp. 231–239, 2010.
- [57] G. M. Garland, E. Suddick, M. Burger, W. R. Horwath, and J. Six, "Direct N₂O emissions following transition from conventional till to no-till in a cover cropped Mediterranean vineyard (*Vitis vinifera*)," *Agriculture, Ecosystems & Environment*, vol. 144, pp. 423–428, 2011.
- [58] S. D. Frey, J. Lee, J. M. Melillo, and J. Six, "The temperature response of soil microbial efficiency and its feedback to climate," *Nature Climate Change*, vol. 3, pp. 395–398, 2013.
- [59] N. Carvalhais, M. Forkel, M. Khomik et al., "Global covariation of carbon turnover times with climate in terrestrial ecosystems," *Nature*, vol. 514, pp. 213–217, 2014.
- [60] F. Peregrina, C. Larrieta, S. Ibáñez, and E. García-Escudero, "Labile organic matter, aggregates, and stratification ratios in a semiarid vineyard with cover crops," *Soil Science Society of America Journal*, vol. 74, pp. 2120–2130, 2010.
- [61] M. Ruiz-Colmenero, R. Bienes, D. J. Eldridge, and M. J. Marques, "Vegetation cover reduces erosion and enhances soil organic carbon in a vineyard in the central Spain," *Catena*, vol. 104, pp. 153–160, 2013.
- [62] F. Zehetner, I. Djukic, R. Hofmann et al., "Soil organic carbon and microbial communities respond to vineyard management," *Soil Use & Management*, vol. 31, pp. 528–533, 2015.
- [63] M. W. Wolff, M. M. Alsina, C. M. Stockert, S. D. S. Khalsa, and D. R. Smart, "Minimum tillage of a cover crop lowers net GWP and sequesters soil carbon in a California vineyard," *Soil and Tillage Research*, vol. 175, pp. 244–254, 2018.
- [64] B. Autret, B. Mary, C. Chenu et al., "Alternative arable cropping systems: a key to increase soil organic carbon storage? Results from a 16 year field experiment," *Agriculture, Ecosystems & Environment*, vol. 232, pp. 150–164, 2016.
- [65] S. M. Devine, K. L. Steenwerth, and A. T. O'Geen, "Soil health practices have different outcomes depending on local soil conditions," *California Agriculture*, vol. 76, pp. 46–55, 2022.
- [66] J. Six, R. T. Conant, E. A. Paul, and K. Paustian, "Stabilization mechanisms of soil organic matter: implications for C-saturation of soils," *Plant and Soil*, vol. 241, pp. 155–176, 2002.

- [67] J. M. Lavalley, J. L. Soong, and M. F. Cotrufo, "Conceptualizing soil organic matter into particulate and mineral-associated forms to address global change in the 21st century," *Global Change Biology*, vol. 26, pp. 261–273, 2020.
- [68] B. Probst, C. Schüler, and R. G. Joergensen, "Vineyard soils under organic and conventional management—microbial biomass and activity indices and their relation to soil chemical properties," *Biology and Fertility of Soils*, vol. 44, pp. 443–450, 2008.
- [69] N. de O. Freitas, A. M. Yano-Melo, F. S. B. da Silva, N. F. de Melo, and L. C. Maia, "Soil biochemistry and microbial activity in vineyards under conventional and organic management at Northeast Brazil," *Scientia Agricola*, vol. 68, pp. 223–229, 2011.
- [70] N. Okur, H. H. Kayikcioglu, F. Ates, and B. Yagmur, "A comparison of soil quality and yield parameters under organic and conventional vineyard systems in Mediterranean conditions (West Turkey)," *Biological Agriculture & Horticulture*, vol. 32, pp. 73–84, 2016.
- [71] S. Di Giacinto, M. Friedel, C. Poll, J. Döring, R. Kunz, and R. Kauer, "Vineyard management system affects soil microbiological properties," *OENO One*, vol. 54, 2020.
- [72] T. M. Bowles, A. D. Hollander, K. Steenwerth, and L. E. Jackson, "Tightly-coupled plant-soil nitrogen cycling: comparison of organic farms across an agricultural landscape," *PLoS One*, vol. 10, pp. 1–24, 2015.